2013-10-02

Stable Isotope and Geochemical Investigations into the Hydrogeology and Biogeochemistry of Oil Sands Reservoir Systems in Northeastern Alberta, Canada

Cowie, Benjamin Ross

UNIVERSITY OF CALGARY

Stable Isotope and Geochemical Investigations into the Hydrogeology and Biogeochemistry of Oil Sands Reservoir Systems in Northeastern Alberta, Canada

by

Benjamin R. Cowie

A THESIS

SUBMITTED TO THE FACULTY OF GRADUATE STUDIES

IN PARTIAL FULFILMENT OF THE REQUIREMENTS FOR THE

DEGREE OF DOCTOR OF PHILOSOPHY

DEPARTMENT OF GEOSCIENCE

CALGARY, ALBERTA

SEPTEMBER, 2013

Abstract

The objective of this thesis was to provide insight into the hydrogeology and biogeochemistry of the heavily biodegraded bitumen reservoirs of the Athabasca oil sands region of Alberta, Canada, using applications of aqueous and stable isotope geochemistry.

Published data were used to generate a regional map of total dissolved solids concentrations in McMurray Formation waters. To explain the regional salinity data, a revised hydrogeological model was developed that incorporates localized upward flow of formation waters from saline Devonian aquifers into the bitumen-bearing McMurray Formation via karst-derived conduits. Where McMurray Formation waters are uninfluenced by connectivity with Devonian aquifers, topographic recharge from meteoric water is the dominant hydrogeological process.

A new method was developed to determine the stable isotope composition and salinity of McMurray Formation waters from porewater samples extracted from drilling fluid-contaminated core. Mixing relationships of $\delta^{2}H$ and $\delta^{18}O$ values in drilling fluid and formation water were used to calculate the original formation water stable isotope composition and salinity from porewater extracted directly from oil sands drill core. Both vertical and lateral heterogeneity were observed on a reservoir-scale, and topographically-derived groundwater recharge was determined to be the dominant hydrogeological process in Suncor-Firebag lease area.

Biogeochemical aspects of oil sands systems were investigated in two studies. The first study examined the impact of variable aqueous geochemistry on oil sands biogeochemistry, specifically methanogenesis and bacterial sulfate reduction, in laboratory-scale microcosms. Changes in aqueous geochemistry induced changes in the total amount of methane generated, and in the stable isotope ratios of carbon and hydrogen of generated methane. The second

experiment measured natural abundance radiocarbon in dissolved inorganic carbon in a coal-bed methane reservoir in the Powder River Basin, Montana, USA. All samples of dissolved inorganic carbon and methane contained no detectable radiocarbon, and thus the carbon flux from biodegradation of coal was much greater than the carbon flux from recent groundwater recharge into the coal-bed aquifer system.

Improved understanding of hydrogeological processes, and better understanding of reservoir biogeochemistry will lead to better decision making by industry and regulators during the development of oil sands resources, while our society transitions away from fossil energy over the coming century.

Acknowledgements

Scientific research is no longer the product of a single principal investigator supervising a graduate student protégé. While this thesis bears my name as author, there are many people who have contributed directly or indirectly to the work within these pages via intellectual discussions, expert technical assistance, access to samples, or occasionally buying a cold beer.

My supervisor Dr. Bernhard Mayer has been a steady guiding presence during my Ph.D. degree. Bernhard has been an invaluable resource during my development as a researcher by sharing his deep understanding of stable isotope geochemistry, the application of these techniques across a wide spectrum of Earth sciences, and ability to communicate science in a clear and concise way. He also possesses incredible organizational capabilities to maintain a large and productive research group, while dedicating substantial time and energy to his family. This balance is something that I truly admire, and I hope to emulate in the future. Thank you, Bernhard, for a fantastic five years in the Applied Geochemistry group.

My thesis examination committee provided substantial feedback that greatly improved this thesis, and the manuscripts that will follow from this work. Dr. Steve Larter, in particular, has provided encouragement and motivation to achieve more, and to think bigger throughout my Ph.D.. Drs. Steve Grasby, Mike Wieser and Ian Clark are also thanked for their presence on my defense committed and their contributions that significantly improved this work.

Bruce James of Suncor Energy Inc. has been a driving force for better understanding of oil sands water systems, and became an important mentor for me as we collaborated on Chapters Two, Three and Four. I thank him for the many coffee chats, insightful comments on both the content and presentation of my research within industry groups, and for improving communication between academia and industry scientists.

The research staff of the Applied Geochemistry group provided a great deal of support and technical expertise. For this I thank Steve Taylor, Mike Nightingale, Maurice Shevalier, Jesusa Pontoy, Nenita Lozano and Jack Goodwin. Mike Nightingale deserves special recognition for his technical and intellectual contribution to the development of the work in Chapters Three and Four.

Collaboration with Lisa Gieg, Jen McIntosh, David Vinson, Sandra Wilson, Hamed Sanei, and Rhonda Clark enriched my doctoral experience, and provided diverse scientific perspectives from my own for which I am very grateful.

Leslie Reid is to thank for her pedagogical expertise and mentorship during my first experience as a university instructor. Learning Assessment days were among the most fun I've ever had in a classroom, and my conceptual model of how all humans learn has been greatly improved thanks to Dr. Reid.

The five years I spent working with the Pavilion Lake Research Project provided me with the desire to build a career in Earth science. While my thesis is unrelated to PLRP, my experience working with this incredible team gave me inspiration and vision for what humans can achieve when enthusiastic people work together toward a common goal. Darlene Lim, Bernard Laval, Greg Slater, Allyson Brady and Donnie Reid are creative and driven leaders who push the project "Deeper toward the Moon and Mars" every year. Margarita Marinova, Alex Forrest, Bekah Shepard, Alfonso Davila, Dale Andersen, Raffy Pendery, Mike Gernhardt, Chris Hadfield, Art Trembanis, Jen Biddle, Mickey and Linda Macri, and many others provided so much energy, humour, inspiration, knowledge and perspective about the human experience on our planet and beyond.

My friends, especially Andrew and Holly Kingston, Duncan Findlay and Stephanie Erickson, are to thank for much encouragement, many unforgettable mountain days, and personal insights over the past five years. You are the best ‘orphan family’ I could hope to have in Calgary, thank you.

I am fortunate to have a supportive immediate and extended family both in Calgary and across Canada. I thank them for their support during this journey. Finally, thank you to my parents, John and Judy for their continued long-distance love and support, and for giving me so many opportunities to grow and succeed throughout my life.

Table of Contents

List of Tables

List of Figures and Illustrations

Chapter One: Introduction

The next frontier in the race to develop fossil energy resources in Alberta, Canada will be the search for water resources and wastewater disposal options in the Athabasca Oil Sands Region (AOSR). Increasing demand for industrial water will necessitate detailed understanding of oil sands hydrogeology, and high-resolution characterization of oil sands reservoir water systems will be required to maximize efficiency of energy and water use during bitumen production. This thesis provides new techniques for water characterization, and new interpretations of the water systems in the Athabasca Oil Sands Region.

1.1 Introduction

Fossil fuels will continue to serve an essential role in the global energy portfolio for the next half-century while societies decarbonize their energy systems (Smil, 2010; IEA World Energy Outlook, 2012). However, easily accessible conventional hydrocarbon resources are becoming depleted, therefore non-conventional sources of fossil fuels are currently being developed to satisfy global demand for energy and petroleum products. The heavily biodegraded Alberta oil sands are the third largest proven reserve of petroleum resources on Earth (Government of Alberta, 2012; World Energy Outlook, 2012) and development of these resources is taking place at a rapid pace. The development of heavy oils and bitumen in Alberta has provided significant economic growth, however, these developments have a large environmental footprint that is not well understood (Hrudey et al., 2010).

The Alberta oil sands are a complicated energy system unlike any previous petroleum system exploited for human consumption. The immense quantity of resources required for extraction, the large footprint of surface operations, and geological complexity of the deposit are all exceptional in the oil and gas industry. Contributing to geological complexity is a challenging sedimentological and stratigraphic framework (Langenberg et al., 2002; Ranger and Gingras,

2003; Fustic et al., 2012), some uncertainty in the regional structural geology (Flach, 1984; Broughton, 2013), the shallow depth of the deposit, ranging from twenty to five hundred metres below ground surface (Government of Alberta, 2013), heavy biodegradation of the oil, resulting in low API° values (Larter et al., 2006; Bennett and Larter, 2008; Fustic et al., 2012; Bennett et al., 2013), and the vast scale of the resource covering a surface area of more than 14 million hectares (Fig. 1.1, Government of Alberta, 2012). Perhaps most significantly, these are the first petroleum deposits exploited by humans that require an exceptionally detailed knowledge of a complex near-surface hydrogeological system, as extraction by steam injection requires an unconventional approach to subsurface reservoir development.

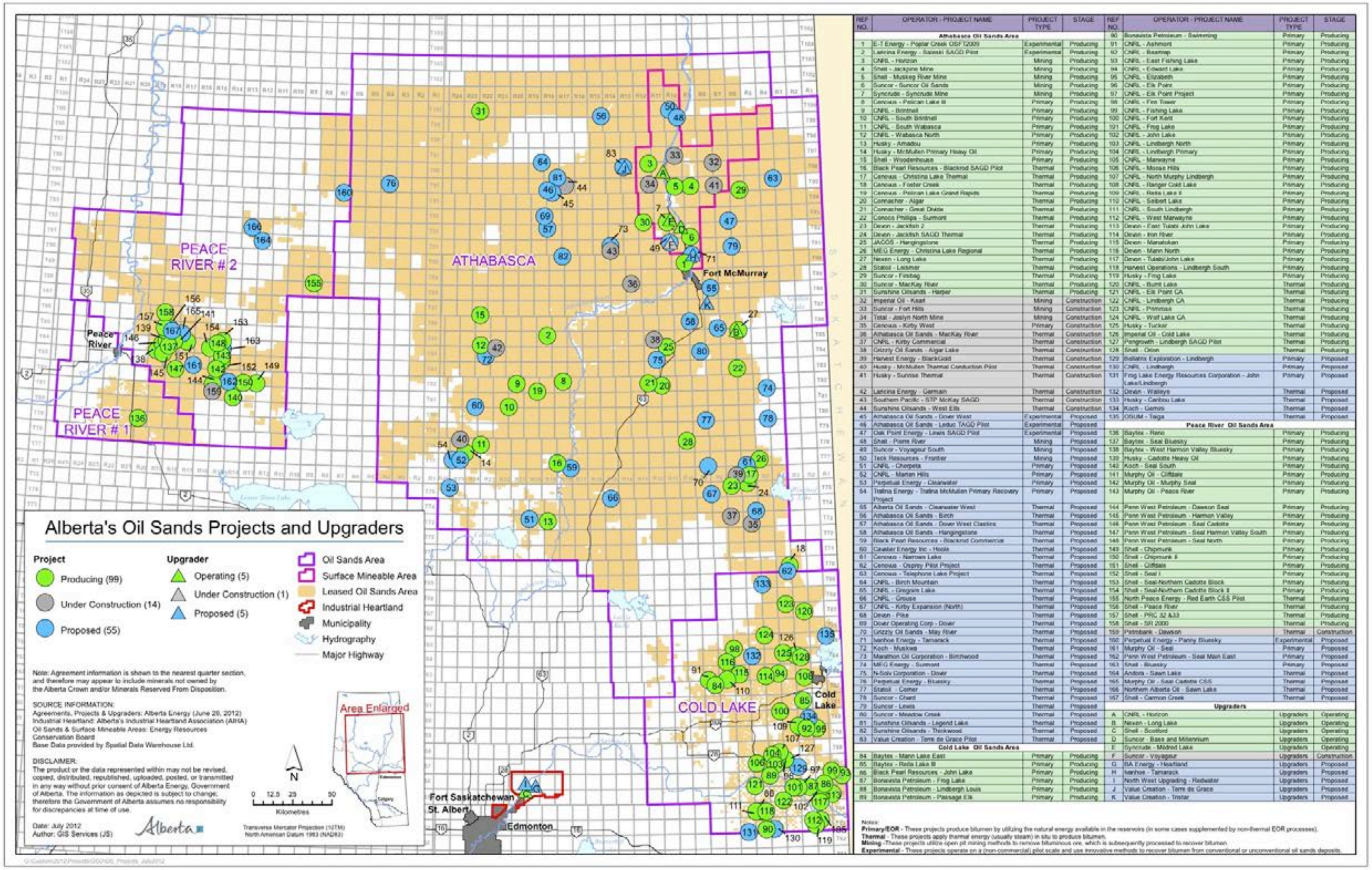

Figure 1.1: Alberta's oil sands lease areas and active oil sands extraction projects (Government of Alberta, 2012).

Acquiring adequate groundwater resources has become an essential step in the development of oil sands resources via in situ methods, as the development of bitumen resources requires between one and ten barrels of water to produce one barrel of synthetic crude oil (Griffiths, 2006; Government of Alberta, 2013). Mining operations in the oil sands regions are all proximal to the Athabasca River, and surface water provides a large water source for industrial processes (Government of Alberta, 2013). However, development of oil sands resources that are too deep to mine also require large quantities of water for fossil fuel extraction by steam assisted gravity drainage and often these deposits are not near a significant surface water source. Therefore energy resource development in the oil sands regions is closely linked to the availability of surface and groundwater resources in northeast Alberta (Gilmour, 2013). During Steam Assisted Gravity Drainage (SAGD) development, steam is injected into the reservoir to lower the viscosity of the bitumen resource and produce the heated liquid to the surface. Detailed knowledge of the reservoir architecture is essential to constrain steam chamber growth within the petroleum-bearing reservoir. Water-saturated zones above, below and within the reservoir must be avoided to maximize production efficiency, as steam preferentially flows into these bitumen-free zones (Rubin et al., 2009). Produced water from SAGD operations is recycled at a high rate (Government of Alberta, 2013), however some industrial wastewater disposal into deep saline aquifers is required at each site (Griffiths et al., 2006; Hrudey et al., 2012).

A major challenge for monitoring resource development in the AOSR is the scarcity of public data on groundwater quality and quantity. While individual companies retain substantial proprietary databases on their individual resource developments, the cumulative effects of development and regional trends in groundwater properties cannot be effectively discerned using

available public data. For government regulators and scientific research, these data are typically unavailable except through Environmental Impact Assessments (EIA) that are local to sub-regional in scope, and data within EIA documents are not peer-reviewed or evaluated for data quality. Data from local-scale EIA have not been synthesized into a broader regional impact assessment, and compiling this data was an objective for some of the work in this thesis.

1.2 Athabasca oil sands: an overview

1.2.1 Geography

There are three major oil sands regions in Alberta: Peace River, Cold Lake and Athabasca (Fig. 1.1). The primary focus of this thesis is on the largest of the three, the Athabasca Oil Sands Region. Most oil sands deposits are overlain on the surface by boreal forest and muskeg. The mean annual temperature at Fort McMurray is 0.7 ºC with January and July averages of −18.8 ºC and 16.8 ºC (National Climate Data and Information Archive, 2013). The mean annual rainfall and snowfall at Fort McMurray are 342 mm and 156 mm respectively, resulting in a total mean annual precipitation of 456 mm (National Climate Data and Information Archive, 2013). Due to the instability of muskeg during the summer months, oil sands drilling is typically conducted during the winter months when the ground is frozen and drilling rigs can access new terrain via ice roads.

1.2.2 Geology of the Athabasca Oil Sands Region

The AOSR is situated on the northeastern fringe of the Alberta foreland basin (Fig. 1.2). Stratigraphic beds dip gently toward the southwest where major tectonic uplift occurred during the Laramide orogeny (Flach, 1984). The Precambrian basement of the North American craton is overlain by thick carbonate and evaporite formations deposited during the Devonian period (Figs. 1.2 & 1.3). Of particular note is the Prairie Evaporite Formation that consists largely of

halite and anhydrite that has been partially removed through dissolution on its easternmost edge (Grobe, 2000). A 250 Myr unconformity separates the Devonian strata from overlying rocks. The paleo-topography of the Devonian surface displays substantial evidence of mature karst and a network of paleo-valleys throughout the Athabasca region (Flach, 1984; Schneider et al., 2012). Deposited above the regional unconformity is the Cretaceous-aged McMurray Formation that hosts most of the oil sands resources in the AOSR. The McMurray Formation has a complex depositional history consisting of lower, middle and upper units (Ranger and Gingras, 2003; Fustic et al., 2012). The lower unit of the McMurray Formation typically consists of coarse-grained sandstone and conglomerate (Ranger and Gingras, 2003). The middle unit that bears the majority of the bitumen resources consists of massive sands with inclined heterolithic stratification, including interbedded shale layers (Ranger and Gingras, 2003). The upper McMurray Formation consists of a horizontally bedded, fine-grained sandstone (Ranger and Gingras, 2003). Above the McMurray Formation, the Cretaceous–aged Mannville group provides a stratigraphic seal for oil migration and acts as a regional aquitard in modern time (Creaney et al., 1994). Quaternary deposits from the most recent continental-scale glaciations rest unconformably above the Mannville group, and provide much of the modern surface topography observed in the AOSR (Andriashek and Atkinson, 2007).

1.3 Hydrogeology of the Athabasca Oil Sands Region

The broad regional hydrostratigraphy of the AOSR has been previously been described by (Hackbarth and Nastasa, 1979; Hitchon, 1990; Bachu and Underschultz, 1993; Bachu, 1995; Anfort et al., 2001; Barson et al., 2001; Adams et al., 2004), however much detail remains to be uncovered. Figure 1.3 illustrates the regional hydrostratigraphic framework determined by Bachu and Underschultz (1993). The major regional aquifer systems can be approximately divided into

Middle Devonian, Upper Devonian, Cretaceous, and Quaternary hydrogeological systems. These systems are described below.

1.3.1 Middle Devonian aquifer system

The Middle Devonian aquifer system consists of the Contact Rapids and Keg River (Winnipegosis) formations. This aquifer system has formation waters with very high TDS values ranging from 350 000 mg/L west of the Prairie evaporite dissolution edge to 100 000 mg/L east of the dissolution edge (Bachu and Underschultz, 1993). This aquifer system is often a candidate for wastewater disposal throughout the AOSR (Rogers, 2012).

1.3.2 Upper Devonian aquifer system

The aquifer system in the Upper Devonian consists of the Waterways (Beaverhill Lake), Cooking Lake, Grosmont, and Winterburn-Wabamun formations. The Waterways-Cooking Lake aquifer system is the only spatially extensive unit in the AOSR, as the Grosmont and Winterburn-Wabamum formations are only present in the far southwest of the AOSR (Bachu and Underschultz, 1993). Published TDS values for the Waterways-Cooking Lake aquifer system range from 140 000 mg/L to 20 000 mg/L (Bachu and Underschultz, 1993).

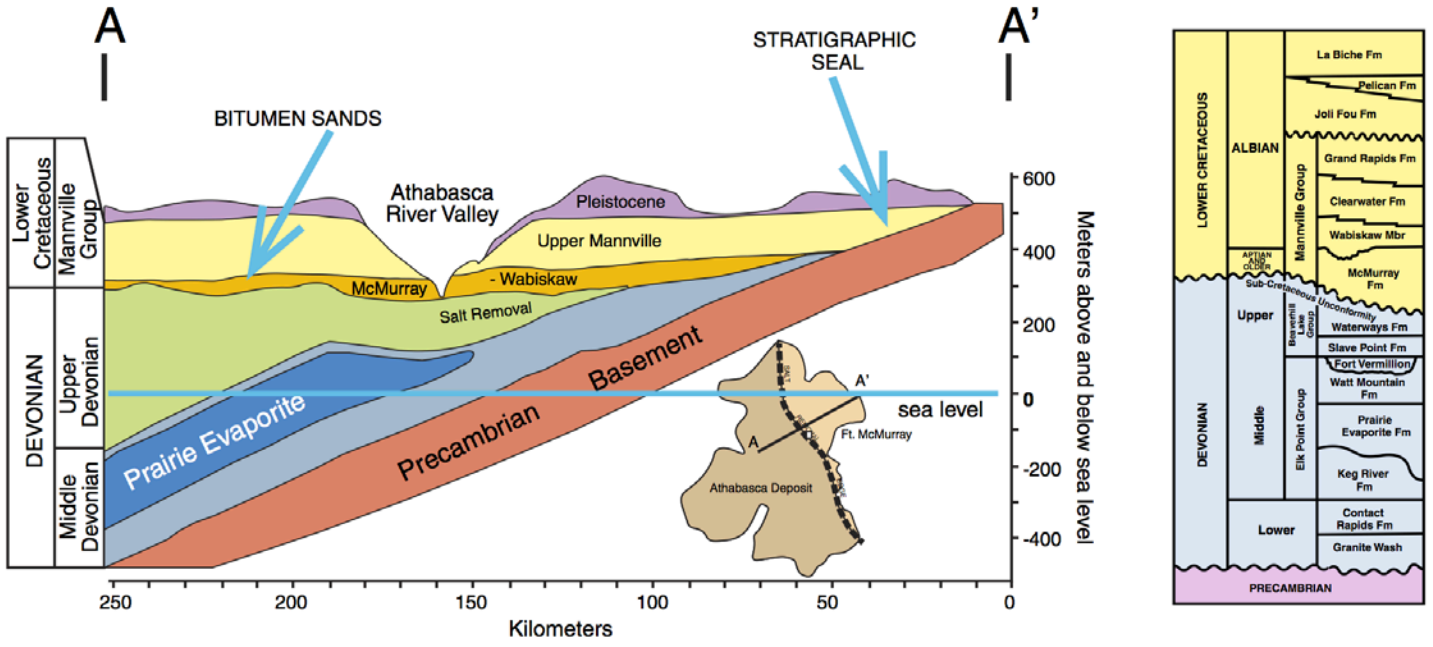

Figure 1.2: Geological cross section and stratigraphy of the Athabasca Oil Sands Region (adapted from Broughton, 2013).

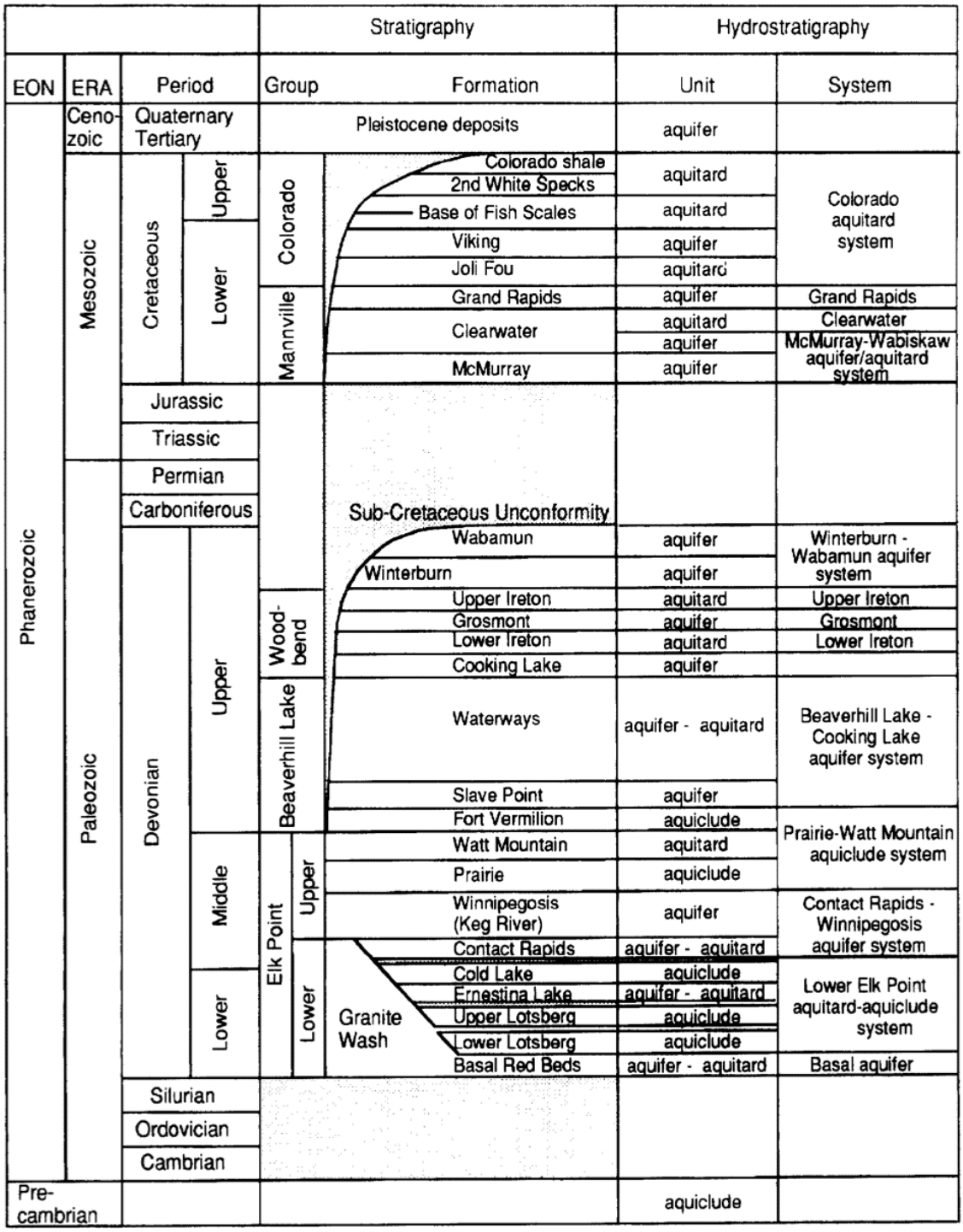

Figure 1.3: Hydrostratigraphy of the Athabasca Oil Sands Region (from: Bachu and Underschultz, 1993).

1.3.3 Cretaceous aquifer system

The Cretaceous aquifer system in the AOSR consists of the McMurray, Clearwater, Grand Rapids, and Viking formations. The Viking and Grand Rapids formations are generally considered to be aquifers, whereas the Clearwater system varies in hydrogeological properties on a local scale in the AOSR from strong aquitard to aquifer (Bachu and Underschultz, 1993). The McMurray and Clearwater formations are regionally extensive throughout the AOSR, whereas the Grand Rapids and Viking formations are absent in parts of the AOSR (Bachu and Underschultz, 1993).

A wide range of TDS values have been previously reported for water from the McMurray Formation, ranging from 300 to 25 000 mg/L (Hackbarth and Nastasa, 1979; Hitchon, 1990; Bachu and Underschultz, 1993). The cause of the variability was explained in several different ways, including depth, temperature, and proximity to evaporite deposits, such the Elk Point aquitard, which can induce salinity of up to 350 g/L in adjacent Devonain aquifer systems (Hackbarth and Nastasa, 1979; Hitchon, 1990; Bachu and Underschultz, 1993). Flow paths in McMurray Formation groundwater are also poorly constrained, however local flow systems for all formations above the sub-Cretaceous unconformity in the AOSR were proposed by Bachu and Underschultz (1993).

1.3.4 Quaternary aquifer systems

The Quaternary aquifer system consists primarily of regionally discontinuous unconsolidated glacial sediments that can reach up to 200 m depth in locations where valleys were carved into bedrock during the last glacial maximum (Bachu and Underschultz, 1993; Andriashek and Atkinson, 2007). These bedrock valleys have locally removed all rock units above the McMurray Formation, thereby creating a direct hydrogeological connection between

the Quaternary aquifer system and the bitumen-saturated McMurray Formation (Andriashek and Atkinson, 2007).

1.3.5 Connectivity between aquifer systems

Understanding cross-formational flow and communication between aquifers is especially important for determining reservoir properties for hydrocarbon extraction, and ensuring elevated pressures generated during steam extraction do not contaminate freshwater aquifers. Recent leaks of bitumen to surface waters that have occurred at the Total-Joslyn Creek facility (Energy Resources Conservation Board, 2010), and the Canadian Natural Resources, Primrose facility (Alberta Energy Regulator, 2013; http://www.aer.ca/about-aer/media-centre/news-releases/3632), demonstrate that connectivity between the shallow bitumen resources and surface waters is indeed possible with anthropogenic stimulation. Hydraulic head measurements indicated that there is some communication through regional aquitards due to heterogeneity, and it cannot be assumed that regional aquitards will effectively separate local hydrogeological processes in northeast Alberta (Bachu and Underschultz, 1993). Local recharge of groundwater is expected in areas of high elevation. Muskeg Mountain and Stony Mountain are indicated as areas of groundwater recharge (WorleyParsons, 2010). In the AOSR, flow between the Cretaceous and Upper Devonian aquifer systems was suggested as a likely possibility by Bachu and Underschultz (1993), as no regional Devonian aquitard exists in this area.

1.4 Composition of oil sands

The oil sands deposits in the McMurray Formation consist of three main components: loosely consolidated minerals, water, and heavily biodegraded oil (bitumen). The mineral phase is dominated by quartz sands and interlaminated shales that have been altered through biodegradation of the oil (Fay, 2011). Secondary carbonate minerals that are highly enriched in

^{13}C indicating methanogenic influence are abundant in oil sands reservoirs (Dimitrakopoulos and Muehlenbachs, 1987). Bitumen and water saturation in the McMurray Formation is variable within a reservoir. Bitumen saturation is usually highest at the top of the reservoir, and decreases through a transition zone to the bottom of the reservoir that typically has water-saturated pores, and is the location of most microbial activity (Bennett et al., 2013). When bitumen fills the pore space entirely, there remains a component of interstitial water within the reservoir surrounding mineral grains in a thin film. It is hypothesized that bitumen retards, but does not prevent groundwater flow at reservoir temperatures and that the bitumen-saturated reservoirs are not significant hydrological barriers over geologic time (Bachu and Underschultz 1993).

Compared to conventional oil, bitumen has low API^{o} gravity, a low hydrogen to carbon ratio, a high boiling point, high sulfur content, and high concentrations of heavy metals, including notably high concentrations of Ni and Va (Table 1.1). In order to be used in refineries, raw bitumen must be upgraded to a synthetic crude oil (SCO) by reducing viscosity, average molecular weight, sulfur and metal content through a variety of energy and water intensive catalyst-driven reactions (Yui, 2008). The upgrading process consumes up to 4 million cubic metres per year (Government of Alberta, 2013).

Table 1.1: Physical and chemical properties of Athabasca bitumen compared to West Texas Intermediate (WTI) petroleum (Rhodes, 1994; Yui, 2008).

Petroleum Properties	Athabasca Bitumen	West Texas Intermediate
API gravity	8º	41º
Density (kg/m^3)	1.01	0.82
H/C Ratio	1.5	2
Viscosity @15ºC (mPa/s)	100 000	5
Saturates %	14	66
Aromatics %	35	26
Resins %	38	6
Asphaltenes %	13	1
Sulfur %	5	0.34
Nitrogen %	0.4	0
Heavy metals (Ni and Va) ppm	100	25

Chemically, bitumen is a complex mixture of high molecular weight hydrocarbons with a poorly-defined structure. There is limited knowledge available about the specific chemical structures in a bitumen mixture (Alex et al., 1994; Peng et al., 1997; Zhao et al., 2000), and it is not yet routine to analyze the distribution of compounds in bitumen and heavy oils. However, the recent application of Fourier-Transform Ion Cyclotron Resonance Mass Spectrometry (FTICR-MS, Petroleomics) has begun to characterize the hundreds of thousands of different compounds in a bitumen or heavy oil, and will likely reveal important insights into the composition and properties of heavily biodegraded oils (Marshall and Rodgers, 2008).

1.5 Biodegradation of petroleum over geologic time

The majority of the world's remaining large petroleum reserves have been exposed to biodegradation over geologic time (Head et al., 2003). Bitumen and heavy oils in the AOSR are formed via anaerobic biodegradation of lighter crude oils, when reservoir physiochemical

conditions are moderate enough to sustain microbial life (Wilhelms et al., 2001; Jones et al., 2007; Huang et al., 2008; Larter et al., 2008; Bennett et al., 2013). The interface between petroleum and water, the oil-water-transition-zone (OWTZ), is the optimal location for microbial growth where the carbon source, nutrients, and water intersect to permit microbial life when temperatures are suitable for microbial growth (< 80ºC) (Roling et al., 2003; Oldenburg et al., 2006; Bennett et al., 2013). Further controls include the presence or absence of sulfate in the reservoir for bacterial sulfate reduction, the surface area of oil-water transition zones, and the depth of the reservoir. Viable prokaryotic microbial communities have been discovered in petroleum reservoirs, and the thermophilic microbes within this environment were found to have diverse metabolic capabilities for carbon, hydrogen and sulfur metabolism (Orphan et al., 2003; Orphan et al., 2000). There have been several studies that have described microbial diversity in modern oil sands systems via molecular methods (Hubert et al., 2012, Sherry et al., 2013; Aitken et al., 2013; Bennett et al., 2013), however this field is in its infancy and much remains to be learned about the specific metabolic processes and pathways by which biodegradation occurs.

The oil in the AOSR has undergone significant biodegadation, with APIº gravity in these regions ranging from 7 to 12º (Larter et al., 2012). Removal of 10% of the hydrocarbons from a reservoir is estimated to take between 1-2 Myr for light oil reservoirs and 5-10 Myr for heavy oil reservoirs (Larter et al., 2006). The most recently proposed mechanism for oil sands biodegradation is the Methanogenic Alkane Degradation dominated by CO_2 Reduction (MADCOR) that proposes a net reaction pathway for an n_{16} alkane that includes biochemical pathways for syntrophic alkane oxidation, syntrophic acetate oxidation, acetoclastic methanogenesis and hydrogenotrophic methanogenesis. The net reaction described by MADCOR is described in Equation 1.

$$4C_{16}H_{34} + 30H_2O \rightarrow 15CO_2 + 49CH_4 \quad [1]$$

Biodegradation can be monitored by a distinct pattern of alkane removal, increases in viscosity, and changes in oil density (Jones et al., 2007, Larter et al., 2003; Larter et al., 2008). Mixing and multiple petroleum charges throughout the history of the basin complicates the signature of biodegradation and elucidating the extent of active degradation can be challenging (Bennett and Larter, 2008).

The extent to which aqueous geochemistry influences microbial processes have thus far been relatively unexplored. As oil migrates from high temperature, high salinity environments to reservoirs with lower temperatures and lower salinities, increasing amounts of biodegradation are possible. However, high salinity and thermodynamic constraints should limit the amount of degradation in deep formation waters in which the temperature is less than 80ºC (Dolfing et al., 2008). Presently the formation water in most oil sands reservoirs have lower formation water TDS concentrations than the proposed geochemical limit for acetoclastic methanogenesis (Chapter Two; Waldron et al., 2008), suggesting modern biodegradation is not limited by salinity.

1.6 Oil sands extraction and water resources

Groundwater resources, both saline and non-saline, are increasingly being exploited in northeastern Alberta for the development of fossil energy reserves. In the coming half-century, demands for groundwater resources will increase, as development in the oil sands region expands (Council of Canadian Academies, 2009). Both mining and SAGD processes consume large quantities of water and fuel to produce and upgrade bitumen to a refinery-quality product, therefore the growth of the oil sands is dependent largely on the availability of water (Chow et al., 2008). Currently total water use is dominated by surface mining, and a net volume of 171.9

million cubic metres of water is withdrawn annually from the Athabasca River (Government of Alberta, 2013). In 2012, in-situ operations consumed an annual net water volume of 30.3 million cubic metres, primarily comprised of groundwater (Government of Alberta, 2013). Bitumen-upgrading facilities consumed a net volume of 4.6 million cubic metres of water during 2012 (Government of Alberta, 2013). The volume of water required to produce one barrel of synthetic crude oil varies depending on the method of extraction. Oil sands mining required an average net water consumption of 2.3 barrels of non-saline water for every barrel of synthetic crude oil produced in 2012 (Government of Alberta, 2013). On average, in-situ extraction techniques consumed 1.7 barrels of non-saline, and 0.4 barrels of saline water to produce one barrel of synthetic crude oil in 2012 (Government of Alberta, 2013). The cumulative impacts of oil sands development on groundwater have not been sufficiently studied (Council of Canadian Academies, 2009) and further investigation is warranted on a regional scale to assess the impacts of multiple operators co-existing in the same region.

1.7 Objective of the thesis

This objective of this thesis was to investigate critical aspects of hydrogeology and biogeochemistry of the McMurray Formation within the Athabasca Oil Sands Region, and oil sands analogues, using aqueous and isotope geochemistry as an essential tool in each study. Novel insight about the recent geological history, modern hydrogeological processes, and reservoir biogeochemical processes were obtained from the five individual studies presented in this thesis.

1.7.1 Chapter Two – Distribution of Total Dissolved Solids in McMurray Formation Water in the Athabasca Oil Sands Region

Total dissolved solids data for McMurray Formation waters in the AOSR were collected and mapped to understand the heterogeneity that can be expected across the region. TDS concentrations ranged from freshwater (minimum observed TDS = 200 mg/L) to brine (maximum observed TDS = 270 000 mg/L), suggesting that distinct local-scale influences are responsible for variability in McMurray Formation water salinity. The regions of highest salinity are consistent with a linear trend of upward vertical flow between the waters of the McMurray and underlying Devonian formations overlying the partial dissolution edge of the Prairie Evaporite Formation. This zone of high vertical connectivity has been explained elsewhere as evaporite karst dissolution potentially associated with a sub-Cretaceous faulting and/or sinkhole structures (Broughton, 2013). Sinkholes are widespread throughout the region on timescales ranging from pre-Cretaceous to modern, suggesting continued hydraulic connectivity through recent time (Broughton, 2013). The driving force for upward movement of groundwater is provided by Pleistocene glacial meltwater that reversed the direction of groundwater flow over the past 2 Ma (Grasby and Chen, 2005). Taken together, the observations of high TDS values and extensive heterogeneity in the salinity of McMurray Formation waters across the AOSR associated with the evaporite dissolution edge, the occurrence of karst hydrogeology, and a plausible driving force has resulted in a modified interpretation of the hydrogeological framework of the Athabasca Oil Sands Region.

1.7.2 Chapter Three – Determination of Total Dissolved Solids and the Stable Isotope Composition of Oil Sands Porewater: A New Tool for Reservoir Fluid Characterization

In this chapter, a new method is described for calculating the total dissolved solids concentration and stable isotope composition of McMurray oil sands reservoir waters. The water

samples required to calculate these parameters were extracted directly from drill core, and the drilling fluids contamination was removed using two end-member mixing calculations. Three case studies are presented that demonstrate the large variability in TDS that is observed in McMurray Formation waters in the AOSR. The development of a tool to directly measure TDS in the reservoir porewater is especially important for accurately calculating the bitumen and water saturation of individual reservoirs, for designing industrial facilities to manage fluids of variable salinity, and for understanding the hydrogeological complexity within an individual oil sands lease area.

1.7.3 Chapter Four – Stable Isotope Geochemistry and Total Dissolved Solids Measurement of Formation Water at the Suncor-Firebag Oil Sands Field from Bitumen Core-Extracted Porewater

The stable isotope composition and total dissolved solids concentration of reservoir porewaters from the Suncor-Firebag lease area were measured to determine the heterogeneity of formation waters in the lease area. Twelve wells from across the Firebag lease were sampled as a proof-of-concept for the technique developed in Chapter Three. The study provided information about the stable isotope composition and heterogeneity in TDS of formation waters within the Firebag lease, and suggested that groundwater in the McMurray Formation at Firebag is largely derived from Holocene recharge, consistent with existing interpretations and regional trends in formation water TDS concentrations. Additional examination of the data set revealed vertical heterogeneity within individual reservoirs, suggesting possible differences in water composition due to geological heterogeneity within and above reservoirs.

1.7.4 Chapter Five – The Influence of Salinity on Methanogenesis in Alberta Oil Sands Microcosms

In this chapter, the influence of aqueous geochemistry on methanogenesis from oil sands substrate was studied in a one-year laboratory experiment. Hydrocarbon-degrading microbial consortia were grown on an oil sands substrate in media containing variable aqueous geochemistry that ranged in TDS concentration from 2 000 to 22 000 mg/L. Differences in the amount of methane generated, and the stable isotope ratios of carbon, hydrogen and sulfur were used to infer the influence of aqueous geochemistry on microbial processes responsible for methane generation.

1.7.5 Chapter Six – Radiocarbon Dating of Biogenic Methane in Powder River Basin Coal Seams

Coalbed methane (CBM) resources in the Powder River Basin, Wyoming, United States, are analogous to oil sands resources in that they are shallow fossil fuel deposits, with near-surface hydrogeological systems and active microbial communities. In the Powder River Basin (PRB), samples of dissolved inorganic carbon in formation waters and methane in produced gases were analyzed for radiocarbon content (^{14}C) to trace microbial carbon cycling and methanogenesis in the PRB. However, despite evidence for recent hydrogeological recharge to the coal seams, all samples measured in this study contained no detectable radiocarbon, thus there has been very little transport of modern carbon from Earth's surface into the CBM reservoir relative to the amount of coal-derived carbon metabolized in the reservoir.

1.8 Summary

This thesis used applications of stable isotope geochemistry to provide novel insight into the hydrogeology and biogeochemistry of the oil sands reservoirs in Alberta. The techniques developed in this thesis, and the information gained from the applications and interpretations

presented here are widely applicable to the rapidly expanding oil sands resource extraction industry in Alberta, and to those involved in regulation of environmental impacts from these industries. Improved understanding of hydrogeological processes, better reservoir characterization, and an improved fundamental understanding of reservoir biogeochemistry will lead to better decision making during the development of these resources, while our society transitions away from fossil energy over the next half-century.

1.9 References

Alberta Energy Regulator (2013). Alberta Energy Regulator orders enhanced monitoring and further steaming restrictions at Primrose and Wolf Lake projects due to bitumen emulsion releases. Press release: July 18, 2013. Available online: http://www.aer.ca/documents/news-releases/AERNR2013-32.pdf

Andriashek, L. D., & Atkinson, N. (2007). Buried Channels and Glacial-Drift Aquifers in the Fort McMurray Region, Northeast Alberta. *Energy and Utilities Board /Alberta Geological Survey Earth Sciences Report* 2007-01 170 pp.

Adams, J.J., Rostron, B.J., Mendoza, C.A. (2004). Coupled fluid flow, heat and mass transport, and erosion in the Alberta basin: implications for the origin of the Athabasca oil sands. *Canadian Journal of Earth Sciences* 41: 1077–1095.

Bachu, S. and Underschultz J.R. (1993). Hydrogeology of formation waters, northeastern Alberta. *AAPG Bulletin, 77*(10), 1745–1768.

Barson, D., Bachu, S., Esslinger, P. (2001). Flow systems in the Mannville Group in the east-central Athabasca area and implications for steam-assisted gravity drainage (SAGD) operations for in situ bitumen production. *Bulletin of Canadian Petroleum Geology* 49(3): 376–392

Bennett, B., & Larter, S. R. (2008). Biodegradation scales: Applications and limitations. *Organic Geochemistry*, *39*(8), 1222–1228.

Bennett, B., Adams, J.J., Gray, N.D., Sherry, A., Oldenburg, T.B.P., Huang, H., Larter, S.R. and Head, I.M. (2013) The controls on the composition of biodegraded oils in the deep subsurface – Part 3. The Impact of microorganism distribution on petroleum

geochemical gradients in biodegraded petroleum reservoirs. *Organic Geochemistry*, 56(3), 94-105.

Broughton, P. L. (2013). Devonian salt dissolution-collapse breccias flooring the Cretaceous Athabasca oil sands deposit and development of lower McMurray Formation sinkholes, northern Alberta Basin, Western Canada. *Sedimentary Geology*, *283*(C), 57–82.

Chow, D., Nasr, T., Chow, R., & Sawatzky, R. (2008). Recovery techniques for Canada's heavy oil and bitumen resources. *Journal Of Canadian Petroleum Technology*, *47*(5), 12–17.

Cooper, D. (2001). Oilsands leak turned mine to pond: Shell finds innovative fix for a never-before-seen problem. *Edmonton Journal*. October 15, 2011

Council of Canadian Academies (2009). *The Sustainable Management of Groundwater in Canada*. Available online: http://www.scienceadvice.ca/en/assessments/completed/groundwater.aspx

Dimitrakopoulous, R., & Muehlenbachs, K. (1987). Biodegradation of petroleum as a source of 13C-enriched carbon dioxide in the formation of carbonate cement. *Chemical Geology*, *65*, 283–291.

Dolfing, J., Larter, S. R., & Head, I. M. (2008). Thermodynamic constraints on methanogenic crude oil biodegradation. *ISME Journal*, 2(4), 442–452.

Energy Resources Conservation Board (2010). *ERCB Staff Review and Analysis: Total E&P Canada Ltd., Surface Steam Release of May 18, 2006.* Available online: http://www.ceaa.gc.ca/050/documents/45468/45468E.pdf

Fay, M. (2010). *The Impact of Petroleum Biodegradation on Oil, Gas, Water and Mineral Geochemistry*. Ph.D. Dissertation. University of Calgary, Gallagher Library 1–424.

Fustic, M., Bennett, B., Hubbard, S. M., Huang, H., Oldenburg, T., & Larter, S. (2012). Impact of Reservoir Heterogeneity and Geohistory on the Variability of Bitumen Properties in the Athabasca Oil Sands, Canada. *AAPG Studies in Geology*, *64*, 1–42.

Griffiths, M., Taylor, A., & Woynillowicz, D. (2006). Troubled Waters, Troubling Trends. *Pembina Institute*, 1–171.

Government of Alberta (2013). *Oil Sands Information Portal*. Retrieved July 21, 2013. http://www.osip.alberta.ca

Grasby, S., & Chen, Z. (2005). Subglacial recharge into the Western Canada Sedimentary Basin - Impact of pleistocene glaciation on basin hydrodynamics. *Geological Society of America Bulletin*, *117*(3-4), 500–514.

Joslyn Creek SAGD Thermal Operation Flach, P. (1984). Oil Sands Geology - Athabasca Deposit North. *Alberta Research Council Bulletin 046*, 1–47.

Hackbarth, D. A., & Nastasa, N. (1979). Groundwater Observation Well Network: Athabasca Oil Sands Area. *Alberta Research Council, Information Series 69*, 1–1272.

Head, I., Jones, D., & Larter, S. (2003). Biological activity in the deep subsurface and the origin of heavy oil. *Nature*, *426*(6964), 344–352.

Hitchon, B. (1991). *Hydrochemistry of Phanerozoic Strata, Northeast Alberta*. Alberta Research Council Open File Report 1991-20, 1–31.

Hrudey, S., Gosselin, P., Naeth, A.M., Plourde, A., Therrien, R., Van Der Kraak, G., Xu, Z., (2012) *Environmental and Health Impacts of Canada's Oil Sands Industry*. Royal Society of Canada Publication 2012-13. Available online: https://rsc-src.ca/en/expert-panels/rsc-reports/environmental-and-health-impacts-canadas-oil-sands-industry

Huang, H. P., Bennett, B., Oldenburg, T., Adams, J., & Larter, S. R. (2008). Geological controls on the origin of heavy oil and oil sands and their impacts on in situ recovery. *Journal Of Canadian Petroleum Technology*, 47(4), 37–45.

Hubert, C., Voordouw, G., & Mayer, B. (2009). Elucidating microbial processes in nitrate- and sulfate-reducing systems using sulfur and oxygen isotope ratios: The example of oil reservoir souring control. *Geochimica et Cosmochimica Acta*, *73*(13), 3864–3879.

Jones, D. M., Head, I. M., Gray, N. D., Adams, J. J., Rowan, A. K., Aitken, C. M., et al. (2007). Crude-oil biodegradation via methanogenesis in subsurface petroleum reservoirs. *Nature*, *451*(7175), 176–180.

International Energy Agency (IEA), (2012). *World Energy Outlook 2012*. Paris, France. 690pp.

Larter, S., Wilhelins, A., Head, I., Koopmans, M., Aplin, A., Di Primio, R., et al. (2003). The controls on the composition of biodegraded oils in the deep subsurface - part 1: biodegradation rates in petroleum reservoirs. *Organic Geochemistry*, *34*(4), 601–613.

Larter, S., Huan, H., Adams, J., Bennett, B., Jokanola, O., Oldenburg, T. (2006). The controls on the composition of biodegraded oils in the deep subsurface: Part II - Geological controls on subsurface biodegradation fluxes and constraints on reservoir-fluid property prediction. *AAPG Bulletin-American Association Of Petroleum Geologists*, 90(6), 921-938.

Larter, S., Huang, H., Adams, J., Bennett, B., & Snowdon, L. R. (2012). A practical biodegradation scale for use in reservoir geochemical studies of biodegraded oils. *Organic Geochemistry*, *45*(C), 66–76.

Langenberg, C.W., Hein, F.J., Lawton, D. and Cunningham, J. (2002). Seismic modeling of fluvial-estuarine deposits in the Athabasca oil sands using ray-tracing techniques,

Steepbank River area, northeastern Alberta. *Bulletin of Canadian Petroleum Geology* 50 178–204

National Climate Data and Information Archive (2013). Fort McMurray Climate Statistics. Available online July 1, 2013: http://climate.weatheroffice.gc.ca/climate_normals/station_metadata_e.html?StnId=2519

Oldenburg, T. B. P., Larter, S. R., & Huang, H. (2006). Nutrient supply during subsurface oil biodegradations - Availability of petroleum nitrogen as a nutrient source for subsurface microbial activity. *Energy and Fuels*, *20*(5), 2079–2082.

Orphan, V., Taylor, L., Hafenbradl, D., & Delong, E. (2000). Culture-dependent and culture-independent characterization of microbial assemblages associated with high-temperature petroleum reservoirs. *Applied And Environmental Microbiology*, *66*(2), 700–711.

Orphan, V., Goffredi, S., Delong, E., & Boles, J. (2003). Geochemical influence on diversity and microbial processes in high temperature oil reservoirs. *Geomicrobiology Journal*, *20*(4), 295–311.

Ranger, M.J., and Gingras, M.K. (2003). Discussion of C.W. Langenberg, F.J. Hein, D. Lawton and J. Cunningham Seismic modeling of fluvial-estuarine deposits in the Athabasca oil sands using ray-tracing techniques, Steepbank River area, northeastern Alberta. *Bulletin of Canadian Petroleum Geology* 51(3) 347–353.

Roling, W., Head, I., & Larter, S. (2003). The microbiology of hydrocarbon degradation in subsurface petroleum reservoirs: perspectives and prospects. *Research in Microbiology*, *154*, 321–328.

Schneider, C.L., Mei, S., Grobe, M., Haug, K. (2012). Beneath the Oil Sands: Stratigraphy and Structural Features of the Devonian of Northeast Alberta. *Geoconvention: 2012*, Calgary, Alberta.

Sherry, A., Gray, N. D., Ditchfield, A. K., Aitken, C. M., Jones, D. M., Röling, W. F. M., et al. (2013). Anaerobic biodegradation of crude oil under sulphate-reducing conditions leads to only modest enrichment of recognized sulphate-reducing taxa. *International Biodeterioration and Biodegradation*, *81*(C), 105–113.

Smil, V., (2010). Energy Transitions: History, Requirements, Prospects. Praeger Publishing.

Waldron, P. J., Petsch, S. T., Martini, A. M., & Nuesslein, K. (2007). Salinity constraints on subsurface archaeal diversity and methanogenesis in sedimentary rock rich in organic matter. *Applied and Environmental Microbiology*, *73*(13), 4171–4179.

Wilhelms, A., Larter, S., Head, I., Farrimond, P., di-Primio, R., & Zwach, C. (2001). Biodegradation of oil in uplifted basins prevented by deep-burial sterilization. *Nature*, *411*(6841), 1034–1037.

WorleyParsons. (2010). Regional Groundwater Quality Study and Monitoring Network Design in the Athabasca Oil Sands: Phase 2: Program Summary. *Regional Municipality of Wood Buffalo: Cumulative Environmental Management Association* Fort McMurray, Alberta, Canada.

Chapter Two: Distribution of Total Dissolved Solids in McMurray Formation Water in the Athabasca Oil Sands Region, Alberta, Canada

2.1 Abstract

Understanding the heterogeneity of the McMurray Formation water salinity is important for hydrogeological interpretation, reservoir characterization, monitoring steam chamber development, and building appropriate facilities to treat saline water extracted from the McMurray aquifer for industrial use. This study mapped total dissolved solids (TDS) of 355 McMurray Formation water samples in the Athabasca oil sands region (54 to 58º N and 110 to 114º W) using published data from recent government reports and Environmental Impact Assessments. McMurray Formation waters varied from non-saline (TDS < 4 000 mg/L) to brine (TDS > 100 000 mg/L) with a regional trend of high salinity water approximately following the dissolution edge of the Prairie Evaporite Formation. The simplest hydrogeological explanation for the observed formation water salinity data is that Devonian aquifers are locally connected to the McMurray Formation via conduits in the sub-Cretaceous karst system in the region overlying the partial dissolution edge of the Prairie Evaporite Formation. The driving force for upward formation water flow was provided by the Pleistocene glaciation events that reversed the regional Devonian flow system over the past 2 Ma in the Athabasca region. This study demonstrates that a detailed approach to hydrogeological assessment is required to elucidate TDS concentrations in McMurray Formation waters at an individual lease-area scale.

2.2 Introduction

The Athabasca oil sands region (AOSR) in northeastern Alberta is a region of significant economic activity and equally significant environmental concern. Rapid development of bitumen resources via surface mining or in-situ extraction by steam-assisted gravity drainage (SAGD)

requires water-intensive extraction and separation processes that will strain Northern Alberta's water supply over the coming decades (Griffiths et al., 2006). The major mining projects in the Athabasca region are sufficiently close to the Athabasca River to draw from its vast surface water resources; however the majority of in-situ extraction facilities must draw upon groundwater resources for industrial use (Hayes, 2013). The McMurray Formation is the primary petroleum-bearing unit in the Athabasca region, however it is also a significant aquifer where it is not saturated with bitumen, and frequently provides water sources for in-situ resource development projects (Hayes, 2013, Wills, 2013).

A detailed hydrostratigraphic description of the Athabasca region was provided by Bachu and Underschultz (1993), and their regional hydrostratigraphic model was reproduced and discussed in Chapter One (Fig. 1.3). The Cretaceous-aged McMurray Formation that bears the majority of the oil sands deposits in the Athabasca region has a complex depositional history with fluvial and estuarine components, and overlies a major unconformity that spans from the upper Devonian to the lower Cretaceous (Fustic et al., 2012). Underlying the sub-Cretaceous unconformity are thick Devonian carbonate and evaporite sequences (Fig. 1.2). Formation waters in Devonian strata in the AOSR are typically more saline than seawater (seawater TDS ≈ 35 000 mg/L), owing to the dissolution of halite and anhydrite evaporite units (Hackbarth and Nastasa, 1979; Bachu and Underschultz 1993; Grasby and Chen, 2005; Gue 2012). Overlying the McMurray Formation is the Cretaceous Clearwater Formation, considered to be a regional aquitard (Fig. 1.3). A second unconformity exists from the upper Cretaceous through to the Pleistocene (Fig. 1.3). The Pleistocene glacial events resulted in the incision of deep valleys that sporadically cross-cut the McMurray Formation and subsequently these channels were infilled with Quaternary aged sediments after downcutting (Andriashek and Atkinson, 2007). These

channels often have aquifer properties and may permit connectivity between shallow groundwater and deeper formation waters where downcutting has occurred. These features provide ample geological complexity to create complicated hydrogeological conditions in the McMurray Formation.

Frequently cited regional flow models have provided somewhat differing interpretations of the sub-Cretaceous hydrogeology. Several models suggest very long flowpaths with formation waters originating far to the south in Montana or far to the West in the Rocky Mountains (Bachu, 1995; Anfort et al., 2001; Barson et al. 2001; Michael et al., 2003). However, mixing between fluids in Devonian and Cretaceous aquifers has been suggested to occur across the sub-Cretaceous unconformity in the AOSR, where the McMurray Formation overlies the Devonian aquifers (Bachu and Underschultz, 1993). However, the location and extent of flow across the sub-Cretaceous interface in the oil sands region remains unconstrained.

Springs in Devonian strata are common along the banks of the Clearwater and Athabasca rivers, indicating that these river valleys are areas of discharge. These waters are typically brackish to saline, with stable isotope compositions that are not indicative of deep basin flow (Grasby and Chen, 2005; Gue, 2012). Very few groundwater samples have ever been obtained from below the sub-Cretaceous unconformity in the AOSR, and the hydrogeological nature of the unconformity has not been studied in great detail in this region. Samples that have been obtained from Devonian strata (Hackbarth and Nastasa, 1979) indicate that formation water TDS in Paleozoic formations underlying the McMurray Formation is greater than that of seawater, with elevated concentrations of Ca and SO_4, suggesting anhydrite dissolution as a possible source of dissolved SO_4.

McMurray Formation water is poorly suited for most domestic water use in the AOSR due to its proximity to bitumen and resulting naturally elevated concentrations of dissolved hydrocarbons (Lemay, 2002a; Hayes, 2013). However, due to its high permeability and relatively shallow depth, the McMurray Formation is an ideal aquifer for industrial water supply. Therefore these water systems have economic value despite their relatively poor water quality (George, 2013). Detailed characterization of aquifer geochemical properties may be beneficial to identify the highest-quality water for industrial processes (Robertson, 2013). Previous regional studies suggest that local processes control McMurray hydrogeology, and that the direction of flow is primarily in the downward direction driven by local meteoric recharge and surface topography (Bachu and Underschultz, 1993; Barson et al., 2001). However, there are many indications suggesting that upward vertical flow, originating from the sub-Cretaceous strata, is an additional important regional-scale hydrogeological process that may impact water quality in some areas of the McMurray Formation in the AOSR. These lines of evidence include drillstem pressure tests that indicated Devonian hydraulic head values exceeding those measured in the McMurray Formation (Nexen Inc and OPTI Canada, 2007), McMurray Formation waters with salinity values greater than seawater (Hackbarth and Nastasa, 1979; WorleyParsons, 2010) and a reported eruption of an H_2S-bearing saline fluid from a Muskeg River mine tailings pit that was attributed to connectivity with artesian Devonian aquifers (Cooper, 2011).

Understanding regional variations in McMurray Formation water TDS is also especially important for in-situ bitumen resource development, both for reservoir characterization and for industrial process design. Geophysical tools used to determine bitumen and water saturation in the McMurray Formation are influenced by elevated salinity in formation waters, and changes in salinity across a bitumen play may lead to incorrect estimates of bitumen saturation with

substantial economic implications. Additionally, the steam-generation process for bitumen recovery requires removal of dissolved solids from the industrial water source, and elevated salinity in the source water adds substantial costs to this process (Robertson, 2013). Therefore there is significant economic benefit to be gained by understanding salinity variations in formation waters within an oil sands reservoir.

Recent research suggests that active karst processes are occurring in the Athabasca region as a result of the dissolution of soluble evaporite and carbonate rock units below the McMurray Formation (Broughton, 2013). These proposed karst processes have substantial implications for McMurray Formation hydrogeology, as the conduit-style preferential flow paths generated in a karst system can create unpredictable water flow paths in groundwater systems (Ford and Williams, 2007), potentially generating conduits for upward vertical flow into the McMurray Formation. Further complicating the system is the influence of meltwater from the Pleistocene glaciation events that has been identified as a major influence in Devonian aquifer systems by geophysical pressure models, geochemical analysis and stable isotope studies (Grasby and Chen 2005; Gue, 2012). Elevated hydraulic head created by several kilometers of glacial ice has generated overpressured, high salinity fluids in the Devonian aquifers that underlie the McMurray Formation (Grasby and Chen, 2005). These glaciogenic fluids containing ions dissolved from Devonian evaporites discharge at outcrops along the Clearwater and Athabasca rivers (Gue, 2012). The McMurray Formation hydrogeology is further influenced by anthropogenic activities via steam injection and groundwater withdrawal. This complex interplay of geological phenomena and anthropogenic activities have created significant variability in the salinity of the McMurray Formation that requires investigation.

The purpose of this study was to map total dissolved solids in waters of the McMurray Formation across the Athabasca oil sands region. Understanding heterogeneity in McMurray Formation water salinity on a regional scale will help to improve the efficiency of oil sands operations, and lower the risk of negative environmental impacts during resource development.

2.3 Methods

Total dissolved solids data for McMurray Formation waters were obtained from a large body of government and industry-level technical reports including: Environmental Impact Assessments, Cumulative Environmental Management Agency (CEMA) documents, Oil Sands Research and Information Network (OSRIN) reports, Energy Resources Conservation Board (ERCB) in-situ operation reports, and Alberta Geological Survey (AGS) reports (Appendix A).

Details of the data source, location, and TDS value for each formation water sample are available in Appendix A. The majority of these samples were obtained from groundwater well sampling, and measured for major and minor cation analysis in commercial laboratories, resulting in a detailed and high quality data set compared to previous formation water samples derived from drill-stem tests or those that use electrical conductivity to measure TDS. Sample access was biased toward the bitumen-bearing commercial lease areas of the Athabasca region, resulting in an uneven spatial distribution across the AOSR. Data were excluded from the database if they were noted in the report as contaminated by drilling fluids or cement (typically resulting in $K^+ > 1\ 000$ mg/L or pH > 10.0). Some studies reported only TDS (e.g. ERCB in-situ progress reports), and these data were not excluded from the data set. Greater than 85% of the TDS data was generated from analysis of a full suite of major and minor cations with a charge balance of < 10%. Samples without major cations and anions are noted in Appendix A. A wide

spatial distribution of groundwater TDS data was obtained, and 355 total data points were included in this study.

2.4 Results

McMurray Formation water TDS data were analyzed by considering the Athabasca region as a whole, and also by dividing the data spatially into three subregions (Fig. 2.1). These subregions were delineated by the Athabasca and Clearwater rivers that incise deep into the geologic strata, and act as major hydrogeological flow barriers in the region (Bachu and Underschultz, 1993). The West subregion consists of all areas west of the Athabasca River; the Northeast subregion consists of the area east of the Athabasca River and north of the Clearwater River, and the Southeast subregion consists of all areas east of the Athabasca River and south of the Clearwater River.

Data from this study were plotted in three different ways to illustrate the observed heterogeneity in the data set. A map of McMurray Formation water TDS was plotted on a regional surface topography map in Figure 2.1. Figure 2.2 presents the regional and subregional TDS data as a box and whisker diagram. Histograms of the regional and subregional TDS values for formation waters are plotted in Figure 2.3. These data illustrated major differences among the subregions and broad variations in formation water TDS emerged.

2.4.1 Athabasca region

A total of 355 McMurray Formation water TDS values were obtained from literature data within the Athabasca region. The median TDS value for the entire Athabasca regional data set was 6 910 mg/L, and the 25th and 75th percentiles were 1 900 and 13 400 mg/L respectively (Table 2.1; Fig. 2.2). The data set displays a very wide range in TDS values, spanning three orders of magnitude from a minimum TDS of 220 mg/L to a maximum of 279 000 mg/L (Table

2.1). Nineteen formation waters had TDS values greater than seawater (seawater TDS ≈ 35 000 mg/L), and seven formation waters had values more than twice the TDS value of seawater (> 70 000 mg/L).

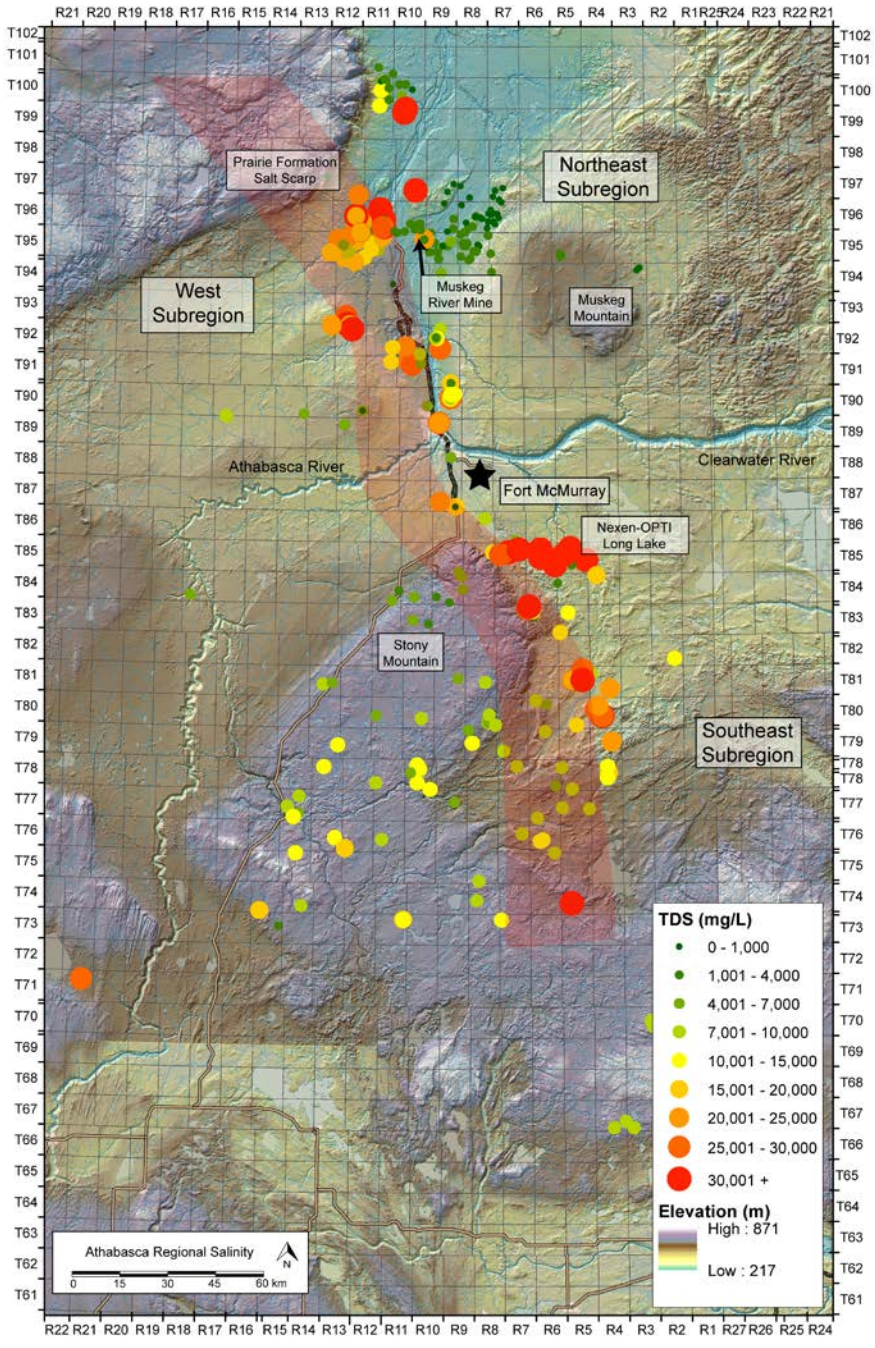

Figure 2.1: McMurray Formation water TDS in the Athabasca oil sands region, overlain on ground surface elevation. Prairie salt scarp (red shading) derived from Broughton (2013). Digital elevation model and base map adapted from Asoian (2012).

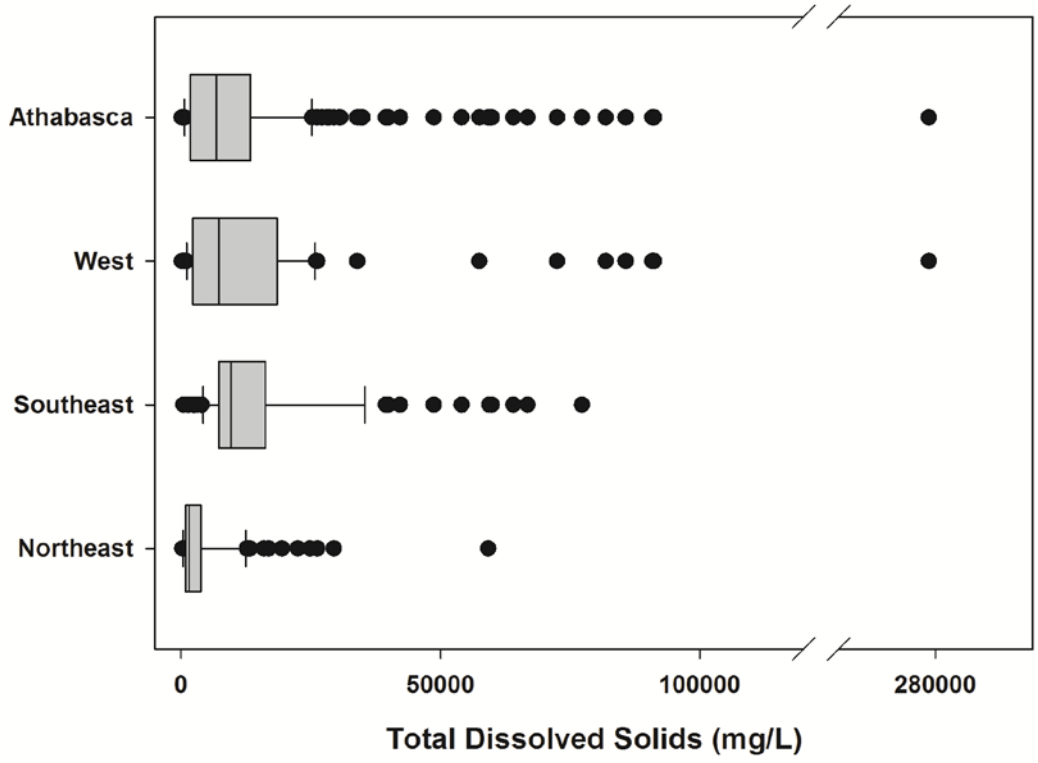

Figure 2.2: Box and whisker plot of McMurray Formation water salinity. The two boxes represent the 2nd and 3rd quartiles, and the extent of the whiskers represent the 10th and 90th percentiles of all data. Dots represent outlying values beyond the 10th and 90th percentile.

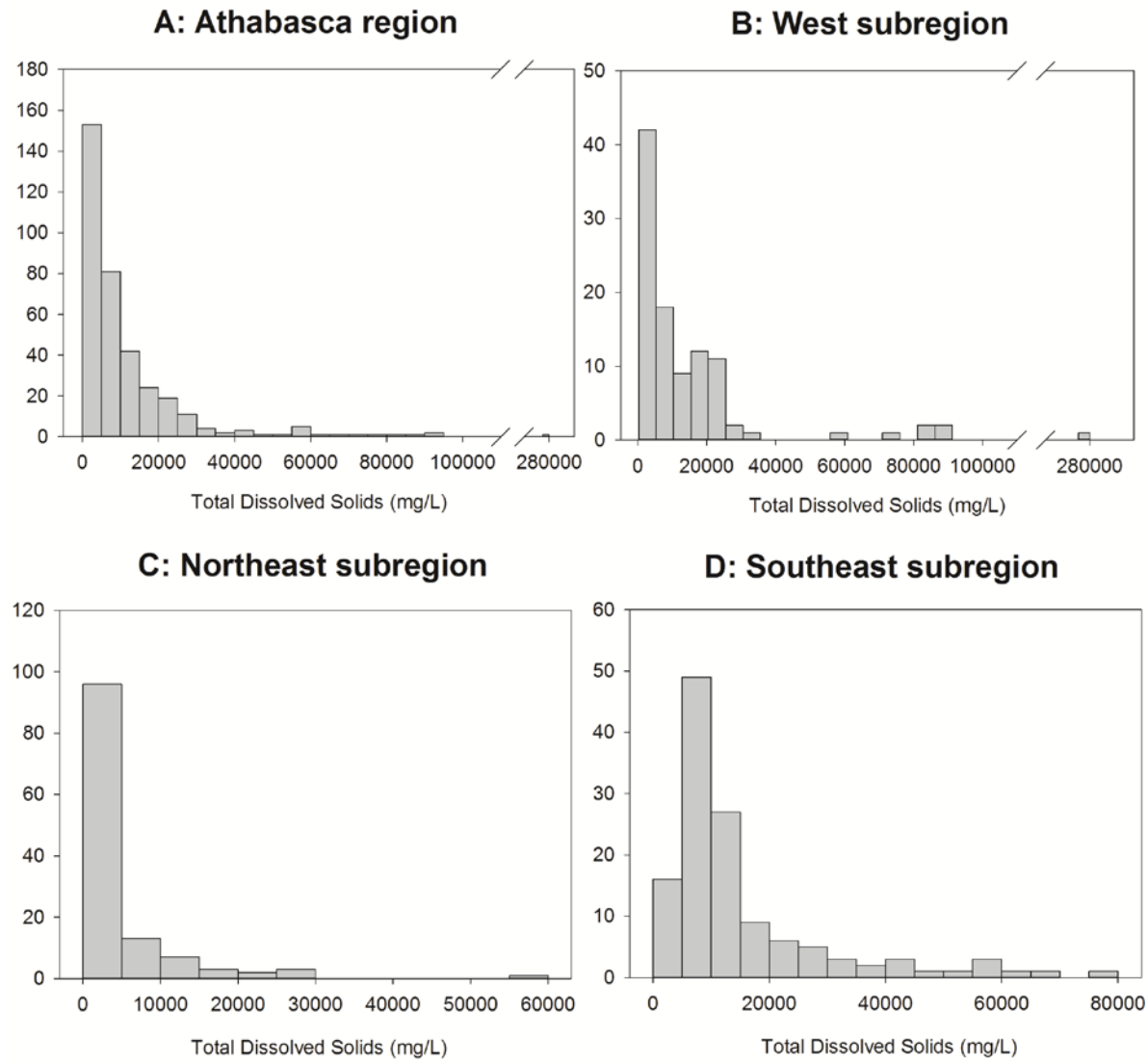

Figure 2.3: Histograms of McMurray Formation water TDS in the Athabasca oil sands region (A) and the three identified subregions, West (B), Northeast (C) and Southeast (D). Bin size is 5 000 mg/L.

Table 2.1: Summary statistics for McMurray Formation water TDS in the Athabasca Oil Sands Region. All values are presented in mg/L.

Region	Median	Minimum	Maximum	25^{th} percentile	75^{th} percentile
Athabasca	6 910	220	279 000	1 900	13 400
West	6 930	220	279 000	2 300	18 200
Northeast	1 570	300	59 200	890	3 870
Southeast	9 600	530	77 300	7 300	16 300

Spatially across the Athabasca region there was a trend of high formation water TDS values above 20 000 mg/L observed from Township 78, Range 4W4 to Township 100, Range 10W4 (Fig. 2.1). This trend approximately overlies the eastern dissolution edge of the Prairie Evaporite Formation, and transcends the regional hydrogeological barriers of the Athabasca and Clearwater rivers, with TDS values above 20 000 mg/L observed in all three subregions (Fig. 2.1). Within ten kilometres of the saline water trend, the highest TDS values in the region are observed. However, the formation water TDS values proximal to the evaporite edge are not exclusively high, suggesting that small-scale local processes, rather than wide-scale regional processes, are responsible for the observed variability.

The histogram of regional TDS values (Fig. 2.3a) shows a strongly skewed distribution toward low TDS values (< 4 000 mg/L), with a long tail of data in the upper range of values (> 20 000 mg/L). While the majority of TDS values plot on the lower end of the distribution, there is a significant group of outliers that require attention due to the challenges posed by high salinity waters in oil sands reservoirs. It should be noted, however, that the shape of the entire Athabasca region formation water TDS histogram (Fig. 2.3a) deviates substantially from those of the subregions (Fig 2.3b–d). Hence, an evaluation of the TDS data by subregion is desirable.

2.4.2 West subregion

The data set for the West subregion included 101 values, primarily from the mining regions of the AOSR. The median salinity was 6 930 mg/L, and the 25th and 75th percentile values were 2 300 and 18 200 mg/L respectively (Table 2.1; Fig. 2.2). The West subregion had the widest range of TDS values of the three subregions, with a minimum observed TDS value of 220 mg/L to a maximum of 279 000 mg/L. Nine of the data points in this subregion were higher than seawater salinity, and the highest salinity value observed in any of the subregions was found

in the West. This brine was observed in Township 96, Range 11W4, and was measured by two different researchers on different sampling dates. In the same township as the brine outlier, TDS values as low as 570 mg/L were also observed in McMurray Formation waters.

Spatially the data in the West subregion were highly variable with few discernible trends apart from the primary regional trend of elevated formation water salinity along the Prairie Evaporite dissolution trend (Fig. 2.1). While the average salinity was 6 930 mg/L in this region, many TDS values below 1 000 mg/L were observed proximal to the high values across the region. In the northernmost mining area (Teck Frontier, Twp 99, Rng 10W4), most TDS values were very low (mean TDS = 4 700 mg/L, n = 28) compared to those obseved at the southern mines. However, two observation wells within the Teck mine had formation waters with significantly higher TDS (~90 000 mg/L) than the rest of the samples. The Teck lease is situated approximately 20 km east of the Prairie evaporite dissolution edge, and overlies large sinkholes in the Devonian surface. West of the Athabasca River and south of Fort McMurray there were fewer available public data upon which to draw interpretations. Water samples from available wells showed variable TDS ranging from 4 000 mg/L to 25 000 mg/L.

The histogram of the West subregion (Fig. 2.3b) depicts a slightly bimodal distribution with twenty-two TDS values greater than 20 000 mg/L. The first modal peak was centred around a TDS value of 3 300 mg/L and the second modal peak was centred on 17 900 mg/L. The tail of high TDS values extended to 279 000 mg/L, with sporadic high TDS values dotting the upper range of formation water TDS values.

2.4.3 Northeast subregion

There were 125 formation water TDS values obtained for the Northeast subregion. The median TDS value was 1 570 mg/L, lowest of the three subregions (Table 2.1). The 25th and

75th percentile values of the data were 890 and 3 870 mg/L respectively (Table 2.1; Fig. 2.2). The Northeast subregion formation water TDS values ranged from 300 to 59 200 mg/L (Table 2.1). There was only one data point that had a TDS value greater than seawater, and generally the formation waters in the Northeast region were less saline than those of the other subregions (Fig. 2.2).

Spatially, the highest TDS values observed in this subregion were proximal to the Athabasca River and the Prairie evaporite dissolution edge (Fig. 2.1). Formation waters with lower TDS values were observed to the east of this boundary. No formation waters with TDS greater than 4 000 mg/L were identified more than 10 km east of the Athabasca river. Formation waters with TDS approaching the value for seawater are found within 10 km of the Athabasca River, however, these data are interspersed with low-TDS formation waters, indicating local, rather than regional, geochemical influence on the formation water salinity in the McMurray Formation.

The histogram for the Northeast subregion (Fig. 2.3c) is skewed toward the low-TDS end of the spectrum, with a large majority of the values (n = 96) falling into the lowest histogram bin (< 5 000 mg/L). However, six TDS values ranging from 20 000 to 59 200 mg/L were identified for McMurray Formation waters in the Northeast subregion.

2.4.4 Southeast subregion

Distinct from the other two subregions that contain mining and in-situ operations, the southeast subregion consists entirely of in-situ energy developments, as the oil sands deposits in this area are too deep to mine. There were 128 data points considered in the Southeast subregion. The median formation water TDS was 9 600 mg/L, highest of the three subregions (Table 2.1). There was some heterogeneity in formation water TDS values, with 25th and 75th percentiles of

7 300 and 16 300 mg/L respectively (Table 2.1; Fig. 2.2). The TDS values in this subregion ranged from a minimum of 530 mg/L to a maximum of 77 300 mg/L (Table 2.1). In the Southeast subregion twelve values had greater TDS values than seawater, the greatest number out of the three subregions.

Examining the spatial distribution of the Southeast subregion, the formation water TDS values were highest in the east, and lower in the west and central portions of the subregion (Fig. 2.1). The lowest TDS values were observed on the Stony Mountain topographic high, centred at Twp 84, Rng 9. The easternmost part of the Southeast subregion was characterized by very elevated TDS values, up to 77 000 mg/L. This region of high salinity is consistent with the broader regional trend of the Prairie evaporite edge, and in the Southeast region, the evaporite edge also coincides with the eastern edge of bitumen-bearing McMurray Formation reservoirs.

The histogram for the Southeast subregion (Fig. 2.3d) was different from those of the other subregions in that the modal peak was in the second histogram bin (5 000 – 10 000 mg/L), indicating that fewer waters with low TDS were present in the Southeast subregion. The modal peak was approximately centred on the median value of 9 600 mg/L for the Southeast subregion (Table 2.1). Similar to the other two subregions, the Southeast region exhibited a long tail toward the high end of TDS in formation water data distribution, with twenty-seven TDS values > 20 000 mg/L measured for McMurray Formation water.

2.5 Discussion

Conceptual models of groundwater flow in the McMurray Formation have described groundwater flow paths as primarily local in nature, driven by topographic recharge (Bachu and Underschultz, 1993; Anfort et al., 2001; WorleyParsons, 2010). However, exclusively downward flow does not satisfactorily explain the variation observed in formation water salinity across the region. While topographically-driven flow does play an important role in the Athabasca oil sands region, additional factors including interactions with fluids from the Devonian units below the sub-Cretaceous unconformity provide a better explanation for the observed variability in TDS. This hypothesis is based on two key principles that have recently been described in the literature: 1) there are widespread karst features underlying the McMurray Formation in the Devonian carbonate and evaporite units (Broughton, 2013), providing conduit-style preferential flow paths between saline aquifers and the McMurray Formation that directly overlies the karst structures and 2) injection of meltwater from Pleistocene ice sheets into the Devonian aquifers that underlie the McMurray Formation (Grasby and Chen, 2005; Gue 2012) has created elevated hydraulic head thus providing a driving force for upward flow of brines into the oil sands reservoirs where conduits exist to enable flow. Hence, a conceptual model is proposed that incorporates both downward and upward groundwater flow into the McMurray Formation to explain the present-day distribution of formation water TDS.

Massive-scale karst caused by carbonate and evaporite dissolution below the sub-Cretaceous unconformity was recently demonstrated to underlie much of the AOSR (Broughton, 2013). Deep, karst-style closed depressions (sinkholes) are apparent throughout the region in the Devonian structural surface, and the continued subsidence of several of these sinkholes has been demonstrated to occur on timescales from pre-Cretaceous to modern (Broughton, 2013). Further

evidence of the presence of sinkholes is provided by geological models developed for Environmental Impact Assessments of many oil sands operations where units above the sub-Cretaceous unconformity have been structurally altered since deposition, suggesting continued subsidence after deposition of these units through Holocene time (e.g. Nexen/OPTI, 2007; Petro Canada, 2001; Teck Resources Limited, 2011). Karst hydrogeological systems consist of a dual porosity system of matrix flow and a network of conduits that can result in groundwater flow rates of up to kilometers per day during periods of high flow (Ford and Williams, 2007). This unique type of hydrogeology that is characterized by preferential flow of fluids through conduits creates significant challenges for groundwater models to recreate. The preferential flow paths generated by karst provide the necessary connectivity to explain the highly localized nature of cross-formation flow between Cretaceous units and Devonian hydrostratigraphic units. The McMurray Formation directly overlies the karst topography of the Devonian system; therefore it should be directly connected to Devonian aquifer systems where conduits exist. Karst provides an explanation consistent with formation waters from adjacent wells having TDS values varying by orders of magnitude, as shown in Figure 2.1. Mixing between fluids from Devonian aquifers and overlying Cretaceous formation waters was first suggested as a possibility by Bachu and Underschultz (1993); however at the time their study was published, there was insufficient data to identify the extent and magnitude of this process. The highly localized nature of upward fluid flow from Paleozoic strata is apparent in the northernmost part of Figure 2.1 (Twp 100, Rng 10W4). In this area of the AOSR, there are groundwater wells drilled into the laterally continuous McMurray Formation that have TDS values ranging from freshwater (< 4 000 mg/L) to those approaching brine concentrations (~90 000 mg/L) over a distance of 10s of kilometres. These locally high TDS values of formation waters are most consistent with hydraulic

connectivity between Devonian and Cretaceous hydrostratigraphic units, however, not all the McMurray Formation waters within this area have high salinity. Therefore the best explanation for the observed variability is that conduits between Cretaceous and Devonian hydrogeological systems exist within the areas of McMurray Formation water with highest salinity, resulting in high TDS values in some areas, but not necessarily in adjacent wells. Therefore, a high degree of variability in formation water TDS values can be expected within the scale of a single oil sands development or lease area.

Connectivity between Cretaceous and Devonian hydrogeological units is insufficient to explain upward flow of high salinity water from underlying units; a driving force is required to move denser, saline water in the opposite direction of gravitational forces. The proposed driving force was previously identified by Grasby and Chen (2005) who provided evidence of subglacial meltwater intrusion into the Devonian carbonate units that underlie the McMurray Formation, and proposed a reversal of the regional groundwater system from a model driven by deep basin flow to one driven by the impact of subglacial recharge. These arguments, based on both physical and chemical arguments, show that modern flow systems are not yet in equilibrium with long-term geological processes (Grasby and Chen, 2005). The data from Grasby and Chen (2005) indicate elevated hydraulic pressures during the Pleistocene glacial events that instigated a reversal in the regional flow system such that groundwater observed in modern Devonian aquifers was recharged with meltwater of ice sheets in the northeast, rather than through deep basin flow from the Rocky Mountains. Geochemical and stable isotope evidence from springs along the Athabasca and Clearwater rivers indicates that the discharging water has elevated salinity, but water stable isotope compositions ($\delta^{2}H$, $\delta^{18}O$) that are dissimilar from deep-basin Devonian brines found elsewhere in Alberta (Connolly et al., 1990; Grasby and Chen, 2005;

Gue, 2012). Instead, the isotopic composition of the discharging brines are consistent with inputs from glacial waters that infiltrated into the Devonian formations and dissolved the evaporite units found within the region. The hydrogeological response from the removal of the continental ice sheets is the northeastern up-dip flow of Devonian formation waters toward the edge of the basin. However, in karst-impacted strata, karst-conduit flow paths are exploited, and saline waters from the Devonian system flow upward into the McMurray Formation.

There are other lines of evidence that provide support for the existence of the Pleistocene basin flow reversal. Evidence of "blowout structures" are described in several locations near the edge of the Western Canada Sedimentary Basin where subsurface pressures exceeded the structural integrity of confining units above the sub-Cretaceous surface. A notable instance of this process is the Howe Lake blowout structure in central Saskatchewan that was described in detail by Christiansen et al. (1982). Recent pressure tests performed for Environmental Impact Assessments provide supporting evidence for upward flow, as several of the wells that were completed in Devonian strata had greater hydraulic head values than wells completed in the overlying McMurray Formation (Nexen Inc. and OPTI Canada Inc., 2007). This evidence suggests that upward flow from the Devonian strata to overlying aquifers has occurred in the recent past, and provides a plausible mechanism for upward flow of high-salinity formation water into the McMurray Formation, across the Athabasca Oil Sands Region from the Devonian aquifers.

The data from this study illustrate that local-scale connectivity across the AOSR between the saline Devonian aquifers and less saline Cretaceous aquifer systems occurs primarily at the edge of the Prairie Evaporite Formation where karst hydrogeology and elevated hydrostatic pressure at depth exist. The presence of karst-derived conduits, where partial dissolution of the

Prairie Evaporite Formation has occurred, and elevated hydraulic head values in some Devonian units due to Pleistocene glacial events provide a geological mechanism and driving force for upward movement of highly saline sub-Cretaceous fluids into areas of the McMurray Formation, especially along the dissolution edge of the Prairie Evaporite Formation (Fig. 2.1). Therefore, hydrogeological models for the Cretaceous units, especially the McMurray Formation must also incorporate the potential for upward flow via conduits from the Devonian aquifers at a local scale. Low salinity McMurray Formation waters are consistent with topographic recharge, as these formations are limited in depth (range ≈ 5 – 560 m), with low temperatures, and radiocarbon dates that suggest groundwater recharge on short time scales on the order of hundreds to thousands of years (Lemay, 2002b).

The data from this study were most consistent with a model of topographic recharge across the region, coupled with local upward formation water flow into the McMurray Formation from the underlying Devonian units. Exclusively downward flow of groundwater from meteoric recharge does not sufficiently explain the substantial variability and spatially incoherent distribution of McMurray Formation waters with elevated TDS values (Figs. 2.1 − 2.3). However, exclusively upward-flow does not explain the low salinity values observed throughout the majority of the region. The NW-SE trending linear feature of high formation water TDS values that coincides with the edge of the Prairie Evaporite Formation provides the conditions most likely to generate upward flow of saline water (Fig. 1). Along this trend, and east of the dissolution edge, significant karsting has developed, leading to the formation of many sinkholes and conduits associated with karst hydrogeology (Broughton, 2013). Also along this trend are evaporite formations of varying thickness (Figure 1.4), with both halite and anhydrite to provide high concentrations of solutes in Devonian formation waters (Grobe, 2000). East of the evaporite

depositional edge (Grobe, 2000), lower TDS values are observed in Devonian formation waters (Grasby and Chen, 2005). West of the evaporite dissolution edge, the evaporite units are largely intact, and therefore the wide-scale karst hydrogeology and conduit system has not yet developed to provide connectivity between the McMurray Formation and underlying Devonian aquifer systems. Therefore McMurray Formation waters with the highest TDS values are observed primarily adjacent to the Prairie evaporite dissolution edge, where karst hydrogeology has created conduits and elevated TDS in Devonian aquifers combine with glaciogenic elevated hydraulic head to force fluid flow in the upward direction into the McMurray Formation waters at many locations across the Athabasca region.

Karst hydrogeology provides a suitable explanation for other unique phenomena in the Athabasca oil sands region. In 2010, during excavation of a new tailings pond at its Muskeg River mine, Shell workers excavated a spring that caused sulfide-rich water (reported TDS ~29 000 mg/L; Ko, 2012) to discharge into the pond at a very high rate of 2×10^6 litres per hour (Cooper, 2011). The simplest explanation for this occurrence of rapid groundwater discharge, and high salinity of the intruding water is the presence of a large conduit connected to an over-pressured Devonian aquifer. These saline water eruptions may possibly be triggered in areas where human development reduces the overlying formation pressure, such as that caused by dewatering and digging of an open-pit mine facility. This study reveals that the most likely location for saline water intrusion occurs to the east of the dissolution edge of the Prairie Evaporite Formation, and detailed hydrogeological work should be conducted before development of oil sands facilities in these areas.

Topographic recharge remains an important process in the Athabasca regional hydrogeological system. Uplands such as Muskeg Mountain and Stony Mountain are likely sites

of groundwater recharge into the McMurray Formation, and McMurray Formation waters with a significant component of Holocene recharge can be expected to have low TDS values below 15 000 mg/L (WorleyParsons, 2010). For example, TDS values measured in the McMurray Formation beneath the area of highest surface elevation at the Stony Mountain upland (2 100 – 6 700 mg/L Fig. 2.1, Twp 84, Rng 9W4) are significantly lower than those of adjacent low-lying areas to the east that are proximal to the evaporite edge (8 300 – 77 000 mg/L; Fig 2.1., Twp 85, Rng 7W4). Groundwater recharge into the units above the McMurray Formation (e.g. glacial sediments, Grand Rapids and Clearwater formations) are likely driven exclusively by topographic recharge, as these formations are separated from the McMurray and Devonian units by the Clearwater regional aquitard, and generally have higher hydraulic head values than the McMurray Formation indicating downward flow (Bachu and Underschultz, 1993). In this respect, previous hydrogeological work in Environmental Impact Assessments is likely correct in interpreting the subsurface system above the McMurray Formation as topographically-driven on a relatively local to subregional scale.

Quaternary incised channels are an additional geological feature that have the capacity to connect surface water directly to the McMurray Formation, bypassing the regional Clearwater aquitards and enabling downward cross-formation flow. These incised channels occur throughout the region and their occurrence and distribution are described in detail by Andriashek and Atkinson (2007). Evidence for direct groundwater recharge to the McMurray Formation is present in the low TDS values in the McMurray Formation around the Nexen-Long Lake development (Fig. 2.1: Twp 84 and 85, Rng 5W4), where the Gregoire Quaternary channel penetrates the McMurray Formation (Nexen-OPTI, 2007). Proximal to the channel, TDS values in McMurray Formation waters are approximately 2 000 mg/L, and distal from the channel these

values increase sharply to > 20 000 mg/L. These large changes in salinity should be noted carefully as they provide early indications of connection between shallow groundwater and McMurray Formation water, and caution should be exercised when operating SAGD facilities near these Quaternary channels

2.6 Conclusions

Highly variable salinity was observed in the McMurray Formation waters throughout the Athabasca oil sands region. Formation water total dissolved solids values ranged from freshwater (TDS = 220 mg/L) to hypersaline brine fluids (TDS = 279 000 mg/L). There is no TDS value that could be considered typical of McMurray Formation water, due to the widespread variability across the AOSR; therefore all TDS measurements should be examined in a regional spatial context to provide insight into local hydrogeological processes. The observed spatial distribution of formation water TDS in the McMurray Formation is best explained by two processes: 1) topographically driven downward infiltration of meteoric water, and 2) upward flow of saline water via localized karst-derived conduits from Devonian aquifers driven by modern response to the basin-scale flow reversal initiated by the Pleistocene glacial events. Both requirements of this interpretation of upward vertical flow from Paleozoic to Cretaceous formations are met in the AOSR through the heavily karst-influenced sub-Cretaceous strata, and elevated hydraulic head in the Devonian aquifers caused by Pleistocene glaciation. Quaternary channels can also facilitate cross-formation flow in the downward direction, bypassing regional aquitards directly connecting modern recharge from precipitation to the McMurray Formation. The result of the groundwater input from Quaternary channels is typically observed as lower TDS values compared to regional McMurray Formation waters. This revised model for McMurray Formation hydrogeology provides an improved explanation for the observed variability in McMurray

Formation water TDS, and the surface discharge events that have been observed in the oil sands region such as the Muskeg River incident. Further investigation is warranted in both the Devonian strata that underlie the McMurray Formation, and on the sub-Cretaceous interface itself. Future work describing hydrogeology in oil sands systems could include detailed stable isotope data of water and its dissolved constituents, and ion-specific geochemical data to better constrain hydrogeological processes in the Athabasca oil sands region.

2.7 References

Andriashek, L. D., & Atkinson, N. (2007). Buried Channels and Glacial-Drift Aquifers in the Fort McMurray Region, Northeast Alberta. *Energy and Utilities Board /Alberta Geological Survey Earth Sciences Report* 2007-01 170 pp.

Anfort, S., Bachu, S., & Bentley, L. (2001). Regional-scale hydrogeology of the Upper Devonian-Lower Cretaceous sedimentary succession, south-central Alberta basin, Canada. *AAPG Bulletin-American Association Of Petroleum Geologists*, *85*(4), 637–660.

Asoian, J. (2012). Regional salinity distribution in the McMurray Formation (map). Suncor Inc. Calgary, AB.

Bachu, S. and Underschultz J.R. (1993). Hydrogeology of formation waters, northeastern Alberta. *AAPG Bulletin, 77*(10), 1745–1768.

Bachu, S. (1995). Synthesis and Model of Formation-Water Flow, Alberta Basin, Canada. *AAPG Bulletin-American Association Of Petroleum Geologists*, *79*(8), 1159–1178.

Barson, D., Bachu, S., & Esslinger, P. (2001). Flow systems in the Mannville Group in the east-central Athabasca area and implications for steam-assisted gravity drainage (SAGD) operations for in-situ bitumen production. *Bulletin of Canadian Petroleum Geology*, *49*(3), 376–392.

Broughton, P. L (2013). Devonian salt dissolution-collapse breccias flooring the Cretaceous Athabasca oil sands deposit and development of lower McMurray Formation sinkholes, northern Alberta Basin, Western Canada. *Sedimentary Geology*, 283(C), 57-82.

Christiansen, E. A., Gendzwill, D. J., & Meneley, W. A (1982). Howe Lake: a hydrodynamic blowout structure. *Canadian Journal Of Earth Sciences*, 19(6), 1122-1139.

Connolly, C., Walter, L., Baadsgaard, H., and Longstaffe, F. (1990). Origin and evolution of formation waters, Alberta basin, Western Canada Sedimentary Basin. 1. Chemistry. *Applied Geochemistry*, *5*(4), 375–395.

Cooper, D. (2001). Oilsands leak turned mine to pond: Shell finds innovative fix for a never-before-seen problem. *Edmonton Journal*. October 15, 2011

Ford D., and Williams, P., (2007). *Karst Hydrogeology and Geomorphology*. John Wiley and Sons Inc.

Fustic, M., Hubbard, S. M., Spencer, R., Smith, D. G., Leckie, D. A., Bennett, B., & Larter, S. (2012). Recognition of down-valley translation in tidally influenced meandering fluvial deposits, Athabasca Oil Sands (Cretaceous), Alberta, Canada. *Marine And Petroleum Geology*, *29*(1), 219–232.

George, R. (2013). Water – policy and government regulation for heavy oil and oilsands development. *Geoconvention: 2013*, Calgary, Alberta.

Grasby, S., & Chen, Z. (2005). Subglacial recharge into the Western Canada Sedimentary Basin - Impact of pleistocene glaciation on basin hydrodynamics. *Geological Society of America Bulletin*, *117*(3-4), 500–514.

Griffiths, M., Taylor, A., & Woynillowicz, D. (2006). Troubled Waters, Troubling Trends. *Pembina Institute*, 1–171.

Gue, A. (2012, December 21). *The geochemistry of saline springs in the Athabasca oil sands region and their impact on the Clearwater and Athabasca rivers*. University of Calgary, M.Sc Thesis. 173pp.

Hayes, B.J. (2013). The changing role of water in the petroleum geologist's "unconventional world." *Geoconvention: 2013*, Calgary, Alberta.

Ko, J. (2011). Accidents Do Happen: Shell Muskeg Tailings Pond. *Water Matters Web Log*. Available Online: http://www.water-matters.org/blog/465

Hackbarth, D. A., & Nastasa, N. (1979). Groundwater Observation Well Network: Athabasca Oil Sands Area. *Alberta Research Council, Information Series 69*, 1–1272.

Lemay, T. (2002). Geochemical and Isotope Data Formation Water from Selected Wells, Cretaceous to Quaternary Succession, Athabasca Oil Sands (In-situ) Area, Alberta. *Alberta Energy and Utilities Board–Alberta Geological Survey Geo-Note 2002-02*, 1–71.

Lemay, T. (2002). Carbon-14 Dating of Groundwater from Selected Wells in Quaternary and Quaternary-Tertiary Sediments, Athabasca Oil Sands (In Situ) Area, Alberta. *Alberta Energy and Utilities Board–Alberta Geological Survey Geo-Note 2002-03*, 1–21.

Michael, K., Machel, H., & Bachu, S. (2003). New insights into the origin and migration of brines in deep Devonian aquifers, Alberta, Canada. *Journal of Geochemical Exploration*, *80*(2-3), 193–219.

Nexen Inc, OPTI Canada Inc. (2007). *Application for the Approval of the Long Lake South Project.* Alberta Energy and Utilities Board and Alberta Environment. Edmonton, Alberta, Canada.

Petro Canada. (2001). *Application for the Approval of the Meadow Creek Project.* Alberta Energy and Utilities Board and Alberta Environment. Edmonton, Alberta, Canada.

Robertson, J. (2013). How produced water and source water qualities influence the operation and environmental footprint of SAGD surface facilities. *Geoconvention: 2013*, Calgary, Alberta.

Teck Resources Ltd. (2011). *Frontier Oil Sands Mine Project Environmental Impact Assessment*. Alberta Energy and Utilities Board and Alberta Environment. Edmonton, Alberta, Canada.

Wills, J. (2013). Hydrogeology 101 for the petroleum geologist. *Geoconvention: 2013*, Calgary, Alberta.

WorleyParsons (2010). *Regional Groundwater Quality Study and Monitoring Network Design in the Athabasca Oil Sands: Phase 2: Program Summary.* Regional Municipality of Wood Buffalo: Cumulative Environmental Management Association, Fort McMurray, Alberta, Canada. Available online: http://library.cemaonline.ca/dms-folders/CEMA-Reports/regional-groundwater-monitoring-network-implementation-in-the-northern-athabasca-oil-sands-contract-number-2008-0003-gwwg/Regional-Groundwater-Monitoring-Network.pdf.

Chapter Three: Determination of Total Dissolved Solids and the Stable Isotope Composition of Oil Sands Reservoir Porewater: A New Tool for Reservoir Fluid Characterization

3.1 Abstract

A new method was developed to calculate the total dissolved solids and stable isotope composition of drill-core derived porewater in Athabasca oil sands reservoirs. Analysis of water samples extracted directly from drill core provides a significant advance in the ability to characterize the properties of reservoir porewater, but requires corrections to account for contamination of drilling fluids. The technique described in this chapter utilizes two end-member mixing relationships between the stable isotope compositions of drilling fluids and formation waters. The method is not dependent on characterization of drilling fluids, however, measuring drilling fluid samples is a useful practice to verify results. Porewater data from three Athabasca oil sands wells are presented in this study. Water derived from these wells had TDS (860 to 45 000 mg/L), δ^2H (−172 to −149‰) and $\delta^{18}O$ (−22.4 to −19.3‰) values that were consistent with regional trends in formation water salinity, and illustrate the wide range of TDS values that can be found in McMurray Formation waters. The ability to characterize aqueous fluids in bitumen reservoirs is particularly important for in-situ extraction techniques that require steam injection, and detailed characterization of reservoir fluids to identify bitumen and water saturation. This methodology will provide geoscientists with a tool to understand the origin and movement of reservoir water due to natural groundwater flow, or anthropogenic influence by steam injection.

3.2 Introduction

The Alberta Oil Sands are the third-largest petroleum reserve in the world representing 1.7 trillion barrels of petroleum hydrocarbons in place (IEA, 2013). Of the three major Alberta oil sands deposits, the Athabasca Oil Sands Region (AOSR) is the largest and shallowest, permitting both surface mining and in-situ recovery near Fort McMurray, Alberta, Canada (Government of Alberta, 2013). The hydrogeology of these heavily biodegraded reservoirs is distinct from conventional petroleum systems due to the relatively shallow reservoir depths and a primarily local nature of most groundwater systems in the Athabasca region (Bachu and Underschultz, 1993). Oil sands reservoirs consist of a loosely consolidated mineral phase, typically quartz sandstone with minor interbedded shales. Pore space in the reservoir is filled with bitumen and water in varying proportions throughout the reservoir. Water saturation increases toward the bottom of the reservoir through a gradual oil-water-transition-zone (OWTZ) that is considered to be the zone of greatest biodegradation of oil (Aitken et al., 2013; Bennett et al., 2013). Below the OWTZ, the reservoir is entirely water saturated and is sometimes described as the "basal water sands."

Recent development of technologies that utilize steam to extract bitumen from reservoirs that are too deep to mine has created a need for detailed understanding of the hydrogeological systems associated with reservoir development. Accurate characterization of the ratio of bitumen to water in a reservoir is paramount to economic recovery of oil sands resources using in situ extraction technology. Steam-assisted gravity drainage (SAGD) and cyclic steam stimulation (CSS) are the most commonly employed in situ extraction technologies in Alberta. Both of these techniques extract petroleum from the subsurface by heating the reservoir to high temperatures

(> 200 ºC) by injecting steam. The steam provides sufficient thermal energy to melt the bitumen resource allowing it to be produced as a mixture of hot bitumen and formation water. SAGD reservoirs utilize paired horizontal wells to produce oil from the reservoir, generating a steam chamber in the bitumen-saturated portion of the reservoir. In an optimal SAGD well pair, the steam chamber is constrained by the hydrophobic bitumen resource, permitting steam to evenly melt the reservoir toward the producing well. However, if the steam chamber penetrates the water-saturated portion of the reservoir, steam preferentially flows toward the water-saturated section, decreasing the efficiency of extraction by mobilizing heat away from the bitumen. Therefore, reservoir engineers require detailed information about the reservoir architecture to drill wells such that the steam chamber will be constrained within the bitumen-saturated zone, and avoiding bitumen-free 'lean-zones' is imperative.

Geophysical tools that use electrical resistivity to determine bitumen and water saturation are sensitive to the salinity of formation waters. However using traditional methods, it is difficult to obtain an accurate measure of formation water salinity in oil sands reservoirs. Water saturation in oil sands systems is calculated using the electrical conductivity of water in the reservoir using Archie's law, and the conductivity of the water is directly related to its dissolved ion composition (Archie, 1942). Typically the salinity of formation waters in one or two observation wells are used for calibration of petrophysical tools over a large lease area. However, the TDS values of water in the McMurray Formation are highly variable over small geographic areas (Chapter Two), and these variations in salinity may generate incorrect estimates of water saturation within the reservoir. Commonly drilled exploration wells do not permit determination of water chemistry because of low water saturation in the reservoir and significant contamination due to

drilling fluids; therefore new tools are required to delineate salinity of reservoir fluids in bitumen-bearing reservoirs of the AOSR.

One of the most powerful uses of isotope hydrogeology is determining the source of water in a groundwater system (Clark and Fritz, 1997). By examining the relationship between δ^2H and $\delta^{18}O$ values, it is possible to delineate water sources, and identify processes that may have affected groundwater through its history. All waters with a meteoric origin plot on the linear trend described by the Global Meteoric Water Line (GMWL, Craig, 1961). Waters condensed and precipitated at warmer temperatures generally have higher δ^2H and $\delta^{18}O$ values than waters condensed and precipitated at colder temperatures, however the linear relationship between δ^2H and $\delta^{18}O$ of precipitation remains approximately consistent through all temperature ranges. The Global Meteoric Water Line has been adapted for Alberta through detailed collection of precipitation records in Edmonton from 1960–1969 (Lemay, 2002; IAEA, 2013). Within the Athabasca region, all waters with a meteoric origin should plot closely to the Edmonton Local Meteoric Water Line (LMWL, Lemay, 2002).

Groundwater sources in the Athabasca region, including relatively recent local groundwater recharge, sub-glacial meltwater, and deep Cretaceous formation water can be differentiated using stable isotopes (Fig. 3.1). Modern recharge into quaternary aquifers has been documented in the Athabasca region as having $\delta^{18}O$ values ranging from −17.7 to −19.8‰ and δ^2H values ranging from −139 to −150‰ (Lemay, 2002). These Quaternary groundwaters plot on the LMWL (Fig. 3.1). Deep regional Cretaceous formation waters in the Alberta basin range in $\delta^{18}O$ from −5.5 to −15.8‰ and range in δ^2H from −82 to −127‰ (Connolly et al., 1990). These deep basin formation waters do not plot on the LMWL, and are isotopically distinct from modern meteoric recharge (Fig. 3.1). Groundwater recharge from sub-glacial meltwater is

thought to be an important process in the Athabasca region (Grasby and Chen, 2005). These waters were derived from melting of continental ice sheets during the Pleistocene epoch, and are depleted in ^{2}H and ^{18}O compared to modern precipitation, but plot on the GWML (Clark et al., 2000; Grasby and Chen, 2005). The isotopic composition of these waters cannot be measured directly, as no pure samples of glacial meltwater remain, however these waters are estimated to have had an isotopic composition plotting on the GMWL, ranging in $\delta^{18}O$ from −25 to −35‰, and a previously modeled $\delta^{18}O$ value for subglacial groundwater recharge was −28‰ (Clark et al., 2000, Fig. 3.1). McMurray Formation waters have $\delta^{18}O$ values ranging from −19.5 to −22.2‰ and $\delta^{2}H$ values ranging from −148 to −172‰ in published studies, and these values are lower than modern recharge in Quaternary formations in the AOSR, suggesting some possible glacial influence in these waters (Lemay, 2002; WorleyParsons, 2010; Gibson et al., 2011). McMurray Formation waters do not have an isotopic signature that is indicative of mixing with deep Cretaceous formation waters, and all previously published McMurray Formation waters plot along the Edmonton LMWL (Fig. 3.1, Connolly et al., 1990; Lemay, 2002; WorleyParsons, 2010; Gibson et al., 2011).

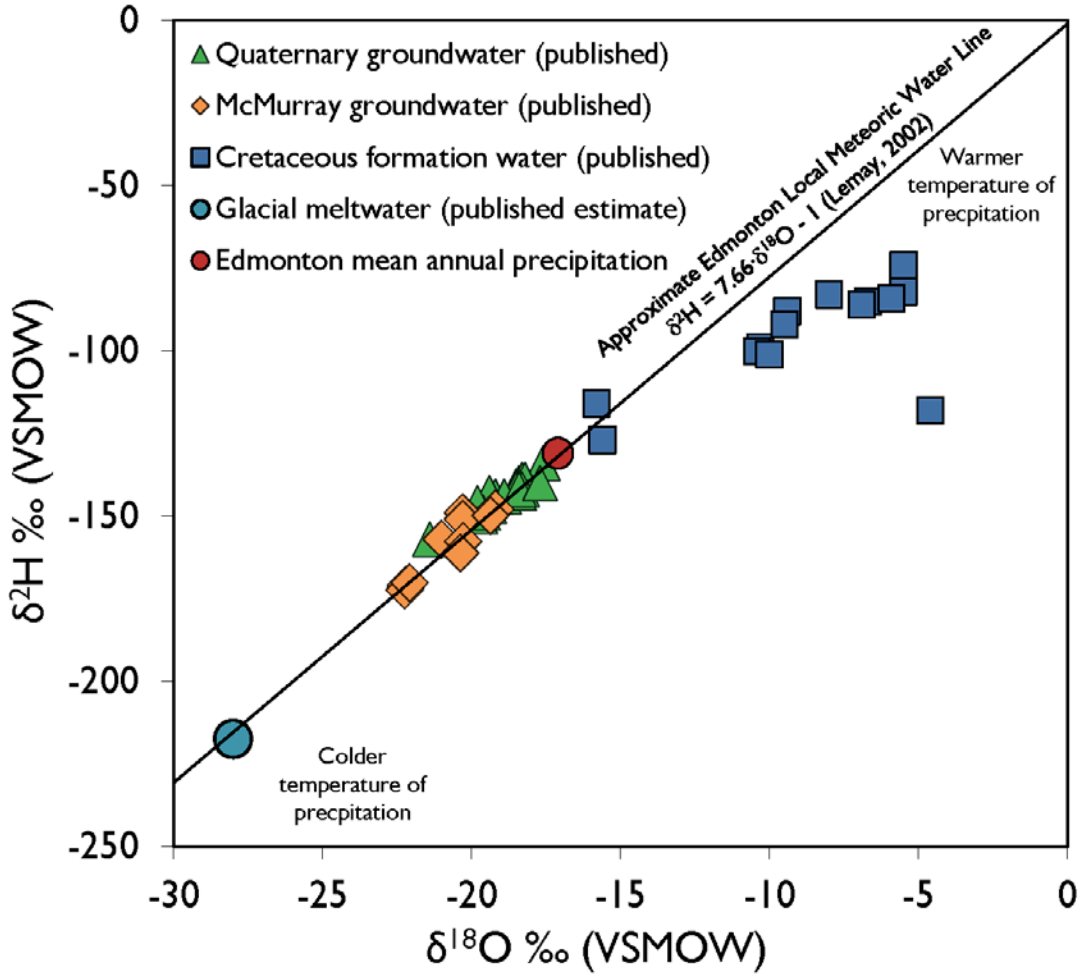

Figure 3.1: Published stable isotope ratios of selected groundwater and formation water samples in Alberta. Data for Quaternary groundwater was derived from Lemay (2002). McMurray Formation water isotope data was derived from Lemay (2002), WorleyParsons (2010) and Gibson et al. (2011). The deep Cretaceous formation water data set was derived from Connolly et al. (1990). An estimate of subglacial meltwater estimate was derived from Clark et al. (2000).

This chapter describes the use of a new water stable isotope approach for determining total dissolved solids and stable isotope ratios of porewater in oil sands reservoirs. This technique measures the properties of porewater squeezed from exploration well drill core that is regularly used for determining the geochemical properties of bitumen (Gushor Inc., 2013), and corrects for the impacts of drilling fluid on formation water measurements. This method represents a significant advance in reservoir characterization for oil sands systems, as increased water sampling density for TDS and stable isotopes within an oilfield will improve estimates of water and bitumen saturation, provide detailed information about local hydrogeological conditions and thus has the potential to increase the efficiency of SAGD extraction methods.

3.3 Experimental approach

3.3.1 Core sampling and water extraction

Core samples obtained from drilling were immediately frozen and shipped from the wellsite to the laboratory within 48 hours to minimize evaporative loss. Porewaters were mechanically extracted from 10 cm of drill core via the Plunger technique (Gushor Inc. 2013, US Patent #8495921). Between six and ten subsamples were taken for analysis from each core, at depth intervals of approximately two to five metres between samples. Oil sands reservoir cores from this study were between ten and thirty metres in length. Volumes of water that are produced by this method are typically less than 15 mL for each 10 cm of core, however some core samples yielded no water. Porewater obtained from plunging was immediately transferred to a glass vial with a teflon-faced lid and refrigerated at 4 ºC until analysis at the University of Calgary.

3.3.2 Drilling mud samples

Four drilling muds were obtained from oil sands drilling operations, and contain a mixture of source waters. These mud samples were not taken from the same wells from which porewaters were extracted from core in this study, however they were obtained from other similar drilling operations in the region. Drilling fluids were sampled at the wellsite in 500 mL glass bottles with teflon faced-lids. Samples were refrigerated at 4 ºC until analysis.

3.3.3 Water sample clean-up

Both porewaters squeezed from core materials and drilling fluids were rich in particulate matter that required clean-up before introduction of water samples into the analytical instruments. Samples were centrifuged at 15 000 RPM for ten minutes to remove suspended matter, and then decanted. A two-step syringe-tip filtration system was subsequently employed, first using a 1.0 µm pre-filter, and a second 0.2 µm GD/X PVDF syringe-tip filter. The clean water sample was divided into an aliquot for water isotope analysis (typically 1.8 mL) and an aliquot for geochemical analysis (sample balance). Where water volumes were less than five millilitres, an aliquot for stable isotope composition was analyzed first, and re-combined with the remaining sample to increase sample volume available for analytical procedures.

3.3.4 Isotope geochemistry

Hydrogen and oxygen isotope ratios were determined using a Los Gatos Research DLT-100 Isotope Ratio Infrared Spectrometer. More than ten injections of each sample were conducted to eliminate memory effects from the previous sample. $\delta^{2}H_{H2O}$ and $\delta^{18}O_{H2O}$ values were normalized using internal laboratory water standards that have been calibrated against international reference materials VSMOW, VSLAP & VGISP. USGS LIMs was used for drift

correction and normalization. Water isotope ratios are reported in delta notation relative to the international VSMOW reference material:

$$\delta^{2}H \text{ or } \delta^{18}O\ (‰) = [R_{sample} / R_{standard} - 1] \times 1000 \qquad [1]$$

Where R represents the measured ratio of $^{2}H/^{1}H$, or $^{18}O/^{16}O$.

Accuracy and precision of $\delta^{18}O$ and $\delta^{2}H$ measurements are generally better than ± 0.1‰ and ± 1.0‰ respectively for replicate measurements of 50 laboratory standards.

3.3.5 Aqueous geochemistry

Analysis of major cations (Na, K, Ca, Mg) was completed using a Varian 725-ES ICP-OES, and a Dionex ICS2000 ion chromatography system was used for major anion concentrations (Cl, SO_4). Analytical precision for cations and anions was typically ± 5% of the measured value for each ion. Laboratory alkalinity (determined as HCO_3) was determined using a Thermo Orion 960 autotitration system, and the typical analytical error for bicarbonate alkalinity was ± 5% of the measured value. Total dissolved solids were calculated for each sample by taking the sum of the concentrations of major cations and anions in each sample.

3.4 Results and discussion

Cores from three representative wells from three different locales within the Athabasca oil sands region were used to demonstrate this new approach to inferring salinity and stable isotope composition of reservoir water in the McMurray Formation. The reservoirs ranged in thickness from ten to thirty metres, and within each reservoir up to ten individual water samples from different depths were obtained and analyzed for stable isotope ratios and geochemical parameters.

The measured TDS values in extracted porewater from Well 1 were highly variable, spanning an order of magnitude from 2 700 mg/L to 28 900 mg/L (Table 3.1). $\delta^{18}O$ values in

porewater samples from Well 1 ranged from −11.2 to −18.2‰, and δ^2H of porewater ranged from −117 to −152‰. There was no observed correlation between TDS or stable isotope composition with depth in the reservoir.

Well 2 also had considerable variability in measured porewater TDS values that ranged from 2 050 to 5 100 mg/L (Table 3.1). The $\delta^{18}O$ values ranged from −13.9 to −17.5‰, and δ^2H_w values ranged from −124 to −141‰ (Table 3.1). There was no observed correlation between TDS or stable isotope composition with depth in the reservoir.

Porewater from Well 3 had the lowest TDS values of the three measured wells, and ranged from 1 020 to 2 800 mg/L (Table 3.1). $\delta^{18}O$ values in Well 3 ranged from −10.8 to −17.9‰, and δ^2H values ranged from −132 to −155‰ (Table 3.1). There was no observed correlation between TDS or stable isotope composition with depth in the reservoir.

Drilling fluids are complicated mixtures of many different water sources and chemicals. Muds are recycled and evaporated during the drilling process, therefore the water isotope signature of drilling fluid expresses an evaporation trend in water isotope ratios that results in a water isotope signature that plots to the right of the LMWL (Clark and Fritz, 1997). Geochemistry and stable isotopes of four mud samples measured in this study are presented in Table 3.2, however, these samples are not likely representative of all drilling fluids used in the Athabasca region and are included as examples only.

To assess the chemical and isotopic composition of reservoir porewater and to determine the impact of drilling fluids on measured water samples, both δ^2H and TDS were plotted against $\delta^{18}O$ values for each of the three wells in Figure 3.2a–c. The $\delta^{18}O$ and δ^2H values were closely correlated in each system, displaying a straight line with a distinct slope plotting to the right of the LMWL (Fig. 3.2). The example drilling mud samples plot near the far right end of the mixing

curves in Figure 3.2. This linear trend of isotope compositions is indicative of a two end-member mixing line between formation waters that plot on the LMWL and drilling fluids that plot to the right of the LMWL. In each of the three wells, the relationship between δ^2H and $\delta^{18}O$ was a tight linear feature (R^2 values from 0.790 to 0.996) that intercepted the LMWL within the range of isotope values that have been previously published for waters in the McMurray Formation (Lemay, 2002; WorleyParsons, 2010; Gibson et al., 2011).

Table 3.1: Geochemical and stable isotope measurements of porewater derived from three selected drill cores in the Athabasca Oil Sands Region

Sample ID	$\delta^{18}O_w$ (‰$_{VSMOW}$)	$\delta^{2}H_w$ (‰$_{VSMOW}$)	TDS (mg/L)	Na (mg/L)	K (mg/L)	Mg (mg/L)	Ca (mg/L)	Cl (mg/L)	SO_4 (mg/L)	HCO_3 (mg/L)
Well 1										
W1–1081	–11.2	–117	2 700	1 390	39	0	14	1 170	58	37
W1–1082	–12.0	–121	4 140	1 860	37	1	39	1 970	96	145
W1–1121	–13.9	–128	10 400	4 200	80	45	159	5 460	279	174
W1–1122	–13.6	–127	9 990	3 900	71	18	162	5 040	224	573
W1–1131	–18.2	–152	28 900	11 400	124	175	121	16 400	232	473
W1–1132	–17.9	–150	29 300	11 000	113	181	134	17 300	277	253
W1–1211	–17.0	–145	24 600	9 440	94	158	79	14 300	198	419
W1–1212	–17.3	–148	23 900	9 050	87	159	76	14 000	185	351
W1–1281	–13.1	–126	10 500	4 220	69	60	169	5 300	301	362
W1–1282	–11.5	–122	15 200	6 170	118	90	241	8 090	507	n.a.
Well 2										
W2–4460	–15.3	–130	3 130	1 190	19	3	9	1 650	93	171
W2–4490	–17.5	–141	5 100	1 910	32	2	4	2 620	200	329
W2–4520	–14.4	–126	3 470	1 300	21	5	14	1 710	220	195
W2–4540	–14.7	–128	3 210	1 230	15	4	10	1 680	165	105
W2–4550	–13.9	–124	2 050	860	14	3	14	950	217	n.a.
W2–4560	–15.5	–131	3 440	1 300	14	4	9	1 900	112	114
Well 3										
W3–2530	–17.9	–155	1 090	580	14	5	15	180	294	560
W3–2570	–14.3	–134	1 710	870	24	23	112	279	406	798
W3–2610	–16.9	–145	1 530	670	22	11	19	250	559	414
W3–2660	–16.7	–150	1 020	560	20	5	12	162	262	636
W3–2700	–10.8	–132	2 800	1 080	59	28	35	331	1 270	n.a.
W3–2750	–14.5	–136	1 560	730	30	10	25	219	545	688
W3–2830	–15.1	–140	1 530	790	24	17	68	192	442	1 092

n.a. denotes the sample was not analyzed for the parameter

Table 3.2: Geochemical and stable isotope measurements of selected drilling fluids used in the McMurray Formation

Sample ID	$\delta^{18}O$ (‰)	$\delta^{2}H$ (‰)	TDS (mg/L)	Na^{+} (mg/L)	K^{+} (mg/L)	Mg^{2+} (mg/L)	Ca^{2+} (mg/L)	Cl^{-} (mg/L)	SO_4^{2-} (mg/L)	HCO_3^{-} (mg/L)
FDM–7	-13.8	-125.2	5 900	1 154	32	37	377	215	44	4 040
FDM–9	-13.0	-122.6	4 700	1 378	36	29	208	336	33	2 680
FDM–11	-14.1	-125.4	2 770	475	113	20	229	81	24	1 830
FDM–15	-14.5	-127.6	3 550	914	41	25	141	173	26	2 230

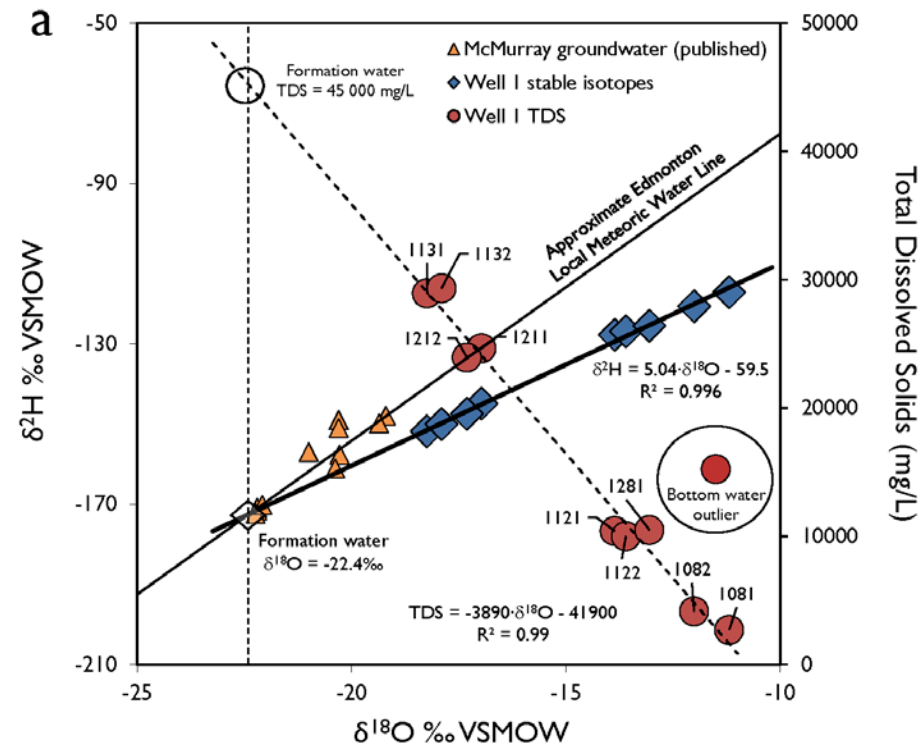
a
McMurray groundwater (published)
Well 1 stable isotopes
Well 1 TDS
Formation water
TDS = 45 000 mg/L
Approximate Edmonton
Local Meteoric Water Line
1131
1132
1212
1211
δ²H = 5.04·δ¹⁸O - 59.5
R² = 0.996
Bottom water
outlier
1281
1121
1122
1082
1081
Formation water
δ¹⁸O = -22.4‰
TDS = -3890·δ¹⁸O - 41900
R² = 0.99
δ²H ‰ VSMOW
Total Dissolved Solids (mg/L)
δ¹⁸O ‰ VSMOW
-50
-90
-130
-170
-210
-25
-20
-15
-10
50000
40000
30000
20000
10000
0

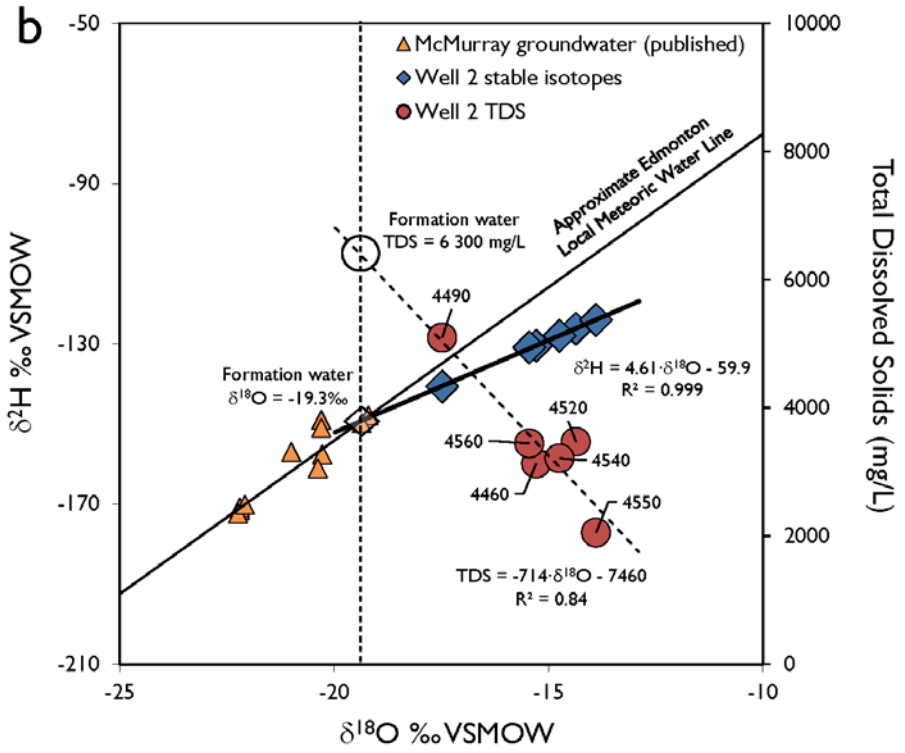
b
McMurray groundwater (published)
Well 2 stable isotopes
Well 2 TDS
Approximate Edmonton
Local Meteoric Water Line
Formation water
TDS = 6 300 mg/L
4490
Formation water
δ¹⁸O = -19.3‰
δ²H = 4.61·δ¹⁸O - 59.9
R² = 0.999
4520
4560
4540
4460
4550
TDS = -714·δ¹⁸O - 7460
R² = 0.84
δ²H ‰ VSMOW
Total Dissolved Solids (mg/L)
δ¹⁸O ‰ VSMOW
-50
-90
-130
-170
-210
-25
-20
-15
-10
10000
8000
6000
4000
2000
0

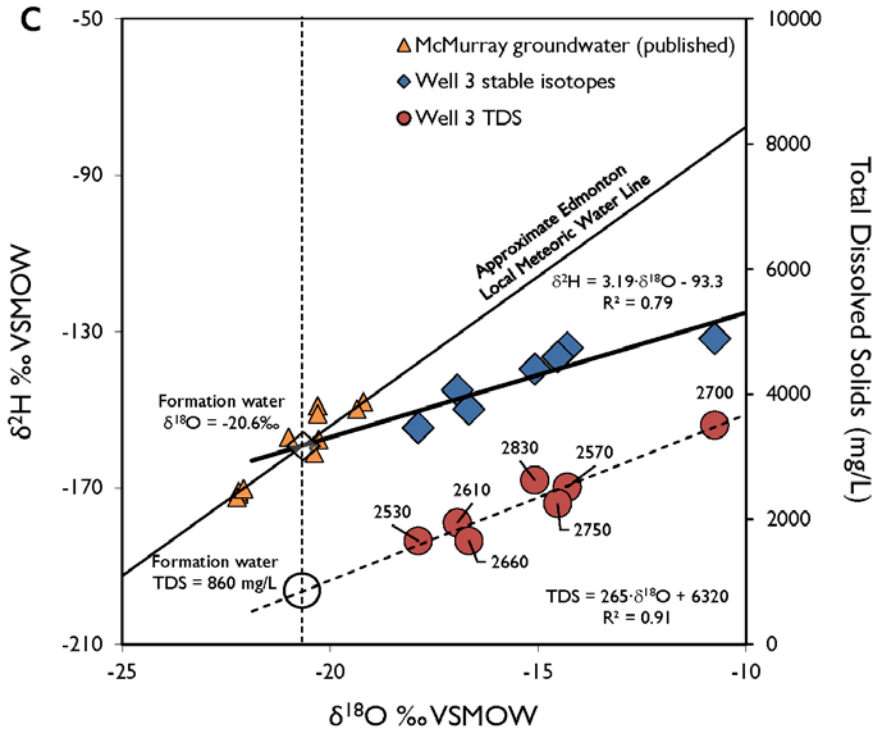

Figure 3.2: Plots of water isotope composition (blue diamonds) and TDS (red circles) for porewater samples obtained from cores from Well #1 (a), Well #2 (b) and Well #3 (c). The labels on the TDS data correspond to individual sample identification numbers in Table 1. Plotted McMurray groundwater samples were obtained from previously published data sources (Lemay, 2002; WorleyParsons, 2010; Gibson et al., 2011). For Well #1, the bottom water outlier was the deepest sample in the reservoir, and represents a different water source, therefore it was not included in the calculation of TDS or stable isotope composition. Analytical error is smaller than data markers, and error is described in Experimental Approach (3.3).

During drilling, mud penetrates the borehole and the extracted drill core. However, because bitumen is hydrophobic, it retards the drilling mud from completely obscuring the formation water signal. Hence, the fluid samples obtained from drill core represent variable mixtures of drilling mud and formation water. Evidence for water samples representing variable mixing between drilling mud and formation water is based on the following observations:

1. The stable isotope ratios of groundwater from all published observation wells in the McMurray Formation plot on the LMWL, strongly suggesting that waters within the reservoirs should also plot on the LMWL.
2. Measured drilling fluids are enriched in ^{2}H and ^{18}O compared with the porewater obtained from drill core, and from published McMurray Formation water data. These drilling fluids plot to the right of the LMWL, suggesting that drilling fluid constitutes the ^{2}H and ^{18}O enriched end-member of the mixing curve, to the right of the LMWL (Fig. 3.2).
3. Porewater samples from all core segments of a given well formed a linear trend in $\delta^{2}H/\delta^{18}O$ space that intercepts the LMWL within the range of water isotope compositions that have been previously published for the McMurray Formation.
4. The isotopic composition of the water samples extracted from cores from a single well are also correlated with TDS, either negatively (Figs 3.2a and 3.2b) or positively (Fig. 3.2c) depending on the TDS of formation water compared to the TDS of the drilling mud (Table 3.2). This provides a second line of evidence for mixing between formation waters with lower $\delta^{18}O$ and $\delta^{2}H$ values and drilling fluids with elevated $\delta^{2}H$ and $\delta^{18}O$ values.

Given these two primary observations that 1) water samples extracted from drill core are a mixture of formation fluids and drilling mud, and 2) the stable isotope composition of

McMurray Formation waters fall on the LMWL, the intercept of a linear least-squares regression line formed by the measured isotope data with the LMWL is interpreted as a close approximation of the original stable isotope composition of the reservoir formation waters. The intersection point of the LMWL and the porewater $\delta^{18}O$– $\delta^{2}H$ regression line was solved using Equations 2–5. The calculated formation water $\delta^{18}O$ value for each investigated well is indicated on Figure 3.2 with an open diamond.

$$\delta^{2}H = 7.66\ (\delta^{18}O) - 1 \qquad [2]$$

Edmonton Local Meteoric Water Line (Lemay, 2002).

$$\delta^{2}H = m_s\ (\delta^{18}O) + b_s \qquad [3]$$

b_s and m_s represent the $\delta^{2}H$-intercept and slope of the mixing line generated by the isotope data for porewaters from each investigated well (Fig. 3.2). Allowing Equations 1 and 2 to have equal $\delta^{2}H$ values, and re-arranging the equation, Equation 3 represents the intersection of the two lines:

$$\delta^{18}O = (b_s - b_{LMWL}) / (m_{LMWL} - m_s) \qquad [4]$$

b_s is the $\delta^{2}H$-intercept and m is the slope of the functions describing the LMWL and linear regression line of the sample. Substituting known constants from the LMWL (Eq. 1) into Equation 3 gives the following:

$$\text{LMWL-Porewater Intercept } \delta^{18}O = (b_s + 1) / (7.66 - m_s) \qquad [5]$$

Equation 4 permits calculation of the reservoir porewater $\delta^{18}O$ value generated by the intersection of the regression line with the LMWL. $\delta^{2}H$ values are calculated by substitution into Equations 2 or 3.

The calculation of TDS values for reservoir water is conducted in a similar fashion to the determination of water isotope composition. A least squares regression line was generated for

TDS–$\delta^{18}O$, and the equation was solved using the $\delta^{18}O$ value calculated in Equation 5. In Well 1 and Well 2, waters with lower $\delta^{18}O$ values had higher TDS concentrations than those with higher $\delta^{18}O$ values, consistent with drilling muds having lower TDS values than reservoir porewater (Table 3.2, Fig. 3.2a and 3.2b). However, in Well 3, TDS decreased with lower $\delta^{18}O$ values, suggesting that the drilling fluid had a greater TDS value than the reservoir porewater (Fig. 3.2c). These observations are consistent with drilling fluids having TDS values approximating the measured range from Table 2, between 2 700 and 5 900 mg/L, and a water isotope signature that plots to the right of the LMWL (Table 3.2).

The calculated $\delta^{18}O$ value for formation water in Well 1 was –22.4‰, in Well 2 the calculated $\delta^{18}O$ value for formation water was –19.3‰, and in Well 3 the calculated $\delta^{18}O$ value for formation water was –20.6‰. The R^2 values generated by the regression lines for each $\delta^{18}O$–TDS system were high, ranging from 0.84 to 0.99. The previously determined formation water $\delta^{18}O$ value from Equation 4 were input into the $\delta^{18}O$–TDS equation for each well to estimate the TDS value for the formation water (Fig. 3.2). The TDS value calculated for formation water, which has not been impacted by drilling fluid, is indicated for each well in Figure 3.2 with an open circle. In Well 1 the calculated formation water TDS value was 45 000 mg/L, in Well 2 the calculated formation water TDS value was 6 300 mg/L, and in Well 3 the calculated formation water TDS value was 860 mg/L.

The TDS results from each well compare favourably with regional formation water chemistry described in Chapter 3.2, suggesting these results provide a close approximation of *in situ* reservoir conditions. Well 1 (TDS = 45 000 mg/L) was drilled in an area west of the Athabasca River, where salinity values greater than seawater are frequently observed (~57 °N, ~112 °W). Well 2 (TDS = 6 300 mg/L) was drilled in the region south of Fort McMurray, where

brackish waters are common in the McMurray Formation (~56 °N, ~111 °W). Well 3 (TDS = 860 mg/L) was drilled in the area northeast of the Athabasca-Clearwater river confluence where non-saline formation waters with TDS below 4 000 mg/L are frequently observed (~57 °N ~111 °W). Therefore the results obtained from this new technique are consistent with regional understanding of heterogeneity in groundwater geochemistry in the McMurray Formation, and suggest that the data are indeed representative of in situ conditions in the reservoir. The results confirm the very large differences in TDS for McMurray Formation waters that need to be considered for resource evaluation.

3.5 Limitations and sample requirements of the reservoir fluid characterization method

The use of this method requires multiple water samples from several depths within a reservoir to be obtained to effectively determine reservoir water chemistry and stable isotope ratios. A minimum of five water samples > 5.0 mL representing different levels of drilling fluid contamination are recommended to generate adequate mixing lines, however the development of this technique is in its infancy and a greater number of samples may be required to characterize a specific reservoir. A greater number of samples measured will likely result in a greater certainty of results, and more detailed vertical spatial resolution. Reservoirs investigated in this study appeared to be relatively homogenous with respect to water chemistry, as the R^2 values of the mixing lines for the three measured wells were very high, and this is expected for a reservoir in equilibrium with a well-mixed aquifer. However, this may not be the case in systems where shales are barriers to fluid flow. Compartmentalized reservoirs and microbial impacts on bitumen properties related to availability of water legs have been noted throughout the oil sands regions by investigating bitumen chemistry (Larter et al., 2003; Larter et al., 2006; Bennett et al., 2013), and it would be unlikely for formation water to transcend these geological barriers over short

time periods. Furthermore, flow along preferential flow paths (e.g. lean zones of low bitumen saturation) may alter the water chemistry of a single part of the reservoir on anthropogenically relevant time scales. Because water flow through the reservoir is slow due to the presence of bitumen, the reservoir may not be in equilibrium if it has been affected by steam injection, or other modern disturbances.

3.6 Conclusions

The approach described in this chapter provides a new method to determine the original oil sands formation water $\delta^{18}O$, $\delta^{2}H$, and TDS directly from drill core samples, by calculating a mixing relationship between formation waters and drilling fluids. The data generated by this technique are independent of the drilling fluid composition, however the results are consistent with measured drilling fluid samples. The stable isotope ratios and total dissolved solids concentrations calculated using this method are consistent with regional TDS and stable isotope trends known from groundwater well sampling, suggesting that accurate values for original porewater can be determined on a well-by-well basis using this technique. It is now possible to obtain information about reservoir water salinity and stable isotope composition on a sub-field scale and greatly increase the frequency of TDS measurements within oil sands lease areas.

The implications of this new method will be improved calibration of geophysical tools for characterization of water and bitumen saturation, and resultant improvement in efficiency of steam-based bitumen recovery techniques based on improved understanding of reservoir architecture. Future deployment of this method will permit detailed characterization of natural hydrochemical variations in the McMurray Formation, assist with hydrogeological model development, and may permit the detection of mobile water from steam injection during in situ energy development.

3.7 References

Aitken, C.M., Jones, D.M., Maguire, M.J., Gray, N.D., Sherry, A. Bowler, B.F.J., Ditchfield, A.K., Larter S. R and Head, I.M. (2013). Evidence that crude oil alkane activation proceeds by different mechanisms under sulfate-reducing and methanogenic conditions. *Geochimica et Cosmochimica Acta* 109(5), 162−174

Archie, G.E. (1942). The electrical resistivity log as an aid in determining some reservoir characteristics. *Petroleum Transactions of AIME* **146**: 54–62.

Bachu, S. and Underschultz J.R. (1993). Hydrogeology of formation waters, northeastern Alberta. *AAPG Bulletin, 77*(10), 1745–1768.

Bennett, B., Adams, J.J., Gray, N.D., Sherry, A., Oldenburg, T.B.P., Huang, H., Larter, S.R. and Head, I.M. (2013) The controls on the composition of biodegraded oils in the deep subsurface – Part 3. The Impact of microorganism distribution on petroleum geochemical gradients in biodegraded petroleum reservoirs. *Organic Geochemistry,* 56(3), 94-105.

Clark, I.D., and Fritz P. (1997). *Environmental isotopes in hydrogeology*. Lewis Publishers: New York. 328pp.

Clark, I.D., Douglas, M., Raven, K., and Bottomley D., (2000). Recharge and preservation of Laurentide glacial meltwater in the Canadian Shield. *Groundwater* 38, 735-742.

Connolly, C.A., Walter, L.M., Baadsgaard H., and Longstaffe, F.J. (1990). Origin and evolution of formation waters, Alberta Basin, Western Canada Sedimentary Basin. Part I and Part II. *Applied Geochemistry* 5, 375-413.

Craig, H. (1961). Isotopic variations in meteoric water. *Science* 133, 1702-1703.

Gibson, J. J., Birks, S. J., Moncur, M., Yi, Y., Tattrie, K., Jasechko, S. (2011). Isotopic and Geochemical Tracers for Fingerprinting Process-Affected Waters in the Oil Sands Industry: A Pilot Study. *Oil Sands Research and Information Network*, 1-120.

Government of Alberta (2013). *Oil Sands Information Portal*. Retrieved June 15, 2013. http://www.osip.alberta.ca

Grasby, S., & Chen, Z. (2005). Subglacial recharge into the Western Canada Sedimentary Basin - Impact of Pleistocene glaciation on basin hydrodynamics. *Geological Society of America Bulletin*, 117(3-4), 500–514.

Gushor Inc. (2013). *The Plunger(tm), patent pending*. Retrieved online April 11, 2013: http://gushor.com/file/page/plunger/plunger.pdf.

International Atomic Energy Agency (2013). *Global Network of Isotopes in Precipitation data: Edmonton*. Retrieved online July 9, 2013: http://www-naweb.iaea.org/napc/ih/IHS_resources_isohis.html

International Energy Agency (IEA), (2012). *World Energy Outlook 2012*. Paris, France. 690pp.

Larter, S., Wilhelms, A., Head, I., Koopmans, M., Aplin, A., Di Primio, R., et al (2003). The controls on the composition of biodegraded oils in the deep subsurface - part 1: biodegradation rates in petroleum reservoirs. *Organic Geochemistry*, 34(4), 601-613.

Larter, S., Huan, H., Adams, J., Bennett, B., Jokanola, O., Oldenburg, T., et al (2006). The controls on the composition of biodegraded oils in the deep subsurface: Part II - Geological controls on subsurface biodegradation fluxes and constraints on reservoir-fluid property prediction. *AAPG Bulletin-American Association Of Petroleum Geologists*, 90(6), 921-938.

Lemay, T (2002). Geochemical and Isotope Data Formation Water from Selected Wells, Cretaceous to Quaternary Succession, Athabasca Oil Sands (In Situ) Area, Alberta. *Alberta Energy and Utilities Board Geo Note 2002-02.* pp 1-71.

WorleyParsons (2010). Regional Groundwater Monitoring Network Implementation in the Northern Athabasca Oil Sands (NAOS) Phase 2 - Program Summary. *Cumulative Environmental Management Agency*, Fort McMurray, Alberta, Canada. 493 pp.

Chapter Four: Stable isotope composition and total dissolved solids measurement of formation waters in the Suncor-Firebag oil sands field from bitumen core-extracted porewater

4.1 Abstract

In the preceding chapter, a method was described to analyze the stable isotope composition and total dissolved solids (TDS) concentration of reservoir porewater directly from bitumen core samples. In this chapter, the method described in Chapter Three was applied to calculate the TDS and stable isotope composition of water samples extracted directly from drill core throughout the Suncor-Firebag oil sands development in northern Alberta, Canada. The application of the porewater technique permitted laterally extensive sampling of these key water parameters throughout the lease area. Some porewater samples provided an indication of vertical heterogeneity within wells, thus providing insight into reservoir connectivity at the Firebag site.

The mean $\delta^{18}O$ and $\delta^{2}H$ values calculated for twelve sampled wells at Firebag were -20.5 ± 1.4‰ and -157 ± 11‰ respectively. The mean total dissolved solids concentration of the twelve sampled wells was $1\,100 \pm 400$ mg/L. These values suggest that the McMurray Formation water was primarily derived from Holocene groundwater recharge. In several of the sampled wells, there was three-dimensional variability observed in both TDS and stable isotope composition of porewater that may indicate barriers to fluid flow, or distinct hydrogeological conditions over several kilometers within the Firebag lease. These results are consistent with regional trends and previously proposed local hydrogeological flow conditions described in the literature. This study represents a significant advance in the aqueous fluid characterization of the McMurray Formation in the Firebag area, and provides substantial insight into the heterogeneity that can be expected of other oil sands developments in the Muskeg Mountain area of the Athabasca Oil Sands Region.

4.2 Introduction

The Alberta Oil Sands are the third-largest petroleum reserve in the world, representing nearly 170 billion barrels of crude oil (Government of Alberta, 2013). These low-quality oil reservoirs are distinct from traditional petroleum systems due to their highly biodegraded nature, relatively shallow reservoir depths, and complex interactions with the regional groundwater system. Recent rapid development of these resources by steam-based technologies has created a need for improved understanding of the hydrogeological environment in the subsurface.

Steam-assisted gravity drainage (SAGD) and cyclic steam stimulation (CSS) are the most commonly employed extraction mechanisms for in-situ extraction of bitumen from oil sands reservoirs. Both of these techniques extract petroleum from the subsurface by heating the bitumen using high temperature steam, melting the resource and producing hot fluids. However, the geology of the McMurray Formation, in which the majority of Athabasca oil sands deposits are found, is highly complex and many challenges were encountered over the course of recent development. The identification of "thief zones" or "lean zones" of low bitumen saturation, and high water saturation is a key factor in steam-based reservoir development, as these conduits can transmit injected steam far away from the intended reservoir zone (Rubin et al., 2009). Identifying and tracing the movement of steam in the subsurface requires detailed characterization of background hydrogeological parameters to identify spatial and temporal changes in formation water properties. Additional challenges include the development of near-surface reservoirs that may be connected to surface waters via quaternary channels, incised into bedrock during the last glacial event. Furthermore, water washing and increased biodegradation due to recent hydrogeological recharge can affect the quality of the bitumen resource, and the value of the resource play. Therefore, accurate characterization of formation water source and

salinity is becoming an essential need for successful development of these complicated energy systems.

Geophysical tools that use electrical resistivity to determine bitumen and water saturation in the reservoir environment are sensitive to the salinity of formation waters, however using present methods, it is difficult to obtain an accurate measure of formation water salinity in oil sands reservoirs. Water saturation (S_w) within a reservoir can be underestimated by up to 20% if the total dissolved solids (TDS) of formation water increases from 10 000 to 20 000 mg/L within the reservoir (Archie, 1942). Typically the salinity of formation waters for an entire oil sands field is determined from one or two observation wells drilled into the water leg of the McMurray Formation. Down-hole geophysical tools that use electrical resistivity to measure water saturation are calibrated using the TDS values from these observation wells. However, due to geological complexity, the TDS in the McMurray Formation water is highly variable over small geographic areas (Chapter Two). Thus, variations in formation water salinity within a field may generate incorrect estimates of water saturation, based on measurements made using resistivity tools, and therefore these tools may not correctly identify lean zones. Frequently drilled exploration wells do not permit direct measurement of reservoir porewater chemistry because of significant formation water contamination by drilling fluids. Other tools such as the Schlumberger MDT down-hole sampling device (Schlumberger, 2013) can provide information about water composition at a single point in the reservoir, however this technique is expensive, and it assumes homogeneous water composition throughout the rest of the reservoir. Therefore new methods are required to directly measure the concentration of total dissolved solids in reservoir formation waters to better understand the heterogeneity within the resource, and to optimize extraction methods.

While knowing the formation water TDS value is important for determining S_w using geophysical techniques, it does not provide substantial insight into the source and movement of formation water. Stable isotope ratios of water (δ^2H, $\delta^{18}O$) are among the most useful tools for determining hydrogeological processes in natural systems (Clark and Fritz, 1997), and may be applied to oil sands reservoirs to help elucidate hydrogeological properties of a resource play. As an intrinsic component of the water molecule, the water isotope composition is highly conservative, thus providing an ideal tracer of formation water sources and subsurface flowpaths. For example, in the Athabasca Oil Sands Region (AOSR), paleo-recharge from glacial meltwater has a stable isotope composition that is distinct from modern recharge, and deep basin waters (e.g. Fig 3.1). Thus it is possible to identify the source and history of groundwater in many cases using a stable isotope approach. Similar to the measurement of TDS in samples obtained from drill core, formation water isotope ratios are also obscured by drilling mud. However, as described in Chapter Three, it is possible to calculate the original TDS and stable isotope composition of formation waters via analysis of extracted porewaters from drill cores, thus permitting higher frequency sampling of formation waters across an oil sands development. Measurement of the stable isotope composition of formation waters provides important information about background hydrogeological conditions prior to steam injection, and may be able to trace steam chamber development upon commencement of steam-based bitumen extraction.

The objective of this study was to characterize the TDS and stable isotope compositions of bitumen reservoirs at the Suncor-Firebag oil sands lease area as a proof of concept study. Using the method described in Chapter Three of this thesis, porewater samples from drill core were extracted from the subsurface, and TDS and stable isotope compositions (δ^2H, $\delta^{18}O$) of

original formation waters were calculated for twelve wells. Additional groundwater and produced water samples were obtained to provide context to the measurements made by the new porewater methodology. This methodology allowed for detailed characterization of bitumen reservoir water and interpretation of hydrogeology within the Firebag lease area.

4.3 Study location details

The Firebag lease area is located northeast of Fort McMurray, approximately centred at 57.24 ºN, 110.85º W. Situated on top of the Muskeg mountain area of the Athabasca Oil Sands Region, Firebag covers an spatial extent of more than 100 km^2. The mean annual temperature at Fort McMurray is 0.7 ºC with January and July averages of −18.8 ºC and 16.8 ºC (National Climate Data and Information Archive, 2013). The mean annual precipitation at Fort McMurray is 456 mm (National Climate Data and Information Archive, 2013). The cold climate experienced in northern Alberta results in comparatively low δ^2H and $\delta^{18}O$ values for precipitation. The $\delta^{18}O$ and δ^2H values for weighted mean annual precipitation in Edmonton were calculated to be −17.1‰ and −132‰ respectively (Lemay, 2002; IAEA 2013). However, groundwater recharge may result from spring snowmelt in the Fort McMurray area, resulting in lower stable isotope values for shallow groundwater recharge (WorleyParsons, 2010a,b). A survey of Quaternary wells in the Athabasca Oil Sands Region resulted in an average $\delta^{18}O$ value of -18.9 ± 0.9‰, and a δ^2H value of -144 ± 5‰ for shallow groundwater (Lemay, 2002); these values are lower than the weighted mean annual precipitation, indicating that recharge due to snowmelt is a likely process. This has been observed in other areas of western Canada including southern Alberta (Grasby

The general hydrostratigraphy of the AOSR was described by Bachu and Underschultz (1993) and can be found in detail in Figure 1.4. The Muskeg Mountain area upon which Firebag

is situated has been identified in previous reports as an area of groundwater recharge, owing to its high elevation relative to the river valleys that surround the region (WorleyParsons, 2010a). Therefore, topographic gravity-driven groundwater recharge is expected within the Firebag region (WorleyParsons, 2010a). However, paleo-recharge from subglacial meltwater has also been an important factor in the AOSR groundwater systems (Grasby and Chen, 2005). Groundwater from glacial meltwater is isotopically distinct from modern recharge, and thus can be identified using stable isotope measurements (Fig. 3.1).

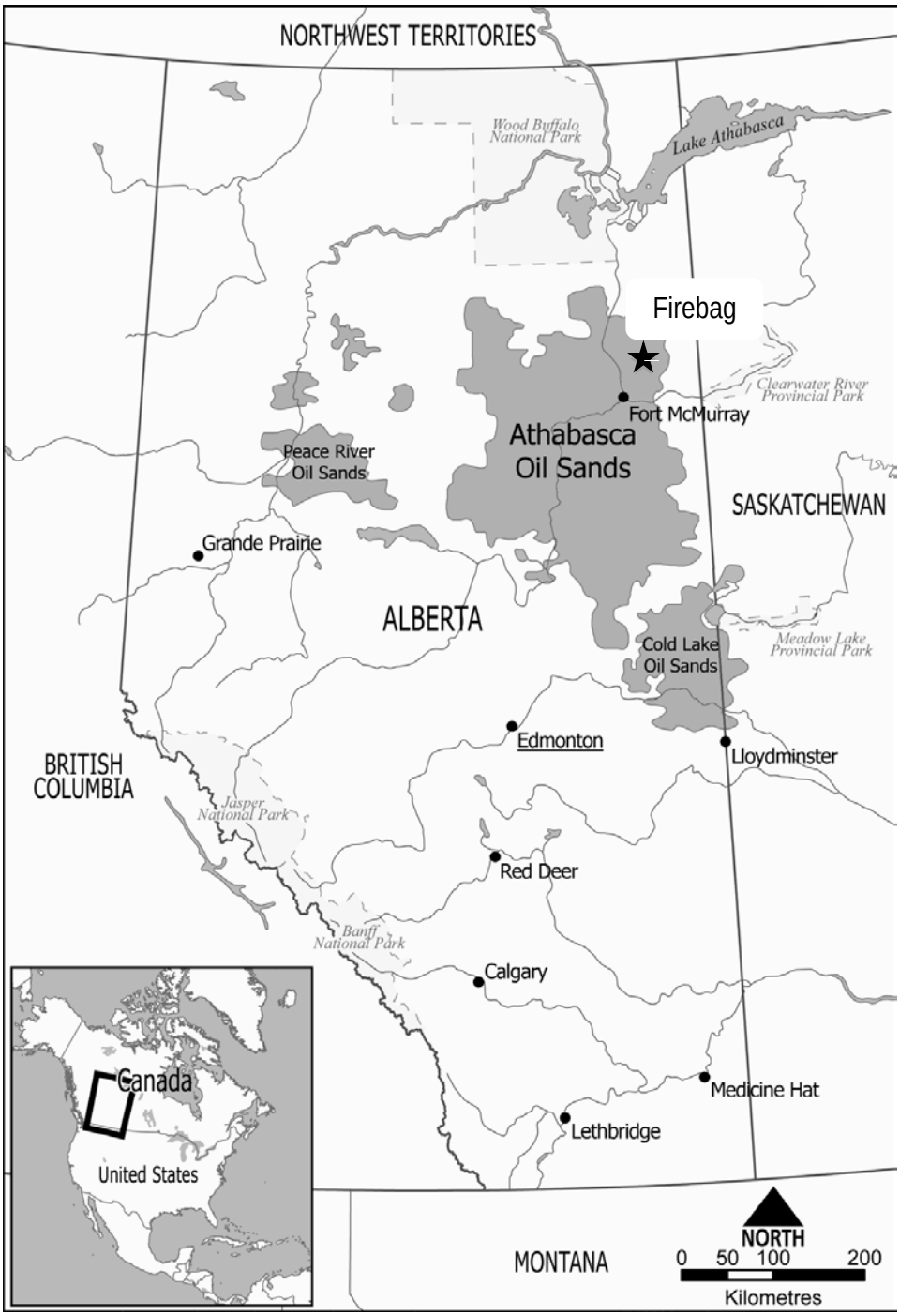

Figure 4.1: Alberta's three oil sands regions. The Suncor-Firebag lease area is indicated with a star on the map (Adapted from Wikimedia Commons, Norman Einstein, 2006).

4.4 Methods

4.4.1 Core sampling and porewater extraction

Drill cores from twelve wells at Firebag were obtained between December 2011 and January 2013. Reservoir depths ranged from 230 − 338 metres below ground surface. Whole drill cores were immediately frozen and shipped from the wellsite to the laboratory within 48 hours to minimize evaporative loss. Between five and thirteen subsamples were taken from each well, at depth intervals of approximately five metres. Porewaters were mechanically extracted from 10 cm of drill core via the Plunger technique at Gushor Inc. (Gushor Inc. 2013, US Patent #8495921). Volumes of water that are produced by this method are typically less than 15 mL for each 10 cm of core, however some samples yielded no water. Porewater obtained from core was immediately transferred to a glass vial with a Teflon-faced lid and refrigerated at 4 ºC until analysis. A complete data set providing details of all samples is available in Appendix B.

4.4.2 Groundwater sampling

Shallow groundwater samples were taken from two wells at approximately 57.24 ºN, 110.73 ºW in a Quaternary aquifer with a screened depth of approximately 60 m. One produced water sample was obtained from a SAGD production well (320 m depth) before the start of steam operations at approximately 57.226 ºN, 110.884 ºW. Groundwater and produced water samples were taken in glass bottles and refrigerated until analysis. No pre-treatment or filtering was completed in the field before transport directly to the University of Calgary laboratory.

4.4.3 Water sample clean-up

Both porewaters squeezed from core materials and produced waters from the pre-SAGD well were rich in mineral content, and these water samples had significant fine suspended mineral content that required clean-up before introduction into the analytical instruments.

Samples were centrifuged at 15 000 RPM for ten minutes to remove suspended matter, and then decanted. A two-step syringe-tip filtration system was subsequently employed to remove solids, first using a 1.0 µm pre-filter, and a second 0.2 µm GD/X PVDF syringe-tip filter. The clean water sample was divided into an aliquot for isotope analysis (typically 1.8 mL) and an aliquot for geochemical analysis (sample balance). Where water volumes were small (< 5 mL), an aliquot of water was analyzed for stable isotope composition and subsequently re-combined with the remaining sample to increase sample volume available for further analytical procedures.

4.4.4 Isotope composition of porewater

Hydrogen and oxygen isotope ratios of water samples were determined using a Los Gatos Research DLT-100 Isotope Ratio Infrared Spectrometer. $\delta^{2}H_{H2O}$ and $\delta^{18}O_{H2O}$ values were normalized using internal laboratory water standards that have been calibrated against international reference materials VSMOW, VSLAP & VGISP. USGS LIMS was used for drift correction and normalization. Water isotope ratios are reported in delta notation relative to the VSMOW international standard:

$$\delta^{2}H \text{ or } \delta^{18}O\ (‰) = [(R_{sample} / R_{standard}) - 1] \times 1000$$

Where R represents the measured ratio of $^{2}H/^{1}H$, or $^{18}O/^{16}O$.

Accuracy and precision of $\delta^{18}O$ and $\delta^{2}H$ measurements are generally better than ± 0.1‰ and ± 1.0‰ respectively for replicate measurements of 50 laboratory standards.

4.4.5 Aqueous geochemistry and calculation of total dissolved solids

Analysis of major cations (Na, K, Ca, Mg) was completed using a Varian 725-ES ICP-OES, and a Dionex ICS2000 ion chromatography system was used for major anions (Cl, SO_4). Analytical precision for cations and anions was typically ± 5% of the reported concentration for each ion. Laboratory alkalinity (reported as HCO_3) was determined using a Thermo Orion 960

autotitration system, with a typical uncertainty of ± 5% of the reported concentration. For samples in which alkalinity measurements were not available due to small sample size, the mean alkalinity value for other samples within that well was used as an estimate. Total dissolved solids were calculated for each sample by taking the sum of major cations and anions in each sample.

4.4.6 Tritium

Tritium analysis was completed on one produced water sample within the Firebag lease area. Tritium concentrations were determined by radiometric detection at the Water Dating Laboratory at GNS Science in Lower Hutt, NZ. Tritium values are reported as Tritium Units (TU, but also sometimes the nomenclature TR is used interchangeably). 1 TU represents a $^{3}H/^{1}H$ ratio of 1×10^{-18}. More information about the tritium measurement process can be found at: http://www.gns.cri.nz/Home/Services/Laboratories-Facilities/Tritium-and-Water-Dating-Laboratory.

4.4.7 Calculation of TDS and stable isotope ratios of formation water

Stable isotope ratios of hydrogen ($\delta^{2}H$) and TDS were plotted against $\delta^{18}O$ values in Cartesian coordinate space. The intersection point of the Local Meteoric Water Line (LMWL) with the regression line generated by the isotope data was calculated using the method described in Chapter Three. TDS was calculated by extrapolation of the $\delta^{18}O$−TDS regression line to the calculated $\delta^{18}O$ value for the formation water.

4.5 Results

For each individual well, δ^2H and TDS were plotted against the $\delta^{18}O$ value of each porewater sub-sample (Figs. 4.2a−m). In each of the wells, the relationship between δ^2H and $\delta^{18}O$ was a linear trend, with slopes ranging from 1.3 to 5.8, that intercepted the Local Meteoric Water Line (LMWL, Lemay, 2002) within the range of previously published stable isotope compositions of McMurray Formation water (Lemay, 2002; WorleyParsons, 2010; Gibson et al., 2011). The local meteoric water line was derived from precipitation data collected in Edmonton from 1960–1969 (Lemay, 2002; IAEA, 2013), and resulted in the relationship between δ^2H and $\delta^{18}O$ described in Equation 1:

$$\delta^2H = 7.66\ \delta^{18}O - 1 \qquad [1]$$

As described in Chapter Three, the linear relationships between $\delta^{18}O$ and δ^2H values represent a two end-member mixing relationship between drilling fluids that plot to the right of the LWML, and formation waters that plot on the LMWL. The $\delta^{18}O$ and TDS values of the extracted porewater samples were also correlated, and the TDS value of the original formation water was calculated using the $\delta^{18}O$ value LMWL intercept. Descriptions of the data trends are presented below. Detailed data tables of individual porewater samples are available in Appendix B.

4.5.1 Firebag 03-18-095-05W4 (Fig. 4.2a)

Seven porewater samples were taken from this well from 253.2 to 283.3 m below ground surface. The $\delta^{18}O$ values for porewater extracted from this well ranged from −17.9 to −10.8‰ and the δ^2H values ranged from −155 to −132‰. The slope of the linear relationship between $\delta^{18}O$ and δ^2H was 3.20, with a moderate R^2 value of 0.79. The isotope mixing line intercepted the LMWL at a $\delta^{18}O$ value of −20.6‰. The TDS values for extracted porewater samples ranged

from 1 650 to 3 500 mg/L. The mixing line between $\delta^{18}O$ and TDS was tightly correlated, having an R^2 value of 0.91. A TDS value of 860 mg/L was calculated for the formation water in this well.

4.5.2 Firebag 03-34-094-06W4 (Fig. 4.2b)

Thirteen porewater samples were taken from this well from 291.3 to 338.4 m below ground surface. The $\delta^{18}O$ values for porewater ranged from −18.2 to −14.7‰ and the $\delta^{2}H$ values ranged from −149 to −130‰. The slope of the linear relationship between $\delta^{18}O$ and $\delta^{2}H$ values was 5.54, with a high R^2 value of 0.97. The isotope mixing line intercepted the LMWL at a $\delta^{18}O$ value of −22.5‰. The TDS values for extracted porewater samples ranged from 2 000 to 3 900 mg/L. The mixing line between $\delta^{18}O$ and TDS was moderately well correlated, with an R^2 value of 0.77. A TDS value of 400 mg/L was calculated for reservoir formation water in this well.

There was one TDS outlier value at 291.3 m from the sample taken at highest elevation in the reservoir, suggesting a geochemical change immediately above the bitumen zone. It had a much higher TDS concentration than samples with similar $\delta^{18}O$ values from the remainder of the well. However, with only a single data point, quantification of fluid properties is not possible for the uppermost portion of the reservoir.

4.5.3 Firebag 07-08-095-05W4 (Fig. 4.2c)

Porewater samples were obtained from 260.2 to 278.0 m below ground surface, and six samples from this well were taken in duplicate at three depths. The $\delta^{18}O$ values for porewater extracted from this well ranged from −15.8 to −13.3‰ and the $\delta^{2}H$ values ranged from −136 to −128‰. The linear relationship between $\delta^{18}O$ and $\delta^{2}H$ values had a slope of 3.58, and an R^2 value of 0.84. The isotope mixing line intercepted the LMWL at a $\delta^{18}O$ value of −19.2‰. The

TDS values for extracted porewater samples ranged from 1 800 to 2 700 mg/L. The TDS values were statistically uncorrelated with $\delta^{18}O$, having an R^2 value of 0.03, suggesting similar TDS concentrations in drilling fluid and formation water. A TDS value of 1 800 mg/L was calculated for the reservoir formation water in this well.

4.5.4 Firebag 09-08-095-05W4 (Fig. 4.2d)

Five porewater samples were taken from this well from 254.4 to 280.3 m below ground surface. The $\delta^{18}O$ values for porewater extracted from this well ranged from −18.1 to −14.9‰ and the $\delta^{2}H$ values ranged from −148 to −131‰. The slope of the linear relationship between $\delta^{18}O$ and $\delta^{2}H$ values was 5.06, with a very high R^2 value of 0.99. The isotope mixing line intercepted the LMWL at a $\delta^{18}O$ value of −21.6‰. The TDS values for extracted porewater samples ranged from 1 400 to 1 900 mg/L. The regression line between $\delta^{18}O$ and TDS was weakly correlated, having an R^2 value of 0.10. A TDS value of 1 300 mg/L was calculated for the reservoir formation water in this well.

4.5.5 Firebag 09-09-095-06W4 (Fig. 4.2e)

Six porewater samples were taken from this well from 262.8 to 285.5 m below ground surface. The $\delta^{18}O$ values for porewater extracted from this well ranged from −16.1 to −14.5‰ and the $\delta^{2}H$ values ranged from −143 to −135‰. The slope of the linear relationship between $\delta^{18}O$ and $\delta^{2}H$ values was 3.16, with an R^2 value of 0.62. The isotope mixing line intercepted the LMWL at a $\delta^{18}O$ value of −19.9‰. The TDS values for extracted porewater samples ranged from 2 100 to 2 500 mg/L. The mixing line between $\delta^{18}O$ and TDS was strongly correlated, having an R^2 value of 0.82. A TDS value of 1 200 mg/L was calculated for the reservoir formation water in this well.

4.5.6 Firebag 15-08-095-05W4 (Fig. 4.2f)

Six porewater samples were taken from this well from 261.2 to 309.2 m below ground surface. The $\delta^{18}O$ values for porewater extracted from this well ranged from −17.4 to −16.0‰ and the $\delta^{2}H$ values ranged from −144 to −136‰. The slope of the linear relationship between $\delta^{18}O$ and $\delta^{2}H$ values was 5.15, with a high R^2 of 0.97. The isotope mixing line intercepted the LMWL at a $\delta^{18}O$ value of −21.0‰. The TDS values for extracted porewater samples ranged from 1 100 to 1 400 mg/L. The $\delta^{18}O$ and TDS values were statistically uncorrelated, having an R^2 value of 0.00. A TDS value of 1 300 mg/L was calculated for the reservoir formation water in this well.

4.5.7 Firebag 01-08-095-06W4 (Fig. 4.2g)

Six porewater samples were taken from this well from 250.8 to 291.1 m below ground surface. The $\delta^{18}O$ values for porewater extracted from this well ranged from −17.4 to −7.0‰ and the $\delta^{2}H$ values ranged from −145 to −125‰. There were two outliers in stable isotope composition and TDS that were obtained from shales above the bitumen-bearing reservoir that are marked on the diagram, and were not included in the calculation of reservoir water properties. The slope of the linear relationship between $\delta^{18}O$ and $\delta^{2}H$ was 1.34, with a high R^2 value of 0.93. The isotope mixing line intercepted the LMWL at a $\delta^{18}O$ value of −19.0‰. The TDS values for extracted porewater samples ranged from 1 800 to 3 600 mg/L. The mixing line between $\delta^{18}O$ and TDS was tightly correlated, having an R^2 value of 0.96. A TDS value of 1 200 mg/L was calculated for the reservoir formation water in this well.

4.5.8 Firebag 11-04-095-06W4 (Fig. 4.2h)

Seven porewater samples were taken from this well from 251.9 to 303.9 m below ground surface. There were two outliers having elevated salinity appearing at the bottom of the reservoir,

below 285 m depth that were not used in the calculation of formation water TDS and isotope composition. The $\delta^{18}O$ values for porewater extracted from this well ranged from −16.7 to −12.9‰ and the $\delta^{2}H$ values ranged from −143 to −135‰. The slope of the linear relationship between $\delta^{18}O$ and $\delta^{2}H$ values was 1.95, with a moderate R^2 value of 0.79. The isotope mixing line intercepted the LMWL at a $\delta^{18}O$ value of −19.0‰. The TDS values for extracted porewater samples ranged from 1 800 to 4 300 mg/L. The mixing line between $\delta^{18}O$ and TDS had a high R^2 value of 0.90. A TDS value of 1 100 mg/L was calculated for the reservoir formation water in this well. The bottom two samples in the well had substantially higher TDS values that could not be quantified due to an inadequate number of data points. However, using an assumed TDS value of 5 000 mg/L for drilling fluid composition, the lower reservoir formation waters likely have a TDS value of 3 000 mg/L or greater.

4.5.9 Firebag 01-10-095-06W4 (Fig. 4.2i)

Nine porewater samples were taken from this well from 269.5 to 308.9 m below ground surface. The $\delta^{18}O$ values for porewater extracted from this well ranged from −16.7 to −13.8‰ and the $\delta^{2}H$ values ranged from −140 to −127‰. There were two distinct groups of samples in this well, separated at approximately 285 m depth. Above 285 m shales were abundant, and below 285 m was dominated by bitumen-saturated sands.

In the shale section, the $\delta^{18}O$ values for extracted porewater ranged from −16.4 to −14.2‰ and the $\delta^{2}H$ values ranged from −140 to −134‰. The slope of the linear relationship between $\delta^{18}O$ and $\delta^{2}H$ values was 2.10 with a moderate R^2 value of 0.66. The isotope mixing line intercepted the LMWL at a $\delta^{18}O$ value of −18.8‰. The TDS values for extracted porewater samples ranged from 2 600 to 3 300 mg/L. The mixing line between $\delta^{18}O$ and TDS had a low R^2

value of 0.04. A TDS value of 2 400 mg/L was calculated for the formation water in the upper portion of this well.

In the sand-dominated bitumen reservoir, below 285 m the $\delta^{18}O$ values for extracted porewater ranged from −16.7 to −13.8‰ and the $\delta^{2}H$ values ranged from −138 to −127‰. The slope of the linear relationship between $\delta^{18}O$ and $\delta^{2}H$ values was 3.92, with a high R^2 value of 0.99. The isotope mixing line intercepted the LMWL at a $\delta^{18}O$ value of −19.3‰. The TDS values for extracted porewater samples ranged from 1 750 to 2 700 mg/L. The mixing line between $\delta^{18}O$ and TDS was tightly correlated, having an R^2 value of 0.90. A TDS value of 850 mg/L was calculated for the reservoir formation water in the lower section of this well.

4.5.10 Firebag 05-06-095-06W4 (Figs. 4.2j & 4.2k)

The data from this well can be presented in two different ways, requiring different interpretations of the data. Given the available data, the reservoir can be considered as one single system, or a two separate water systems consisting of formation waters with distinct properties.

Considering the well as a single system (Fig. 2j), eleven porewater samples were taken from 243.5 to 297.7 m below ground surface. There was an outlier at the bottom of the well at a depth of 297.7 m with unusually low $\delta^{2}H$ and TDS values; therefore it was excluded from all calculations. The $\delta^{18}O$ values for porewater extracted from this well ranged from −18.0 to −13.3‰ and the $\delta^{2}H$ values ranged from −149 to −124‰. The slope of the linear relationship between $\delta^{18}O$ and $\delta^{2}H$ was 5.53, with a high R^2 value of 0.96. The isotope mixing line intercepted the LMWL at a $\delta^{18}O$ value of −23.2‰. The TDS values for extracted porewater samples ranged from 2 700 to 4 200 mg/L. The mixing line between $\delta^{18}O$ and TDS had an R^2 value of 0.68. A TDS value of 1 200 mg/L was calculated for the formation water if it is considered a single entity.

Considering the reservoir as a separated water system requires two different drilling muds with distinct water isotope compositions (Fig 2k). Drilling mud switches are common in oil sands operations; therefore a change in mud composition is a plausible explanation for the data. This system is separated at approximately 260 metres below ground surface.

In the upper section, above 260 m, the $\delta^{18}O$ values for extracted porewater ranged from −18.0 to −16.2‰ and the $\delta^{2}H$ values ranged from −149 to −143‰. The slope of the linear relationship between $\delta^{18}O$ and $\delta^{2}H$ values was 2.10 with an R^2 value of 0.85. The isotope mixing line intercepted the LMWL at a $\delta^{18}O$ value of −19.7‰. The TDS values for extracted porewater samples ranged from 2 700 to 3 500 mg/L. The mixing line between $\delta^{18}O$ and TDS had an R^2 value of 0.47. A TDS value of 2 500 mg/L was calculated for the formation water above the reservoir.

In the lower section, below 260 m, the $\delta^{18}O$ values for extracted porewater ranged from −17.2 to −13.6‰ and the $\delta^{2}H$ values ranged from −146 to −124‰. The slope of the linear relationship between $\delta^{18}O$ and $\delta^{2}H$ values was 5.79, with a high R^2 value of 0.99. The isotope mixing line intercepted the LMWL at a $\delta^{18}O$ value of −24.1‰. The TDS values for extracted porewater samples ranged from 2 700 to 4 200 mg/L. The mixing line between $\delta^{18}O$ and TDS had an R^2 value of 0.66. A very low TDS value of 80 mg/L was calculated for the reservoir formation water in this well.

4.5.11 Firebag 07-10-095-06W4 (Fig. 4.2l)

This well displayed a clear distinction between formation waters that exist above and below 300 m depth.

In the upper system, above the bitumen reservoir, five porewater samples were taken from 275.3 to 295.6 m below ground surface. The $\delta^{18}O$ values for porewater extracted from this

well ranged from −17.5 to −12.8‰ and the δ^2H values ranged from −146 to −128‰. The slope of the linear relationship between $\delta^{18}O$ and δ^2H values was 3.71, with a high R^2 value of 0.96. The isotope mixing line intercepted the LMWL at a $\delta^{18}O$ value of −20.6‰. The TDS values for extracted porewater samples ranged from 1 700 to 3 200 mg/L. The mixing line between $\delta^{18}O$ and TDS had a high R^2 value of 0.95. A TDS value of 900 mg/L was calculated for the formation water in this well above 300 m.

In the lower section that comprises the bitumen reservoir, three porewater samples were taken from 301.3 to 319.7 m below ground surface. The $\delta^{18}O$ values for porewater extracted from this well ranged from −16.2 to −13.4‰ and the δ^2H values ranged from −137 to −128‰. The slope of the linear relationship between $\delta^{18}O$ and δ^2H values was 3.42, with an R^2 value of 0.86. The isotope mixing line intercepted the LMWL at a $\delta^{18}O$ value of −19.3‰. The TDS values for extracted porewater samples ranged from 2 600 to 3 600 mg/L. The mixing line between $\delta^{18}O$ and TDS was tightly correlated, having an R^2 value of 0.96. A TDS value of 1 500 mg/L was calculated for the reservoir formation water in this well.

4.5.12 Firebag 15-31-094-06W4 (Fig. 4.2m)

Eight porewater samples were taken from this well from 285.7 to 286.9 m below ground surface. There were two outliers having elevated salinity appearing at the bottom of the reservoir, below 285 m depth that were not used in the calculation of formation water TDS and isotope composition. The $\delta^{18}O$ values for porewater extracted from this well ranged from −16.5 to −14.0‰ and the δ^2H values ranged from −142 to −128‰. The slope of the linear relationship between $\delta^{18}O$ and δ^2H values was 5.25, with an R^2 value of 0.95. The isotope mixing line intercepted the LMWL at a $\delta^{18}O$ value of −21.4‰. The TDS values for extracted porewater samples ranged from 2 200 to 3 600 mg/L. The mixing line between $\delta^{18}O$ and TDS had an R^2

value of 0.79. A TDS value of 200 mg/L was calculated for the reservoir formation water in this well.

Figure 4.2 : For each well, $\delta^{2}H$ and TDS are plotted against $\delta^{18}O$ for each individual data point within a sampled well. Measured water isotope data are shown as blue diamonds, and an open diamond indicates the intercept of the LMWL with the isotope mixing line. Red circles indicate TDS data points, and the TDS value at the LMWL intercept is indicated with an open circle. Subsurface depths (m) from which the samples were taken are indicated on the TDS data points. Published McMurray Formation water isotope data (Lemay, 2002; WorleyParsons, 2010b; Gibson et al., 2011) are indicted using orange triangles. The analytical error on each data point is smaller than the marker in both isotope and TDS space.

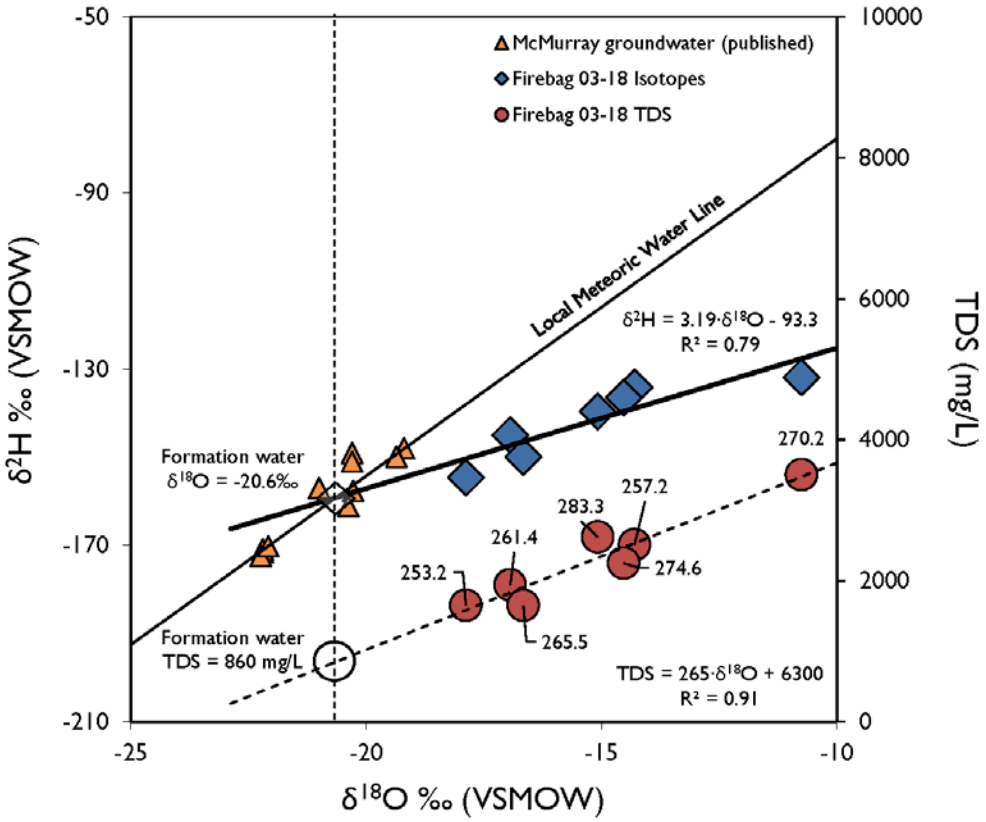

Figure 4.2a: Stable isotope composition and TDS data from well 03-18-095-5W4.

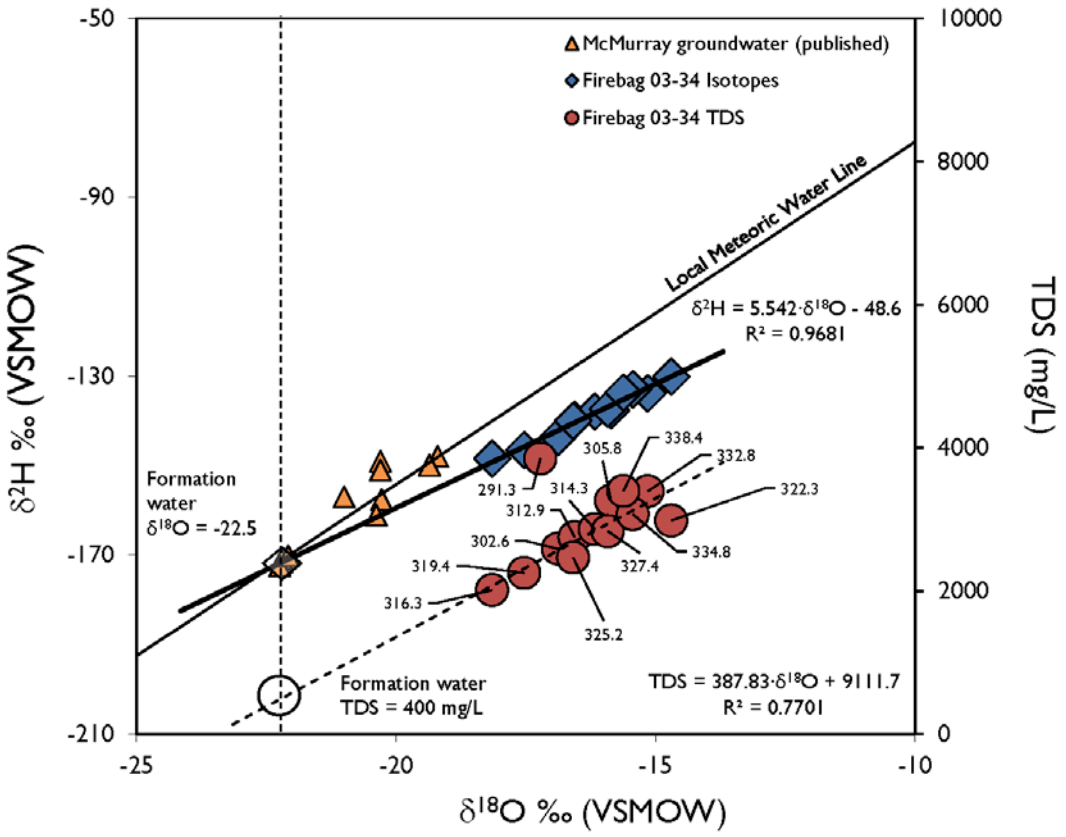

Figure 4.2b: Stable isotope composition and TDS data from well 03-34-094-06W4.

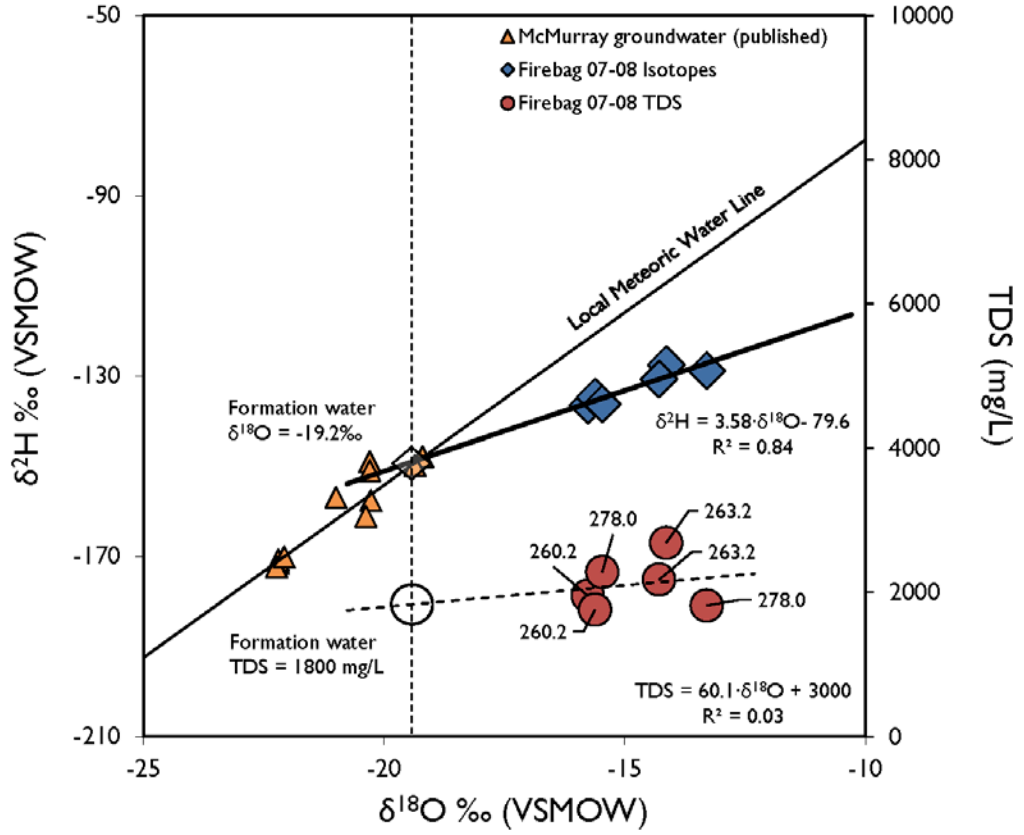

Figure 4.2c: Stable isotope composition and TDS data from well 07-08-095-05W4.

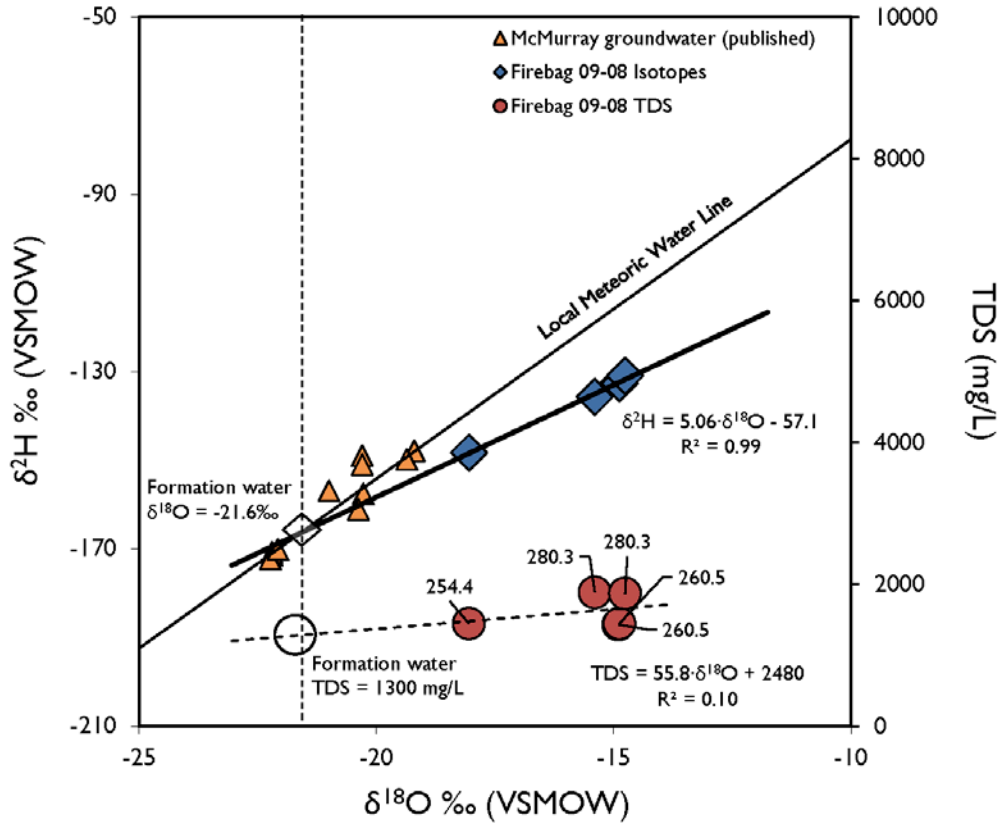

Figure 4.2d: Stable isotope composition and TDS data from well 09-08-095-05W4.

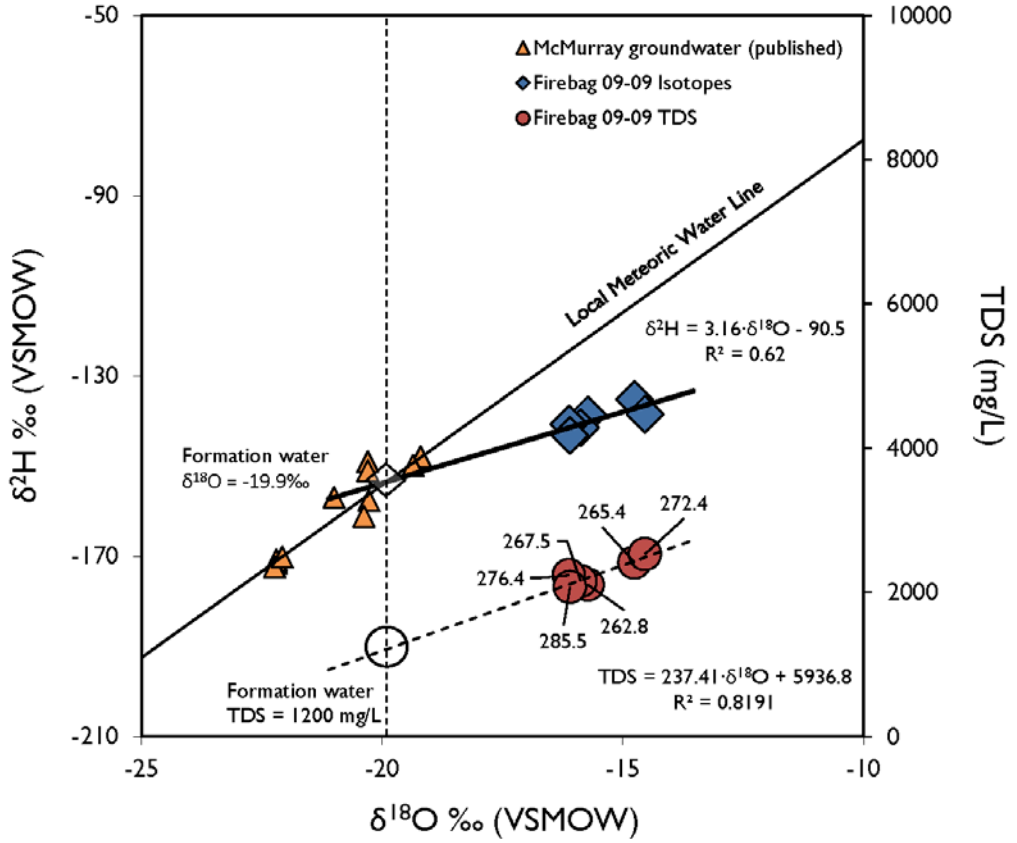

Figure 4.2e: Stable isotope composition and TDS data from well 09-09-095-06W4.

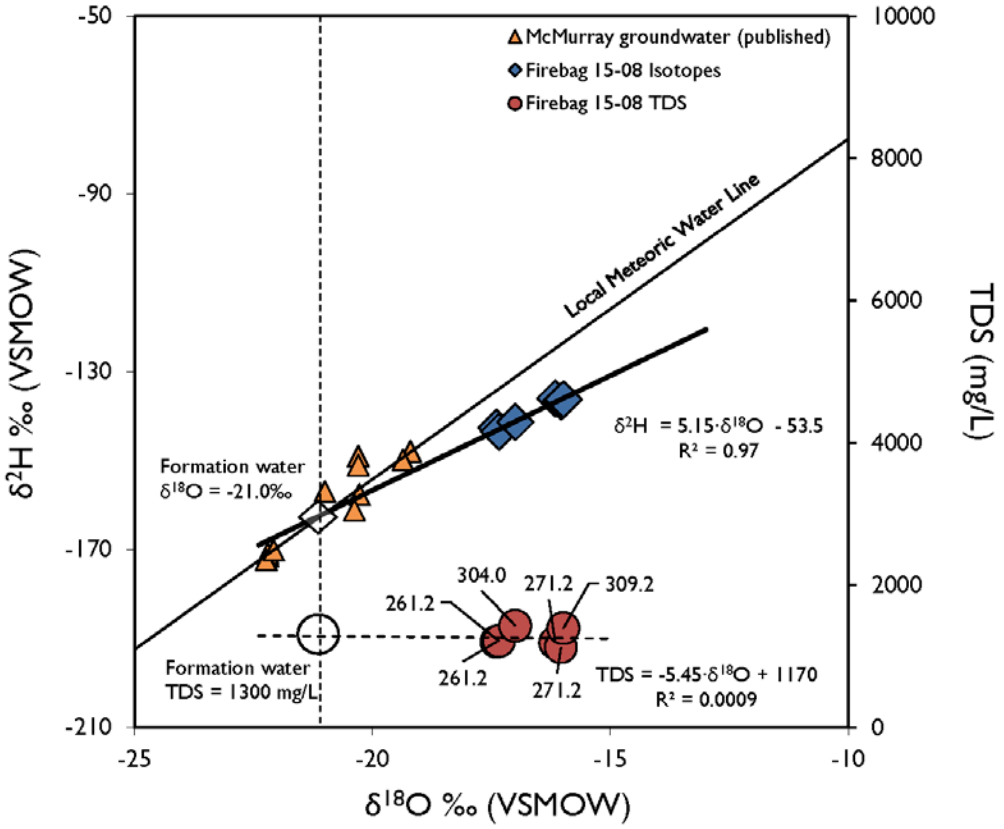

Figure 4.2f: Stable isotope composition and TDS data from well 15-08-095-05W4.

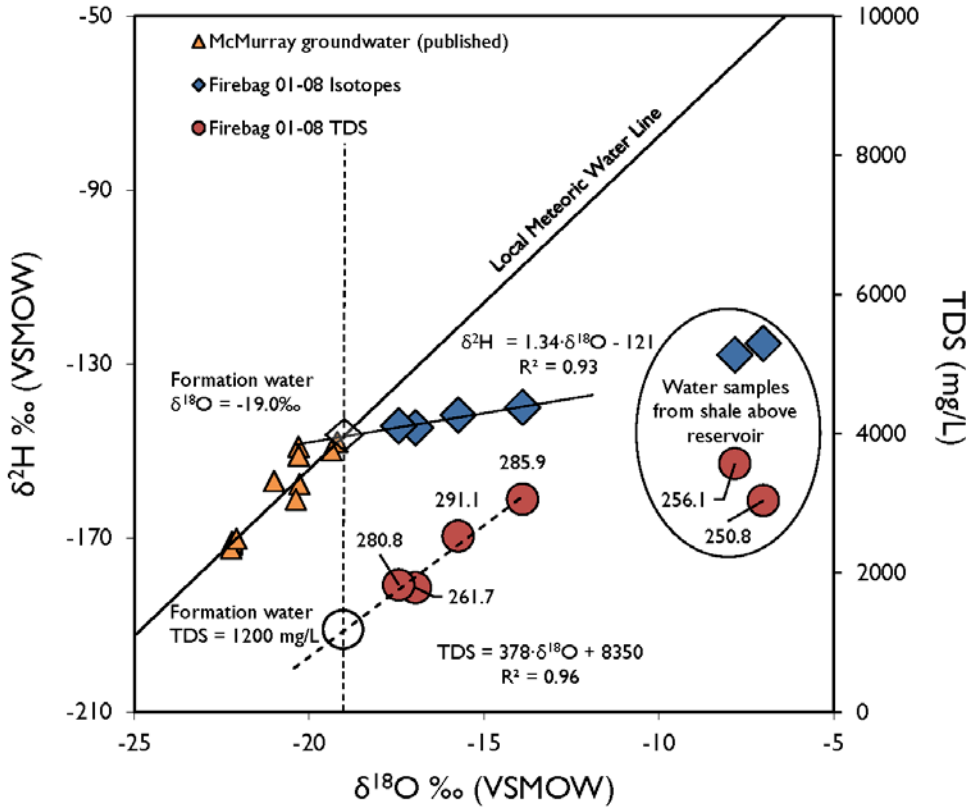

Figure 4.2g: Stable isotope composition and TDS data from well 01-08-095-06W4. The samples at 256.1 and 250.8 m were taken above the bitumen reservoir, and likely represent a change in formation water TDS in these samples.

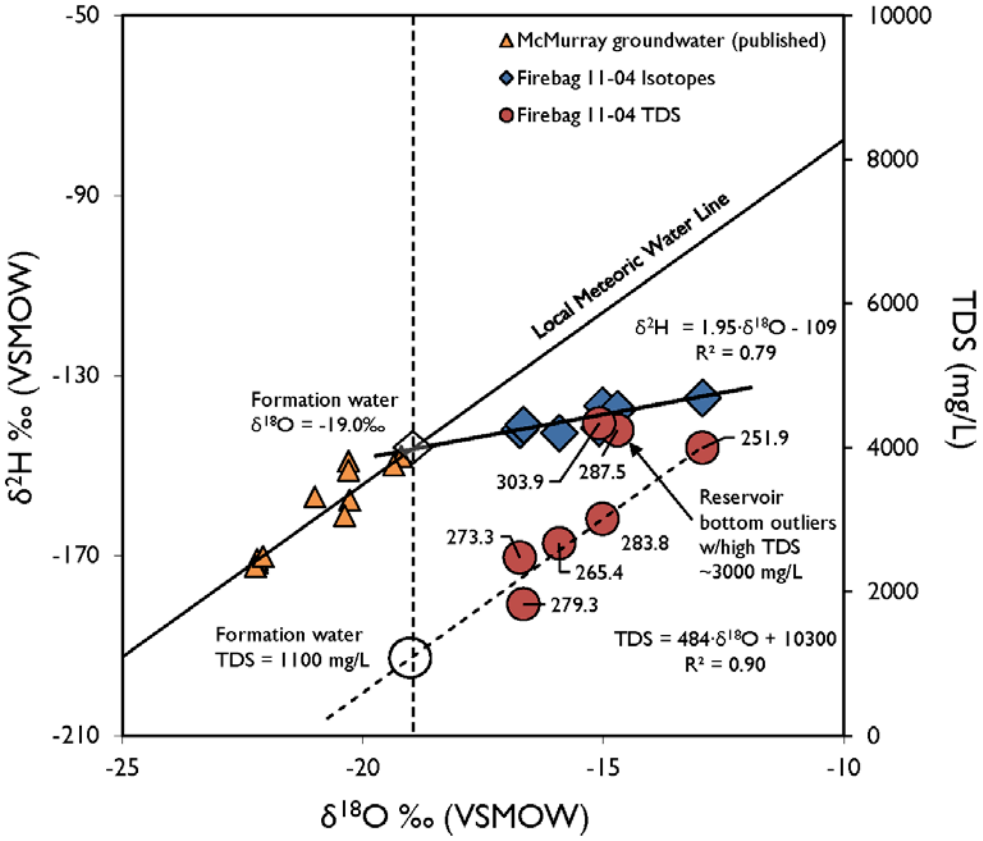

Figure 4.2h: Stable isotope composition and TDS data from well 11-04-095-06W4. The two deepest samples in the reservoir had substantially higher TDS values than the upper part of the well.

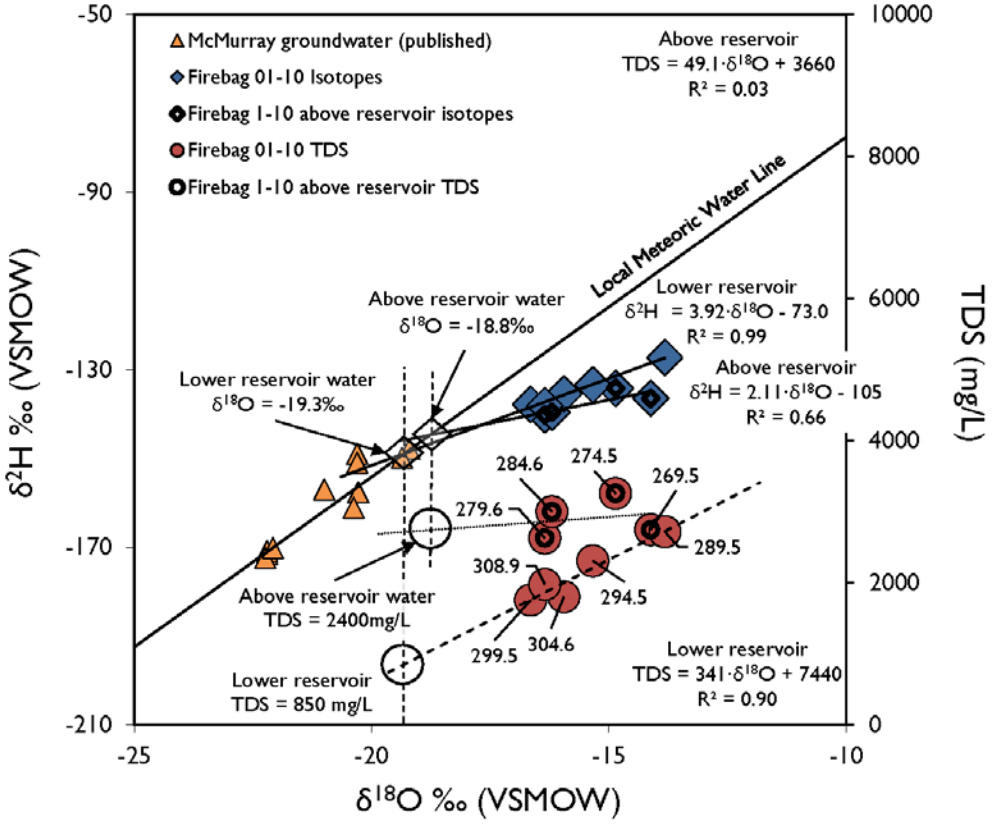

Figure 4.2i: Stable isotope composition and TDS data from well 01-10-095-06W4. Samples from above reservoir are distinguished from the lower reservoir by open black diamonds and circles inside the existing markers for isotopes and TDS.

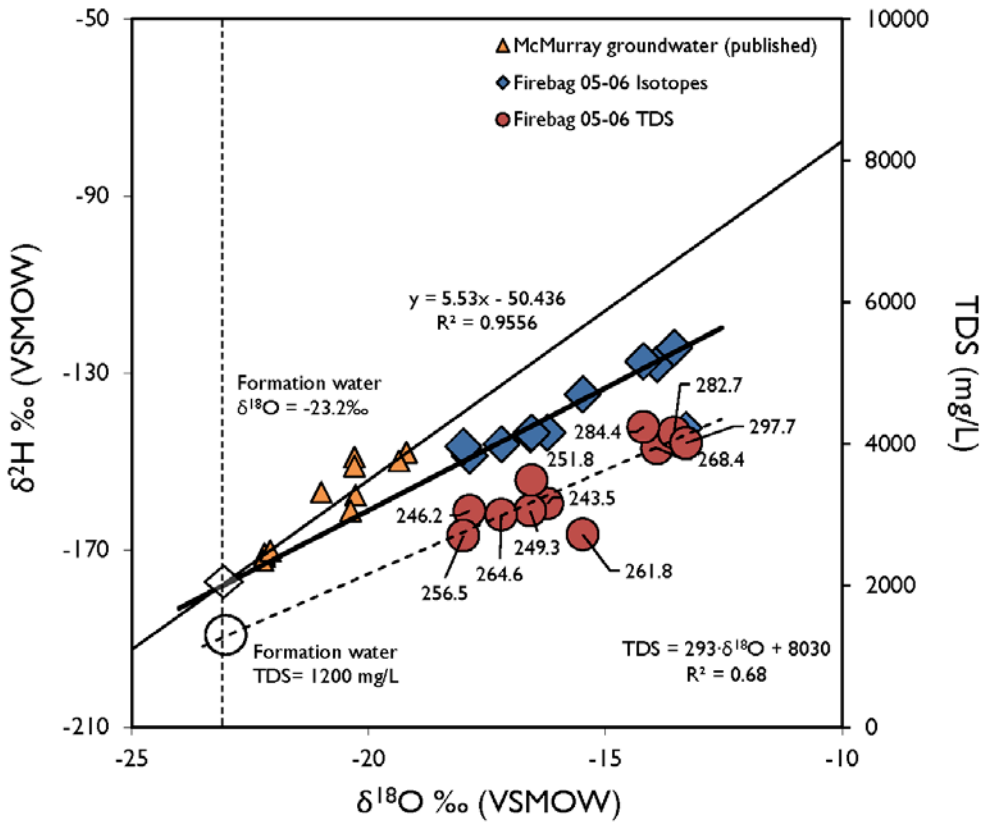

Figure 4.2j: Stable isotope composition and TDS data from well 05-06-095-06W4, presented as a homogeneous reservoir system.

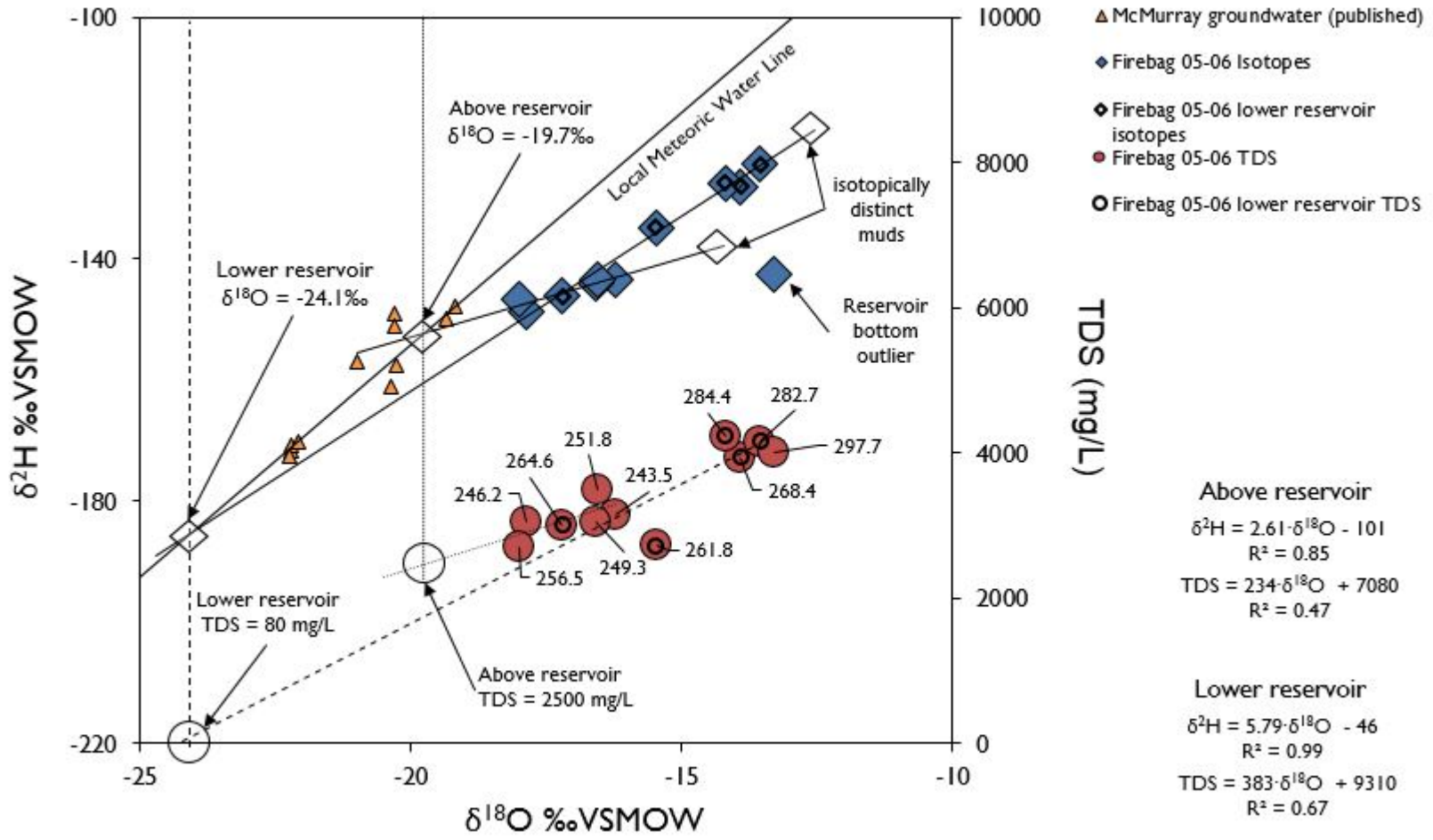

Figure 4.2k: Stable isotope composition and TDS data from well 05-06-095-06W4, presented as a separated water system.

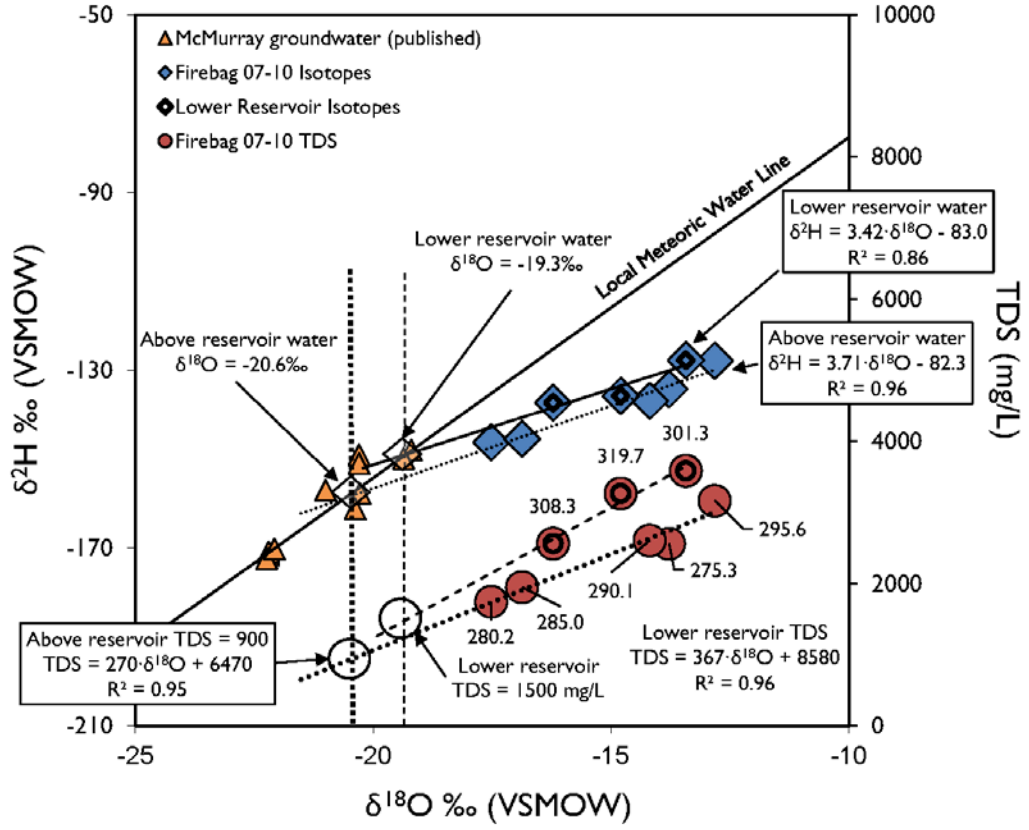

Figure 4.2l: Stable isotope composition and TDS data from well 07-10-095-06W4. Equations for the reservoir below 300 m are presented. Lower reservoir isotope data are distinguished by black diamonds inside the isotope markers.

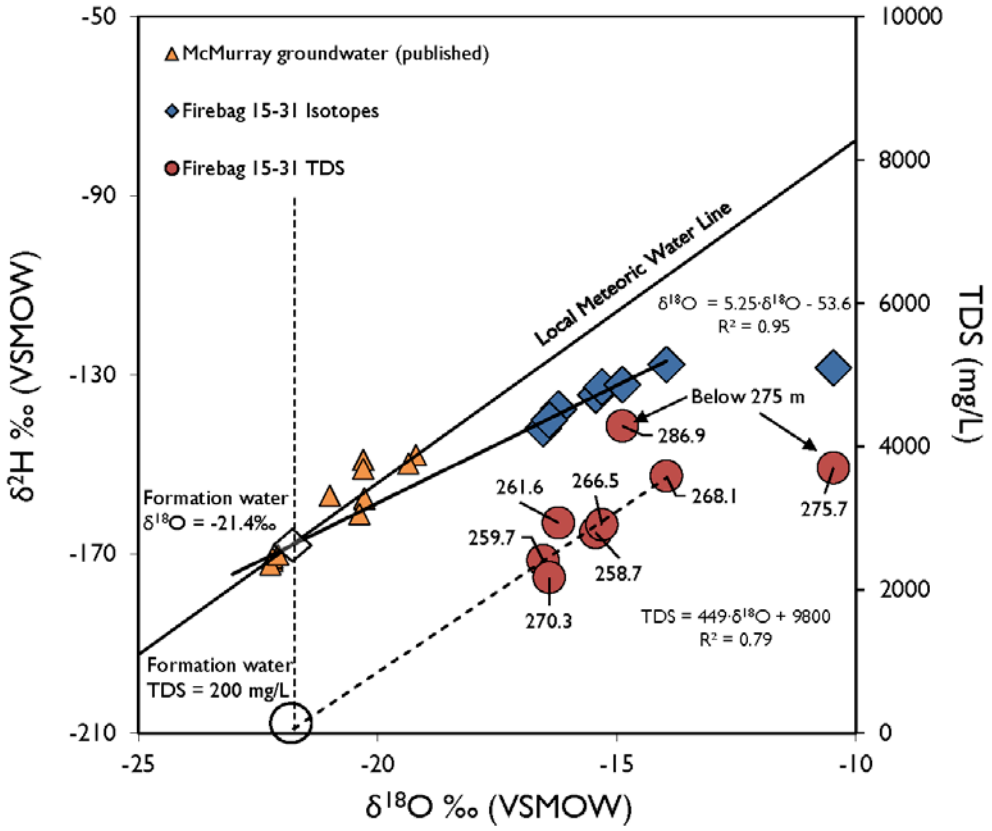

Figure 4.2m: Stable isotope composition and TDS data from well 15-31-094-06W4.

4.5.13 Quaternary groundwater

Two quaternary groundwater samples at Firebag were measured for aqueous geochemistry and stable isotope composition. Q1 had a TDS value of 476 mg/L and Q2 had a TDS value of 409 mg/L. The $\delta^{18}O$ and $\delta^{2}H$ values were −20.0‰, and −154‰ for Q1 and −19.4‰, and −149‰ for Q2 (Table 4.1).

4.5.14 McMurray Formation produced water

Water produced from a SAGD well that had not yet started steam injection yielded a stable isotope composition of the formation waters of −20.2‰ for $\delta^{18}O$ and −157‰ for $\delta^{2}H$ (Table 4.1). The TDS concentration was 1 240 mg/L in the produced water sample.

The sample from well 5P6 was analyzed for tritium concentration to determine if some of this water was recharged into the reservoir in the past fifty years. The measured tritium concentration was determined to be 0.346 ± 0.086 (1σ) TU.

Table 4.1: Geochemical and stable isotope measurements of selected groundwater samples

Sample ID	$\delta^{18}O$ (‰)	$\delta^{2}H$ (‰)	TDS (mg/L)	Na (mg/L)	K (mg/L)	Mg (mg/L)	Ca (mg/L)	Cl (mg/L)	SO_4 (mg/L)	HCO_3 (mg/L)
Quaternary Source Water										
Q1	−20.0	−154	476	11	2	24	72	4	3	361
Q2	−19.4	−149	409	7	1	15	70	4	2	309
McMurray Formation Pre-SAGD Produced well 5P6										
5P6	−20.2	−157	1 226	326	10	4	5	79	5	798

4.6 Discussion

The data generated in this study provide a spatially detailed stable isotope composition and TDS information for McMurray Formation waters at Firebag. Collectively, these results provide a framework for interpretation of hydrogeological processes. There was heterogeneity observed in measured stable isotope compositions and TDS values between wells across the Firebag region, but also within individual wells, suggesting vertical heterogeneity with different water properties within single wells.

4.6.1 Field-scale heterogeneity in stable isotope composition of formation waters

Calculated $\delta^{18}O$ values of McMurray Formation water in the Firebag samples from this study ranged from −19.0‰ to −24.1‰ (n = 12 wells); and the mean value of the twelve sampled wells was −20.5‰ ± 1.4‰ (1σ). The mean McMurray Formation water $\delta^{18}O$ was slightly lower than the average value for Quaternary groundwater in this study (−19.7‰), and lower than that of shallow groundwater in the Athabasca region (−18.9 ± 0.9‰; Lemay, 2002). The lower average $\delta^{18}O$ value of McMurray Formation waters may suggest that reservoir formation water consists of a mixture of recently infiltrated groundwater with a small component of colder temperature groundwater recharge, possibly a remnant of Pleistocene glacial meltwater (Grasby and Chen, 2005).

Across the Firebag lease area, there was variability in $\delta^{18}O$ values in McMurray Formation waters that suggests different amounts of modern recharge throughout the field. A map illustrating the locations of the sampled wells and the properties of their respective formation waters is provided in Figure 4.3. Because groundwater in Quaternary aquifers have higher $\delta^{18}O$ values than existing McMurray Formation waters, continued topographically-driven recharge of modern water should increase the $\delta^{18}O$ value of McMurray Formation water with

greater amounts of groundwater recharge. Shaded boxes on Figure 4.3 indicates reservoir formation water $\delta^{18}O$ values that were higher than −20‰, whereas unshaded boxes indicate $\delta^{18}O$ values in formation waters that were lower than −20‰. The formation water in the centre of the lease area appeared to have higher $\delta^{18}O$ values than formation water toward the field edges, however the observed differences are typically less than 2‰. A possible explanation that is consistent with this spatial trend is that the water in the centre of the Firebag area is recharged with water derived from modern precipitation at a faster rate than water at the edges of the lease, as these values are closer to what was observed in the Quaternary groundwater systems in the AOSR. Thus, higher $\delta^{18}O$ values of McMurray Formation waters at Firebag may be indicative of zones of increased amounts of Holocene groundwater recharge in these areas.

The $\delta^{18}O$ values calculated for McMurray Formation waters in this study are consistent with the range of values observed elsewhere in the Athabasca region for McMurray Formation waters (Fig. 4.4). The mean $\delta^{18}O$ value of the data set from this study (−20.5‰) was identical to the mean of previously published values (−20.6‰) within analytical error (Lemay, 2002; WorleyParsons, 2010b; Gibson et al., 2011). However, the range of $\delta^{18}O$ values calculated in this study (−24.1 to −19.0‰) slightly exceeded the range of published McMurray Formation water $\delta^{18}O$ values (−22.2 to −19.2‰) at both high and low ends of the range (Lemay, 2002; WorleyParsons, 2010b; Gibson et al., 2011). The similarity between the wells in this study, and the published wells from the McMurray Formation suggests similar regional processes by which groundwater reaches the McMurray Formation. Additionally, the mean stable isotope composition calculated by the porewater method ($\delta^{18}O$ = −20.5‰) was similar to the pre-SAGD produced water sample ($\delta^{18}O$ = −20.1‰) obtained from the centre of the field (Figs. 4.3 & 4.4),

providing supporting evidence that the new method for calculating reservoir isotope composition is capable of generating accurate results.

Typically, waters in the McMurray Formation have lower formation water $\delta^{2}H$ and $\delta^{18}O$ values compared with isotope values measured in the Quaternary aquifers, however there is substantial overlap in the respective data ranges of these waters (Fig. 4.4). The waters from this study that were most similar to the Quaternary groundwater at Firebag are spatially located in the central area of the Firebag lease, and shaded gray on Figure 4.3. It is plausible that higher formation water $\delta^{2}H$ and $\delta^{18}O$ values in the McMurray Formation represent areas of increased contribution of Holocene groundwater.

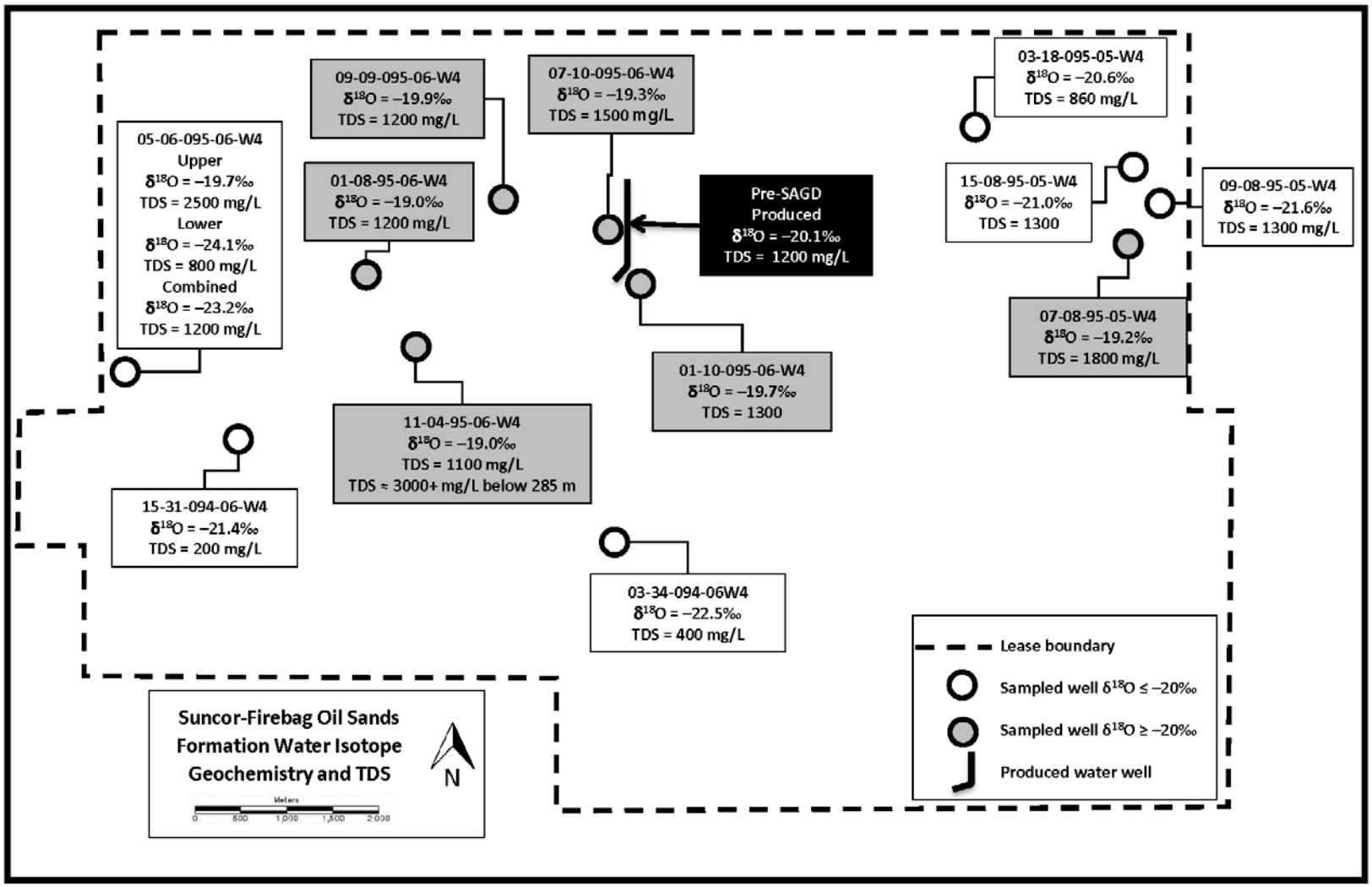

Figure 4.3: Stable isotope composition and TDS of sampled wells in the Firebag region.

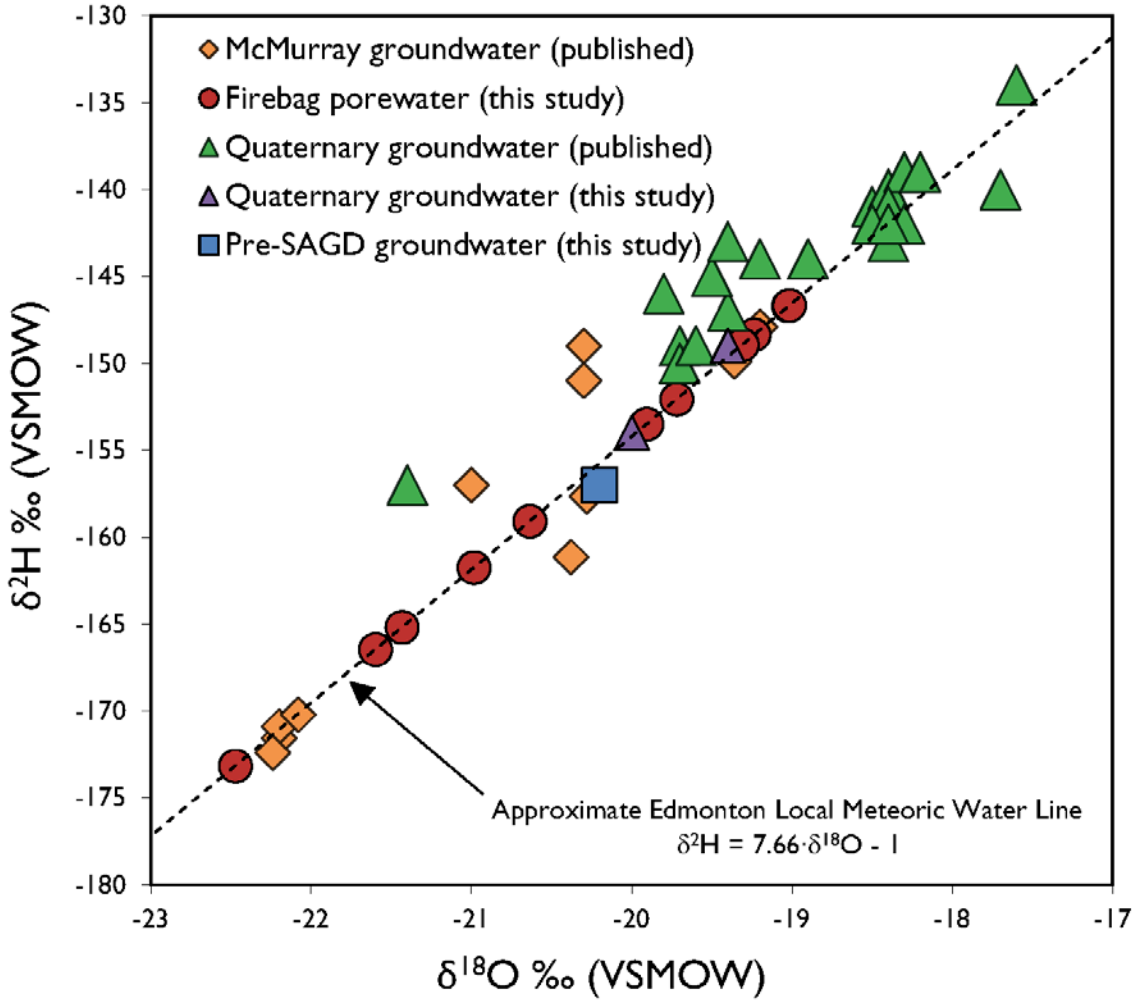

Figure 4.4: Stable isotope compositions of formation waters calculated in this study compared to published values from groundwater samples throughout the Athabasca oil sands region (data sources for published values: Lemay, 2002; WorleyParsons 2010b; Gibson et al., 2011).

4.6.2 Field-scale heterogeneity in total dissolved solids of formation waters

The calculated TDS values for McMurray Formation waters at Firebag ranged from 80 mg/L to a maximum value of 2 500 mg/L. The mean TDS value for the data set was 1 100 mg/L, and the standard deviation of TDS values was 400 mg/L. The range of TDS values observed at Firebag is very small compared to the range of TDS values observed in the McMurray Formation within the Athabasca Oil Sands Region (Chapter Two, AOSR TDS range: 200−279 000 mg/L). In this study, all sampled formation waters at Firebag were within the guideline classification for "non-saline" water as defined by Alberta Environment regulations (TDS < 4 000 mg/L). This range represents a very small amount of heterogeneity in the data set as a whole, and indicates lower formation water salinity than most oil sands lease areas in the Athabasca region (Chapter Two). With the limited heterogeneity in TDS values, it is difficult to draw any substantial conclusions from the data. There were no apparent spatial correlations, or correlations between the calculated formation water $\delta^{18}O$ and TDS values observed. However, the TDS values for formation waters at Firebag are typical for formation waters of surrounding regional McMurray Formation groundwater (Chapter Two). The TDS values calculated by the porewater method are very similar in TDS (mean TDS = 1 100 mg/L) compared with the pre-SAGD produced water sample obtained from the centre of the field that had a TDS value of 1 200 mg/L (Figs. 4.3 & 4.4). The similarity of traditional groundwater sampling and the porewater method provides supporting evidence for the accuracy of TDS values generated by the new technique.

4.6.3 Vertical heterogeneity within wells

While porewaters sampled from several of the wells generated mixing lines for $\delta^{18}O$, TDS and $\delta^{2}H$ between drilling fluid and formation water with high R^2 values through the entire

reservoir, other wells had significant variability that required additional explanation. Significant deviations from the mixing lines in isotope and TDS space were observed in several wells, and these deviations may suggest intra-reservoir heterogeneity, caused by differences in geology, or mixing with a third water source.

In three wells (Figs. 4.2h, 4.2l, and 4.2m), the TDS values increased near the bottom of the reservoir, and in four wells (Figs 4.2b, 4.2g, 4.2i, and 4.2j-k) there was intra-reservoir heterogeneity or higher TDS values near the top of the reservoir. The substantial increases in salinity at the reservoir bottom may suggest that a barrier to freshwater recharge exists in these reservoirs.

In well number 11-04-095-6W4 (Fig. 4.2h) there were two samples with very high salinity compared to the other subsamples from this well, and these were the deepest subsamples from this well. However, it is difficult to interpret two points quantitatively using the porewater technique. A conclusion one could draw from these data is that the lower portion of this well is in connectivity with the sub-Cretaceous system, and therefore has higher salinity in this portion of the reservoir. A qualitative, but conservative estimate of TDS, that assumes a drilling fluid TDS value of 5 000 mg/L, would be that the lower portion of this well below 285 m has a salinity that is greater than 3 000 mg/L. While not as high as the Devonian samples observed elsewhere in the AOSR, 3 000 mg/L is a substantially higher TDS value than any samples observed anywhere else at Firebag, or within the broader Muskeg Mountain region of the AOSR (Chapter Two). Further sampling may assist with quantifying a TDS value with higher precision in this section of the field.

Within well number 07-10-095-6W4 (Fig. 4.2l) there are two distinct mixing trends between drilling mud and formation water that suggest a barrier to water flow in the reservoir at

approximately 300 m depth. The small difference in TDS above and below 300 m in this well does not support the hypothesis of upward flow of highly saline Devonian fluids. However, it is consistent with differences in geology, as the samples above 300 m are shaley components of the Upper McMurray, whereas below the 300 m the bitumen-saturated reservoir sands of the Middle McMurray.

Well 15-31-094-6W4 (Fig. 4.2m) had one high and one low TDS values off the main regression line below 275 m in the reservoir. Theses samples both had smaller initial volumes of water 1.2 and 1.0 mL for 275.7 m and 286.9 m respectively, therefore the scatter may be due to increased analytical uncertainty rather than geological variability.

Well 03-34-94-6W4 (Fig. 4.2b) had one distinct outlier at the top of the reservoir (291.3 m). The 291.3 m sample had measured TDS value of 3 850 mg/L, that was considerably higher than any of the other subsamples. This sample was taken more than 10 m higher in the reservoir than any other subsample in this well, and it is possible that its elevated TDS is due to sampling from a shale bed in this reservoir that has retained higher salinity of its associated waters than the rest of the reservoir.

Well 01-08-095-6W4 (Fig. 4.2g) produced mixing lines with little scatter in isotope space ($R^2 = 0.93$) and TDS space ($R^2 = 0.96$). However, two samples that were taken from shale above the bitumen reservoir at 250.8 and 256.1 m depth had very distinct isotope compositions and TDS from the rest of the reservoir. These samples from the shale beds had $\delta^{18}O$ values that were higher than any of the drilling fluids sampled (Table 3.2) and therefore the TDS values cannot be interpreted in the same way as the samples taken from the bitumen reservoir. These data suggest interesting and distinct geochemical conditions in water derived from shale that requires substantial further investigation to fully comprehend.

The vertical heterogeneity in well 01-10-095-6W4 (Fig. 4.2i) was substantial in both TDS and stable isotope ratios, and had two distinct trends above and below 285 m. The high TDS value was calculated to be 2 400 mg/L in the above-reservoir system, and the low TDS value was calculated to be 850 mg/L in the lower bitumen reservoir system. A low degree of correlation was observed above the reservoir ($R^2 = 0.03$), and a high degree of correlation was observed in the reservoir ($R^2 = 0.90$). Additional sampling of formation waters may be required to unravel the complexity generated above the reservoir, however the lower reservoir data appears to have homogeneous formation water composition.

Finally, the interpretation of well 05-06-095-6W4 (Fig. 4.2j & 4.2k) was difficult due to the apparent presence of multiple drilling fluids. If the reservoir is interpreted as being influenced by only one drilling mud, Figure 4.2j illustrates a unified approach to interpreting the data that result in a TDS value of 1 200 mg/L. However, Figure 4.2k shows that it is plausible that there are two distinct trends in the data, with a shale bed at approximately 260 m depth. The top samples in the reservoir combine to make one distinct regression line between δ^2H and $\delta^{18}O$, intercepting the LMWL at a $\delta^{18}O$ value of −19.7‰, whereas the lower reservoir intercepts the LMWL at −24.1‰. There is presently no reason to favour one interpretation over the other, however the data set for this well suggests a challenge in interpreting this new data that must be accounted for in future studies.

4.6.4 Insights from tritium analysis of formation water

Tritium is a useful tool for investigating groundwater recharged in the last fifty years. Modern tritium values in groundwater range from 5 to 15 TU, however atmospheric nuclear weapons testing provided a spike up to 50 TU or higher for recharge that occurred during the peak atmospheric weapons testing period of the 1960s (Clark and Fritz, 1997). Tritium decays

with a half-life of 12.3 years, resulting its use being limited to waters recharged in only the most recent past (Clark and Fritz, 1997). The single tritium measurement of groundwater at Firebag from the pre-SAGD producing well yielded a very low tritium content of 0.34 TU, suggesting very little influence from waters recharged in the last fifty years, and little mixing contamination from nearby steam injection that uses water from modern shallow aquifers that likely contain tritium in measurable quantities. Qualitative interpretation of tritium values are described in Clark and Fritz (1997) as follows:

< 0.8 TU: sub-modern, recharged prior to 1952

0.8 to 4 TU: mixture between sub-modern and recent recharge

5 to 15 TU: Modern (5 to 10 year recharge)

15 to 30 TU: Some "bomb" ^{3}H present

>30 TU: Considerable recharge from 1960s/1970s

>50 TU: Dominantly 1960s recharge

The expected tritium contents for steam injected water is likely within the 5 to 15 year recharge period, as shallow groundwater is rapidly recharged in the Quaternary strata of the Athabasca region (Lemay, 2002; Gibson et al., 2011). It would be unexpected to find naturally recharged tritium-containing waters in the McMurray Formation, except possibly where a Quaternary channel has penetrated the cap rock of the McMurray Formation and recent infiltration has occurred. Alternatively, tritium content above 0.8 TU may indicate contamination of formation water by steam injection, because steam is derived from a shallow groundwater source that has likely received meteoric recharge in the past fifty years. The low tritium content in the sampled well from Firebag suggests that any infiltration from modern groundwater

recharge occurred primarily before 1950, although little can be gleaned from a single preliminary measurement.

4.7 Conclusions

This is the first study to utilize the porewater technique described in Chapter Three to calculate stable isotope composition and TDS of porewater obtained from drill core within an oil sands field. Stable isotope ratios of extracted porewater from drill core enabled the calculation of formation water TDS, $\delta^{18}O$, and $\delta^{2}H$ values in the Firebag region laterally across the lease area, and vertically within a single reservoir drill core, resulting in a three-dimensional characterization of formation water in an oil sands lease area. The new method is consistent with regional geochemical and isotopic trends obtained by traditional well sampling techniques, suggesting accurate results were obtained by the new method. Changes in formation water TDS and stable isotope composition were observed between wells over a geographical scale of several kilometres, and within wells on a vertical scale of 10s of metres. The major conclusions of this work are summarized below:

1. McMurray Formation waters at Firebag are mainly homogeneous in TDS and stable isotope composition compared to the distribution of values in the McMurray Formation across the Athabasca Oil Sands Region. The McMurray Formation waters at Firebag had a mean TDS of 1 100 mg/L, with a standard deviation of ± 400 mg/L, and a mean $\delta^{18}O$ value of -20.5 ± 1.4‰. In the centre of the Firebag lease area, the lower $\delta^{18}O$ values may indicate greater Holocene recharge than the amount or recharge occurring around the edges of the lease area. The stable isotope composition of Firebag waters is indicative of primarily Holocene recharge with potentially a minor component of subglacial meltwater associated with the Pleistocene glaciation.

2. The porewater technique is possibly capable of identifying changes in formation water chemistry within a single reservoir that may be due to changes in geology via transitions from above-reservoir shales to within-reservoir bitumen-saturated sands (01-10-095-6W4, 07-10-095-06W4M).

3. Water obtained from a SAGD-producing well prior to start of steam operations had similar TDS, $\delta^{2}H$ and $\delta^{18}O$ values to waters generated by the porewater method. Water from this well had a $\delta^{18}O$ value of −20.1‰ that was lower than shallow groundwater, and a TDS value of ≈ 1 250 mg/L that was higher than overlying shallow groundwater. Its tritium content of 0.34 TU was consistent with no groundwater recharge in the McMurray Formation in the last 50 years.

4.8 References

Andriashek and Atkinson (2007). *Buried Channels and Glacial-Drift Aquifers in the Fort McMurray Region, Northeast Alberta.* EUB/AGS Earth Science Report 2007-01. 170 pp.

Archie, G.E. (1942). The electrical resistivity log as an aid in determining some reservoir characteristics. *Petroleum Transactions of AIME* **146**: 54–62.

Bachu, S. and Underschultz J.R. (1993). Hydrogeology of formation waters, northeastern Alberta. *AAPG Bulletin, 77*(10), 1745–1768.

Berthold, S., Bentley, L.R., and Hayashi, M. (2004). Integrated hydrogeological and geophysical study of depression-focused groundwater recharge in the Canadian prairies. Water Resources Research 40(6): W0605 1–14.

Broughton, P. L. (2013). Devonian salt dissolution-collapse breccias flooring the Cretaceous Athabasca oil sands deposit and development of lower McMurray Formation sinkholes, northern Alberta Basin, Western Canada. *Sedimentary Geology*, 283(C), 57−82.

Clark, I., and Fritz P., (1997) *Environmental isotopes in hydrogeology*. Lewis Publishers: New York. 328pp.

Ford D., and Williams, P., (2007). *Karst Hydrogeology and Geomorphology*. John Wiley and Sons Inc.

Gibson, J. J., Birks, S. J., Moncur, M., Yi, Y., Tattrie, K., Jasechko, S., et al. (2011). Isotopic and Geochemical Tracers for Fingerprinting Process-Affected Waters in the Oil Sands Industry: A Pilot Study. *Oil Sands Research and Information Network*, 1−120.

Government of Alberta, Department of Energy (2013). *Alberta's Oil Sands*. Available online: http://www.energy.gov.ab.ca/OilSands/pdfs/FactSheet_OilSands.pdf

Gue, A. (2012). *The geochemistry of saline springs in the Athabasca oil sands region and their impact on the Athabasca and Clearwater rivers*. M.Sc. Thesis, University of Calgary: Gallagher Library.

Gushor Inc. (2013). *The Plunger(tm), patent pending*. Retrieved online April 11, 2013: http://gushor.com/file/page/plunger/plunger.pdf.

Grasby, S., & Chen, Z. (2005). Subglacial recharge into the Western Canada Sedimentary Basin - Impact of Pleistocene glaciation on basin hydrodynamics. *Geological Society of America Bulletin*, 117(3-4), 500−514.

Grasby, S.E., Osborn, J., Chen, Z., Wozniak, P.R.J. (2010). Influence of till provenance on regional groundwater geochemistry. *Chemical Geology* 273: 225–237.

International Atomic Energy Agency (2013). *Global Network of Isotopes in Precipitation data: Edmonton*. Retrieved online July 9, 2013: http://www-naweb.iaea.org/napc/ih/IHS_resources_isohis.html

Lemay, T. (2002). *Geochemical and Isotope Data Formation Water from Selected Wells, Cretaceous to Quaternary Succession, Athabasca Oil Sands (In Situ) Area, Alberta.* Alberta Energy and Utilities Board, 1−71.

National Climate Data and Information Archive (2013). Fort McMurray Climate Statistics. Avaialble online July 1, 2013: http://climate.weatheroffice.gc.ca/climate_normals/ station_metadata_e.html?StnId=2519

Norman Einstein (2006). Athabasca Oil Sands map. Wikimedia Commons: retrieved online March 8, 2009: http://commons.wikimedia.org/wiki/File:Athabasca_Oil_Sands_map.png Worldwide public domain image.

Rubin, E., Winter, T., and Garner, D.L. (2009). Simulation-Based Forecasting of Oilsands SAGD Performance with Thief Zones and Barrier Risks. *Gussow Geoscience Conference*, October 5−7 2009, Banff, Alberta.

Schlumberger Limited (2013). *Downhole sampling*. Retrieved July 31, 2013: http://www.slb.com/services/characterization/testing/reservoir_sampling/downhole_sampling.aspx

WorleyParsons. (2010a). Regional Groundwater Quality Study and Monitoring Network Design in the Athabasca Oil Sands: Phase 1 (No. 2007-0039) Regional Municipality of Wood Buffalo: *Cumulative Environmental Management Association*, Fort McMurray, AB. 157 pp.

WorleyParsons. (2010b). Regional Groundwater Monitoring Network Implementation in the Northern Athabasca Oil Sands (NAOS) Phase 2 - Program Summary. Regional Municipality of Wood Buffalo: *Cumulative Environmental Management Association*, Fort McMurray, AB., 1–493.

Chapter Five: Influence of Aqueous Geochemistry on Methanogenesis in Alberta Oil Sands Microcosms

5.1 Abstract

This study examined the relationship between water chemistry and biogeochemical activity in the Alberta oil sands using a bench-scale experiment. The biodegradation of light oil over geological time via methanogenesis has been proposed to be an important post-emplacement alteration process of the oil sands reserves in western Canada. Methanogenesis is common in many shallow hydrocarbon reservoir systems and is thought to be a central process in the geological history of Alberta's oil sands. Shallow hydrocarbon reservoir environments are favorable to methanogenic communities that require low temperature, moderate pH and reducing geochemical conditions to conduct their metabolic processes. In the McMurray Formation, the predominant Athabasca oil sands reservoir, formation water geochemistry is variable and salinity ranges from freshwater to brine (Chapter Two). Furthermore, quaternary-aged glacial channels have brought fresh groundwater into contact with some parts of the oil sands deposits since the last glaciation, possibly stimulating increased methanogenic activity in oil sands reservoirs. Therefore the relationship between microbial processes and aqueous geochemistry requires investigation to gain insight into potential mechanisms and rates of hydrocarbon biodegradation and methane formation in oil sands systems.

Laboratory cultures of methanogenic communities were grown on an oil sands substrate with three different aqueous geochemical compositions that are typical of the Athabasca region. Methane generation rates, microbial community composition and stable isotope geochemistry of the carbon and sulfur systems were determined over twelve months to assess the influence of variable salinity on biodegradation of oil sands via methanogenesis.

Microbial methane generation was variable among replicates with similar chemical water compositions. However, mean methane generation rates were higher in brackish and freshwater enrichment cultures than in saline cultures. Carbon isotope measurements indicated acetoclastic methanogens were dominant, however a component of CH_4 generated by CO_2 reduction was also prevalent in each replicate. A mixed methanogenic community was most likely active in all three geochemical variants. Sulfur isotope data suggested that bacterial sulfate reduction (BSR) is a likely process in the saline cultures where sulfate concentrations were elevated. However, in the cultures with active BSR, methanogenesis was not completely inhibited.

Based on these experiments, the geochemical makeup of the water in oil sands formation is likely a major control on the amount of biodegradation and methanogenesis in the Athabasca oil sands area.

5.2 Introduction

The oil sands of northern Alberta are comprised of severely biodegraded petroleum systems, and methanogenesis by a microbial consortium of bacteria and archaea is hypothesized to be the dominant biodegradation process for degrading light oil to bitumen over geologic time (Head et al., 2003; Larter et al., 2003; Larter et al., 2006; Jones et al., 2007; Bennett et al., 2013). The biochemical pathways under which biodegradation occurs anaerobically have become more thoroughly understood over the past several decades (van der Linden and Thijsse, 1965; Atlas, 1981; Leahy and Colwell, 1990; Watkinson and Morgan, 1990; Atlas and Bartha, 1992; Cerniglia, 1992; Atlas, 1995; van Beilen and Funhoff, 2007; Aitken et al., 2013). The time period required for removal of 10% of the alkane fraction from an oil column range from 1–5 Ma for a light oil column and up to 10 Ma for equivalent biodegradation in a heavy oil column (Larter et al., 2006). Microbes responsible for anaerobic biodegration of hydrocarbons require moderate temperatures, below 80 ºC (Zengler et al., 1999; Wilhelms et al., 2001; Adams et al., 2006; Jones et al. 2007); however, methanogenic biodegradation may also be hampered by elevated salinity in formation waters (Waldron et al., 2008; McIntosh, 2011).

There are two primary pathways by which methane can be generated from other carbon sources by methanogenic archaea. CO_2 reduction (hydrogenotrophic methanogenesis, Eq. 1) converts hydrogen and CO_2 into methane, and acetate fermentation (acetoclastic methanogenesis, Eq. 2) breaks down small organic molecules into methane and CO_2. These reactions proceed by the following simplified reactions:

$$4H_2 + CO_2 \rightarrow CH_4 + 2H_2O \qquad [1]$$

$$CH_3COO^- + H^+ \rightarrow CH_4 + CO_2 \qquad [2]$$

Both methanogenic pathways can be inhibited by high water salinity, however, the microbes that carry out acetoclastic methanogenesis are more sensitive to high salinity than hydrogenotrophic microbes. Elevated chloride concentrations ([Cl] > 35 g/L) have been demonstrated to inhibit acetoclastic methanogenesis, and these high levels of chloride have been observed in several oil sands reservoirs in Alberta (Waldron et al., 2008; Chapter Two). The upper limit for methanogenic CO_2 reduction in hydrocarbon systems has been proposed to be 126 g/L Cl, and this level of salinity has been found in one oil sands reservoir in Alberta (Waldron et al., 2008, Chapter Two).

The formation waters in the Athabasca oil sands regions (AOSR) are hydrochemically complex, and range in salinity from sodium-chloride brines with 270 g/L total dissolved solids, and 170 g/L Cl, to relatively fresh sodium bicarbonate type waters with less than 1 000 mg/L total dissolved solids and 0.2 g/L Cl (Chapter Two, this thesis). This variability can be observed over a geographic area of less than ten kilometres in some locations (Chapter Two, this thesis). Many shallow reservoirs in the AOSR are thought to be influenced by interactions with shallow groundwater through channels incised during the Pleistocene deglaciation events and infilled with Quaternary sediments (Andriashek and Atkinson, 2007). These channels may provide conduits for lower salinity waters into oil sands reservoirs over Holocene time scales (Andriashek and Atkinson, 2007; Lemay 2002). Below the McMurray Formation, upward flow of sulfate-rich brines from Devonian formations (Gue, 2012) can occur through karst-style conduits (Chapter Two; Broughton, 2013) providing a sulfate source to oil sands reservoirs. Furthermore, it has been hypothesized that the entire Athabasca oil sands regional hydrogeological system was impacted by a large influx of glacial meltwater during the Pleistocene epoch (Grasby and Chen, 2005). This influx of low salinity meltwater and in situ or

external nutrients (Oldenburg et al., 2006) may have exerted a significant impact on the modern rates of biodegradation of bitumen and natural gas generation in areas where freshwater displaced deep formation brines.

Stable isotopes can provide critical insight into methanogenic processes in environmental systems. Whiticar (1999) provided a comprehensive overview of the stable isotope ratios associated with methane of both biogenic and thermogenic origin in natural systems. Typically methane derived from thermal degradation of organic matter has δ^2H values that range from −250 to −100‰ and $\delta^{13}C$ values that range from −55 to −25‰ (Whiticar, 1999; Fig 5.1). Biogenic methane produced via the CO_2-reduction pathway has very low $\delta^{13}C$ values, ranging from −110 to −60‰, and methane produced via acetate fermentation has intermediate $\delta^{13}C$ values ranging from −65 to −50‰ (Fig. 5.1) (Gelwicks et al., 1994). Methanogenesis by CO_2 reduction can also have a substantial effect on the carbon isotope ratios of CO_2. As methanogenesis consumes CO_2 and partitions the light isotopes into CH_4, the $\delta^{13}C_{CO2}$ value increases to maintain isotope mass balance with the low $\delta^{13}C$ values of the methane. Thus, in a closed system, as methane is generated by CO_2 reduction, the $\delta^{13}C$ value of CO_2 will increase from its baseline value.

Hydrogen isotope ratios of biogenic methane are closely related to the hydrogen isotope ratio of the water from which it is produced. During CO_2 reduction all four hydrogen atoms of methane are derived from water (Whiticar, 1999). Equation 3 describes the relationship of hydrogen isotope ratios of water to that of methane generated by CO_2 reduction (Whiticar, 1999):

$$\delta^2H_{CH4} = \delta^2H_{H2O} - \beta \qquad [3]$$

The value β in this equation represents an empirically observed fractionation value for CO_2 reduction in natural systems, typically 160‰ (Whiticar, 1999).

Equation 4 describes the hydrogen isotope composition in methane generated by acetate fermentation (Whiticar, 1999):

$$\delta^2H_{CH4} = [(f_{methyl} \times \delta^2H_{methyl}) + (f_{H2O} \times \delta^2H_{H2O})] - \beta \quad [3]$$

The f_{methyl} value represents the fraction of methane hydrogen atoms derived from the methyl group of acetate and the f_{H2O} value represents the fraction of hydrogen atoms derived from addition of the final hydrogen atom onto the methyl group. Values for f_{methyl} and f_{H2O} are 0.75 and 0.25 respectively, as three hydrogen atoms are derived from the methyl group of the acetate, and one is derived from the final hydrogen molecule added to the methane product, typically considered to be derived from water (Whiticar, 1999). While the emprical fractionation factor β is less well constrained for fermentation reactions than CO_2 reduction, a typical value for β is large, and ranges from 300 to 370‰ (Whiticar 1999). δ^2H_{methyl} values are variable, and can range from −150 to −50‰ depending on the source of organic carbon (Schimmelmann et al., 2006; Whiticar, 1999). The isotope value of the final hydrogen atom added to the methane is more difficult to measure, and may depend on the activity of dissolved hydrogen in water (Burke, 1993; Sugimoto and Wada, 1995). Also associated with fermentation is the possibility of hydrogen isotope exchange with water, however how much exchange may be occurring remains uncertain (Whiticar, 1999). While the details of hydrogen incorporation into methane by acetate fermentation remain mechanistically unconstrained, the δ^2H values from fermentation are typically more negative than those for methane formed by CO_2 reduction. Thus by measuring stable isotope ratios of carbon and hydrogen in methane, the origin of the gas can be determined

and information can be gleaned about the biochemical processes occurring in an environmental system.

The objective of this study was to measure differences in rates and pathways of methanogenesis in bench-scale oil sands microcosms using chemical and isotopic parameters. It was hypothesized that lower water salinity would be more favorable for methanogenesis in oil sands; and conversely that elevated salinity conditions would slow the microbial generation of methane. Understanding how microbial communities are impacted by variable formation water geochemistry at a laboratory scale is the first step toward identifying large-scale variability in biodegradation levels across the Alberta oil sands regions. By studying the impacts of aqueous geochemistry on methenogenesis in oil sands microcosms, this study aimed to provide a framework for future studies linking hydrochemistry and biodegradation in the AOSR.

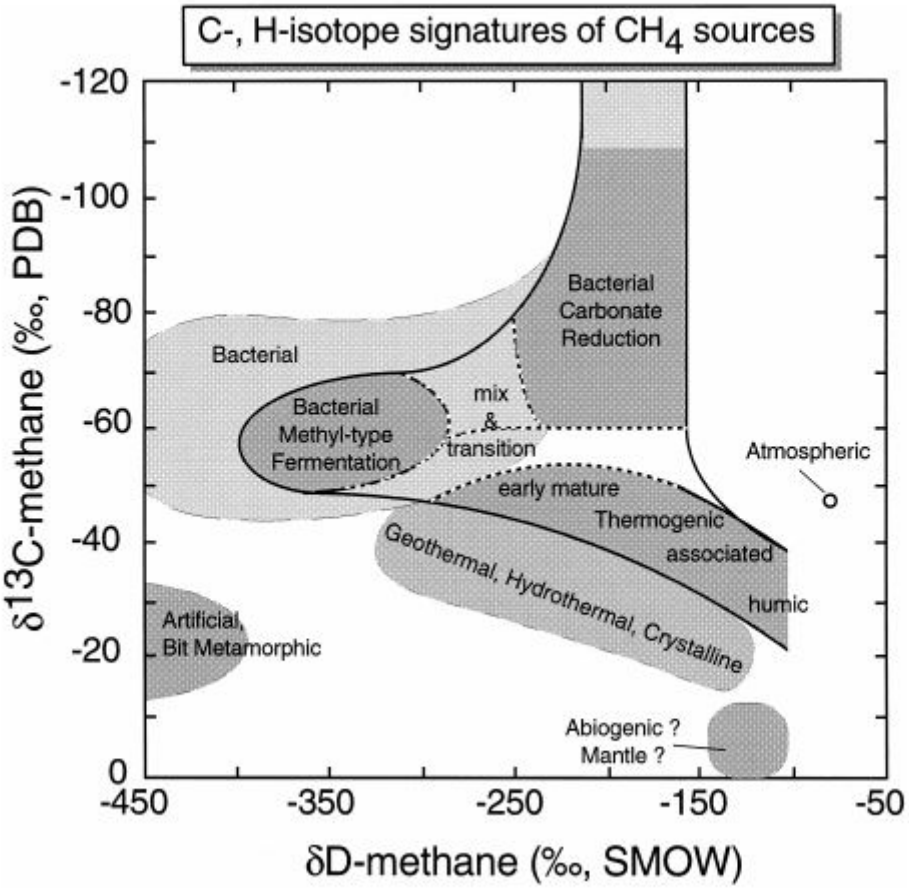

Figure 5.1: Stable isotope ratios of hydrogen and carbon in methane from biogenic and thermogenic sources (from: Whiticar, 1999).

5.3 Methods

5.3.1 Microcosm preparation

Three types of aqueous media, representative of oil sands formation water chemistry in the Athabasca Oil Sands Region (Chapter Two), were created and are designated "Fresh", "Brackish", and "Saline" throughout this chapter. Each type of media was created in bulk in four litre flasks. Fresh media consisted of 1.8 L distilled water, 0.75 g NaCl, 75 mL Pfennig I (10 g/L K_2HPO_4), 75 mL Pfennig II (6.6 g/L $MgCl_2$-$6H_2O$; 8.0 g/L NaCl; 8.0 g/L NH_4Cl; 1.0 g/L $CaCl_2$-$2H_2O$), 15 mL Wolin metals (0.5 g/L EDTA; 3.0 g/L $MgSO_4$; 0.5 g/L $MnSO_4$-H_2O; 1.0 g/L NaCl; 0.1 g/L $CaCl_2$**.**$2H_2O$; 0.1 g/L $ZnSO_4$**.**$7H_2O$; 0.1 g/L $FeSO_4$**.**$7H_2O$; 0.01 g/L $CuSO_4$**.**$5H_2O$; 0.01 g/L Na_2MoO_4**.**$2H_2O$; 0.01 g/L H_3BO_3; 0.005 g/L Na_2SeO_4; 0.003 g/L $NiCl_2$**.**$6H_2O$), 15 mL Balch vitamins (2.0 mg/L biotin; 2.0 mg/L folic acid; 10.0 mg/L pyridoxine-HCl; 5.0 mg/L thiamine-HCl; 5.0 mg/L riboflavin; 5.0 mg/L nicotinic acid; 5.0 mg/L DL calcium pantothenate; 0.1 mg/L vitamin B12; 5.0 mg/L PABA; 5.0 mg/L lipoic acid; 5.0 mg/L mercaptoethane-sulfonic acid (MESA), and 1.5 mL of Resazurin. Brackish media consisted of 1.8 L distilled water, 7.5 g NaCl, 75 mL Pfennig I, 75 mL Pfennig II, 15 mL Wolin metals, 15 mL Balch vitamins and 1.5 mL Resazurin. Saline media consisted 1.8 L distilled water, 30 g NaCl, 7.5 g $NaHCO_3$, 4.5 g $MgCl_2$-$6H_2O$, 0.22 g $CaCl_2$-$2H_2O$, 6.0 g Na_2SO_4, 0.37g NH_4Cl, 0.29 g KH_2PO_4, 0.75 g KCl, 15 mL Wolin metals, 15 mL Balch vitamins, and 1.5 mL Resazurin. All media types were pH adjusted to 7.0 using NaOH, and boiled for one hour. Media were subsequently cooled under a stream of 80:20 N_2:CO_2 gas to prevent oxygenation. The final geochemical composition of each water type is presented in Table 5.1.

For each geochemical condition, twelve microcosms, and six controls were prepared in an anaerobic chamber, for a total of thirty-six replicates and eighteen control samples.

Microcosms were prepared in sterile 120 mL serum bottles. In each microcosm, 95 mL of aqueous media, and 50 ± 1 grams of homogenized Cold Lake oil sands material was added. Initial headspace gas was a mixture of 90% N_2 and 10% CO_2. Finally, each bottle was augmented with 2 mL of microbial culture derived from a petroleum-degrading mixed methanogen enrichment culture subsisting on a 2,6-dimethylbenzene carbon source derived from the same consortium as used by Berdugo-Clavijo et al. (2012).

Three types of control samples were created in duplicate for each geochemical condition. Media-only controls (no microbes, no oil sands −M/−OS) contained only the sterile aqueous media. Microbes, no oil sands controls (+M/−OS) were augmented with the mixed methanogen culture, but did not contain any oil-sands substrate. Oil-sands controls (−M/+OS) consisted of media and oil sands, but were not augmented with the microbial enrichment culture.
The experiment was conducted over an approximate one-year period, with samples taken at experiment start, 0 weeks (T0), 11 weeks (T1), 22 weeks (T2), 35 weeks (T3) and 49 weeks (T4).

5.3.2 Aqueous geochemistry and stable isotope analysis

Samples for aqueous geochemistry were taken from each bottle at the T0, T2 and T4 time steps. Using a sterile syringe needle, 2 mL of water was drawn from each bottle and filtered using a 0.45 µm syringe tip filter. Geochemical sampling for concentrations of major cations (Na, K, Mg, Ca) was conducted by ICP-OES. Major anion concentrations (Cl, SO_4, NO_3) were determined using an ion chromatography system (Dionex ICS 2000).

5.3.3 Stable isotope composition of water

Stable isotope ratios of hydrogen and oxygen in the microcosms were measured on a Los Gatos Research laser isotope analyzer. δ^2H_{H2O} and $\delta^{18}O_{H2O}$ values are normalized using internal

laboratory water standards that have been calibrated against international reference materials VSMOW, VSLAP & VGISP. USGS LIMs was used for drift correction and normalization. Water isotope ratios are reported in delta notation relative to the VSMOW international standard:

$$\delta^{2}H \text{ or } \delta^{18}O\ (‰) = [R_{sample} / R_{standard} - 1] \times 1000 \qquad [4]$$

Where R represents the measured ratio of $^{2}H/^{1}H$ or $^{18}O/^{16}O$.

Accuracy and precision of $\delta^{2}H$ measurements are generally better than ±1.0‰ for replicate measurements of 50 laboratory standards. Oxygen isotope ratios of water were not used in this study.

5.3.4 Headspace methane concentration measurement

Headspace methane concentrations were measured at all five time steps using a Varian gas chromatograph equipped with a flame ionization detector. Using a sterile needle, 0.1 mL of headspace gas was removed from each bottle and injected into the injection port. Gas chromatograph system parameters were as follows: inlet temperature 150 ºC, oven temperature 30 ºC, detector temperature 250 ºC. Methane concentration measurements, measured in mole percent headspace concentration, were calibrated against external standards for which reproducibility was 10% relative to the measured value.

5.3.5 Headspace stable isotope measurements

Stable isotope ratios of carbon were measured for CO_2 and CH_4 in the headspace gas at all five time steps of the study. Stable isotope ratios of hydrogen in methane were measured at T3 and T4 when sufficient CH_4 concentrations were generated to measure $\delta^{2}H$ values. Approximately 0.1 mL was sampled for each $\delta^{13}C$ and $\delta^{2}H$ measurement from each vial with a sterile syringe. Isotope ratio measurements were all conducted on a Thermo MAT 253 GC-IRMS system equipped with a combustion and a pyrolysis furnace.

Carbon isotope ratios of CO_2 were analyzed by GC-IRMS using a PlotU column. The gas chromatograph injector temperature was 180 ºC, the helium carrier gas flow rate was 2.4 mL/min, and the GC oven temperature was 120 ºC. Reproducibility of daily laboratory standards for $\delta^{13}C_{CO2}$ was better than 0.5‰ (2σ). Carbon isotope ratios of methane were analyzed in combustion mode on a GC-C-IRMS using a Molsieve column. The injector temperature was 150 ºC, the oven temperature was 30 ºC, and the flow rate was 1.2 mL/min. Reproducibility of daily laboratory standards for $\delta^{13}C_{CH4}$ was better than 1.0‰ (2σ).

Hydrogen isotope ratios of methane were measured in pyrolysis mode using a Molsieve column. The injector temperature was 150 ºC, the oven temperature was 30 ºC, and the flow rate was 1.2 mL/min. Reproducibility of laboratory standards for $\delta^{2}H_{CH4}$ was less than 10‰ (2σ). Isotope ratios of carbon for CO_2 and CH_4 are reported in delta notation in comparison to the international standard PDB. Isotope ratios of hydrogen in CH_4 are reported in delta notation relative to the VSMOW international standard.

$$\delta^{13}C \text{ or } \delta^{2}H\ (‰) = [R_{sample} / R_{standard} - 1] \times 1000 \qquad [5]$$

Where R represents the measured ratio of $^{13}C/^{12}C$ or $^{2}H/^{1}H$.

5.3.6 Stable sulfur isotopes of dissolved sulfate

Stable isotopes of sulfur in dissolved sulfate were measured in the saline enrichment cultures at T0, T2, and T4. One millilitre of water was removed from each bottle using a sterile syringe and dissolved sulfate was precipitated to $BaSO_4$ by injection into a 0.1 M $BaCl_2$ solution. Barium sulfate precipitates were removed from solution by filtration, and were washed and dried following filtration. These samples were transferred into tin cups and analyzed for $\delta^{34}S$ using a Carlo Erba NA 1500 elemental analyzer interfaced to a Thermo Delta+XL mass spectrometer.

Sulfur isotope ratios are reported relative to the Canyon Diablo Troilite (CDT) international standard. Analytical precision of replicate standards was typically better than 0.5‰ (2σ).

Table 5.1: Average major cation and anion concentrations for replicate microcosms (n=12) and +M/−OS control groups (n=2). Total dissolved solids (TDS) values were calculated by addition of measured cations and anions.

	Na (mg/L)	K (mg/L)	Ca (mg/L)	Mg (mg/L)	Cl (mg/L)	SO_4 (mg/L)	TDS (mg/L)
Brackish							
T0	3 700	130	4	12	3 300	n.d.	7 100
T4	3 500	100	8	11	3 200	n.d.	6 800
Control							
T0	3 700	130	1	4	3 200	n.d.	7 000
T4	3 400	120	9	6	3 200	n.d.	6 800
Fresh							
T0	880	86	10	19	890	n.d.	1 800
T4	890	79	7	15	900	n.d.	1 900
Control							
T0	750	120	9	33	840	n.d.	1 900
T4	750	120	5	27	860	n.d.	1 800
Saline							
T0	9 200	260	53	330	11 000	2 100	23 000
T2	n.m.	n.m.	n.m.	n.m.	11 000	2 000	n.m.
T4	8 500	250	48	230	11 000	1 900	22 000
Control							
T0	9 200	270	28	320	11 000	2 100	23 000
T2	n.m.	n.m.	n.m.	n.m.	11 000	2 000	n.m.
T4	8 400	270	31	220	11 000	2 100	22 000

n.d. denotes samples that were below instrument detection levels
n.m. denotes the parameter was not measured at a given time step

5.4 Results

Summary data of the experimental results are presented in this chapter. A complete data set including all measured geochemical and stable isotope parameters is available in Appendix C.

5.4.1 Methane generation in experimental microcosms

Mean headspace methane concentrations of the twelve replicates of each geochemical makeup are presented at each time step in Figure 5.2. Methane was not detected in the headspace of any replicates after the initial bottle construction at the T0 time step. After one year (T4), methane concentrations were highest in the Brackish microcosms (22.8 mol%), and lowest in the Saline microcosms (8.1 mol%) with intermediate CH_4 concentrations in the Fresh microcosms (12.4 mol%). There was a large variability in the amount of methane produced among replicates. At the T4 time step, Fresh enrichments ranged from 0 to 35 mol% methane headspace, Saline samples ranged from 0 to 28 mol%, and Brackish samples ranged from 3 to 35 mol%. A complete data set for all geochemical and stable isotope parameters is available in Appendix C.

5.4.2 Methane generation in controls

Unexpectedly, the microbial-control samples (+M/−OS, designated F1, F2, B1, B2, S1, and S2 throughout this chapter) generated methane in the absence of an oil sands substrate. Up to 12 mol% and 4 mol% methane was detected in headspace in the Brackish and Fresh microcosms respectively at the T4 time step. The Saline (+M/−OS) control samples generated detectable, but not quantifiable amounts of methane (< 0.5 mol%). None of the (−M/+OS) or (−M/−OS) control samples generated methane under any geochemical condition.

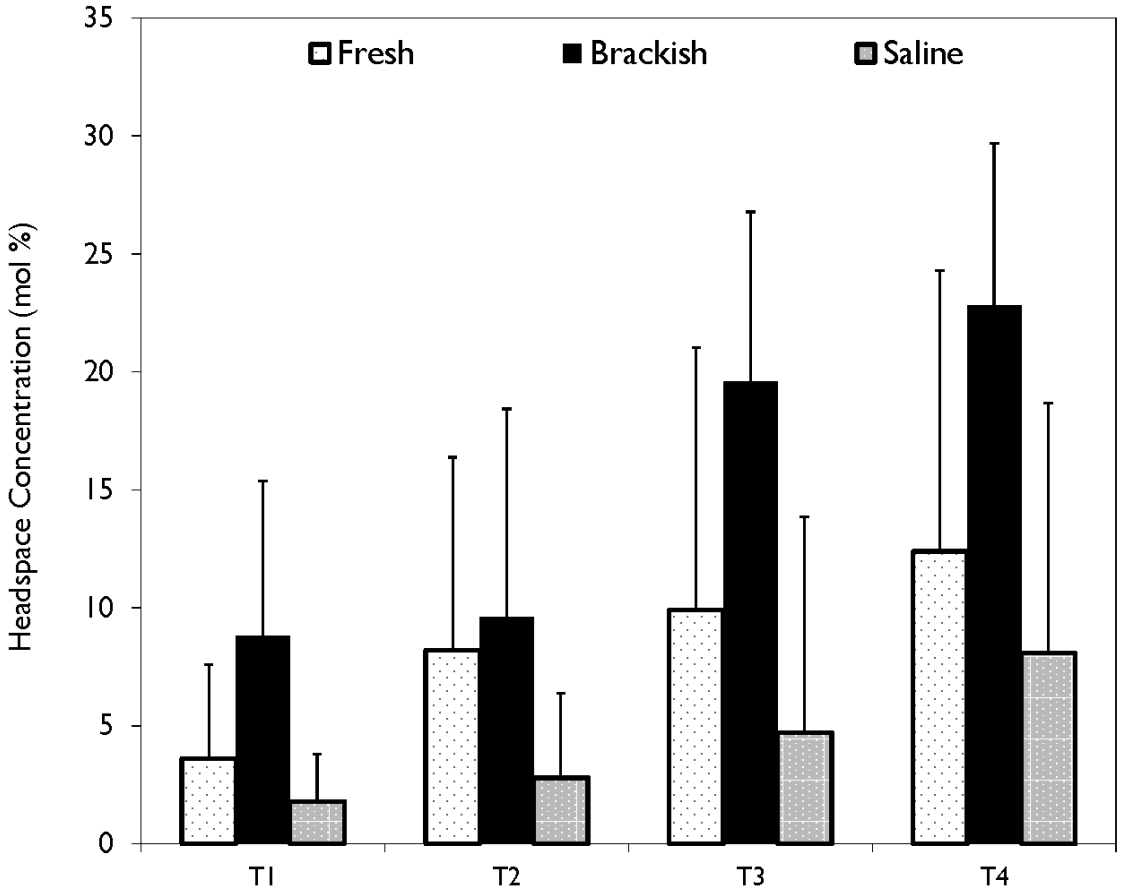

Figure 5.2: Mean headspace methane concentrations for each geochemical condition (n = 12 replicates of each Fresh, Brackish and Saline). Error bars represent one standard deviation of observed methane concentrations in the twelve replicates of each geochemical condition.

5.4.3 Stable isotopes of carbon and hydrogen

$\delta^{13}C$ values of CO_2 are presented for each individual microcosm in Figure 5.3a-c. The $\delta^{13}C$ values of CO_2 increased from the T0 value of −29.9‰ to a mean value of −25.7‰ at T4 in the Fresh enrichments, from a T0 value of −29.6‰ to −28.4‰ at T4 in the Brackish enrichments, and from −31.0‰ at T0 to −29.3‰ at T4 in the Saline enrichments. CO_2 concentrations in headspace gas were not quantified in the experiment, however the peak amplitude of CO_2 on IRMS measurements became diminished over the course of the experiment, qualitatively suggesting microbial consumption of inorganic carbon at a rate greater than generation of CO_2 from petroleum hydrocarbon biodegradation.

$\delta^{13}C$ values of methane for Fresh, Brackish and Saline conditions are presented as a time series in Figure 5.4 a-c. All enrichments had initially low $\delta^{13}C_{CH4}$ values that became progressively enriched in ^{13}C over the course of the experiment. At T1, the mean $\delta^{13}C$ values for methane were −63.1‰, −71.8‰ and −71.8‰ for the Fresh, Brackish, and Saline enrichments respectively. After the T4 timestep, the mean $\delta^{13}C_{CH4}$ was −52.9‰ for the Fresh microcosms, −43.4‰ for the Saline microcosms, and −35.6‰ for the Brackish microcosms. The $\delta^{13}C$ values for the Saline and Brackish microcoms were higher at T4 than expected for biogenic methane produced in open environmental systems whereas the Fresh microcosms fell within the expected range for methane formed in natural freshwater systems (Whiticar, 1999).

Hydrogen isotope ratios provided additional insight into the pathway of methane generation over the experimental period. Hydrogen isotope ratios were measured at the T3 and T4 timesteps only. A dual isotope plot of $\delta^{2}H$ and $\delta^{13}C$ values for methane is presented in Figure 5.5. All CH_4 samples were very depleted in ^{2}H, and ranged in $\delta^{2}H$ values from −458 to

−379‰. The mean δ^2H values of methane for the Fresh, Brackish and Saline groups at T4 were −409‰, −399‰, and −399‰.

Figure 5.3: $\delta^{13}C$ values of CO_2 for microcosms at the start of the experiment and at each sampled time step.

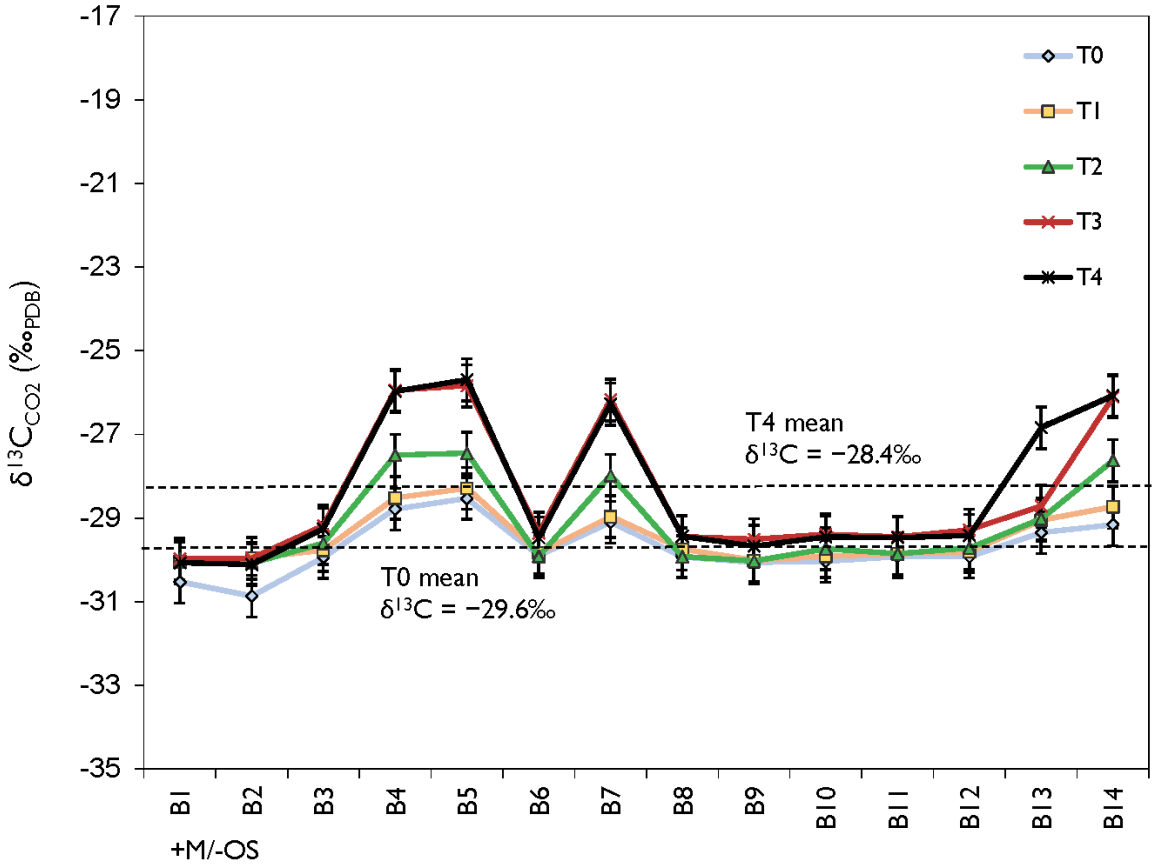

Figure 5.3a: $\delta^{13}C$ values of CO_2 for Brackish microcosms at the start of the experiment and at each sampled time step. B1 and B2 represent +M/−OS controls, and B3 through B14 represent individual +M/+OS microcosm samples. The two dashed lines represent the mean value of B3–B14 at T0 and T4 as indicated.

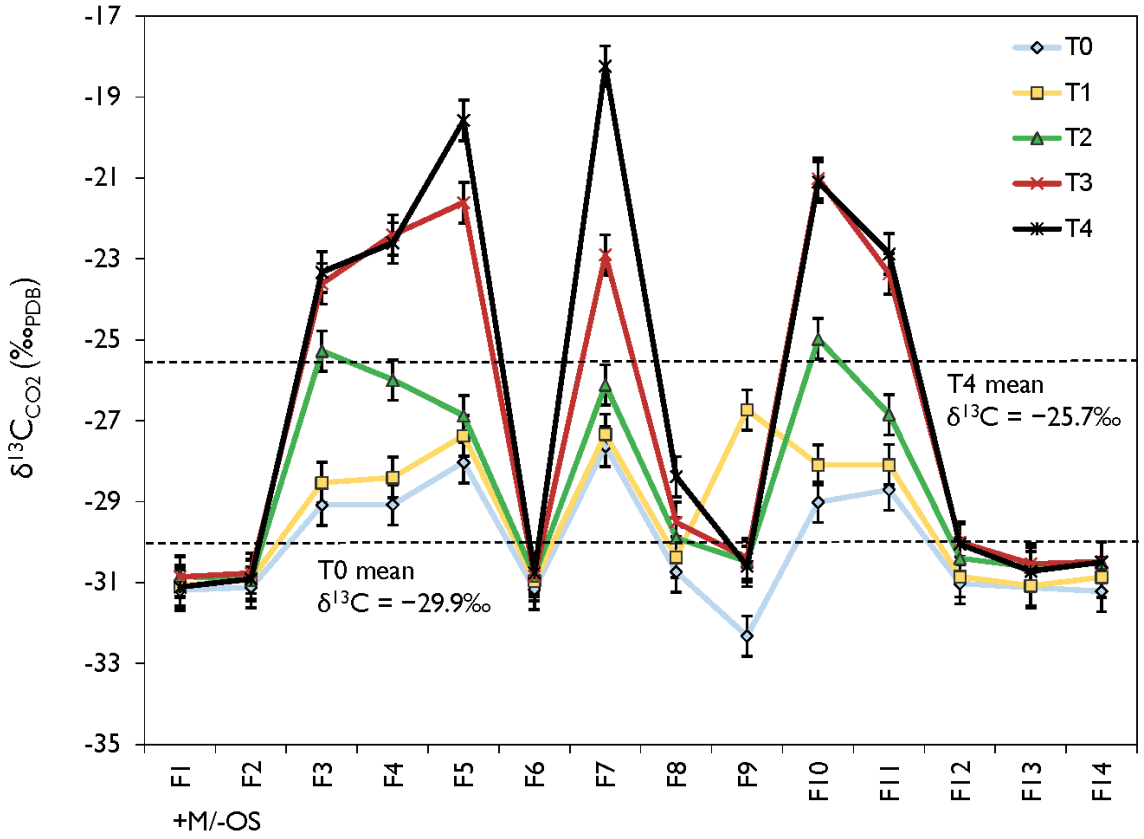

Figure 5.3b: $\delta^{13}C$ values of CO_2 for Fresh microcosms at the start of the experiment and at each sampled time step. F1 and F2 represent +M/−OS controls, and F3 through F14 represent individual +M/+OS microcosm samples. The two dashed lines represent the mean $\delta^{13}C_{CO2}$ value in F3–F14 at T0 and T4 as indicated.

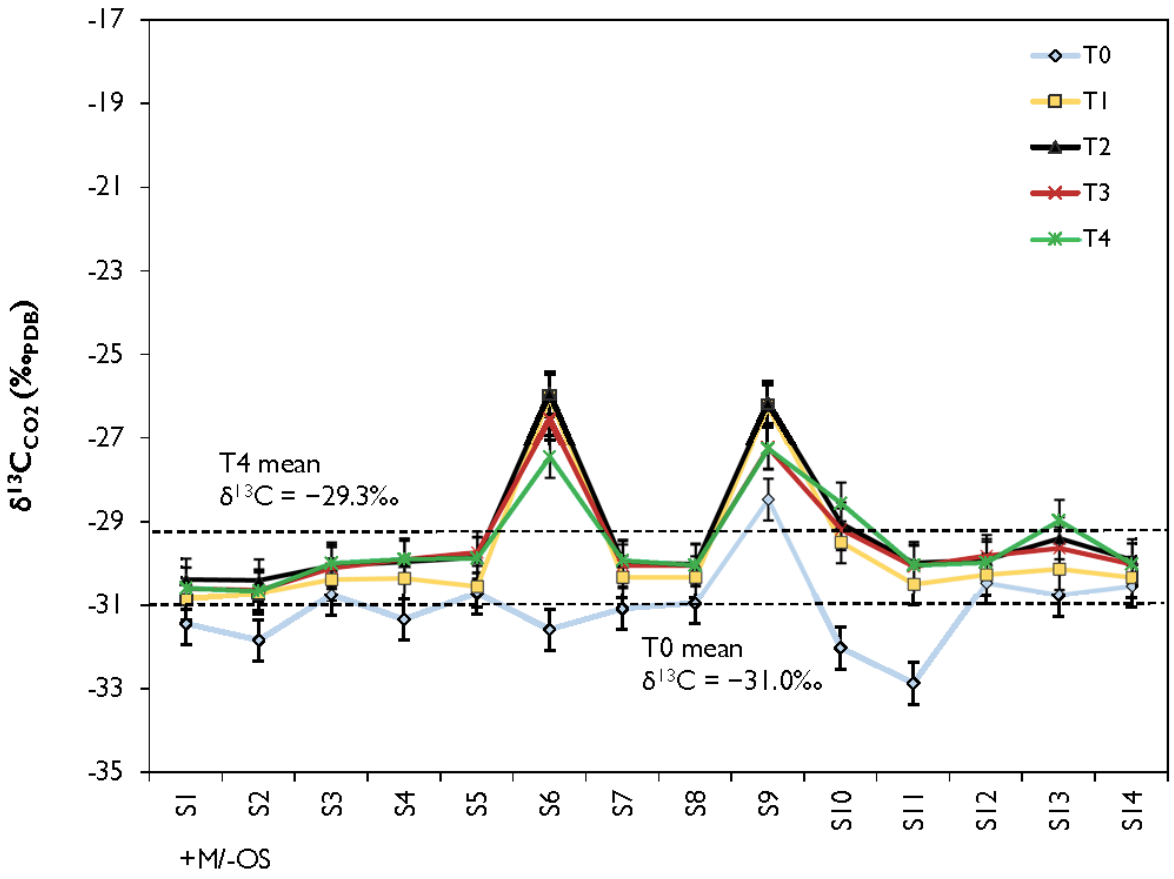

Figure 5.3c: $\delta^{13}C$ values of CO_2 for Saline microcosms at the start of the experiment and at each sampled time step. S1 and S2 represent +M/−OS controls, and S3 through S14 represent individual +M/+OS microcosm samples. The two dashed lines represent the mean $\delta^{13}C_{CO2}$ value in S3–S14 at T0 and T4 as indicated.

Figure 5.4 $\delta^{13}C$ values of CH_4 for microcosms at the start of the experiment and at each sampled time step.

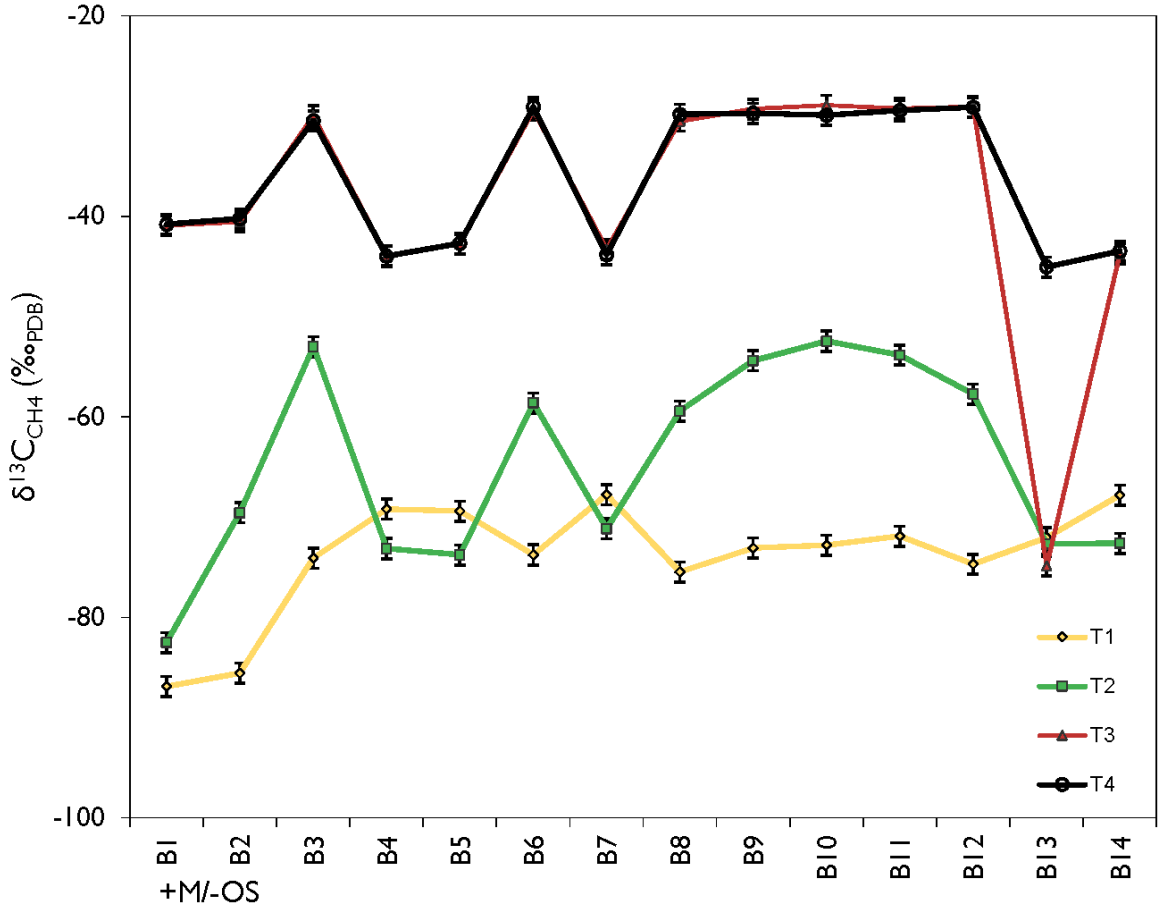

Figure 5.4a: $\delta^{13}C$ values of CH_4 of the Brackish microcosms. B1 and B2 represent +M/−OS controls, and B3 through B14 represent individual +M/+OS microcosm samples.

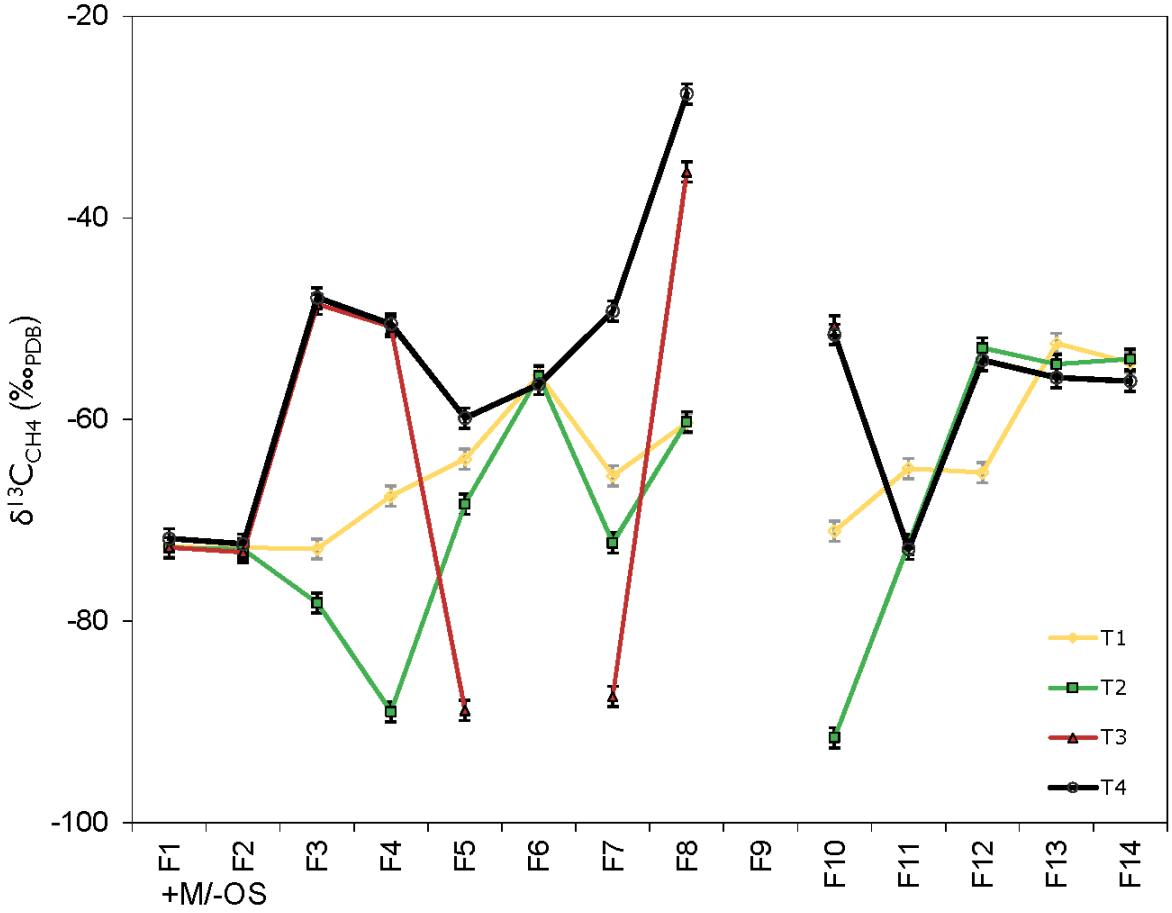

Figure 5.4b: $\delta^{13}C$ values of CH_4 of the Fresh microcosms. F1 and F2 represent +M/−OS controls, and F3 through F14 represent individual +M/+OS microcosm samples.

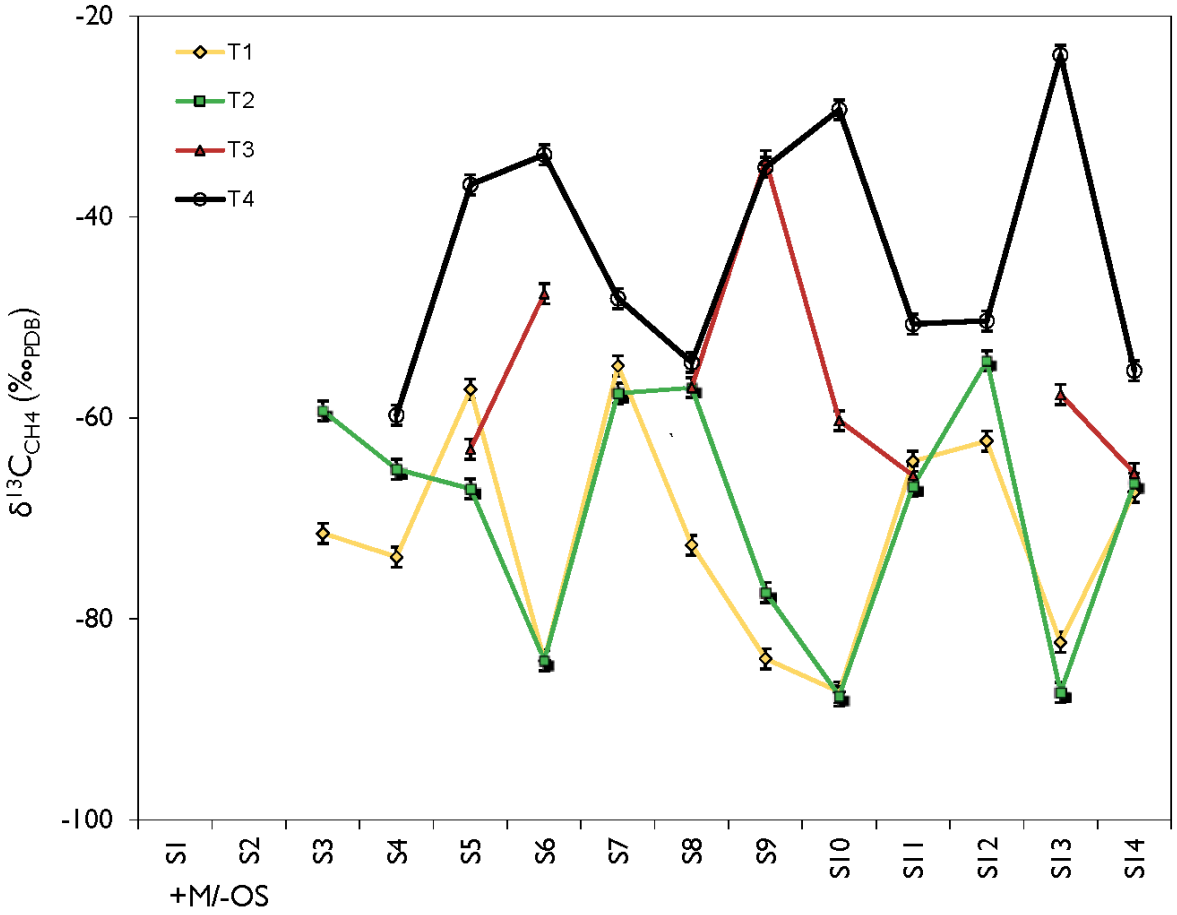

Figure 5.4c: $\delta^{13}C$ values of CH_4 of the Saline microcosms. S1 and S2 represent +M/−OS controls, and S3 through S14 represent individual +M/+OS microcosm samples.

5.4.4 Aqueous geochemistry and water stable isotopes

Aqueous geochemistry was measured at T0 and T4 to evaluate the microbial impact on dissolved constituents. Mean values for inorganic geochemistry are presented in Table 5.1. The total dissolved solids (TDS) values at T0 for the Fresh, Brackish and Saline groups were 1 900, 6 800, and 22 000 mg/L respectively, representing the variability of formation waters in the McMurray Formation in the AOSR (Chapter Two).

Major cations and anions did not vary within analytical error over the course of the experiment in either the Fresh or Brackish microcosms (Table 5.1). However, in the Saline microcosms, there was a significant decrease in sulfate concentration over the course of the experiment. The mean sulfate concentration in the Saline microcosms decreased from an initial value of 2 100 mg/L at T0 to 1 900 mg/L at T4. This represents a mean decrease in dissolved sulfate concentration of approximately 10% over a one year period. Water stable isotope composition was measured in each microcosm at T0. These waters had a $\delta^{18}O$ value of −19.1 ± 0.4‰ (2σ), and a $\delta^{2}H$ value of −148‰ ± 1.5‰ (2σ).

5.4.5 Stable sulfur isotope ratios

The $\delta^{34}S$ values of sulfate increased in all Saline enrichments by several permil over the course of the experiment. There was no detectable sulfate in the Fresh or Brackish microcosms. The sulfate used to prepare the aqueous media for Saline microcosms had an initial $\delta^{34}S_{SO4}$ value of +15.2‰, however minor contributions from oil sands substrate diminished this value in most microcosms to an average $\delta^{34}S_{SO4}$ value of +13.7‰ at T0 (Appendix C). Over the one year experimental period, the $\delta^{34}S_{SO4}$ value in the twelve Saline microcosms increased by an average of +4.8‰, to a mean value of +18.5‰. This increase was greater than the observed increase in $\delta^{34}S_{SO4}$ in the −M/+OS control (+0.67‰), and the +M/–OS control (+1.8‰).

5.5 Discussion

In this experiment, aqueous geochemistry strongly influenced the amount of methane generated, and the carbon isotope ratios of methane produced in the microcosms. In all microcosm types, both carbon and hydrogen isotope ratios indicated a strong contribution of methane derived from acetate fermentation, however, the $\delta^{13}C_{CO2}$ indicated some contribution of methane from CO_2 reduction, especially in the Fresh microcosms. In the Saline microcosms, bacterial sulfate reduction was observed via an increase in $\delta^{34}S_{SO4}$ accompanying the decrease in concentration of sulfate over the experimental time period. The presence of sulfate did not completely inhibit methanogenesis, as both processes were observed over the course of the experiment. These findings, further discussed below, are consistent with a diverse microbial community using a variety of biochemical pathways for the biodegradation of petroleum hydrocarbons.

5.5.1 Brackish microcosms

The mean $\delta^{13}C_{CH4}$ value for methane in the Brackish enrichments was −35.6 ± 7‰ at T4, and this value was substantially higher than is typical for biogenic methane in environmental systems (Whiticar, 1999). Within the Brackish microcosms, there were two distinct sub-groups of microcosms: one that had a mean $\delta^{13}C_{CH4}$ value at T4 of –29.7‰ (n=7), and a second group that had a mean $\delta^{13}C_{CH4}$ value at T4 of −43.8‰ (n=5). In the seven replicates in which the $\delta^{13}C_{CH4}$ reached −30‰ at T4, $\delta^{13}C_{CO2}$ remained unchanged within analytical precision from T0–T4, and in the other five replicates, the $\delta^{13}C_{CO2}$ value increased over the course of the experiment by an average of 2.8‰. The elevated $\delta^{13}C_{CH4}$ values observed in the first group of Brackish microcosms are best explained by the predominance of acetate fermentation, and the complete conversion of the entire resevoir of acetate to methane over the course of the experiment. To

maintain isotope mass balance, $\delta^{13}C_{CH4}$ will approach the $\delta^{13}C$ value of organic carbon in the oil sands substrate as the fraction of acetate-derived carbon converted to methane approaches 100%, and the $\delta^{13}C_{CH4}$ value in the Brackish microcosms was comparable to the initial bulk oil sands $\delta^{13}C$ value of −30‰. The $\delta^{13}C_{CO2}$ value was unchanged at approximately −30‰ suggesting no difference between the $\delta^{13}C$ values of methyl and carboxyl carbon atoms in the acetate molecule. Therefore, acetate fermentation was determined to be the predominant biodegradation process in the first group of Brackish microcosms. In the second group, where the $\delta^{13}C_{CO2}$ values increased from T0 to T4, the co-existence of CO_2 reduction and acetoclastic methanogenesis is suggested.

A carbon isotope mass balance approach was used in the second group of Brackish microcosms to estimate the contribution of the methane derived from acetate fermentation and CO_2 reduction pathways. The contribution of methane from acetate fermentation was given a $\delta^{13}C_{CH4\text{-}fermentation}$ value of −30‰ due to the probable complete conversion of acetate to CH_4 that was observed in all replicates, and methane from CO_2 reduction was given a typical $\delta^{13}C_{CH4\text{-}CO2\ reduction}$ value of −90‰ (Whiticar 1999).

$$\delta^{13}C_{CH4} = f \times \delta^{13}C_{CH4\text{-}CO2\ reduction} + (1 - f) \times \delta^{13}C_{CH4\text{-}fermentation} \qquad [6]$$

This carbon mass balance approach for methane indicated that in the second group of Brackish microcosms where $\delta^{13}C_{CO2}$ increased during the experiment, up to 10% of the methane was generated by CO_2 reduction. In the first group of samples where there was no change in the $\delta^{13}C_{CO2}$ value during the experiment, there was also no evidence of CO_2 reduction in the $\delta^{13}C$ values of methane. It is unclear why CO_2 reduction was observed in some of the microcosms, but not in others, as all microcosms received the same initial geochemical treatment and inoculation. Biological complexity and microbial ecosystem interactions may be responsible for the observed variability.

The Brackish +M/−OS control produced quantifiable amounts of methane. The mean amount of methane measured in the headspace at the end of the experiment by these two controls was approximately 10 mol%. This was unexpected, as the only additional organic carbon that was intentionally added to the bottle was a small amount of EDTA and vitamins from the media mixture. The $\delta^{13}C_{CO2}$ in the +M/−OS control samples was unchanged at a mean value of −30.2 ± 0.3‰ over the course of the experiment, suggesting in agreement with $\delta^{13}C_{CH4}$ values, that acetate fermentation was the dominant methanogenic process. As there was little initial organic carbon added to these controls, it is suggested that consumption of dead cells, inoculum hydrocarbons (a small amount of 2,6 dimethylbenzene carried over from the previous culture in 2 mL of inoculum), or degradation of EDTA may have generated the observed methane (e.g. Thomas et al., 1998).

Hydrogen isotope ratios were used as an additional tool to assess the methane generation pathways in the microcosms. The hydrogen isotope model proposed by Whiticar (1999) generates methane derived from the acetoclastic pathway that is typically more depleted in ^{2}H than methane derived from CO_2 reduction (Fig. 5.1). The measured hydrogen isotope composition of water in this study ($\delta^{2}H_{H2O}$ = −148‰), was input into Equation 3, and typical values for Alberta oil sands hydrocarbon compouds ($\delta^{2}H_{oil\ sands}$ = −140‰, Marcano et al., 2013) and β (320‰, Whiticar, 1999) were added into Equation 4. These values resulted in a calculated $\delta^{2}H_{CH4}$ value for methane generated by CO_2 reduction of −308‰, and the expected $\delta^{2}H$ value for methane generated by acetate fermentation was calculated to be −462‰. At T4, the group of Brackish microcosms that had methane primarily derived from acetoclastic methanogenesis had a mean $\delta^{2}H$ value of −392‰, and the group that derived methane from both pathways had a mean $\delta^{2}H$ value of −415‰. Thus, the hydrogen isotope system in the Brackish microcosms was

unusual in that the enrichments with evidence of CO_2 reduction also exhibited large depletions of ^2H in the methane generated relative to the samples that were dominated by the fermentation pathway. This was unexpected, as typical values for δ^2H_{CH4} in CO_2 reduction are higher than those for acetate fermentation (Whiticar 1999). However, this phenomenon of very ^2H depleted hydrogen isotope ratios in methane generated by CO_2 reduction has been observed previously in other laboratory studies and was explained by several different mechanisms. These mechanisms include a greater reservoir of available hydrogen available in freshwater compared to marine systems (Burke, 1993; Sugimoto and Wada, 1995), or exceptionally high rates of methane generation (Sugimoto and Wada, 1995). In this study, the Brackish samples generated greater amounts of methane than the Fresh or Saline microcosms, therefore any of these proposed explanations may be consistent with the observed results. This represents a significant deviation from natural systems and illustrates a challenge with working at the bench scale to test geomicrobiological phenomena.

5.5.2 Fresh microcosms

The Fresh microcosms generated an intermediate amount of methane compared with the Brackish and Saline microcosms. There was substantial variability within the Fresh microcosm replicates, with some replicates generating less methane than the control group (+M/−OS), and others generating up to 35 mol% in the headspace. The mean headspace methane concentration for the twelve Fresh microcosms was 12.4 mol%.

The mean $\delta^{13}C_{CH4}$ value for the Fresh microcosms was −52.9‰ at T4. This $\delta^{13}C_{CH4}$ value was lower than those of the Brackish ($\delta^{13}C_{CH4}$ = −36.4‰) or Saline ($\delta^{13}C_{CH4}$ = −43.4‰) enrichments at T4, and was most consistent with observed natural systems of similar geochemistry (Whiticar, 1999). The Fresh microcosms also had the highest mean $\delta^{13}C_{CO2}$ value

(−25.7‰), suggesting CO_2 reduction played a greater role in methane generation in the Fresh microcosms compared to the Brackish or Saline systems.

Hydrogen isotope ratios provided insight into the pathways of methanogenesis in the Fresh microcosms. However, there were fewer δ^2H_{CH4} values (n = 7) for samples from the Fresh microcosms because the concentrations of methane were too low in the other five replicates, and the quantification limits of GC-Py-IRMS analyses for hydrogen isotope ratios are greater than GC-C-IRMS analyses for carbon isotope ratios. The mean δ^2H_{CH4} for the Fresh microcosms at T4 was −404‰, and that value was in between the values for Brackish microcosms with CO_2 reduction (δ^2H_{CH4} = −414‰) and those with only fermentation (δ^2H_{CH4} = −392‰). This δ^2H value more closely approximated the modeled δ^2H_{CH4} value of −462‰ for acetate fermentation than the modeled δ^2H_{CH4} value of −308‰ for CO_2 reduction. However, because the $\delta^{13}C_{CO2}$ values for the Fresh microcosms increased in all microcosms by an average of 4.8‰ between T0 and T4, a component of methane produced by the CO_2 reduction pathway is still inferred for the Fresh system.

There were two individual Fresh microcosms that produced outlying data that require careful attention. At the T3 timestep, the samples most depleted in ^2H were F5 (δ^2H_{CH4} = −459‰) and F7 (δ^2H_{CH4} = −449‰). Between T2 and T3, there was a substantial increase in $\delta^{13}C_{CO2}$ (Fig. 5.3a), suggesting a high rate of methane generation by CO_2 reduction for these two samples over this time period. Also consistent with high amounts of CO_2 reduction was an observed decrease in $\delta^{13}C_{CH4}$ to a value approaching −90‰, that is lower than would be expected for acetate fermentation. These observations are similar to those made for the Brackish microcosms, in that in this study CO_2 reduction generated a very low value for δ^2H_{CH4}. Subsequently in the F5 and F7 microcosms between T3 and T4, several observations were

consistent with a shift in the dominant pathway of methanogenesis including: 1) an increase in δ^2H_{CH4} by 46‰ and 51‰, 2) an increase in $\delta^{13}C_{CH4}$ of 29‰ and 38‰ and, 3) a greatly increased headspace methane concentration that was higher by 12.0 and 20.0 mol% in F5 and F7, respectively. Taken together, these three results are consistent with a shift from predominantly CO_2 reduction to predominantly acetoclastic methanogenesis between T3 and T4. However, between T3 and T4, $\delta^{13}C_{CO2}$ increased by 2.0‰ and 4.6‰ in F5 and F7, suggesting continued production of some methane via the CO_2 reduction pathway during this time period.

The Fresh +M/−OS controls generated detectable methane amounts, approximately 2 mol% in the headspace gas. There was no change in the $\delta^{13}C_{CO2}$ in the +M/−OS controls over the course of the experiment, and the δ^2H_{CH4} for the control samples was −427‰, more closely approximating the modeled value of −462‰ value for δ^2H_{CH4} in acetate fermentation than the modeled value of −308‰ for CO_2 reduction. Therefore the methanogenic pathway of the control group appeared to be dominated by acetate fermentation. Similar to the Brackish microcosms, the carbon source for methanogenesis in the controls could be the small amount of carbon substrate transferred from the initial inoculum or the vitamins and EDTA from the media mixture.

5.5.3 Saline microcosms

The Saline microcosms were distinct from the Fresh and Brackish groups because they contained significant quantities of dissolved sulfate; a suitable electron acceptor for biodegradation of petroleum hydrocarbons that is competitive with methanogenesis for certain substrates (Berkowitz et al., 2010; Mbadinga et al., 2011). Sulfate is present in several Athabasca oil sands reservoirs; however, the source of sulfate in natural oil sands systems is poorly understood. The oil sands deposits overlie Devonian carbonate and anyhydrite-bearing evaporite

formations with high formation water salinity (Gue, 2012) that could provide a significant sulfate source to some reservoirs if vertical flow was occurring (Chapter Two). In traditional redox models, sulfate is consumed by BSR before the initiation of methanogenesis (Berkowitz et al., 2010); therefore under the favorable conditions that exist in these reservoirs, sulfate should be eliminated before the commencement of methanogenesis over geologic time.

The Saline microcosms generated the least methane after one year at T4 (mean = 6.75 mol%) compared to either the Fresh (12.4 mol%) or Brackish (22.8 mol%) microcosms. There were two apparent sub-groups in the Saline data set: one group with high methane generation (n = 4), and a second group with very low methane generation (n = 10). The four enrichments that generated substantial methane were: S5 (18.7 mol%), S9 (28.5 mol%), S10 (14.5 mol%) and S13 (17.1%). The mean methane generation for the other ten Saline microcosms was significantly lower (0.3 mol%). This finding provides ambiguous evidence for the impact of elevated salinity on the growth of methanogenic microbes on oil sands. The low overall methane generation suggests that a geochemical control is possible, however the four microcosms that produced substantial methane suggest that rapid methanogenesis is also possible under saline conditions.

The Saline +M/−OS controls generated no quantifiable methane, suggesting that the microbial consortium was not as well adapted to the salinity of this sample group. This was unexpected, as the Fresh and Brackish microcosms did have evidence of methanogenesis, and because the original microbial enrichment culture was derived from a saline oil field (Berdugio-Clavio et al., 2012). These control microcosms received the same initial vitamins and organic carbon sources as the Brackish and Fresh microcosms, therefore this result suggests that elevated salinity played a role in the amount of methane generated from oil sands by these microcosms.

Carbon isotope systems provided evidence that acetate fermentation predominated as the main methanogenic pathway in the Saline microcosms. The mean $\delta^{13}C_{CO2}$ value was only slightly altered over the course of the experiment from −31.0‰ at T0 to −29.3‰ at T4 (Figure 3c), and the mean $\delta^{13}C_{CH4}$ value after one year (T4) was −43.4‰. Both of these values suggest methanogenesis by acetate fermentation, and the carbon isotope ratios of methane suggest that the systems are approaching complete conversion of acetate to methane in a closed system, comparable to the Brackish microcosms.

Hydrogen isotope ratios of methane in saline enrichments presented an analytical challenge due to the low headspace methane concentration in many of the samples. Only two data points were obtained at T3, and six data points were obtained at T4. The majority of Saline T4 samples plotted in the same range for $\delta^{2}H_{CH4}$ as the methane from the Fresh and Brackish microcosms, ranging from −422 to −383‰ (Fig. 5.6), indicating likely dominance of the acetoclastic pathway in the saline systems. This was supported by the unaltered $\delta^{13}C_{CO2}$ values throughout the course of the experiment suggesting CO_2-reduction was not a dominant biochemical process.

Qualitatively, the $\delta^{13}C_{CO2}$, $\delta^{13}C_{CH4}$ and $\delta^{2}H_{CH4}$ values in the Saline microcosms all reflect major contributions of methane from acetate fermentation, and a minor contribution from CO_2 reduction. $\delta^{13}C_{CH4}$ was very ^{13}C enriched relative to what would be expected for CO_2 reduction, and $\delta^{2}H_{CH4}$ values plot within the expected range for acetate fermentation (Fig. 5.5). $\delta^{13}C_{CO2}$ increased slightly in some bottles between T0 and T4, suggesting a contribution of CO_2 reduction in S6, S9, S10 and S11. It was unexpected that acetate fermentation would predominate the Saline group, as CO_2 reduction tends to be less influenced by salinity than acetoclastic methanogens (Whiticar 1999; Waldron et al., 2008). However, in the experimental

design the concentration of chloride was not intended to be high enough to completely inhibit acetoclastic methanogens at ~1M Cl^- (Waldron et al., 2008).

Bacterial sulfate reduction (BSR) was observed in all Saline microcosms. Strong evidence for BSR is presented in Figure 5.6 that shows both a decrease in the fraction remaining of initial sulfate and a corresponding increase in $\delta^{34}S_{SO4}$. The relationship between decreasing sulfate concentration and ^{34}S enrichment in the remaining sulfate reservoir from T0 to T4 corresponds approximately to a closed-system Rayleigh fractionation factor (α) of 1.035, that is typical for sulfate reducing bacteria (Clark and Fritz, 1997; Habicht and Canfield, 1997). Therefore BSR was determined to be an active microbial process in these sulfate-containing microcosms.

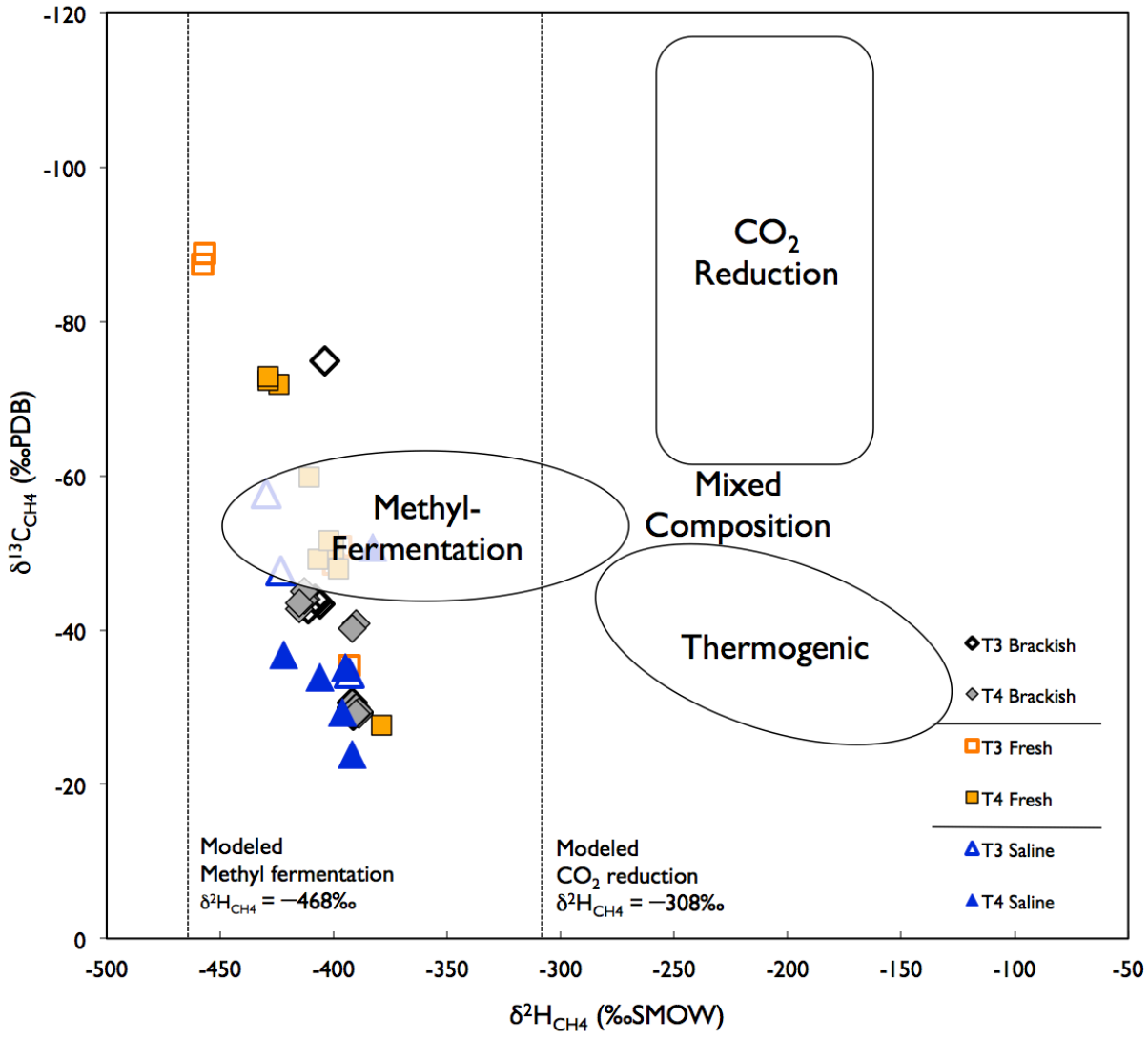

Figure 5.5: Methane dual-isotope plot for microcosms at T3 and T4. Modeled δ^2H values for methane produced by CO_2 reduction and acetate fermentation were −308‰ and −468‰ respectively and are indicated by dotted lines. Boxes indicating methane generation pathway are derived from Whiticar (1999). 1σ error bars are smaller than markers in both δ^2H and $\delta^{13}C$ space.

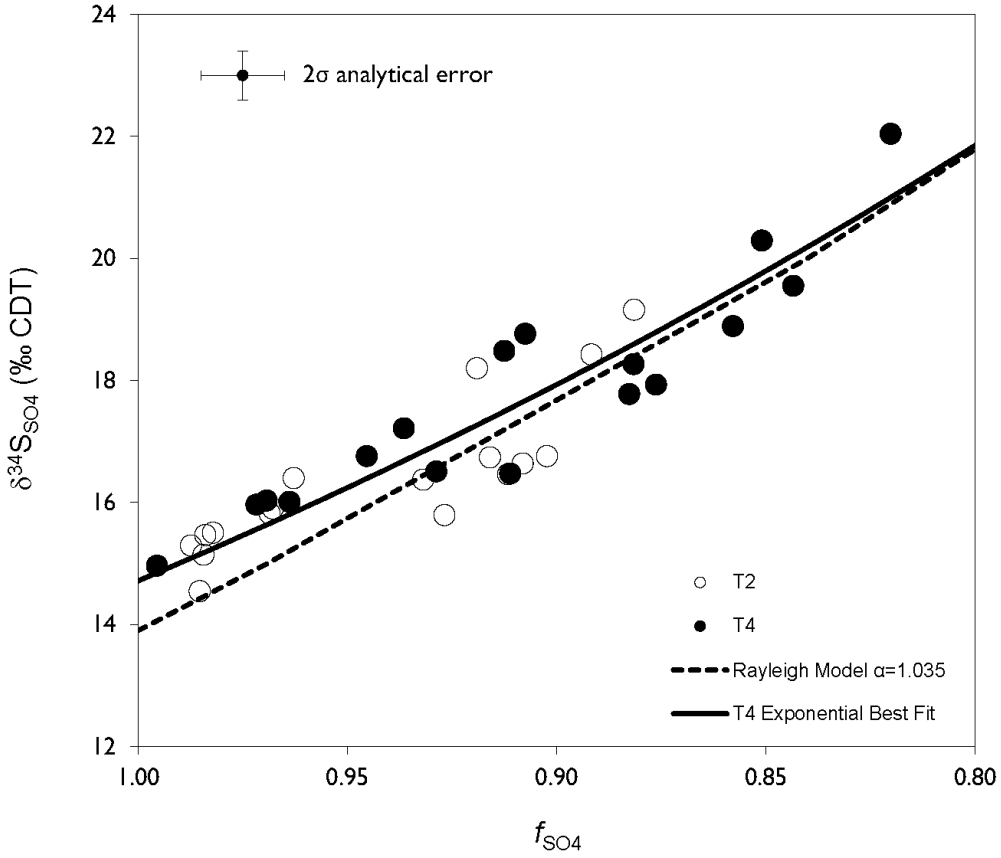

Figure 5.6: Dissolved sulfate fraction remaining from T0 and $\delta^{34}S$ values of sulfate from Saline microcosms at T2 and T4 compared with a closed-system Rayleigh model for bacterial sulfate reduction using a fractionation factor $\alpha = 1.035$.

Bacterial sulfate reduction may negatively impact rates of methanogenesis in the Saline microcosms. Under traditional redox models, methanogenesis and bacterial sulfate reduction do not typically co-exist because they compete for the acetate and hydrogen substrates (Oremland and Polcin, 1982). Furthermore, H_2S that is generated as a byproduct of sulfate reduction is toxic to most organisms including methanogens at concentrations less than 5% (Krishnanand et al., 1993). In petroleum reservoir systems, H_2S can be removed through advection, or can be made unavailable to biological activity through reactions with iron to form sulfide minerals such as pyrite. H_2S concentration was not measured in this experiment, however its presence was observed by odour during microcosm sampling. Therefore, bacterial sulfate reduction may have reduced the rate of methanogenesis through competition for substrate or H_2S toxicity in microcosms with abundant sulfate.

Increasing amounts of headspace methane over the course of the experiment, coupled with decreasing concentrations of sulfate that became enriched in ^{34}S provide unequivocal evidence of co-existing BSR and methanogenic biochemical pathways for petroleum biodegradation in this experiment. Increasing headspace methane concentrations, combined with isotopic evidence for predominantly acetoclastic methanogenesis conclusively demonstrated that methanogenesis was an active process in the Saline microcosms. Decreasing concentrations of sulfate and increases in the $\delta^{34}S_{SO4}$ value indicate bacterial sulfate reduction was prevalent in all Saline microcosms. Therefore, methanogenesis and bacterial sulfate reduction were observed to co-exist in these laboratory experiments. Extrapolation to reservoir systems from bench-scale studies in not straightforward. However these results suggest that reservoirs with significant sulfate concentrations in formation water may have both BSR and methanogenic processes contributing to biodegradation of petroleum hydrocarbons.

An individual microcosm, S13, was unique among replicates of all geochemical conditions in that the $\delta^{13}C$ value of methane was significantly higher than the starting oil sands material. In the S13 microcosm, $\delta^{13}C_{CH4}$ increased from −57.7‰ to −23.9‰ between T3 and T4; and the $\delta^{2}H_{CH4}$ value increased from −430‰ to −392‰. The carbon isotope value is substantially higher than the bulk isotopic composition of the initial oil sands substrate. The combined carbon and hydrogen isotope values between T3 and T4 cannot be explained by methane oxidation because the absolute amount of methane in the bottle increased from T3 to T4 from 4 mol% to 17 mol% in headspace, making it highly unlikely that oxidation generated the observed increases in $\delta^{13}C_{CH4}$ and $\delta^{2}H_{CH4}$ values. A suitable explanation for this phenomenon is the co-metabolism of acetate by methanogens and sulfate reducing bacteria where BSR generates a ^{13}C enrichment in the acetate reservoir. Goevert and Conrad (2008, 2009) observed significant isotope discrimination in the $\delta^{13}C$ of acetate when metabolised by sulfate reducing bacteria. In their experiment, $\delta^{13}C$ values of acetate had increased by up to 19.3‰ compared to a control sample in an experiment where Desulfobacca acetoxidans consumed both acetate and sulfate. A ^{13}C enrichment in the acetate reservoir of the S13 replicate could explain the high $\delta^{13}C_{CH4}$ values observed in this microcosm. The methane formed from the ^{13}C-enriched acetate pool would also have high $\delta^{13}C$ values as a result of the small carbon isotope fractionation due to the complete consumption of acetate over the course of the experiment. The hydrogen isotope values are best explained by comparison of the $\delta^{2}H_{CH4}$ value at T4 with other acetoclastic microcosms, where the predominantly fermentation-driven microcosms in the Fresh, Brackish and Saline systems had a $\delta^{2}H_{CH4}$ value of −390‰. Co-metabolism of acetate by SRB and methanogens to produce ^{13}C-enriched methane is a plausible process when sufficient reservoirs of acetate are available, and acetoclastic methanogenesis is the dominant methane-producing pathway.

5.5.4 Impact of geochemistry on methanogenesis in oil sands microcosms

The geochemical conditions in the microcosms created considerable variability in the amounts of methane produced and pathways of methanogenesis in these oil sands enrichment cultures, although these differences were not entirely consistent with the hypothesis that decreasing salinity increases the rate of methanogenesis. Taking the mean values over a one year period, the Brackish microcosms produced the most methane, followed by the Fresh microcosms and the least methane was generated by the Saline microcosms.

Methanogenic pathways also varied considerably depending on the geochemical composition of the water. It was unexpected that samples from Fresh microcosms had the strongest evidence for CO_2 reduction, as typically this pathway is found in saline and marine environments compared to the acetoclastic pathway that is generally characteristic of freshwater systems (Whiticar, 1999). It was also unexpected to observe methane in the Saline microcosms to be predominantly derived from acetate fermentation, as CO_2 reduction is more typical in saline systems.

Caution should be taken in interpretation of these results due to the closed-system nature of the experiments, and the heterogeneity in the results among identical replicates of the same geochemical makeup. Major differences from natural systems may be due to the greater availability of nutrients in these enrichments, or a different consortium of microbes than currently exists in natural oil sands reservoirs.

The methanogenic activity of the +M/−OS controls was unexpected and provides insight into how each set of microbes was adapted to the geochemical conditions without a major carbon substrate. The brackish +M/−OS controls produced the most methane, the fresh +M/−OS controls produced a small amount and the saline +M/−OS controls produced almost no

detectable methane. The relative amounts of methane produced by the control samples matched the oil sands microcosms, suggesting that the salinity of the media did have an effect on these microbes.

While controlled conditions can be advantageous for studying biogeochemical processes, microbes can behave very differently in a small-scale closed-system experiment compared with a natural reservoir environment. The isotopic composition of methane generated in this study by the Brackish and Saline microcoms was not comparable to results from the field, that typically fall within the range of CO_2-reduction-dominated systems (Whiticar, 1999). Understanding the causes of differences between field observations and laboratory studies may provide significant insight into the biogeochemical processes that govern biodegradation over geological time.

5.6 Conclusions

In these laboratory experiments, variable aqueous geochemistry impacted both the amount of methane generation and the dominant pathway by which it was produced. The Brackish microcosms produced the highest amount of methane, predominantly via acetate fermentation. A small sub-group of the Brackish microcosms had a substantial methane contribution from CO_2 reduction that induced a very large hydrogen isotope effect, typical of closed-system conditions that are not typically observed in natural environments. The Fresh microcosms generated, on average, less methane than the Brackish microcosms, however, the Fresh systems had contributions from both CO_2 reduction and acetate fermentation in methane generated. This was unexpected, as fermentation is typically described as a freshwater process, and CO_2 reduction as primarily marine. Similar to the Brackish microcosms, very large hydrogen isotope effects were also observed in Fresh microcosms with substantial CO_2 reduction. The Saline microcosms generated, on average, the least methane out of the three salinity groups, and the methane that was generated was predominantly via the acetate fermentation pathway. Bacterial sulfate reduction was observed in all Saline microcosms, and BSR may have negatively influenced methanogenic activity through competition for carbon substrates or H_2S toxicity. This initial attempt at understanding the influence of salinity on biogeochemistry of oil sands reservoirs strongly suggests that geochemistry is an important control on microbial activity and biodegradation in oil sands systems.

5.7 References

Adams, J., Riediger, C., Fowler, M., & Larter, S. (2006). Thermal controls on biodegradation around the Peace River tar sands: Paleo-pasteurization to the west. *Journal of Geochemical Exploration*, *89*(1-3), 1–4.

Aitken, C. M., Jones, D. M., Maguire, M. J., Gray, N. D., Sherry, A., Bowler, B. F. J., et al. (2013). Evidence that crude oil alkane activation proceeds by different mechanisms under sulfate-reducing and methanogenic conditions. *Geochimica Et Cosmochimica Acta*, 1–44.

Andriashek, L. D., & Atkinson, N. (2007). Buried Channels and Glacial-Drift Aquifers in the Fort McMurray Region, Northeast Alberta. *Alberta Geological Survey*, 1–170.

Atlas, R. M. (1981). Microbial degradation of petroleum hydrocarbons: an environmental perspective. *Microbiological Reviews*, *45*(1), 180–209.

Atlas, R.M. and R. Bartha, 1992. Hydrocarbon biodegradation and oil spill bioremediation. *Advances in Microbial Ecology* 12: 287-338.

Atlas, R. (1995). Petroleum Biodegradation and Oil Spill Bioremediation. *Marine Pollution Bulletin*, *31*, 178–182.

Beilen, J. B., & Funhoff, E. G. (2007). Alkane hydroxylases involved in microbial alkane degradation. *Applied microbiology and biotechnology*, *74*(1), 13–21.

Berkowitz, B., Dror, I., Yaron, B. 2008 *Contaminant Geochemistry: Interactions and Transport in the Subsurface Environment*. Springer.

Bennett, B., Adams, J.J., Gray, N.D., Sherry, A., Oldenburg, T.B.P., Huang, H., Larter, S.R. and Head, I.M. (2013) The controls on the composition of biodegraded oils in the deep subsurface – Part 3. The Impact of microorganism distribution on petroleum

geochemical gradients in biodegraded petroleum reservoirs. *Organic Geochemistry*, 56(3), 94-105.

Berdugo-Clavijo, C., Dong, X., Soh, J., Sensen, C. W., & Gieg, L. M. (2012). Methanogenic biodegradation of two-ringed polycyclic aromatic hydrocarbons. *FEMS Microbiology Ecology*,

Broughton, P. L (2013). Devonian salt dissolution-collapse breccias flooring the Cretaceous Athabasca oil sands deposit and development of lower McMurray Formation sinkholes, northern Alberta Basin, Western Canada. *Sedimentary Geology*, 283(C), 57-82.

Burke, R.A. Jr., 1993. Possible influence of hydrogen concentra- tion on microbial methane stable hydrogen isotopic composition. *Chemosphere* 26, 55–67.

Cerniglia, C. E.; Sutherland, J. B.; Crow, S. A. (1992) in : *Microbial degradation of natural products* ed : Winkelmann, G.. Wiley-Blackwell.

Clark, I., & Fritz, P. (1997). *Environmental Isotopes in Hydrogeology*. Lewis Publishers.

Gelwicks, J., Risatti, J. B., & Hayes, J. M. (1994). Carbon isotope effects associated with aceticlastic methanogenesis. *Applied and Environmental Microbiology*, *60*(2), 467–472.

Goevert, D., & Conrad, R. (2008). Carbon Isotope Fractionation by Sulfate-Reducing Bacteria Using Different Pathways for the Oxidation of Acetate. *Environmental Science and Technology*, *42*(21), 7813–7817.

Goevert, D., & Conrad, R. (2009). Effect of Substrate Concentration on Carbon Isotope Fractionation during Acetoclastic Methanogenesis by Methanosarcina barkeri and M. acetivorans and in Rice Field Soil. *Applied and Environmental Microbiology*, *75*(9), 2605–2612.

Grasby, S., & Chen, Z. (2005). Subglacial recharge into the Western Canada Sedimentary Basin - Impact of pleistocene glaciation on basin hydrodynamics. *Geological Society of America Bulletin*, *117*(3-4), 500–514.

Gue, A. (2012, December 21). *The geochemistry of saline springs in the Athabasca oil sands region and their impact on the Clearwater and Athabasca rivers*. M.Sc. thesis. University of Calgary.

Habicht, K. S., & Canfield, D. E. (1997). Sulfur isotope fractionation during bacterial sulfate reduction in organic-rich sediments. *Geochimica et Cosmochimica Acta*, *61*(24), 5351–5361.

Head, I., Jones, D., & Larter, S. (2003). Biological activity in the deep subsurface and the origin of heavy oil. *Nature*, *426*(6964), 344–352.

Jones, D. M., Head, I. M., Gray, N. D., Adams, J. J., Rowan, A. K., Aitken, C. M., et al. (2007). Crude-oil biodegradation via methanogenesis in subsurface petroleum reservoirs. *Nature*, *451*(7175), 176–180.

Maillacheruvu, K. Y., Parkin, G. F., Peng, C. Y., Kuo, W.-C., Oonge, Z. I., & Lebduschka, V. (1993). Sulfide toxicity in anaerobic systems fed sulfate and various organics. *Water environment research : a research publication of the Water Environment Federation*, 100–109.

Larter, S., Wilhelins, A., Head, I., Koopmans, M., Aplin, A., Di Primio, R., et al. (2003). The controls on the composition of biodegraded oils in the deep subsurface - part 1: biodegradation rates in petroleum reservoirs. *Organic Geochemistry*, *34*(4), 601–613.

Larter, S., Huan, H., Adams, J., Bennett, B., Jokanola, O., Oldenburg, T., et al. (2006). The controls on the composition of biodegraded oils in the deep subsurface: Part II -

Geological controls on subsurface biodegradation fluxes and constraints on reservoir-fluid property prediction. *AAPG Bulletin-American Association of Petroleum Geologists*, *90*(6), 921–938.

Leahy, J. G., & Colwell, R. R. (1990). Microbial degradation of hydrocarbons in the environment. *Microbiological reviews*, *54*(3), 305–315.

Lemay, TG. (2002a). Geochemical and Isotope Data Formation Water from Selected Wells, Cretaceous to Quaternary Succession, Athabasca Oil Sands (In Situ) Area, Alberta. *Alberta Energy and Utilities Board*, 1–71.

Mbadinga, S. M., Wang, L.-Y., Zhou, L., Liu, J.-F., Gu, J.-D., & Mu, B.-Z. (2011). Microbial communities involved in anaerobic degradation of alkanes. *International Biodeterioration and Biodegradation*, *65*(1).

McIntosh, J.C., Walter, L.M., and Martini, A.M. (2002). Pleistocene recharge to midcontinent basins : Effects on salinity structure and microbial gas generation. *Geochimica et Cosmochimica Acta* 66 : 1681–1700.

Oldenburg, T. B. P., Larter, S. R., & Huang, H. (2006). Nutrient supply during subsurface oil biodegradations - Availability of petroleum nitrogen as a nutrient source for subsurface microbial activity. *Energy and Fuels*, *20*(5), 2079–2082.

Schimmelmann, A., Sessions, A., & Mastalerz, M. (2006). Hydrogen isotopic (D/H) composition of organic matter during diagenesis and thermal maturation. *Annual Review Of Earth And Planetary Sciences*, *34*, 501–533.

Thomas, R. A. P., Lawlor, K., Bailey, M., & Macaskie, L. E. (1998). Biodegradation of metal-EDTA complexes by an enriched microbial population. *Applied and Environmental Microbiology*, *64*(4), 1319–1322.

Sugimoto, A., & Wada, E. (1995). Hydrogen isotopic composition of bacterial methane: CO 2/H 2 reduction and acetate fermentation. *Geochimica et Cosmochimica Acta, 59*(7), 1329–1337.

Van Der Linden, A. C., and Thijsse, J. E., (1965). *The Mechanisms of Microbial Oxidations of Petroleum Hydrocarbons*. John Wiley and Sons.

Waldron, P. J., Petsch, S. T., Martini, A. M., & Nuesslein, K. (2007). Salinity constraints on subsurface archaeal diversity and methanogenesis in sedimentary rock rich in organic matter. *Applied and Environmental Microbiology*, *73*(13), 4171–4179.

Watkinson, R. J., & Morgan, P. (1990). Physiology of aliphatic hydrocarbon-degrading microorganisms. *Biodegradation*, *1*, 79–92.

Whiticar, M. (1999). Carbon and hydrogen isotope systematics of bacterial formation and oxidation of methane. *Chemical Geology*, *161*, 291–314.

Wilhelms, A., Larter, S., Head, I., Farrimond, P., di-Primio, R., & Zwach, C. (2001). Biodegradation of oil in uplifted basins prevented by deep-burial sterilization. *Nature*, *411*(6841), 1034–1037.

Zengler, K., Richnow, H., Rossello-Mora, R., Michaelis, W., & Widdel, F. (1999). Methane formation from long-chain alkanes by anaerobic microorganisms. *Nature*, *401*(6750), 266–269.

Chapter Six: Radiocarbon Dating of Methane and Dissolved Inorganic Carbon in Powder River Basin Coal Seams

6.1 Abstract

Radiocarbon (^{14}C) measurements of dissolved inorganic carbon and methane were conducted on samples from the northernmost Powder River Basin, MT, USA to better constrain the timing and formation processes of natural gas generation in coal bed methane deposits. The radiocarbon measurements of dissolved inorganic carbon revealed that all tested samples had no quantifiable modern radiocarbon, suggesting no contribution of carbon from the Earth's surface to the underlying aquifers over the past 50 000 years. Radiocarbon measurements of methane in produced gases were also radiocarbon-dead within error, with one exception, suggesting little to no contribution of recent carbon to the subsurface carbon cycle in this region of the Powder River Basin. Evidence from previous studies suggests that recent recharge is prevalent in the Basin, however, rapid carbon cycling due to biodegradation of coal could be responsible for lowering the ^{14}C contents of methane and dissolved inorganic carbon below detection limits.

6.2 Introduction

Coal-bed methane (CBM) production has increased markedly over the past decade to supply natural gas resources for electricity generation, heating fuel, and increasingly as transportation fuel. The Powder River Basin (PRB) in the United States is one of the most prolific producing regions of CBM in the world (United States Energy Information Agency, 2007). Investigations in other coalbed methane deposits in the Antrim, Marcellus and Illinois basins in the United States have provided evidence for substantial recent microbial gas generation in the Holocene period (e.g. McIntosh et al., 2002; Martini et al., 2003; McIntosh et al., 2004; McIntosh and Walter, 2005; Strapoc et al., 2007; Fomolo et al., 2008a,b; Strapoc et al., 2008ab; Strapoc et al., 2010), and this previous work has identified a large fraction of the gas deposits in the PRB to be biological in origin. The origin of coal-bed methane gases in the PRB was determined through microbial studies and geochemical analysis of produced fluids from several locations in the Powder River Basin (Formolo et al., 2008; Rice et al., 2008). Further studies have demonstrated a distinction between 'early-stage' methane of primarily biogenic origin on the edges of the basin where modern recharge is thought to be occurring, and 'late stage' methane in the centre of the basin that contains a mixture of biogenic and thermogenic methane (Flores et al., 2008, Bates et al., 2011).

Debate exists over the origin and timing of methane accumulation in the PRB. Claypool (2001) postulated that the bulk of the methane accumulated in the PRB was generated during the Holocene (Claypool 2001; Luca Technologies 2004). However, evidence presented by Flores et al. (2008) suggested that both "old" and "new" gases in the PRB originated from the Paleogene to modern day, with increased in situ gas generation along basin margins over the last 12–2 Ma due to increased groundwater flow. This question is significant with respect to in situ biogenic

gas production, and the potential for continued microbial methanogenesis to replenish the energy source in these reservoirs over time.

Notwithstanding the timing of generation, biological methanogenesis is thought to be one of the major processes responsible for methane generation over geologic time in the PRB (Flores et al., 2008; Bates et al., 2011). Methanogenesis proceeds by two pathways that use different sources of carbon and different electron acceptors. CO_2 reduction (Eq. 1) and acetoclastic methanogenesis (Eq. 2) are both thermodynamically favourable reactions thought to be carried out under different geochemical conditions in coal seams (Martini et al., 1996; Martini et al., 1998; Strapoc et al., 2011; McIntosh et al., 2004).

$$4H_2 + CO_2 \rightarrow CH_4 + 2H_2O \quad [1]$$

$$CH_3COO^- + H^+ \rightarrow CH_4 + CO_2 \quad [2]$$

Carried out by microbes, these reactions have distinct stable isotope fractionation factors for carbon and hydrogen that can be used to determine the origin of methane in an environmental system (Whiticar, 1999). CO_2 reduction is generally favoured in marine environments whereas methyl fermentation is more prevalent in terrestrial systems (Whiticar, 1999).

The hydrogeology of the PRB is complex, and reservoir fluids are likely a mixture of surface recharge and deeper basin fluids (Flores et al., 2008; Bates et al., 2011). Water isotope analysis of fluids from the PRB are indicative of meteoric recharge from a water source with low $\delta^{18}O$ and $\delta^{2}H$ values that is typical of modern precipitation in the region (Flores et al. 2008; Bates et al., 2011). Radiocarbon analysis conducted by Bates et al. (2011) reported up to 0.041 fraction modern carbon (fm) in dissolved inorganic carbon (DIC) at several locations in the PRB where modern recharge was suspected to be occurring. If modern groundwater recharge reaches the coal-seam aquifers, recent carbon from groundwater may also provide a measurable modern-

carbon input to the subsurface carbon cycle, and should result in a detectable radiocarbon signals in the coal seam methane as DIC is converted to methane (Eq. 1).

Radiocarbon (^{14}C) is an important tool to trace carbon cycling in near-surface systems, although it is limited in time scale by its relatively short half-life of 5 570 years, resulting in no detectable radiocarbon signal after approximately 50 ka (Stuiver and Polach, 1977; Trumbore, 2009). Hydrocarbons derived from coal contain no detectable ^{14}C due to radioactive decay over millions of years since deposition. Conversely, carbon fixed from atmosphere by plants during the recent geological past (50 ka) has modern levels of ^{14}C derived from interactions between ^{14}N and cosmic rays in the upper atmosphere (Clark and Fritz, 1997). Decaying plant matter is metabolized into DIC in the soil by microorganisms, which can be subsequently transported by groundwater flow into deeper aquifers (Trumbore, 2009). The distinction in ^{14}C between coal and surface-derived carbon in a CBM reservoir provides a label that can be exploited to overcome the limitations of indistinguishable $\delta^{13}C$ values between the coal-derived or surface-derived carbon reservoirs.

The objective of this study was to use natural-abundance radiocarbon (^{14}C) measurements of DIC and methane from CBM wells to determine whether substantial methanogenesis using modern carbon has occurred in the recent past (50 ka). Groundwater recharge from shallow aquifers is suspected to occur in this region on a time scale of less than 50 ka, and this process is responsible for transport of radiocarbon into the reservoir from the surface in the form of DIC (Flores et al., 2008; Trumbore, 2009; Bates et al., 2011). As methanogens convert inorganic carbon to methane, an above-background ^{14}C signal may be measurable in the methane. Therefore, if surface carbon has contributed recent carbon to the reservoir, and microbes have converted the modern carbon to methane, natural gas generated in the PRB during the last 50 ka

should be enriched in ^{14}C above detection limits. If radiocarbon values in methane are not above detection levels, it is likely that metabolism of organic carbon from coal is the nearly-exclusive flux of carbon into the PRB formation waters and natural gas deposits. Therefore under this scenario, in-situ microbial activity would overwhelm the signature of modern carbon from groundwater recharge, and result in a radiocarbon-dead signature in bicarbonate and methane in the reservoir.

6.3 Study area and stratigraphy

This study examined a region in the northern part of the Powder River Basin in southern Montana, USA, where active CBM production is ongoing. The Powder River Basin is a structural basin located on the border between northern Wyoming and southern Montana (Fig. 6.1). It is constrained by the Black Hills in the east and the Bighorn Mountains in the west. The coal seams in the basin are primarily Paleogene in age and were deposited during the retreat of the Western Interior Seaway (Anna, 1986; Bartos and Ogle, 2002). The gas and water samples for this study were obtained from the northwest corner of the Powder River Basin. Sample depths in this study range from 80 m to 527 m below ground surface (Table 6.1). All samples described in this chapter are derived from the Wyodak-Anderson coal zone, an upper subunit of the Paleogene (66–58 Ma) Fort Union Formation (Fig. 6.2), and an active zone of CBM production. The Paleogene succession is considered to be a regional aquifer (Bates et al. 2011).

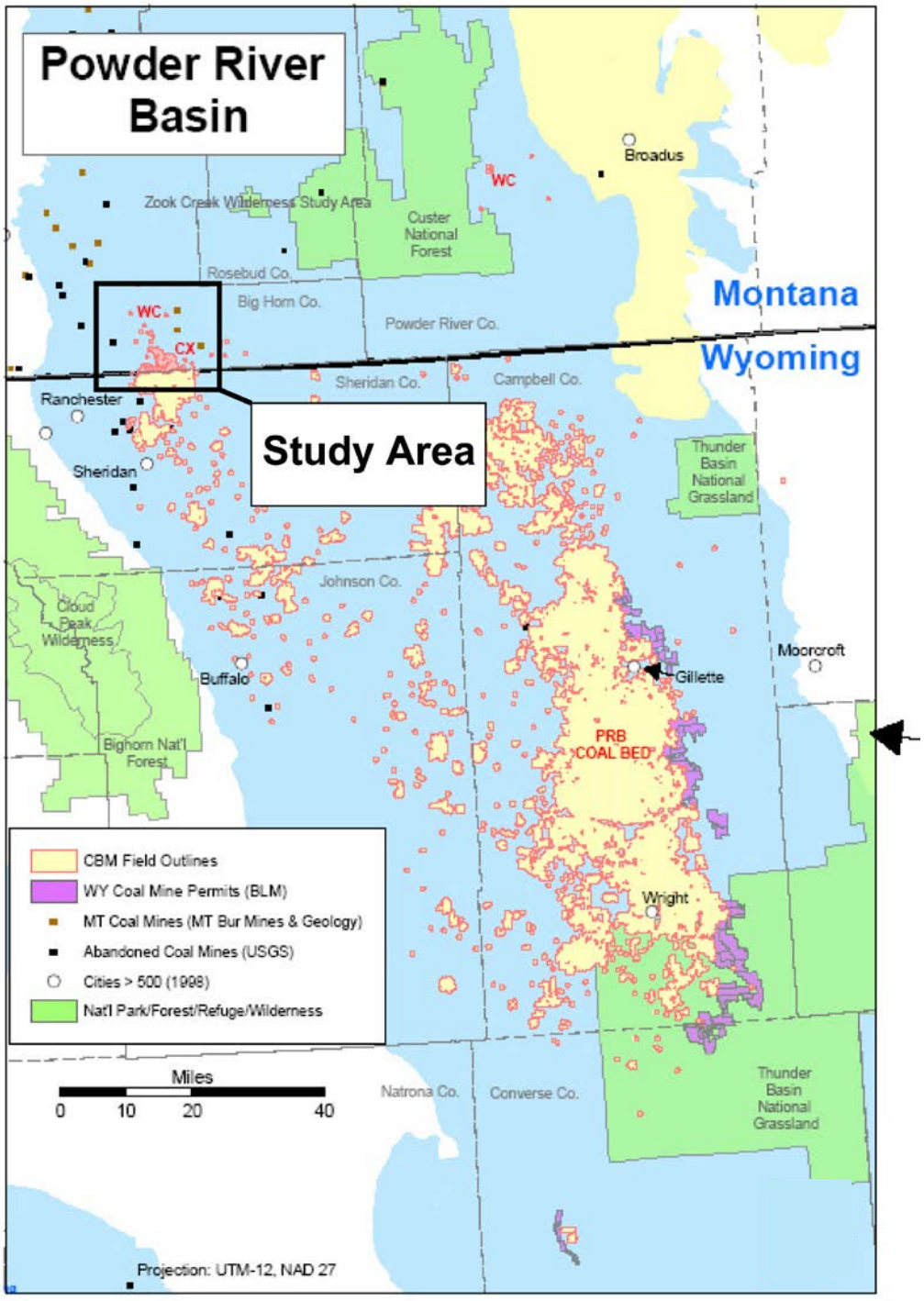

Figure 6.1: Regional coal development within the Powder River Basin. Adapted from Limerick (2004)

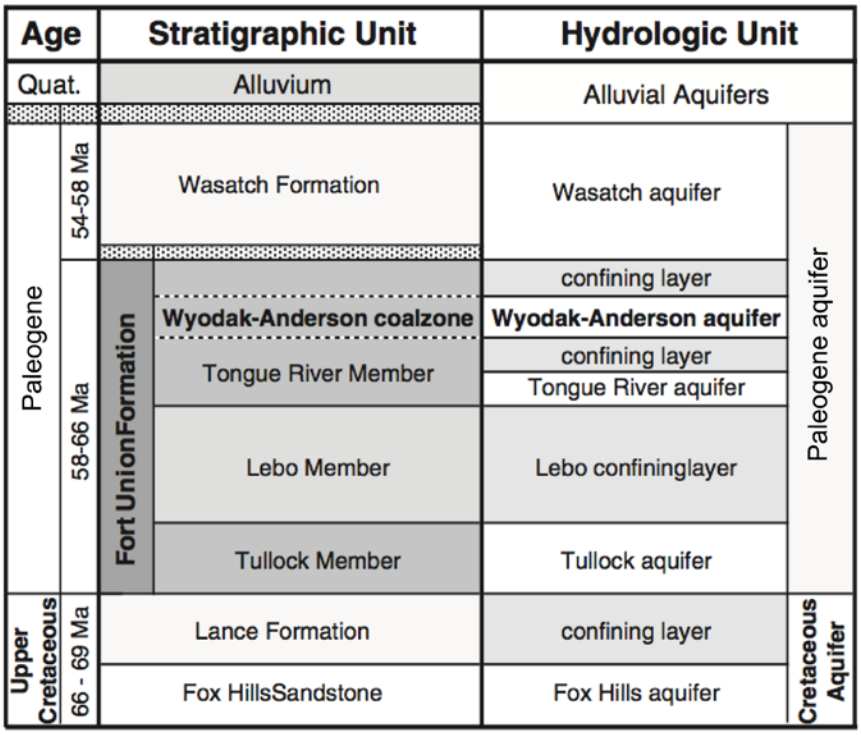

Figure 6.2: Stratigraphy of the Powder River Basin within the study area. Adapted from Bates et al. (2011).

6.4 Methods

6.4.1 Field Sampling

Produced gas samples from eight wells were obtained directly from the wellhead using the Isotube sampling system (Isotech Inc.). Groundwater samples for radiocarbon analysis were obtained from each of the eight wellheads by pumping unfiltered water into 500 mL type III soda-lime glass bottles with PTFE-faced lids until overflowing. Groundwater samples were sealed immediately and refrigerated at 4 ºC until analysis.

6.4.2 Stable isotope geochemistry

Stable isotope ratios of carbon and hydrogen that are displayed in Table 6.1 were measured by Vinson (personal communication, 2012), and will be published elsewhere. Stable isotope ratios of carbon are reported in delta notation relative to VPDB, and stable isotope ratios for hydrogen are reported relative to VSMOW.

$$\delta^{2}H \text{ or } \delta^{13}C\ (‰) = [(R_{sample} / R_{standard}) - 1] \times 1000 \qquad [3]$$

Where R represents the measured ratio of $^{13}C/^{12}C$ or $^{2}H/^{1}H$.

Precision for isotope measurements on hydrocarbons by gas-chromatography-isotope-ratio-mass-spectrometry (GC-IRMS) is typically ± 0.5‰ for carbon, and ± 5‰ for hydrogen.

Stable isotope ratios of hydrogen in water were reported by Vinson (personal communication, 2012). Stable isotope ratios of hydrogen in water are presented in delta notation, as per Equation 3, relative to VSMOW, with a typical precision of ± 1‰.

6.4.3 Gas line methane separation and combustion for radiocarbon analysis

To measure radiocarbon in methane, the methane must first be separated from other constituents of the mixed gas obtained from the wellhead (e.g. N_2, CO_2, C_2–C_5), and combusted to CO_2 to produce a pure sample for analysis. Samples were separated on a three-stage flow-

through pyrex gas line with ultra-high-purity helium (UHP-He) used as the carrier gas (Fig. 6.3). The gas line was evacuated and subsequently purged with helium for twenty minutes before each separation. Gas samples were introduced under low pressure by penetrating both sampling ports of the Isotube simultaneously with a needle. The flow rate of He gas was approximately 20 mL/min, and samples were flushed for 25 minutes each, equivalent to five volumes of the Isotube. The gas mixture was passed through a two-stage liquid N_2 trap to remove water, CO_2 and higher hydrocarbons (Stage 1). Methane was combusted to CO_2 in-line using a CuO furnace with a Pt catalyst at 850 ºC (Stage 2). The CO_2 resulting from methane combustion was trapped using a dual-coil liquid N_2 cryogenic trap, and the carrier gas was vented (Stage 3). After completely flushing the gas sample through the apparatus, stage three was sealed, and remaining volatile gases were evacuated by pumping. Subsequently, the CO_2 sample was released from the trap using a mixture of dry ice and ethanol and transferred to a Pyrex finger using a liquid N_2 trap. The Pyrex finger containing pure sample CO_2 was sealed and removed from the system using a blowtorch.

In-house laboratory methane standards were subjected to the same procedure as the samples, and subsequently analyzed for $\delta^{13}C$ to determine if complete combustion was achieved in the gas line. Methane standards that were combusted on the gas line and analyzed as CO_2 were within 1‰ of the accepted $\delta^{13}C$ value, indicating complete combustion was achieved in the system.

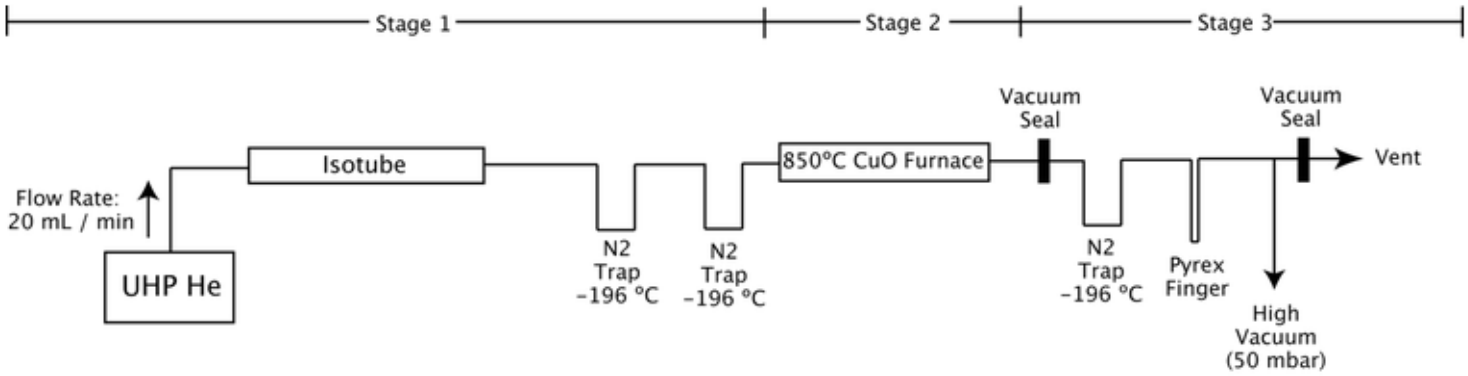

Figure 6.3: Schematic illustration of laboratory apparatus for separation of methane from CO_2 and other hydrocarbon gases. All higher hydrocarbons are trapped by the two-stage liquid nitrogen traps ahead of the furnace in Stage 2. Methane was combusted in the high temperature furnace and was trapped as CO_2 in Stage 3 of the apparatus.

6.4.4 AMS analysis

Methane-derived CO_2 in Pyrex tubes and untreated produced water samples were transported to the Rafter Radiocarbon Laboratory in Lower Hutt, New Zealand, for analysis by accelerator mass spectrometry (AMS). Radiocarbon values are reported as fraction modern (fm) compared with the ^{14}C Standard Reference Material 4990B, oxalic acid (Stuiver and Polach, 1977).

$$fm = [(^{14}C/^{12}C)_{sample}] / [0.95 \times (^{14}C/^{12}C)_{OX1}] \qquad [4]$$

OX1 represents the standard reference material 4990B.

Radiocarbon data were normalized to $\delta^{13}C$ of –25‰ to eliminate mass-dependent isotope effects, and were age corrected for the year of collection (2011). Stable isotope ratios of carbon were also measured for DIC at the Rafter Radiocarbon Laboratory and are reported in delta notation ($\delta^{13}C$) relative to the VPDB standard reference material. A University of Calgary thermogenic methane calibration standard was combusted and converted to CO_2 using the same separation apparatus as shown in Figure 6.3, and an fm value of 0.0021 was measured. For the purposes of this study, this value represents the minimum background radiocarbon level that can be attained for methane derived from produced gases, due to small amounts of contamination of samples by laboratory air.

Measured values of $\delta^{13}C_{CH4}$ from the sampled methane and $\delta^{13}C_{CO2}$ derived from combustion were compared to identify potential contamination during sample processing. All but one of the samples had a difference of less than 2‰, between $\delta^{13}C_{CH4}$ before combustion, and $\delta^{13}C_{CO2}$ after combustion, indicating that complete combustion was attained, and that there was minimal contamination from outside carbon sources. However, the stable isotope mass balance conducted on the pre-combustion $\delta^{13}C_{CH4}$ and post-combustion $\delta^{13}C_{CO2}$ values for sample PRB-3

suggested that this sample was contaminated with up to 10% atmospheric CO_2 during processing. Because of the elevated radiocarbon level, and elevated $\delta^{13}C_{CO2}$, the methane radiocarbon data for PRB-3 was discarded as contaminated.

6.5 Results and discussion

The stable isotope ratios of carbon and hydrogen indicated that the methane measured in this study was primarily biogenic in origin. $\delta^{13}C$ values of methane ranged from −78.2 to −57.9‰, and $\delta^{2}H_{CH4}$ values ranged from −327 to −279‰ (Table 6.1). Formation waters from the reservoirs in which the methane samples were obtained ranged in $\delta^{2}H$ values from −164 to −129‰ (Table 6.1). Figure 6.4 shows a hydrogen isotope plot comparing hydrogen isotope ratios of water and methane. $\delta^{2}H$ values in methane were consistently lower than $\delta^{2}H$ values in water by approximately 160‰. These data are consistent with the hydrogen isotope separation expected for biological CO_2 reduction, as described by Equation 5:

$$\delta^{2}H_{CH4} = \delta^{2}H_{H2O} - 160 \pm 10 \qquad [5]$$

$\delta^{13}C$ values for DIC ranged from −11.0‰ to +16.2‰. Figure 6.5 shows a dual-isotope plot of carbon isotope separation between DIC and methane ($\Delta^{13}C_{DIC\text{-}CH4}$), versus the hydrogen isotope composition of methane.

$$\Delta^{13}C_{DIC\text{-}CH4} = \delta^{13}C_{DIC} - \delta^{13}C_{CH4} \qquad [6]$$

Typical carbon isotope separation values between DIC and methane during microbial CO_2 reduction range from 49 to 95‰, and separation factors for methyl fermentation typically range from 39 to 58‰ (Whiticar, 1999). In this study, isotope separation between DIC and methane ranged from 61.6 to 82.0‰, suggesting that CO_2 reduction is the predominant process for forming CH_4 in these samples (Whiticar, 1999). Hence, carbon and hydrogen isotope ratios strongly suggest CO_2 reduction as the primary pathway of methanogenesis. Combining the

expected hydrogen isotope fractionation from Equation 3 with the expected carbon isotope separation between DIC and methane, the gas samples from this study are all consistent with a biogenic origin via the CO_2 reduction pathway.

Radiocarbon results for DIC and CH_4 are presented in Table 6.1. Radiocarbon data in organic-rich reservoirs do not represent true ages due to the potential for respiration and carbonate exchange reactions in the subsurface (Clark and Fritz 1997). Therefore, all radiocarbon analyses in this study are presented as fraction modern (fm), as opposed to an absolute radiocarbon date. All formation water DIC samples were considered radiocarbon dead within analytical and sampling error, with fm values ranging from 0.0003 to 0.0051. Seven out of eight radiocarbon values measured for methane were considered to be radiocarbon-dead falling into a range of fm values from 0 to 0.0071. One exception, PRB-5, had a measured fm value of 0.0401, that was above background levels. This sample may have also been contaminated by laboratory processing because the ^{14}C values for DIC in this well displayed a background fm value of 0.0018.

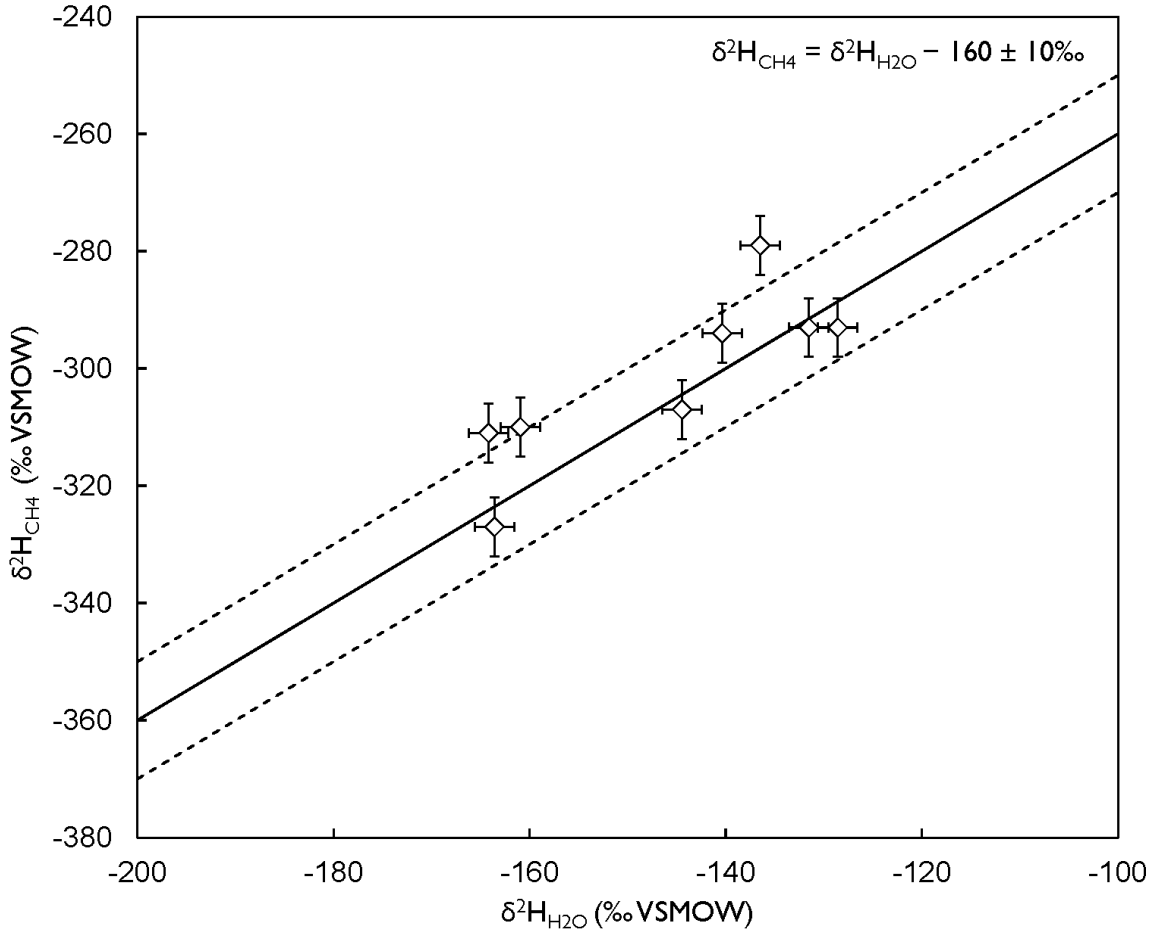

Figure 6.4: Comparison of δ^2H values for methane and produced water from measured samples in the PRB. The values fall within the expected range for CO_2 reduction, plotted on the graph as a solid line with ± 10‰ indicated by dashed lines (Whiticar, 1999).

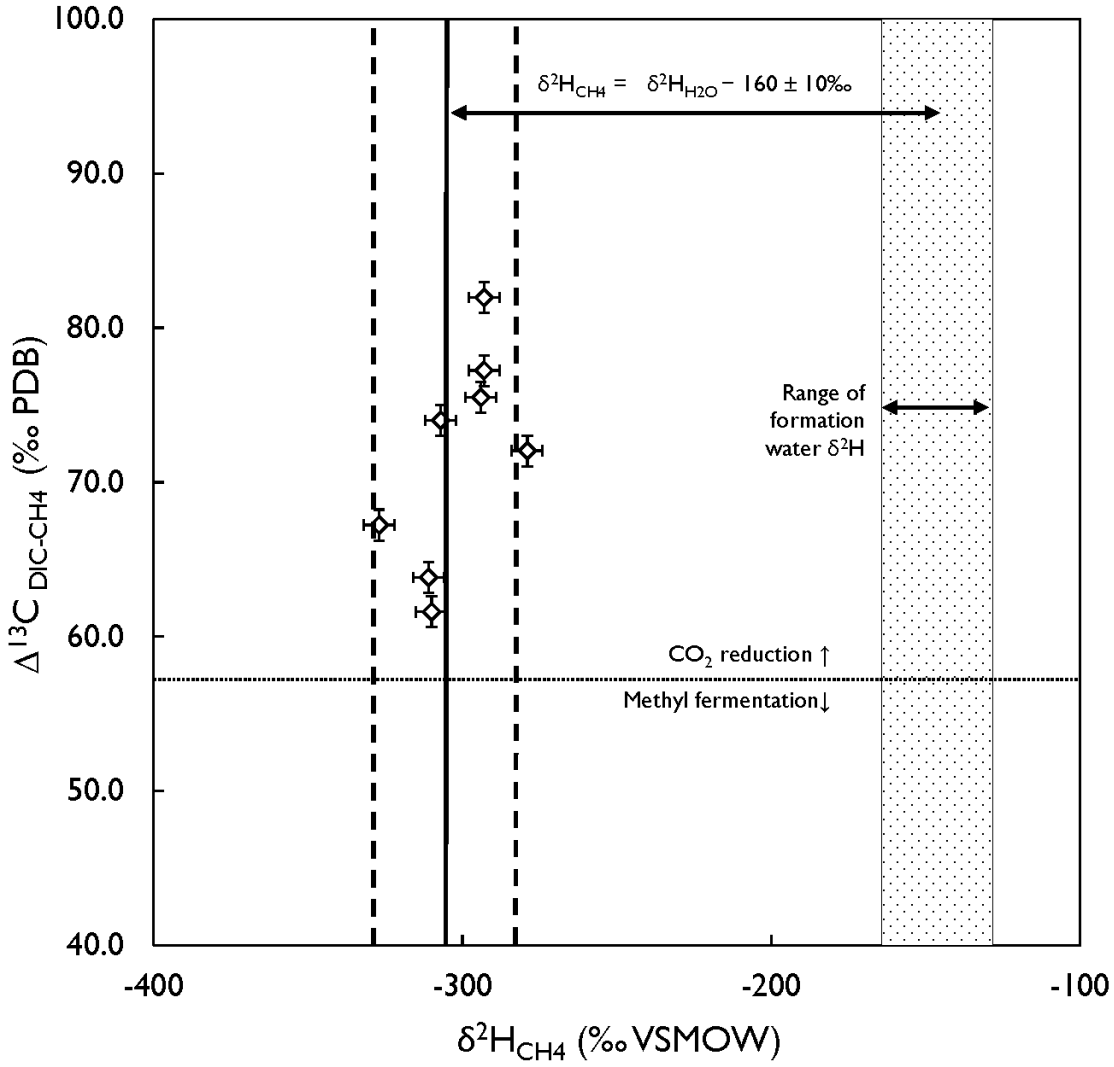

Figure 6.5: Dual-isotope plot showing δ^2H of methane against the carbon isotope separation between DIC and CH_4 for the produced samples. The range of δ^2H for PRB formation waters is illustrated as a dotted range, and the expected hydrogen isotope value for methane derived from CO_2 reduction is plotted as a solid vertical line with 10‰ uncertainty represented by dashed lines. The dotted horizontal line represents the expected offset between $\delta^{13}C$ of DIC and methane for the CO_2 reduction (above the line) and methyl fermentation (below the line) pathways (Whiticar, 1999).

Table 6.1: Selected fluid properties from measured wells in the Powder River Basin.

Sample ID	Latitude	Longitude	Depth (m)	C1/ (C2−C5)	δ^2H_{H2O} (‰)	δ^2H_{CH4} (‰)	$\delta^{13}C_{CH4}$ (‰)	$\delta^{13}C_{DIC}$ (‰)	DIC *f*m	CH_4 *f*m
PRB-1	44.97613	−106.76998	376	868	−140	−294	−59.3	16.2	0.0033	0.0071
PRB-2	44.90754	−106.71326	527	1 475	−129	−293	−62.6	14.6	0.0003	−0.0005
PRB-3	45.03003	−106.88097	190	1 231	−161	−310	−64.0	−2.4	0.0024	n.m.
PRB-4	45.01158	−106.91223	166	585	−164	−327	−78.2	−11.0	0.0026	0.0010
PRB-5	44.97296	−106.86689	218	521	−144	−307	−57.9	16.1	0.0018	0.0401
PRB-6	45.04324	−106.90211	179	615	−164	−311	−62.3	1.5	0.0023	0.0040
PRB-7	45.12535	−106.48363	80	2 534	−131	−293	−69.4	12.6	0.0009	−0.0006
PRB-8	45.43497	−106.39206	117	10 933	−137	−279	−67.4	4.6	0.0051	−0.0004
CH_4 blank	n.a.	n.a.	n.a.	n.a.	n.a.	n.a.	−36.2	n.a.	n.a.	0.0021

n.m. sample was not measured for ^{14}C content due to contamination during laboratory processing
n.a. = lab standard of thermogenic methane used to verify separation and combustion methodology

The simplest explanation for the radiocarbon-dead values observed for DIC and CH_4 in this study is that groundwater recharge has not occurred in these reservoirs over the past 50,000 years. However, this interpretation is not consistent with suggested modern recharge in the hydrogeological system as previously proposed by Flores et al. (2008) and Bates et al. (2011). The majority of radiocarbon in groundwater recharge is derived from the metabolism of organic matter in the soil zone and subsequent infiltration into the subsurface (Trumbore, 2009). The amount of dissolved inorganic carbon in shallow groundwater is approximately 50 mg of carbon per litre in the PRB region (Sharma and Frost, 2007), and an approximate hundred-fold dilution with ancient ^{14}C-free carbon would be required to lower the radiocarbon value of DIC below detection limits.

Several processes may contribute to the elimination of modern carbon in DIC and CH_4 including radioactive decay along a slow flow path, carbon exchange with carbonate minerals, bacterial sulfate reduction and, most likely, methanogenesis of coal-derived carbon.

Carbonate exchange and dissolution reactions occur in the shallow subsurface, diluting the radiocarbon signal of DIC and causing an over-estimate of the ^{14}C age of groundwater (Clark and Fritz, 1997). There are models available to correct radiocarbon signals to account for exchange reactions, however, correction factors cannot be used when radiocarbon is below detection limits, as is the case in this study.

Bacterial sulfate reduction (BSR) is an important process in anoxic reservoirs where sulfate is an abundant anion. When coal is the carbon source for BSR, one mole of radiocarbon-dead DIC is generated for each mole of SO_4^{2-} consumed by microbes. None of the eight waters derived from the eight sampled wells contained detectable dissolved sulfate (Vinson, personal communication, 2012). However, Rice et al. (2008) reported substantial dissolved sulfate in

shallower CBM reservoirs and aquifers in the region and attributed its source to oxidation of pyrite and anhydrite dissolution. Due to the availability of coal-derived organic carbon in these aquifers, sulfate that infiltrated with groundwater would be rapidly consumed by bacterial sulfate reduction on the margins of the basin where infiltration occurred. Therefore the absence of sulfate in these reservoirs, and presence of sulfate in overlying aquifers suggest that bacterial sulfate reduction likely contributed a component of radiocarbon-dead DIC to this system, substantially diluting the modern carbon signature of downward infiltrating DIC.

Subsequent to removal of sulfate, methanogenesis becomes the dominant reservoir biogeochemical process. Methanogenesis results in net production of radiocarbon-dead DIC and CH_4 due to the biodegradation of coal hydrocarbons, thus continuously overwhelming the modern radiocarbon signal of DIC from groundwater recharge (Equation 7, Jones et al., 2008; Strapoc et al., 2011). Four of the eight groundwater wells sampled (PRB-1, PRB-2, PRB-5, and PRB-7) contained DIC that was enriched in ^{13}C (Table 6.1), thus was suggestive of active methanogenesis. Coal hydrocarbons are chemically distinct from petroleum due to their origin as terrestrial plant matter as opposed to marine biomass. However, biodegradation in the subsurface likely proceeds via similar mechanisms and pathways to petroleum biodegradation, generating products that dilute any modern radiocarbon in both the DIC and methane carbon pools. For example, the methanogenic alkane degradation by CO_2 reduction (MADCOR) stoichiometry proposed by Jones et al. (2008) results in the generation of forty-nine moles of methane and fifteen moles of CO_2 from four moles of an n_{16} alkane, that would further dilute the modern radiocarbon signature of DIC during active methanogenesis (Equation 7).

$$4C_{16}H_{34} + 30H_2O \rightarrow 15CO_2 + 49CH_4 \qquad [7]$$

Even more significant would be the generation of one mole of CO_2 for every mole of CH_4 if acetoclastic methanogenesis was a significant process within the reservoir (Equation 2), however, the stable isotope results appear to indicate CO_2 reduction as the primary pathway. Therefore if the rate of methanogenesis and associated in situ CO_2 generation in the reservoir is much greater than the rate of carbon influx from surface waters, the modern radiocarbon input from surface water could be rapidly diluted by active microbial communities, leading to the observed radiocarbon-dead signature in DIC. A radiocarbon-dead signature in DIC would lead to a radiocarbon-dead signature in CH_4, because no detectable radiocarbon would exist in the DIC pool for methanogens to metabolize. Methane derived from coal would also have a radiocarbon-dead signature.

The above-background ^{14}C value observed in the PRB-5 methane sample, fm = 0.0401, was challenging to explain given the available data. The $\delta^{13}C_{CH4}$ value was unchanged before and after the collection and laboratory separation process, therefore laboratory processing did not likely contaminate the sample. The DIC in the reservoir was radiocarbon-dead, indicating that any modern methane generated in this reservoir would also be radiocarbon-dead. By all other metrics (e.g. geographic location, aqueous geochemistry, depth, water stable isotopes) the well was not unusual from the other sampled wells.

6.6 Conclusions

While the studied section of the Powder River Basin contained significant amounts of biogenic methane, and is suggested to have modern groundwater recharge, none of the DIC or CH_4 measured in this study contained measurable amounts of radiocarbon. Therefore, the amount of carbon reaching the CBM reservoirs from surface recharge of groundwater is insignificant compared to the amount of carbon metabolized within the reservoir itself.

Previous models of regional groundwater flow provide multiple lines of evidence that remain supportive of recent recharge, however this study provides evidence that DIC from shallow groundwater recharge is not a significant component of the carbon cycle in these CBM reservoirs. The conspicuous absence of radiocarbon in the basin should not be used to discount the hypothesis of modern recharge-driven methanogenesis, as these ideas are not mutually exclusive due to the possibility of rapid biogeochemical cycling in the subsurface. It is plausible that the recent recharge provides nutrients and supports geochemical conditions conducive to methanogenesis. However, according to the presented data, the modern groundwater system does not provide the carbon source for methane generation in the studied section of the PRB.

6.7 References

Anna, L. O. (1986). *Geologic Framework of the Groundwater System in Jurassic and Cretaceous Rocks in the Northern Great Plains, in Parts of Montana, North Dakota,* South *Dakota, and Wyoming* (No. 1402-B) (pp. 1–45). United States Geological Survey.

Bates, B. L., Mcintosh, J. C., Lohse, K. A., & Brooks, P. D. (2011). Influence of groundwater flowpaths, residence times and nutrients on the extent of microbial methanogenesis in coal beds: Powder River Basin, USA. *Chemical Geology*, *284*(1-2), 45–61.

Bartos, T. T., & Ogle, K. M. (2002). *Water Quality and Environmental Isotopic Analyses of Groundwater Samples Collected from the Wasatch and Fort Union Formations in Areas of Coalbed Methane Development – Implications to Recharge and Groundwater Flow, Eastern Powder River Basin, Wyoming* (No. 02-4045). United States Geological Survey (pp. 1–96).

Clark, I., & Fritz, P. (1997). *Environmental Isotopes in Hydrogeology*. Lewis Publishers.

Claypool, G.E., 2001. Geochemical characterization of biogenic gas and coalbed methane in shallow gas fields: Eastern Denver Basin, Powder River Basin and Williston Basin. Luca Technologies Internal Report (http://www.lucatechnologies.com).

Flores, R. M., Rice, C. A., Stricker, G. D., Warden, A., & Ellis, M. S. (2008). Methanogenic pathways of coal-bed gas in the Powder River Basin, United States: The geologic factor. *International Journal of Coal Geology*, *76*(1-2), 52–75.

Formolo, M. J., Salacup, J. M., Petsch, S. T., Martini, A. M., & Nusslein, K. (2008a). A new model linking atmospheric methane sources to Pleistocene glaciation via methanogenesis in sedimentary basins. *Geology*, *36*(2), 139–142.

Formolo, M., Martini, A., & Petsch, S. (2008b). Biodegradation of sedimentary organic matter associated with coalbed methane in the Powder River and San Juan Basins, U.S.A. *International Journal of Coal Geology*, *76*(1-2), 86–97.

Jones, D. M., Head, I. M., Gray, N. D., Adams, J. J., Rowan, A. K., Aitken, C. M., Bennett, B., Huang, H., Brown, A., Bowler, B. J. F., Oldenburg, T., Erdmann, M., and Larter S.R. (2008). Crude-oil biodegradation via methanogenesis in subsurface petroleum reservoirs. *Nature*, *451*(7175), 176–180.

Limerick, S. H. (2004) Coalbed Methane in the United States: A GIS Study. *AAPG Annual Meeting*, Dallas, Texas, April 18-21, 2004. Available online: http://www.searchanddiscovery.com/documents/2004/limerick/index.htm

LucaTechnologies. (2004). *Active Biogenesis of Methane in Wyoming's Powder River Basin*. Luca Technologies Inc., 9 pp. (http://www.lucatechnologies.com).

Martini, A. M., Budai, J. M., Walter, L. M., & Schoell, M. (1996). Microbial generation of economic accumulations of methane within a shallow organic-rich shale. *Nature* 383(6596): 155-158.

Martini, A. M., Walter, L. M., Budai, J. M., Ku, T., Kaiser, C. J., & Schoell, M. (1998). Genetic and temporal relations between formation waters and biogenic methane: Upper Devonian Antrim Shale, Michigan Basin, USA. *Geochimica Et Cosmochimica Acta*, *62*(10), 1699–1720.

Martini, A. M., Walter, L. M., Ku, T. C. W., Budai, J. M., McIntosh, J. C., & Schoell, M. (2003). Microbial production and modification of gases in sedimentary basins: A geochemical case study from a Devonian shale gas play, Michigan basin. *AAPG Bulletin-American Association of Petroleum Geologists*, *87*(8), 1355.

McIntosh, J., Walter, L., & Martini, A. (2002). Pleistocene recharge to midcontinent basins: Effects on salinity structure and microbial gas generation. *Geochimica Et Cosmochimica Acta*, *66*(10), 1681–1700.

Mcintosh, J. C., Walter, L. M., & Martini, A. M. (2004). Extensive microbial modification of formation water geochemistry: Case study from a Midcontinent sedimentary basin, United States. *Geological Society of America Bulletin*, *116*(5), 743.

McIntosh, J. C., & Walter, L. M. (2005). Volumetrically significant recharge of Pleistocene glacial meltwaters into epicratonic basins: Constraints imposed by solute mass balances. *Chemical Geology*, *222*(3-4), 292–309.

Rice, C. A., Flores, R. M., Stricker, G. D., & Ellis, M. S. (2008). Chemical and stable isotopic evidence for water/rock interaction and biogenic origin of coalbed methane, Fort Union Formation, Powder River Basin, Wyoming and Montana U.S.A. *International Journal of Coal Geology*, *76*(1-2), 76–85.

Sharma, S., & Frost, C. D. (2007). Tracing Coalbed Natural-Gas-Coproduced Water Using Stable Isotopes of Carbon. *Groundwater*, *46*(2), 329–334.

Strąpoć, D., Mastalerz, M., Eble, C., & Schimmelmann, A. (2007). Characterization of the origin of coalbed gases in southeastern Illinois Basin by compound-specific carbon and hydrogen stable isotope ratios. *Organic Geochemistry*, *38*(2), 267–287.

Strapoc, D., Picardal, F. W., Turich, C., Schaperdoth, I., Macalady, J. L., Lipp, J. S., et al. (2008). Methane-Producing Microbial Community in a Coal Bed of the Illinois Basin. *Applied and Environmental Microbiology*, *74*(8), 2424–2432.

Strąpoć, D., Mastalerz, M., Schimmelmann, A., Drobniak, A., & Hedges, S. (2008). Variability of geochemical properties in a microbially dominated coalbed gas system from the eastern margin of the Illinois Basin, USA. *International Journal of Coal Geology*, *76*(1-2), 98–110.

Strąpoć, D., Mastalerz, M., Schimmelmann, A., Drobniak, A., & Hasenmueller, N. R. (2010). Geochemical constraints on the origin and volume of gas in the New Albany Shale (Devonian–Mississippian), eastern Illinois Basin. *Aapg Bulletin-American Association of Petroleum Geologists*, *94*(11), 1713–1740.

Strąpoć, D., Mastalerz, M., Dawson, K., Macalady, J., Callaghan, A. V., Wawrik, B., et al. (2011). Biogeochemistry of Microbial Coal-Bed Methane. *Annu. Rev. Earth Planet. Sci.*, *39*(1), 617–656.

Stuiver, M., & Polach, H. A. (1977). Discussion: Reporting of 14C Data. *Radiocarbon*, *19*(3), 355–363.

Trumbore, S. (2009). Radiocarbon and Soil Carbon Dynamics. *Annual Review Of Earth And Planetary Sciences*, *37*, 47–66.

United States of America, Office of Integrated Analysis and Forecasting, E. I. A. (2007). *Annual Energy Outlook 2007*: With Projections to 2030, 1–243.

Vinson, D. (2012). Stable isotope and geochemical parameters of the Powder River Basin wells analyzed in this study were provided as a personal communication to the author ahead of publication by the University of Arizona research team. *University of Arizona*, Tuscon, AZ.

Whiticar, M. (1999). Carbon and hydrogen isotope systematics of bacterial formation and oxidation of methane. *Chemical Geology*, *161*, 291–314.

Chapter Seven: Summary of Major Findings and Future Work

7.1 Thesis summary

The objective of this thesis was to advance knowledge and understanding of hydrogeology and biogeochemistry in the oil sands systems of the Athabasca oil sands region of Alberta. The following is a summary of major conclusions derived from the preceding chapters.

Chapter Two described how the salinity of McMurray Formation water in the Athabasca Oil Sands Region (AOSR) has been influenced by upward groundwater flow from Devonian strata that lie beneath the oil sands resources. A linear feature of elevated TDS in McMurray Formation waters was observed above the dissolution edge of the Prairie Evaporite Formation, spanning the entire length of the AOSR. The Devonian strata beneath the McMurray Formation are heavily influenced by karst hydrogeology, providing a network of conduits for rapid groundwater flow. The proposed driving force for upward formation water flow is the basin scale response to meltwater injection via continental ice sheets during the Pleistocene epoch. Possible impacts of high-salinity formation water influx on oil sands leases in the AOSR include the potential for reservoir souring via bacterial sulfate reduction, misinterpretation of geophysical logs that rely on electrical resistivity to calculate water saturation, and the unplanned discharge of high-salinity formation waters into surface water systems.

In Chapter Three a new technique was developed to determine the stable isotope composition and total dissolved solids concentration of porewater samples extracted from oil sands drill cores. Drilling mud contamination of fluids from drill core was eliminated using a two end-member isotope mixing calculation. This technique provided a mechanism to identify heterogeneity in formation water stable isotope composition and total dissolved solids concentration, both laterally within an oil sands lease area, and vertically within a single well by

direct measurements from drill core. This technique has the capacity to dramatically increase water sampling frequency within an oil sands lease area and to provide hydrogeologists with a new tool to determine groundwater heterogeneity in oil sands systems.

Chapter Four described a proof-of-concept study at the Suncor-Firebag oil sands area that demonstrated the applicability of the method developed in Chapter Three. Minor variations in TDS and stable isotope compositions were observed across the Firebag field, however all data at Firebag were consistent with the regional topographically-driven hydrogeology described in previous research (WorleyParsons, 2010). An additional important finding of this study was the identification of wells with vertical heterogeneity, where aqueous fluid properties changed with depth within a single well. Compartmentalized reservoirs have been described previously using organic geochemistry (Fustic et al., 2012), and therefore the observation of wells with distinct porewater TDS values above and below a physical barrier was not unexpected. The widespread application of the porewater technique for measuring formation water compositions in oil sands will enable three-dimensional assessment of reservoir water within an oil sands lease area, and has the capability to provide exceptionally detailed characterization of the hydrogeology and water sources of oil sands reservoirs.

The heterogeneity observed in oil sands formation water TDS across the AOSR in Chapter Two led to another question, “How are reservoir microbial communities impacted by changes in formation water chemistry?” The laboratory experiments describd in Chapter Five illustrated important differences in biogeochemical processes that occur in oil sands systems. Changes in the geochemistry of the aqueous media, from freshwater with no sulfate (TDS = 1 900 mg/L), to brackish water with no sulfate (TDS = 7 000 mg/L), to saline water with 2 000 mg/L of dissolved sulfate (TDS = 22 000 mg/L) resulted in significant changes in the

biogeochemical processes responsible for methane generation, and suggested that aqueous geochemistry may be an important control on biodegradation of oil over geological time in the AOSR. However, despite the differences in microbial methane generation pathways among the samples with distinct aqueous geochemistry, the laboratory experiment generated results that were atypical of natural systems. Thus, further investigation is warranted to explain the differences of results obtained under laboratory and field conditions, and more thoroughly understand how aqueous geochemistry impacts oil sands reservoir microbial processes.

Understanding the rates and pathways of methanogenesis is important in field studies as well as laboratory studies. Chapter Six attempted to use natural abundance radiocarbon to trace methanogenesis in an oil-sands analogue site: a coalbed methane system in the Powder River Basin of Montana, USA. However, despite evidence of recent hydrogeological recharge from other studies, no radiocarbon was detected in the dissolved inorganic carbon or methane found in the reservoir. This suggests substantially more carbon cycling occurs via microbial metabolism of radiocarbon-dead coal than is input into the basin via transport of DIC from the surface. A non-zero radiocarbon signature has been detected in DIC from several oil sands formation waters throughout the AOSR (Lemay, 2003), and therefore a natural abundance radiocarbon approach may be more useful for tracing microbial methane generation within these reservoirs than within the Powder River Basin.

7.2 Future work

The research described within this thesis has provided insight into the hydrogeological and biogeochemical systems in the AOSR. However there is substantial work that could follow in the future to broaden the scope of the applications described, and to fill gaps in understanding.

The number of groundwater observation wells that have been drilled in the AOSR has increased rapidly as development of bitumen resources accelerates. Physical hydrogeological and geochemical data from these groundwater wells are readily available through Environmental Impact Assessment (EIA) documents. The focus of the EIA is often local to sub-regional and these documents neglect the AOSR as a whole. Substantial improvements could be made to the understanding of regional hydrogeological processes via a regional-scale synthesis of all available data. The scope of the work in Chapter Two was exclusively focused on the McMurray Formation waters, however the data from the overlying and underlying formations exist, and could be synthesized to improve upon the existing regional groundwater models. The regional hydrogeology article by Bachu and Underschultz (1993) remains one of the most frequently cited regional groundwater studies in Environmental Impact Assessment documents and industry literature. However, more data have been collected in the twenty years since publication of this report than was available for the interpretation provided in the Bachu and Underschultz article (1993). Therefore, improved interpretation of regional processes would likely result from re-examination of currently available data. Both the oil sands industry and government regulators would benefit from a synthesis of the currently available groundwater data. It is the author's opinion that such a synthesis would be best conducted by government scientists (e.g. the Alberta Geological Survey or Alberta Energy Regulator), as permanent staff would be best able to maintain a current database with new data added as they are reported. However, in present-day Alberta the apparent lack of government resources dedicated to thorough science-based environmental monitoring in the oil sands may require an academic institution to continue this type of research.

There is substantial future work required to fully develop the potential of the porewater technique for determining oil sands formation water properties (Chapters Three and Four). Future method development may enable the characterization of formation water geochemistry on an ion-specific basis. However, initial attempts to approach this challenge were unsuccessful, possibly due to the similarity of TDS values of Firebag waters and drilling fluids. The reservoir porewater characterization technique could be applied to hundreds of uncharacterized lease areas across the AOSR, and combined with GIS and spatial statistical analysis to provide a detailed understanding of formation water chemistry in oil sands reservoirs. Detailed TDS and stable isotope mapping of formation water within individual leases, such as what was conducted at Firebag in Chapter Four, can provide essential information about groundwater flow, assist with geophysical log interpretation of water saturation, and perhaps be used to directly measure steam movement in the subsurface during in-situ energy recovery. Determining formation water TDS and isotope composition with high spatial resolution is especially relevant in areas that may have elevated formation water salinity, such as the areas above the Prairie evaporite dissolution edge described in Chapter Two. Variations in TDS within a lease area have been observed in the AOSR (Teck Resources Ltd., 2011), and exploring these variations in detail before development of a new resource play could lead to better decisions about well configuration, design of industrial water treatment facilities, and avoid environmental risk from reservoir souring due to bacterial sulfate reduction or pipe scaling due to incompatible water geochemistry. The porewater technique for reservoir water characterization has the potential to become a standard tool in the development of in situ resources in the AOSR, and the next step will be the adoption of the method by oil sands operators. At the time of writing, Suncor will contribute to two additional ongoing but incomplete formation water characterization studies using the porewater

technique during the 2014 winter drilling season. Three other companies have expressed preliminary interest in this type of analysis within their own lease areas.

The relationship between microbial processes and aqueous geochemistry in shallow fossil energy reservoirs remains poorly constrained and understood. Chapter Five yielded suggestive, but far from conclusive results about the impact of aqueous geochemistry on microbial processes and Chapter Six suggested that biodegradation of coal contributes substantially more carbon to a coal bed methane carbon cycle than recent groundwater transport of carbon from Earth's surface. Integration of molecular biology with isotope geochemistry in future studies will likely yield essential gains in understanding of microbial processes in shallow reservoir systems. By using molecular biology and isotope geochemistry in tandem, thus combining the two key questions, "what microbes are living in a reservoir?" and, "what processes and metabolic pathways are the microbes utilizing?" an improved understanding of the reservoir microbial system may be obtained in the future.

Continued in-situ energy resource development in the oil sands regions of Alberta will necessitate the exploitation of substantial groundwater resources, and demand improvements in water use efficiency for steam-based bitumen recovery. Future in-situ energy developments may incorporate biological recovery of resources that will require a detailed knowledge of the reservoir microbial communities and the geochemical processes that these microbes perform. This thesis has provided novel insights into both biogeochemical and hydrogeological processes relevant to oil sands exploitation in Alberta. Improved water and energy efficiency in resource recovery, gained from improved characterization of oil sands systems, will be beneficial to society while we transition to a decarbonized energy economy over the next century.

7.3 References

Bachu, S. and Underschultz J.R. (1993). Hydrogeology of formation waters, northeastern Alberta. *AAPG Bulletin, 77*(10), 1745–1768.

Fustic, M., Bennett, B., Hubbard, S. M., Huang, H., Oldenburg, T., & Larter, S. (2012). Impact of Reservoir Heterogeneity and Geohistory on the Variability of Bitumen Properties in the Athabasca Oil Sands, Canada. *AAPG Studies in Geology*, *64*, 1–42.

Lemay, T. (2002a). *Geochemical and Isotope Data Formation Water from Selected Wells, Cretaceous to Quaternary Succession, Athabasca Oil Sands (In Situ) Area, Alberta.* Alberta Energy and Utilities Board Geo-Note 2002-02, 1−71.

Lemay, T. (2002b). *Carbon-14 Dating of Groundwater from Selected Wells in Quaternary and Quaternary-Tertiary Sediments, Athabasca Oil Sands (In Situ) Area*, Alberta. Alberta Energy and Utilities Board Geo-Note 2002-03, 1–21.

Teck Resources Ltd. (2011). *Frontier Oil Sands Mine Project Environmental Impact Assessment*. Alberta Energy and Utilities Board and Alberta Environment. Edmonton, Alberta, Canada.

APPENDIX A: SUPPORTING INFORMATION FOR CHAPTER TWO

Table A1: Data Source, Location and TDS values of McMurray Formation waters presented as summary data in Chapter 2. Unless otherwise indicated, TDS values were calculated by addition of major cations and anions with a charge balance of less than 10%.

Source	Latitude	Longitude	TDS (mg/L)
Canadian Natural Resources Ltd. 2006	57.3280301	-111.6892675	278 652
Canadian Natural Resources Ltd. 2006	57.3971505	-111.8246233	23 106
Canadian Natural Resources Ltd. 2006	57.3680779	-111.6960397	5 080
Canadian Natural Resources Ltd. 2006	57.3316944	-111.7434073	21 500
Canadian Natural Resources Ltd. 2006	57.3243726	-111.6892664	22 900
Canadian Natural Resources Ltd. 2006	57.3571211	-111.7095629	72 500
Canadian Natural Resources Ltd. 2006	57.3280301	-111.6892675	570
Shell Canada Limited, 2002	57.2844453	-111.1476851	3 280
Shell Canada Limited, 2002	57.2190438	-111.2424672	2 330
Shell Canada Limited, 2002	57.2553863	-111.3845924	982
Shell Canada Limited, 2002	57.2371638	-111.4116567	2 290
Shell Canada Limited, 2002	57.2153593	-111.2492379	2 792
Shell Canada Limited, 2002	57.2262905	-111.2898579	1 800
Shell Canada Limited, 2002	57.2553775	-111.2763148	1 252
Shell Canada Limited, 2002	57.2553816	-111.2627752	1 397
Shell Canada Limited, 2002	57.2589901	-111.2763146	1 284
Shell Canada Limited, 2002	57.2626027	-111.2763144	2 296
Shell Canada Limited, 2002	57.2371473	-111.4522508	3 830
Shell Canada Limited, 2002	57.2626027	-111.2763144	1 572
Shell Canada Limited, 2002	57.2626062	-111.4251868	2 930
Shell Canada Limited, 2002	57.2662235	-111.4590155	2 660
Shell Canada Limited, 2002	57.25678287	-111.3575744	1 370
Shell Canada Limited, 2002	57.26416291	-111.4252563	2 930
Shell Canada Limited, 2002	57.26651519	-111.4588421	2 660
Shell Canada Limited, 2002	57.2626088	-111.2560049	1 410
Shell Canada Limited, 2002	57.28785438	-111.2919806	3 280
Shell Canada Limited, 2002	57.21920135	-111.4063914	2 330
Shell Canada Limited, 2002	57.2542435	-111.3840032	982
Shell Canada Limited, 2002	57.23906678	-111.4108514	2 290
Shell Canada Limited, 2002	57.2153593	-111.2492379	2 792
Shell Canada Limited, 2002	57.2262905	-111.2898579	1 800
Shell Canada Limited, 2002	57.2553775	-111.2763148	1 252
Shell Canada Limited, 2002	57.2553816	-111.2627752	1 397
Shell Canada Limited, 2002	57.2378743	-111.4495398	3 910
Shell Canada Limited, 2002	57.26334283	-111.2785899	1 572
Shell Canada Limited, 2002	57.2589901	-111.2763146	1 284

Source	Latitude	Longitude	TDS (mg/L)
Shell Canada Limited, 2002	57.2626027	-111.2763144	2 296
WorleyParsons Komex, 2007	57.33168102	-111.3264432	1 470
WorleyParsons Komex, 2007	57.37033643	-111.286022	729
WorleyParsons Komex, 2007	57.37511556	-111.3770574	990
WorleyParsons Komex, 2007	57.39158882	-111.2456296	534
WorleyParsons Komex, 2007	57.40797901	-111.3606319	485
WorleyParsons Komex, 2007	57.42405295	-111.2932866	573
WorleyParsons Komex, 2007	57.42982735	-111.3277767	454
Imperial Oil Limited, 2007	57.41181982	-111.1136408	548
Imperial Oil Limited, 2007	57.37879768	-111.0797115	440
Imperial Oil Limited, 2007	57.39449154	-111.1234368	422
Imperial Oil Limited, 2007	57.41896424	-111.0732224	342
Imperial Oil Limited, 2007	57.38638988	-111.0906068	404
Imperial Oil Limited, 2007	57.31057824	-111.2284828	1 540
Imperial Oil Limited, 2007	57.29530674	-111.2694563	1 286[b]
Imperial Oil Limited, 2007	57.33855131	-111.2132067	1 461
Imperial Oil Limited, 2007	57.33178309	-111.1813767	488 [b]
Imperial Oil Limited, 2007	57.30438039	-111.3295219	1 237 [b]
Imperial Oil Limited, 2007	57.30672865	-111.2499206	1 130
Imperial Oil Limited, 2007	57.33567239	-111.1877414	692
Imperial Oil Limited, 2007	57.30640631	-111.1541967	446
Imperial Oil Limited, 2007	57.32106675	-111.2626043	332
Deer Creek Energy, Total E&P, 2006	57.22164355	-111.7882358	12 700
Deer Creek Energy, Total E&P, 2006	57.24316111	-111.7190003	8 620
Deer Creek Energy, Total E&P, 2006	57.24303443	-111.7543918	13 400
Deer Creek Energy, Total E&P, 2006	57.24303443	-111.7543918	14 400
Deer Creek Energy, Total E&P, 2006	57.26414667	-111.7675565	14 200
Deer Creek Energy, Total E&P, 2006	57.2771694	-111.6961366	15 200
Deer Creek Energy, Total E&P, 2006	57.20850656	-111.8386302	15 400
Deer Creek Energy, Total E&P, 2006	57.21874098	-111.8930451	18 400
Deer Creek Energy, Total E&P, 2006	57.21874098	-111.8930451	15 800
Deer Creek Energy, Total E&P, 2006	57.23574155	-111.8988404	9780
Deer Creek Energy, Total E&P, 2006	57.24197318	-111.942157	17 700
Deer Creek Energy, Total E&P, 2006	57.26113928	-111.9173306	18 900
Deer Creek Energy, Total E&P, 2006	57.26491634	-111.8356174	16 500
Deer Creek Energy, Total E&P, 2006	57.27399609	-111.8858414	20 100
Deer Creek Energy, Total E&P, 2006	57.27123028	-111.9280123	22 800
Deer Creek Energy, Total E&P, 2006	57.29141658	-111.8082935	21 900
Deer Creek Energy, Total E&P, 2006	57.23424288	-111.9663791	17 700
Deer Creek Energy, Total E&P, 2006	57.3062584	-111.6892508	57 500
Deer Creek Energy, Total E&P, 2006	57.29783281	-111.7393497	7 970

Source	Latitude	Longitude	TDS (mg/L)
Deer Creek Energy, Total E&P, 2006	57.29741471	-111.8429256	19 900
Suncor Inc, 2003	56.869167	-111.338611	2 324
Lemay, 2002	55.174896	-113.143097	25 200
Lemay, 2002	55.726726	-110.723283	8 680
Lemay, 2002	56.264247	-112.650671	5 560
Lemay, 2002	56.520851	-111.309494	15 016
Lemay, 2002	56.520851	-111.309494	18 136
Lemay, 2002	56.660206	-111.336723	5 434
Lemay, 2002	56.769241	-112.489243	9 518
Gibson et al., 2011	57.26	-111.27	1 965
Gibson et al., 2011	57.26	-111.27	1 909
Gibson et al., 2011	57.24	-111.45	427
WorleyParsons, 2010	57.2371526	-111.4454851	519
WorleyParsons, 2010	57.2626027	-111.2763144	2 350
WorleyParsons, 2010	57.182521	-111.129322	2 169
WorleyParsons, 2010	56.7897504	-111.7898274	1 056
WorleyParsons, 2010	56.7897504	-111.7898274	3 384
WorleyParsons, 2010	56.8042642	-111.4573884	5 745
WorleyParsons, 2010	57.146173	-111.6390328	531
WorleyParsons, 2010	57.2916795	-111.4454845	3 068
WorleyParsons, 2010	57.2916361	-111.6217154	3 326
WorleyParsons, 2010	57.2190437	-111.404892	3 063
Canadian Natural Resources Ltd. 2007	55.3573323	-111.0740892	14 500[a]
Cenovus Inc., 2009a	55.0732334	-110.3393894	9 100[a]
Cenovus Inc., 2009b	55.0696196	-110.3393895	9 000[a]
Cenovus Inc., 2009b	55.0549998	-110.3266775	9 100[a]
Statoil Canada Limited, 2012	55.7825825	-111.4841259	13 000[a]
Statoil Canada Limited, 2012	55.7244012	-111.432395	13 100[a]
Statoil Canada Limited, 2012	55.7426325	-111.4970586	13 500[a]
Statoil Canada Limited, 2012	55.7935559	-111.4970585	13 300[a]
Statoil Canada Limited, 2012	55.7789444	-111.5035248	12 800[a]
Canadian Natural Resources Ltd. 2011	54.771415	-110.523912	7 300[a]
Canadian Natural Resources Ltd. 2011	54.7895026	-110.4665237	7 300[a]
Canadian Natural Resources Ltd. 2011	54.7714	-110.42863	7 300[a]
Nexen Inc, 2011	56.3716995	-110.6479306	40 000[a]
Nexen Inc, 2011	55.4044631	-110.7269784	40 000[a]
Husky Energy Inc., 2008	57.233513	-111.1341496	1 170[a]
Husky Energy Inc., 2008	57.233513	-111.1341496	1 160[a]
Husky Energy Inc., 2008	57.3171525	-111.1138325	667[a]
Husky Energy Inc., 2008	57.34622	-111.1476813	518[a]
Husky Energy Inc., 2008	57.3243973	-111.1206019	628[a]

Source	Latitude	Longitude	TDS (mg/L)
Husky Energy Inc., 2008	57.342611	-111.1341411	534[a]
Husky Energy Inc., 2008	57.3353795	-111.0935209	510[a]
Husky Energy Inc., 2008	57.3462334	-111.1138308	516[a]
Husky Energy Inc., 2008	57.3571289	-111.1341409	520[a]
Husky Energy Inc., 2008	57.3243865	-111.1476821	650[a]
Husky Energy Inc., 2008	57.2553834	-111.1950765	967[a]
Husky Energy Inc., 2008	57.2589975	-111.2018461	818[a]
Husky Energy Inc., 2008	57.2408239	-111.2221571	1 240[a]
Husky Energy Inc., 2008	57.2408224	-111.2086174	1 060[a]
Canadian Natural Resources Ltd. 2012	55.3573408	-111.5611964	15 579
Canadian Natural Resources Ltd. 2012	55.3573408	-111.5611964	14 744
Canadian Natural Resources Ltd. 2012	55.3354923	-112.1765489	3 155
Canadian Natural Resources Ltd. 2012	55.3936838	-112.0675759	8 633
Canadian Natural Resources Ltd. 2012	55.542644	-112.0986339	10 794
Canadian Natural Resources Ltd. 2012	55.5826325	-111.671682	9 087
Canadian Natural Resources Ltd. 2012	55.5862881	-111.9045572	13 292
Canadian Natural Resources Ltd. 2012	55.5571985	-111.8527936	15 591
Harvest Operations Corp. 2013	55.5462509	-110.8112521	7 506
Harvest Operations Corp. 2013	55.5789829	-110.8824233	12 635
Harvest Operations Corp. 2013	55.5826424	-110.8694819	11 932
Harvest Operations Corp. 2013	55.4662871	-111.1865586	9 346
Harvest Operations Corp. 2013	55.3791114	-112.2727045	18 509
Harvest Operations Corp. 2013	55.6008197	-110.9730101	8 943
Harvest Operations Corp. 2013	55.4118607	-111.1958215	8 296
Harvest Operations Corp. 2013	55.5462509	-110.8112521	7 785
Ivanhoe Energy, 2010	56.826432	-111.33962	5 445
Ivanhoe Energy, 2010	56.826432	-111.33962	8 600
Ivanhoe Energy, 2010	56.826432	-111.33962	29 480
Ivanhoe Energy, 2010	56.826432	-111.33962	8 416
Ivanhoe Energy, 2010	56.826432	-111.33962	12 710
Ivanhoe Energy, 2010	56.826432	-111.33962	3 216
Ivanhoe Energy, 2010	56.826432	-111.33962	16 000
Ivanhoe Energy, 2010	56.826432	-111.33962	19 500
Ivanhoe Energy, 2010	56.826432	-111.33962	13 300
Ivanhoe Energy, 2010	56.826432	-111.33962	8 220
Ivanhoe Energy, 2010	56.826432	-111.33962	9 430
Ivanhoe Energy, 2010	56.826432	-111.33962	8 110
Ivanhoe Energy, 2010	56.826432	-111.33962	8 340
Ivanhoe Energy, 2010	56.8370242	-111.3378996	11 900
Ivanhoe Energy, 2010	56.8370118	-111.3180291	12 300
Ivanhoe Energy, 2010	56.8370118	-111.3180291	11 100

Source	Latitude	Longitude	TDS (mg/L)
Ivanhoe Energy, 2010	56.8370222	-111.3312726	12 400
Ivanhoe Energy, 2010	56.7570776	-111.3975247	26 300
Ivanhoe Energy, 2010	56.7570776	-111.3975247	24 900
Cenovus Energy Inc., 2011	57.1861911	-110.3781456	300
Cenovus Energy Inc., 2011	57.1934798	-110.3647301	350
Teck Resources Ltd., 2011	57.337825	-111.834692	2 320
Teck Resources Ltd., 2011	57.337825	-111.834692	1 780
Teck Resources Ltd., 2011	57.337825	-111.834692	4 900
Teck Resources Ltd., 2011	57.337825	-111.834692	1 880
Teck Resources Ltd., 2011	57.337825	-111.834692	81 900
Teck Resources Ltd., 2011	57.337825	-111.834692	85 800
Teck Resources Ltd., 2011	57.337825	-111.834692	18 000
Teck Resources Ltd., 2011	57.6879311	-111.6850495	2 100
Teck Resources Ltd., 2011	57.7170153	-111.7124134	2 200
Teck Resources Ltd., 2011	57.7170109	-111.685053	1 300
Teck Resources Ltd., 2011	57.6479077	-111.7192483	9 100
Teck Resources Ltd., 2011	57.6915485	-111.7124112	2 400
Teck Resources Ltd., 2011	57.7387851	-111.6508562	2 100
Teck Resources Ltd., 2011	57.7242373	-111.691894	1 800
Teck Resources Ltd., 2011	57.666072	-111.6713656	2 600
Teck Resources Ltd., 2011	57.7569307	-111.7260967	2 500
Teck Resources Ltd., 2011	57.6879311	-111.6850495	6 400
Teck Resources Ltd., 2011	57.7170153	-111.7124134	5 600
Teck Resources Ltd., 2011	57.7170109	-111.685053	3 400
Teck Resources Ltd., 2011	57.6479077	-111.7192483	11 000
Teck Resources Ltd., 2011	57.6769908	-111.6029645	4 700
Teck Resources Ltd., 2011	57.6915485	-111.7124112	12 000
Teck Resources Ltd., 2011	57.7387851	-111.6508562	2 300
Teck Resources Ltd., 2011	57.6951763	-111.5482604	727
Teck Resources Ltd., 2011	57.7097321	-111.5824576	3 220
Teck Resources Ltd., 2011	57.7242373	-111.691894	1 900
Teck Resources Ltd., 2011	57.6515809	-111.5892841	1 000
Teck Resources Ltd., 2011	57.666072	-111.6713656	1 900
Teck Resources Ltd., 2011	57.7097222	-111.6166515	1 870
Teck Resources Ltd., 2011	57.7569307	-111.7260967	2 900
Teck Resources Ltd., 2011	57.6987643	-111.67137	2 800
Teck Resources Ltd., 2011	57.6297822	-111.5892669	90 900
Teck Resources Ltd., 2011	57.6406214	-111.5824335	91 200
Teck Resources Ltd., 2011	57.7170153	-111.7124134	280[b]
Southern Pacific Resources Corp., 2011	57.7242373	-111.691894	2 050
Southern Pacific Resources Corp., 2011	57.0334718	-111.8602844	18 000

Source	Latitude	Longitude	TDS (mg/L)
Southern Pacific Resources Corp., 2011	56.7897504	-111.7898274	704[a]
Southern Pacific Resources Corp., 2011	56.7678716	-112.487669	9 712
Southern Pacific Resources Corp., 2011	57.018998	-111.8468655	34 000
Southern Pacific Resources Corp., 2011	56.7788188	-112.0889117	6 930
Southern Pacific Resources Corp., 2011	56.7497601	-111.882876	5 480
Southern Pacific Resources Corp., 2011	56.7897504	-111.7898274	6 900
Southern Pacific Resources Corp., 2011	56.8042642	-111.4573884	5 600
Petro Canada, 2001	56.2881188	-111.2735407	5 500
Petro Canada, 2001	56.2517417	-111.3393659	3 846
Petro Canada, 2001	56.2662933	-111.4051908	2 716
Petro Canada, 2001	56.2663164	-111.5171007	4 311
Petro Canada, 2001	56.2553866	-111.6290157	6 921
Petro Canada, 2001	56.2844673	-111.5960979	3 803
Petro Canada, 2001	56.3062099	-110.7928522	3 204
Petro Canada, 2001	56.3571557	-110.7203901	2 508
Petro Canada, 2001	56.4262569	-111.0036174	6 179
Petro Canada, 2001	56.4262569	-111.0036174	5 969
Petro Canada, 2001	56.1899068	-111.4446834	2 289
Petro Canada, 2001	56.2009007	-111.5236797	4 020
Gulf Canada and ConocoPhillips, 2001	55.7717069	-110.5394941	16 564
Gulf Canada and ConocoPhillips, 2001	56.4262569	-111.0036174	4 314
Gulf Canada and ConocoPhillips, 2001	55.9135122	-111.1443318	7 477
Gulf Canada and ConocoPhillips, 2001	56.0334852	-110.7201807	22 149
Gulf Canada and ConocoPhillips, 2001	55.6735339	-110.7724328	8 892
Gulf Canada and ConocoPhillips, 2001	55.9752981	-110.9028876	9 770
Gulf Canada and ConocoPhillips, 2001	55.9316624	-110.5700623	30 721
Gulf Canada and ConocoPhillips, 2001	56.2335353	-110.9442616	27 248
Gulf Canada and ConocoPhillips, 2001	56.2226292	-110.7402159	13 408
Gulf Canada and ConocoPhillips, 2001	55.8480075	-111.8947949	13 344
Gulf Canada and ConocoPhillips, 2001	56.2407721	-110.9376976	64 067
Gulf Canada and ConocoPhillips, 2001	55.7862415	-111.9627914	12 486
Gulf Canada and ConocoPhillips, 2001	56.2116782	-110.911305	1 419
Gulf Canada and ConocoPhillips, 2001	56.2116782	-110.911305	1 590
Gulf Canada and ConocoPhillips, 2001	55.7717069	-110.5394941	15 130
Gulf Canada and ConocoPhillips, 2001	56.0080156	-110.5309055	21 110
Gulf Canada and ConocoPhillips, 2001	55.9498329	-110.6026945	27 100
Gulf Canada and ConocoPhillips, 2001	56.0516507	-110.6222762	9 168
Gulf Canada and ConocoPhillips, 2001	56.0516507	-110.6222762	7 052
Gulf Canada and ConocoPhillips, 2001	56.3280636	-110.5952455	20 000
Gulf Canada and ConocoPhillips, 2001	55.9135122	-111.1443318	6 090
Gulf Canada and ConocoPhillips, 2001	55.7426175	-111.7040263	7 641

Source	Latitude	Longitude	TDS (mg/L)
Gulf Canada and ConocoPhillips, 2001	55.7899933	-110.9988916	8 203
Gulf Canada and ConocoPhillips, 2001	56.0370712	-111.2944087	5 836
Gulf Canada and ConocoPhillips, 2001	55.7717101	-111.5293901	5 080
Gulf Canada and ConocoPhillips, 2001	55.6553767	-112.0857	4 346
Gulf Canada and ConocoPhillips, 2001	56.0334852	-110.7201807	19 935
Gulf Canada and ConocoPhillips, 2001	56.1680732	-110.7797282	11 127
Gulf Canada and ConocoPhillips, 2001	55.8589665	-110.5243774	20 650
Gulf Canada and ConocoPhillips, 2001	56.2226292	-110.7402159	10 577
Gulf Canada and ConocoPhillips, 2001	55.8916414	-111.2422057	6 823
Gulf Canada and ConocoPhillips, 2001	55.7026427	-112.0856975	8 082
Gulf Canada and ConocoPhillips, 2001	55.6735339	-110.7724328	7 567
Gulf Canada and ConocoPhillips, 2001	55.6698662	-110.6365538	7 260
Gulf Canada and ConocoPhillips, 2001	55.7353837	-110.8047833	4 650
Gulf Canada and ConocoPhillips, 2001	55.9752981	-110.9028876	8 014
Gulf Canada and ConocoPhillips, 2001	55.9644004	-110.8506822	5 906
Gulf Canada and ConocoPhillips, 2001	56.0262207	-111.1573736	7 330
Gulf Canada and ConocoPhillips, 2001	55.7862206	-110.772431	7 445
Gulf Canada and ConocoPhillips, 2001	56.2407721	-110.9376976	19 009
Gulf Canada and ConocoPhillips, 2001	55.6880808	-111.3094827	6 079
Gulf Canada and ConocoPhillips, 2001	55.9353017	-111.1378045	8 383
Gulf Canada and ConocoPhillips, 2001	56.091656	-110.2046933	13 202
Gulf Canada and ConocoPhillips, 2001	55.6444743	-110.8953691	8 748
Gulf Canada and ConocoPhillips, 2001	55.8334418	-111.0660791	7 153
Gulf Canada and ConocoPhillips, 2001	55.9316624	-110.5700623	28 600
Gulf Canada and ConocoPhillips, 2001	56.226242	-110.9178938	12 154
Gulf Canada and ConocoPhillips, 2001	55.9243438	-111.4771317	8 205
Gulf Canada and ConocoPhillips, 2001	56.0188765	-111.9731021	7 640
Gulf Canada and ConocoPhillips, 2001	55.6735526	-112.1439191	8 072
Gulf Canada and ConocoPhillips, 2001	56.0625656	-110.6679645	25 300
Gulf Canada and ConocoPhillips, 2001	55.8880491	-110.8572097	9 437
Gulf Canada and ConocoPhillips, 2001	55.6444713	-112.1115742	10 870
Gulf Canada and ConocoPhillips, 2001	56.0334793	-110.6679638	35 000
Gulf Canada and ConocoPhillips, 2001	55.8480075	-111.8947949	11 520
Gulf Canada and ConocoPhillips, 2001	56.2407721	-110.9376976	59 896
Gulf Canada and ConocoPhillips, 2001	56.2407721	-110.9376976	59 424
Gulf Canada and ConocoPhillips, 2001	56.2407721	-110.9376976	59 913
Gulf Canada and ConocoPhillips, 2001	55.7898866	-110.5459632	11 438
Gulf Canada and ConocoPhillips, 2001	55.9061714	-111.1051896	8 951
Gulf Canada and ConocoPhillips, 2001	55.7862415	-111.9627914	11 211
Gulf Canada and ConocoPhillips, 2001	55.7571419	-110.5459652	13 826
Gulf Canada and ConocoPhillips, 2001	55.9607449	-110.5896422	24 000

Source	Latitude	Longitude	TDS (mg/L)
Gulf Canada and ConocoPhillips, 2001	55.9062294	-110.7005918	10 690
Gulf Canada and ConocoPhillips, 2001	55.8553382	-111.2226311	10 100
Gulf Canada and ConocoPhillips, 2001	55.9316228	-111.7055527	5 270
Gulf Canada and ConocoPhillips, 2001	56.0225316	-111.9274184	6 180
Nexen Inc and OPTI Canada, 2007	56.3935104	-111.1221127	14 374
Nexen Inc and OPTI Canada, 2007	56.3790338	-110.8784678	66 822
Nexen Inc and OPTI Canada, 2007	56.4008321	-110.878463	48 732
Nexen Inc and OPTI Canada, 2007	56.3790336	-110.8718812	77 252
Nexen Inc and OPTI Canada, 2007	56.3935166	-111.043116	42 233
Nexen Inc and OPTI Canada, 2007	56.4880929	-111.1616445	8 295
Nexen Inc and OPTI Canada, 2007	56.3898762	-111.0497104	14 725
Nexen Inc and OPTI Canada, 2007	56.3862572	-111.0825798	28 198
Nexen Inc and OPTI Canada, 2007	56.4008292	-110.9904073	34 671
Nexen Inc and OPTI Canada, 2007	56.5352558	-111.3911476	20 857
Nexen Inc and OPTI Canada, 2007	56.3862333	-110.7599152	54 084
Nexen Inc and OPTI Canada, 2007	56.4044631	-110.7269784	39 492
Nexen Inc and OPTI Canada, 2007	56.3571466	-110.8060366	30 478
Hackbarth and Nastasa, 1979	57.3280301	-111.6892675	2 480
Hackbarth and Nastasa, 1979	57.3971505	-111.8246233	23 706
Hackbarth and Nastasa, 1979	57.4480105	-111.9871068	220
Hackbarth and Nastasa, 1979	57.2371473	-111.4522508	3 910
Hackbarth and Nastasa, 1979	57.2626027	-111.2763144	968
Hackbarth and Nastasa, 1979	57.2626027	-111.2763144	1 556
Hackbarth and Nastasa, 1979	57.182521	-111.129322	1 560
Hackbarth and Nastasa, 1979	56.52075	-111.3114067	526
Hackbarth and Nastasa, 1979	56.7897504	-111.7898274	940
Hackbarth and Nastasa, 1979	57.2371487	-111.872028	9 320
Hackbarth and Nastasa, 1979	56.7678716	-112.487669	9 764
Hackbarth and Nastasa, 1979	57.3062595	-111.6960133	26 070
Hackbarth and Nastasa, 1979	57.2916482	-111.8111152	20 896
Hackbarth and Nastasa, 1979	57.2916482	-111.8111152	19 435
Hackbarth and Nastasa, 1979	57.2553666	-111.8991046	4 420
Hackbarth and Nastasa, 1979	57.317151	-111.5537821	1 828
Hackbarth and Nastasa, 1979	57.295258	-111.6352763	1 998
Hackbarth and Nastasa, 1979	57.3462375	-111.1002906	462
Hackbarth and Nastasa, 1979	57.2735342	-111.4793181	22 544
Hackbarth and Nastasa, 1979	57.2735342	-111.4793181	3 590
Hackbarth and Nastasa, 1979	57.178891	-111.3908081	6 940
BOVAR Environmental, 1996	57.2626027	-111.2763144	968
BOVAR Environmental, 1996	57.2626027	-111.2763144	1 556
BOVAR Environmental, 1996	57.2371473	-111.4522508	1 138

Source	Latitude	Longitude	TDS (mg/L)
BOVAR Environmental, 1996	57.31715105	-111.5018109	1 160
BOVAR Environmental, 1996	57.30100043	-111.5015246	1 970
BOVAR Environmental, 1996	57.31725705	-111.5089684	1 056
BOVAR Environmental, 1996	57.29517111	-111.5806787	1 660
BOVAR Environmental, 1996	57.30199302	-111.5310798	1 460
BOVAR Environmental, 1996	57.29615657	-111.3605449	330
BOVAR Environmental, 1996	57.3	-111.5	1 957
BOVAR Environmental, 1996	57.3	-111.5	1 913
BOVAR Environmental, 1996	57.3	-111.5	1 521
BOVAR Environmental, 1996	57.3	-111.5	1 726
Suncor Inc., 2007	56.928099	-111.5585063	23 900
Suncor Inc., 2007	56.9281047	-111.6457167	14 200
Suncor Inc., 2007	56.9207875	-111.5383849	26 300
Suncor Inc., 2007	56.9716406	-111.5718515	21 600
Suncor Inc., 2007	56.9680437	-111.6389791	11 700
Suncor Inc., 2007	56.9244551	-111.4914466	5 520
Suncor Inc., 2007	56.9498697	-111.4981348	7 660
Suncor Inc., 1998	57.2680657	-111.3406107	5 445
Suncor Inc., 1998	57.02111733	-111.3922701	8 601
Suncor Inc., 1998	56.96559493	-111.3934956	29 480
Suncor Inc., 1998	56.99527842	-111.4097746	12 710
Suncor Inc., 1998	56.99515366	-111.4203073	8 416
Suncor Inc., 1998	56.99697116	-111.4140728	3 216
True North Energy L.P., 2001	57.4116415	-111.5267569	577[c]
True North Energy L.P., 2001	57.4116415	-111.5267569	6 090[c]
True North Energy L.P., 2001	57.4116415	-111.5267569	59 206[c]

[a] The TDS value provided in the reference did not include detailed geochemical information

[b] The charge balance for these samples ranged between 10–25%. These values were exclusively low-salinity samples that would be influenced by inaccurate alkalinity measurements, and therefore were included in the database.

[c] Three TDS values from groundwater wells within the True North Energy L.P. mine were provided without location data. An arbitrary location in the centre of the mine was selected for each of these points.

References

BOVAR Environmental (1996). *Environmental impact assessment for the Syncrude Canada Limited Aurora Mine.* Alberta Environmental Protection and Alberta Energy and Utilities Board. Edmonton, Alberta, Canada.

Canadian Natural Resources Limited (2003). *Horizon Oil Sands Project Application for Approval.* Alberta Energy and Utilities Board and Alberta Environment. Edmonton, Alberta, Canada.

Canadian Natural Resources Limited (2011). *Kirby SAGD In Situ Performance Presentation*. Alberta Energy Resources Conservation Board. Available Online: http://www.ercb.ca/data-and-publications/activity-and-data/insitu-progress

Canadian Natural Resources Limited (2012). *Primrose Wolf Lake CSS In Situ Performance Presentation.* Alberta Energy Resources Conservation Board. Available Online: http://www.ercb.ca/data-and-publications/activity-and-data/insitu-progress

Canadian Natural Resources Limited (2012). *Application for Approval of the Grouse In Situ Oil Sands Project.* Alberta Energy and Utilities Board and Alberta Environment. Edmonton, Alberta, Canada.

Cenovus Energy Inc. (2009a). *Foster Creek SAGD In Situ Performance Presentation.* Alberta Energy Resources Conservation Board. Available Online: http://www.ercb.ca/data-and-publications/activity-and-data/insitu-progress

Cenovus Energy Inc. (2009b). *Christina Lake SAGD In Situ Performance Presentation.* Alberta Energy Resources Conservation Board. Available Online: http://www.ercb.ca/data-and-publications/activity-and-data/insitu-progress

Cenovus Energy Inc. (2011). *Telephone Lake project: Application for approval and supplemental information request 1.* Alberta Energy and Utilities Board and Alberta Environment. Edmonton, Alberta, Canada.

Deer Creek Energy Limited, Total E&P Canada Limited (2006). *Applications for the Deer Creek Energy Limited Joslyn North Mine Project.* Alberta Energy and Utilities Board and Alberta Environment. Edmonton, Alberta, Canada.

Gulf Canada Resources, ConocoPhillips. (2001). *Application for the Approval of the Surmont Project.* Alberta Energy and Utilities Board and Alberta Environment. Edmonton, Alberta, Canada.

Hackbarth, D. A., & Nastasa, N. (1979). Groundwater Observation Well Network: Athabasca Oil Sands Area. *Alberta Research Council, Information Series 69*, 1–1272.

Harvest Operations Corp. (2013). *BlackGold Expansion Project Application for Approval.* Alberta Energy and Utilities Board and Alberta Environment. Edmonton, Alberta, Canada.

Husky Energy Inc. (2011). *Sunrise SAGD In Situ Performance Presentation.* Alberta Energy Resources Conservation Board. Available Online: http://www.ercb.ca/data-and-publications/activity-and-data/insitu-progress

Ivanhoe Energy (2010). *Application for Approval and Supplemental Information Requests 1, 2 and 3 Tamarack Integrated Oil Sands Project.* Alberta Energy and Utilities Board and Alberta Environment. Edmonton, Alberta, Canada.

Imperial Oil Limited (2006). *Kearl Oil Sands Project - Mine Development Environmental Impact Assessment.* Alberta Energy and Utilities Board and Alberta Environment. Edmonton, Alberta, Canada.

Lemay, T. (2002). Geochemical and Isotope Data Formation Water from Selected Wells, Cretaceous to Quaternary Succession, Athabasca Oil Sands (In-situ) Area, Alberta. *Alberta Energy and Utilities Board–Alberta Geological Survey Geo-Note 2002-02*, 1–71.

Nexen Inc, OPTI Canada Inc. (2007). *Application for the Approval of the Long Lake South Project.* Alberta Energy and Utilities Board and Alberta Environment. Edmonton, Alberta, Canada.

Nexen Inc. (2012). *Long Lake SAGD In Situ Performance Presentation.* Alberta Energy Resources Conservation Board. Available Online: http://www.ercb.ca/data-and-publications/activity-and-data/insitu-progress

Petro Canada. (2001). *Application for the Approval of the Meadow Creek Project.* Alberta Energy and Utilities Board and Alberta Environment. Edmonton, Alberta, Canada.

Shell Canada Limited (2002). *Application for Approval of the Jackpine Mine - Phase 1.* Alberta Energy and Utilities Board and Alberta Environment. Edmonton, Alberta, Canada.

Southern Pacific Resources Corp. (2011). *STP McKay Thermal Project Integrated ERCB Application and Environmental Impact Assessment Report.* Alberta Energy and Utilities Board and Alberta Environment. Edmonton, Alberta, Canada.

Statoil Canada Limited (2012). *Leismer SAGD In Situ Performance Presentation.* Alberta Energy Resources Conservation Board. Available Online: http://www.ercb.ca/data-and-publications/activity-and-data/insitu-progress

Suncor Inc. (1998). *Project Millennium Application.* Alberta Energy and Utilities Board and Alberta Environment. Edmonton, Alberta, Canada.

Suncor Inc. (2007). *Application for the Approval of the Voyageur South Project.* Alberta Energy and Utilities Board and Alberta Environment. Edmonton, Alberta, Canada.

Suncor Energy Incorporated (2003). *South Tailings Pond Project.* Alberta Energy and Utilities Board and Alberta Environment. Edmonton, Alberta, Canada.

Teck Resources Ltd. (2011). *Frontier Oil Sands Mine Project Environmental Impact Assessment*. Alberta Energy and Utilities Board and Alberta Environment. Edmonton, Alberta, Canada.

TrueNorth Energy L.P. (2001). *Application for the Approval of the Fort Hills Oil Sands Project.* Alberta Energy and Utilities Board and Alberta Environment. Edmonton, Alberta, Canada.

WorleyParsons Komex (2007). *Shell Canada Limited Jackpine Mine Expansion and Pierre River Mine Project Base Case Report.* Alberta Energy and Utilities Board and Alberta Environment. Edmonton, Alberta, Canada.

WorleyParsons. (2010). Regional Groundwater Quality Study and Monitoring Network Design in the Athabasca Oil Sands: Phase 2: Program Summary. *Regional Municipality of Wood Buffalo: Cumulative Environmental Management Association* Fort McMurray, Alberta, Canada.

WorleyParsons. (2011). Surface water – groundwater interactions in the lower Athabasca Region Final Report Phase 2: Program Summary. *Cumulative Environmental Management Agency* Fort McMurray, Alberta, Canada, 1–493.

APPENDIX B: MEASURED STABLE ISOTOPE AND GEOCHEMICAL PARAMETERS FOR POREWATERS EXTRACTED FROM FIREBAG DRILL CORES

Table B1: Geochemical and stable isotope measurements of porewater derived from the twelve drill cores examined in Chapter 4

Well ID and Depth (m)	$\delta^{18}O_w$ (‰$_{VSMOW}$)	$\delta^{2}H_w$ (‰$_{VSMOW}$)	TDS (mg/L)	Na^+ (mg/L)	K^+ (mg/L)	Mg^{2+} (mg/L)	Ca^{2+} (mg/L)	Cl^- (mg/L)	SO_4^{2-} (mg/L)	HCO_3^- (mg/L)
03-18-095-5W4										
253.2	-17.9	-155	1 651	583	14	5	15	180	294	560
257.2	-14.3	-134	2 511	869	24	23	112	279	406	798
261.4	-16.9	-145	1 942	667	22	11	19	250	559	414
265.5	-16.7	-150	1 652	556	20	5	12	162	262	636
270.2	-10.8	-132	3 503	1 079	59	28	35	331	1 273	698
274.6	-14.5	-136	2 250	734	30	10	25	219	545	688
283.3	-15.1	-140	2 622	787	24	17	68	192	442	1 092
03-34-094-06W4										
291.3	-17.2	-146	3 851	1 213	115	8	12	715	477	1 312
302.6	-16.9	-144	2 590	854	25	11	27	264	471	939
305.8	-15.9	-138	3 262	972	34	23	75	246	1 218	694
312.9	-16.6	-140	2 753	989	36	34	88	307	600	699
314.3	-16.2	-138	2 861	1 000	31	26	130	246	778	651
316.3	-18.2	-148	2 012	764	24	21	53	225	429	495
319.4	-17.5	-146	2 253	755	28	14	36	174	483	762
322.3	-14.7	-130	2 985	1 114	43	28	116	287	424	973
325.2	-16.6	-140	2 468	940	27	30	59	284	675	454
327.4	-15.9	-137	2 835	922	30	25	92	252	820	694
332.8	-15.2	-134	3 392	1 188	90	40	118	395	652	908
334.8	-15.4	-133	3 072	1 082	34	38	133	460	822	503
338.4	-15.6	-134	3 397	1 209	41	45	177	548	814	562
07-08-095-5W4										
260.2	-15.8	-136	1 953	596	27	29	128	185	255	734
260.2	-15.6	-135	1 759	574	21	21	95	174	253	621
263.2	-14.1	-128	2 686	1 074	34	23	158	397	370	630
263.2	-14.3	-131	2 176	789	21	17	127	214	309	699
278.0	-13.3	-129	1 817	590	40	30	53	470	314	320
278.0	-15.5	-136	2 280	722	110	24	74	445	287	616
09-08-095-5W4										
254.4	-18.1	-148	1 444	698	24	12	27	338	231	781
260.5	-14.9	-133	1 429	682	23	28	72	324	314	638
260.5	-14.9	-133	1 445	674	25	29	76	329	318	639

Well ID and Depth (m)	$\delta^{18}O_w$ (‰VSMOW)	$\delta^{2}H_w$ (‰VSMOW)	TDS (mg/L)	Na^+ (mg/L)	K^+ (mg/L)	Mg^{2+} (mg/L)	Ca^{2+} (mg/L)	Cl^- (mg/L)	SO_4^{2-} (mg/L)	HCO_3^- (mg/L)
280.3	-15.4	-136	1 884	997	34	28	104	352	375	948
280.3	-14.8	-131	1 867	1 011	29	22	90	350	366	966
09-09-095-6W4										
262.8	-15.7	-139	2 104	695	20	11	57	170	459	691
265.4	-14.8	-135	2 412	785	24	15	87	194	516	791
267.5	-15.9	-141	2 155	792	26	11	22	235	594	476
272.4	-14.5	-138	2 529	749	19	13	85	161	623	878
276.4	-16.1	-141	2 237	665	23	15	56	178	640	660
285.5	-16.1	-143	2 073	749	28	16	38	203	578	462
15-08-095-5W4										
261.2	-17.4	-143	1 203	665	32	12	25	206	175	725
261.2	-17.3	-144	1 211	661	32	11	24	206	176	733
271.2	-16.2	-136	1 190	685	34	20	67	159	208	672
271.2	-16.0	-137	1 126	662	31	19	58	153	201	636
304.0	-17.0	-141	1 427	692	112	18	36	356	208	667
309.2	-16.0	-136	1 392	862	41	25	66	279	290	653
01-08-095-6W4										
250.8	-7.0	-125	3 039	1 418	23	1	2	303	346	945
256.1	-7.8	-128	3 567	1 175	22	0	3	288	521	1 559
261.7	-17.0	-145	1 788	599	18	7	25	142	194	802
280.8	-17.4	-144	1 827	607	19	21	88	158	460	475
285.9	-13.9	-140	3 058	817	41	33	50	251	920	945
291.1	-15.7	-142	2 527	642	28	18	38	221	634	945
11-04-095-6W4										
251.9	-12.9	-135	3 996	1363	25	7	9	781	569	1 243
265.4	-15.9	-143	2 670	897	17	4	5	371	451	926
273.3	-16.7	-142	2 472	826	16	5	17	331	506	771
279.3	-16.7	-141	1 825	608	15	6	23	225	332	616
283.8	-15.0	-137	3 011	842	24	20	63	334	716	1 011
287.5	-14.7	-138	4 242	1 463	37	14	22	555	1 139	1 011
303.9	-15.1	-142	4 335	1 414	65	1	4	762	587	1 502
01-10-095-6W4										
269.5	-14.1	-137	2 744	965	25	4	17	442	617	674
274.5	-14.9	-134	3 255	1 168	49	11	44	707	601	675
279.6	-16.4	-140	2 628	957	35	5	14	323	439	856
284.6	-16.2	-140	2 999	1 541	51	4	26	253	450	674

Well ID and Depth (m)	$\delta^{18}O_w$ (‰VSMOW)	$\delta^{2}H_w$ (‰VSMOW)	TDS (mg/L)	Na^+ (mg/L)	K^+ (mg/L)	Mg^{2+} (mg/L)	Ca^{2+} (mg/L)	Cl^- (mg/L)	SO_4^{2-} (mg/L)	HCO_3^- (mg/L)
289.5	-13.8	-127	2 715	1 052	31	14	90	212	642	674
294.5	-15.3	-133	2 307	871	23	11	35	187	507	674
299.5	-16.7	-138	1 753	548	14	5	19	147	345	674
304.6	-16.0	-136	1 801	512	21	14	45	135	401	674
308.9	-16.4	-138	1 975	615	32	18	59	166	595	490
269.5	-14.1	-137	2 744	965	25	4	17	442	617	674
05-06-095-6W4										
243.5	-16.2	-143	3 155	966	44	23	102	398	1 109	513
246.2	-17.9	-149	3 052	1 023	25	7	9	396	643	948
249.3	-16.6	-144	3 056	1 042	27	7	14	459	615	892
251.8	-16.6	-144	3 484	1 234	27	8	13	702	603	898
256.5	-18.0	-147	2 701	893	23	8	31	423	534	787
261.8	-15.5	-135	2 720	1 007	25	12	39	290	773	574
264.6	-17.2	-146	3 001	1 008	29	9	11	328	666	949
268.4	-13.9	-128	3 937	1 379	163	26	169	556	1 183	461
282.7	-13.6	-124	4 157	1 318	46	24	175	447	1 226	920
284.4	-14.2	-127	4 236	1 451	53	21	164	572	1 204	771
297.7	-13.3	-142	4 012	1 237	47	29	47	898	983	771
07-10-95-6W4										
275.3	-13.8	-134	2 560	774	21	4	21	331	661	748
280.2	-17.5	-146	1 745	590	16	3	8	223	244	662
285.0	-16.9	-145	1 948	660	20	4	7	233	334	691
290.1	-14.2	-137	2 606	839	67	4	7	306	447	935
295.6	-12.8	-128	3 165	1 058	49	3	9	432	485	1 128
301.3	-13.4	-128	3 587	1 613	74	6	84	490	572	748
308.3	-16.2	-137	2 564	754	27	12	36	179	809	748
319.7	-14.8	-136	3 269	1 096	124	8	21	415	1 281	324
15-31-094-6W4										
258.7	-15.4	-135	2 797	917	36	26	117	253	631	816
259.7	-16.5	-142	2 409	738	24	19	55	258	309	1 007
261.6	-16.2	-138	2 934	966	44	23	102	287	466	1 047
266.5	-15.3	-133	2 910	1 097	48	23	127	287	479	848
268.1	-14.0	-128	3 586	1 338	57	30	107	345	860	848
270.3	-16.4	-140	2 169	915	26	3	8	281	413	523
275.7	-10.5	-128	3 700	1 683	46	2	5	364	752	848
286.9	-14.9	-132	4 284	1 348	62	35	108	339	1545	848

APPENDIX C: MEASURED STABLE ISOTOPE AND GEOCHEMICAL PARAMETERS FOR OIL SANDS MICROCOSMS IN CHAPTER FIVE.

Table C1: Headspace methane concentration in individual microcosms at T0−T4. All values expressed in mol%.

Sample ID	T0	T1	T2	T3	T4
B1	n.d.	3.7	4.6	12.9	n.a.
B2	n.d.	2.4	4.8	9.4	n.a.
B3	n.d.	3.9	3.4	16.9	n.a.
B4	n.d.	15.2	22.1	34.2	34.5
B5	n.d.	18.7	1.5	21.7	27.0
B6	n.d.	4.1	4.5	15.9	19.0
B7	n.d.	15.9	18.2	14.8	27.5
B8	n.d.	4.3	5.8	14.8	17.9
B9	n.d.	3.2	5.0	14.6	n.a.
B10	n.d.	3.0	2.1	19.1	n.a.
B11	n.d.	2.8	1.8	19.4	n.a.
B12	n.d.	3.7	6.1	21.2	22.0
B13	n.d.	17.0	23.8	10.2	12.0
B14	n.d.	14.1	21.1	32.6	22.4
B15	n.d.	n.d.	n.d.	n.d.	n.d.
B16	n.d.	n.d.	n.d.	n.d.	n.d.
B17	n.d.	n.d.	n.d.	n.d.	n.d.
B18	n.d.	n.d.	n.d.	n.d.	n.d.
S1	0	0.0	0.7	0.30	0.3
S2	0	0.0	0.4	0.32	0.2
S3	0	0.3	0.9	0.44	0.2
S4	0	0.4	0.7	0.52	0.5
S5	0	0.4	1.1	0.56	0.5
S6	0	5.0	7.1	11.8	18.7
S7	0	0.3	0.8	0.4	n.d.
S8	0	4.1	4.6	0.6	n.d.
S9	0	5.6	12.2	31.7	28.5
S10	0	0.5	1.4	4.5	14.5
S11	0	0.3	0.6	0.64	0.7
S12	0	1.9	3.3	0.41	0.3
S13	0	1.8	1.2	4.01	17.1
S14	0	0.8	0.1	0.58	0.1
S15	n.d.	n.d.	n.d.	n.d.	n.d.
S16	n.d.	n.d.	n.d.	n.d.	n.d.
S17	n.d.	n.d.	n.d.	n.d.	n.d.
S18	n.d.	n.d.	n.d.	n.d.	n.d.
F1	n.d.	4.1	3.5	1.9	2.0
F2	n.d.	4.0	5.1	1.5	1.8
F3	n.d.	3.0	12.1	22.7	20.0
F4	n.d.	4.0	15.0	24.7	17.2
F5	n.d.	9.3	17.6	10.0	22.3
F6	n.d.	0.5	1.0	0.5	0.5
F7	n.d.	10.7	17.0	14.0	34.2
F8	n.d.	0.3	0.6	4.4	12.8
F9	n.d.	0.1	0.1	0.1	0.1

Sample ID	T0	T1	T2	T3	T4
F10	n.d.	4.0	21.5	31.6	25.6
F11	n.d.	9.1	9.9	10.2	14.6
F12	n.d.	0.6	0.9	0.4	0.5
F13	n.d.	0.6	1.1	0.4	0.3
F14	n.d.	0.6	1.2	0.2	0.5
F15	n.d.	n.d.	n.d.	n.d.	n.d.
F16	n.d.	n.d.	n.d.	n.d.	n.d.
F17	n.d.	n.d.	n.d.	n.d.	n.d.
F18	n.d.	n.d.	n.d.	n.d.	n.d.

n.a. denotes that the value was not measured due to analytical instrument failure
n.d. denotes that there was no methane detected in the microcosm

Table C2: $\delta^{13}C$ values of CO_2 in individual microcosms at T0−T4. All values expressed in permil VPDB (‰).

Sample ID	T0	T1	T2	T3	T4
B1	−30.5	−30.0	−30.0	−30.0	−30.1
B2	−30.9	−30.0	−30.1	−30.0	−30.1
B3	−29.9	−29.8	−29.6	−29.2	−29.3
B4	−28.8	−28.5	−27.5	−26.0	−26.0
B5	−28.5	−28.3	−27.4	−25.8	−25.7
B6	−29.9	−29.8	−29.9	−29.4	−29.5
B7	−29.1	−29.0	−28.0	−26.2	−26.3
B8	−29.9	−29.7	−29.9	−29.4	−29.4
B9	−30.1	−30.0	−30.0	−29.5	−29.7
B10	−30.0	−29.9	−29.7	−29.4	−29.5
B11	−29.9	−29.9	−29.9	−29.5	−29.5
B12	−29.9	−29.8	−29.7	−29.3	−29.4
B13	−29.4	−29.1	−29.0	−28.7	−26.8
B14	−29.2	−28.7	−27.6	−26.1	−26.1
B15	−28.0	−27.3	−27.7	−27.6	−27.8
B16	−30.6	−30.6	−30.2	−30.3	−30.4
B17	−30.9	n.a.	−30.3	−30.3	−30.5
B18	−30.9	n.a.	−30.4	−30.4	−30.6
S1	−31.4	−30.9	−30.4	−30.6	−30.6
S2	−31.8	−30.7	−30.4	−30.6	−30.7
S3	−30.7	−30.4	−30.0	−30.1	−30.0
S4	−31.3	−30.4	−30.0	−29.9	−29.9
S5	−30.7	−30.6	−29.9	−29.7	−29.9
S6	−31.6	−26.0	−25.9	−26.6	−27.4
S7	−31.1	−30.3	−30.0	−30.0	−29.9
S8	−31.0	−30.3	−30.0	−30.0	−30.0
S9	−28.5	−26.2	−26.2	−27.2	−27.2
S10	−32.0	−29.5	−29.0	−29.2	−28.6
S11	−32.9	−30.5	−30.0	−30.1	−30.0
S12	−30.5	−30.3	−29.9	−29.8	−30.0
S13	−30.8	−30.1	−29.4	−29.6	−29.0
S14	−30.5	−30.3	−29.9	−30.0	−30.0
S15	−31.6	−29.7	−29.3	−29.3	−29.4
S16	−31.4	−30.5	−30.3	−30.5	−30.4
S17	−31.5	−31.1	−30.5	−30.7	−30.6
S18	−32.0	−30.8	−30.5	−30.5	−30.7
F1	−31.2	−31.1	−30.8	−30.9	−31.1
F2	−31.1	−30.9	−30.9	−30.8	−30.9
F3	−29.1	−28.5	−25.3	−23.6	−23.3
F4	−29.1	−28.4	−26.0	−22.4	−22.6
F5	−28.0	−27.4	−26.9	−21.6	−19.6
F6	−31.2	−31.0	−30.8	−30.8	−30.8
F7	−27.6	−27.3	−26.1	−22.9	−18.2
F8	−30.7	−30.4	−29.9	−29.5	−28.4
F9	−32.3	−26.7	−30.5	−30.4	−30.6
F10	−29.0	−28.1	−25.0	−21.0	−21.1
F11	−28.7	−28.1	−26.9	−23.4	−22.9
F12	−31.0	−30.9	−30.4	−30.0	−30.1
F13	−31.1	−31.1	−30.6	−30.5	−30.7
F14	−31.2	−30.9	−30.5	−30.5	−30.5

Sample ID	T0	T1	T2	T3	T4
F15	−31.4	−31.5	−31.3	−31.2	−31.4
F16	−32.0	−30.8	−30.6	−30.6	−30.6
F17	−32.3	−32.3	−32.0	−32.1	−32.3
F18	−32.3	−32.4	−32.1	−32.0	−32.4

n.a. denotes that the value was not measured at this time step

Table C3: $\delta^{13}C$ values of CH_4 in individual microcosms at T1−T4. All values expressed in permil VPDB (‰).

Sample ID	T1	T2	T3	T4
B1	−86.9	−82.5	−40.9	−40.8
B2	−85.6	−69.6	−40.5	−40.2
B3	−74.1	−53.0	−30.0	−30.5
B4	−69.2	−73.1	−43.9	−44.0
B5	−69.4	−73.8	−42.8	−42.7
B6	−73.8	−58.6	−29.4	−29.1
B7	−67.8	−71.2	−43.3	−43.8
B8	−75.5	−59.4	−30.5	−29.8
B9	−73.1	−54.4	−29.3	−29.7
B10	−72.8	−52.5	−28.9	−29.9
B11	−71.9	−53.8	−29.3	−29.4
B12	−74.7	−57.7	−29.1	−29.1
B13	−72.0	−72.7	−74.9	−45.1
B14	−67.8	−72.6	−43.7	−43.5
B15	n.d.	n.d.	n.d.	n.d.
B16	n.d.	n.d.	n.d.	n.d.
B17	n.d.	n.d.	n.d.	n.d.
B18	n.d.	n.d.	n.d.	n.d.
S1	n.d.	n.d.	n.d.	n.d.
S2	n.d.	n.d.	n.d.	n.d.
S3	−71.5	−59.3	n.d.	n.d.
S4	−73.9	−65.1	n.d.	−59.7
S5	−57.1	−67.1	−63.1	−36.8
S6	−84.1	−84.2	−47.7	−33.8
S7	−54.8	−57.6	n.d.	−48.1
S8	−72.7	−57.0	−57.0	−54.5
S9	−84.0	−77.4	−34.4	−35.1
S10	−87.3	−87.7	−60.3	−29.3
S11	−64.3	−66.8	−65.7	−50.7
S12	−62.3	−54.3	n.d.	−50.4
S13	−82.3	−87.3	−57.7	−23.9
S14	−67.4	−66.5	−65.5	−55.3
S15	n.d.	n.d.	n.d.	n.d.
S16	n.d.	n.d.	n.d.	n.d.
S17	−71.5	−59.3	n.d.	n.d.
S18	−73.9	−65.1	n.d.	−59.7
F1	−72.6	−72.7	−72.7	−71.8
F2	−72.7	−72.9	−73.2	−72.3
F3	−72.8	−78.2	−48.6	−47.9
F4	−67.6	−89.0	−50.8	−50.5
F5	−63.9	−68.4	−88.8	−59.8
F6	−55.6	−55.7	n.d.	−56.5
F7	−65.6	−72.2	−87.5	−49.2
F8	−60.3	−60.2	−35.4	−27.7
F9	n.d.	n.d.	n.d.	n.d.
F10	−71.1	−91.6	−50.7	−51.6
F11	−64.9	−72.4	n.d.	−72.9
F12	−65.3	−52.9	n.d.	−54.1
F13	−52.5	−54.5	n.d.	−55.9
F14	−54.4	−54.0	n.d.	−56.2

Sample ID	T1	T2	T3	T4
F15	n.d.	n.d.	n.d.	n.d.
F16	n.d.	n.d.	n.d.	n.d.
F17	n.d.	n.d.	n.d.	n.d.
F18	n.d.	n.d.	n.d.	n.d.

n.d. denotes that the IRMS peak height for methane was below quantification limits

Table C4: δ^2H values of CH_4 in individual microcosms at T3−T4. All values expressed in permil VSMOW (‰).

Sample ID	T3	T4
B1	−392	−390
B2	−396	−392
B3	−392	−392
B4	−408	−412
B5	−411	−415
B6	−391	−389
B7	−406	−413
B8	−392	−391
B9	−389	−390
B10	−391	−390
B11	−390	−389
B12	−392	−390
B13	−404	−413
B14	−407	−415
B15	n.d.	n.d.
B16	n.d.	n.d.
B17	n.d.	n.d.
B18	n.d.	n.d.
S1	n.d.	n.d.
S2	n.d.	n.d.
S3	n.d.	n.d.
S4	n.d.	n.d.
S5	n.d.	−422
S6	−423	−406
S7	n.d.	n.d.
S8	n.d.	n.d.
S9	−393	−395
S10	n.d.	−396
S11	n.d.	−383
S12	n.d.	n.d.
S13	−430	−392
S14	n.d.	n.d.
S15	n.d.	n.d.
S16	n.d.	n.d.
S17	n.d.	n.d.
S18	n.d.	n.d.
F1	−435	−424
F2	−437	−429
F3	−400	−398
F4	−397	−400
F5	−457	−411
F6	n.d.	n.d.
F7	−458	−407
F8	−393	−379
F9	n.d.	n.d.
F10	−401	−402
F11	n.d.	−429
F12	n.d.	n.d.
F13	n.d.	n.d.
F14	n.d.	n.d.

Sample ID	T3	T4
F15	n.d.	n.d.
F16	n.d.	n.d.
F17	n.d.	n.d.
F18	n.d.	n.d.

n.d. denotes that the IRMS peak height for methane was below quantification limits

Table C5: $\delta^{34}S$ values of dissolved sulfate in Saline microcosms. All values expressed in permil CDT (‰).

Sample ID	T0	T2	T4
S1	14.8	15.5	16.0
S2	14.5	15.1	16.8
S3	12.6	16.8	17.9
S4	12.7	n.a	19.6
S5	13.8	18.4	20.3
S6	14.6	15.9	17.2
S7	13.2	16.7	18.3
S8	12.8	16.5	18.9
S9	14.5	15.8	16.0
S10	14.9	16.4	18.8
S11	14.1	19.2	22.0
S12	12.7	15.8	16.5
S13	14.8	18.2	18.5
S14	12.8	16.6	17.8
S15	13.6	16.4	16.5
S16	13.9	14.5	13.6
S17	14.8	15.3	15.0
S18	14.8	15.5	16.0

n.a. denotes that the sample was not measured

Table C6: Water stable isotope composition of individual microcosms at T0. All values expressed in permil VSMOW (‰).

Sample ID	$\delta^{18}O$	$\delta^{2}H$
B1	−18.9	−148
B2	−19.4	−149
B3	−19.3	−148
B4	−19.0	−148
B5	−19.0	−147
B6	−18.9	−147
B7	−19.1	−148
B8	−19.0	−148
B9	−19.2	−148
B10	−19.1	−149
B11	−19.0	−148
B12	−18.9	−148
B13	−18.9	−148
B14	−19.0	−148
B15	−19.2	−149
B16	−19.2	−148
B17	−19.3	−148
B18	−19.2	−148
S1	−19.4	−149
S2	−19.3	−148
S3	−18.9	−147
S4	−19.1	−147
S5	−19.2	−148
S6	−18.9	−147
S7	−19.2	−147
S8	−19.4	−148
S9	−19.2	−147
S10	−19.3	−147
S11	−19.2	−146
S12	−19.1	−146
S13	−19.3	−148
S14	−19.3	−147
S15	−19.4	−147
S16	−18.9	−147
S17	−19.6	−148
S18	−19.6	−148
F1	−19.1	−150
F2	−19.2	−149
F3	−18.9	−149
F4	−19.0	−149
F5	−18.9	−148
F6	−19.0	−148
F7	−18.9	−147
F8	−19.1	−147
F9	−19.3	−149
F10	−19.0	−148
F11	−19.0	−148
F12	−19.2	−148
F13	−19.2	−148
F14	−19.2	−148

Sample ID	$\delta^{18}O$	$\delta^{2}H$
F15	−19.0	−147
F16	−19.3	−148
F17	−19.2	−149
F18	−19.1	−148

Table C7: Major cation concentrations for each microcosm at T0 and T4.

Depth (m)	T0				T4			
	Na^+ (mg/L)	K^+ (mg/L)	Mg^{2+} (mg/L)	Ca^{2+} (mg/L)	Na^+ (mg/L)	K^+ (mg/L)	Mg^{2+} (mg/L)	Ca^{2+} (mg/L)
B1	3 726	125	2	1	3 484	125	0	12
B2	3 578	131	5	0	3 366	117	12	6
B3	3 925	113	8	3	3 444	89	10	6
B4	3 853	121	15	8	3 422	92	10	6
B5	3 406	113	12	3	3 362	97	10	8
B6	3 718	130	13	7	3 372	92	9	6
B7	3 625	111	13	7	3 519	116	12	8
B8	3 652	269	5	0	3 415	95	14	13
B9	3 810	114	9	2	3 559	121	9	7
B10	3 765	113	12	4	3 595	98	14	14
B11	3 938	121	16	6	3 518	88	9	4
B12	3 667	122	14	2	3 610	98	10	4
B13	3 760	116	16	6	3 517	121	9	7
B14	3 616	110	12	0	3 649	141	12	10
B15	3 857	102	10	3	3 507	103	10	6
B16	3 957	102	7	4	3 518	94	14	9
B17	3 677	127	11	2	3 546	120	12	7
B18	3 833	134	7	5	3 921	149	13	5
S1	9 183	255	319	30	8 311	240	200	23
S2	9 176	282	324	27	8 403	299	248	40
S3	9 164	259	318	47	8 921	280	264	50
S4	9 343	241	315	48	8 432	218	211	47
S5	9 295	242	310	46	8 761	272	256	49
S6	8 968	237	305	48	8 154	206	204	47
S7	9 111	254	316	50	8 251	221	222	48
S8	9 502	259	337	49	8 556	225	214	47
S9	9 353	270	321	50	8 365	220	198	52
S10	9 366	264	314	46	9 610	278	259	56
S11	9 279	260	313	39	7 989	256	224	38
S12	8 764	300	333	49	8 247	255	236	46
S13	8 918	267	333	58	7 894	234	217	45
S14	9 113	269	391	110	8 803	271	251	48
S15	9 382	321	376	62	8 493	261	240	42
S16	9 152	260	385	74	8 846	200	222	50

Depth (m)	T0				T4			
	Na^+ (mg/L)	K^+ (mg/L)	Mg^{2+} (mg/L)	Ca^{2+} (mg/L)	Na^+ (mg/L)	K^+ (mg/L)	Mg^{2+} (mg/L)	Ca^{2+} (mg/L)
S17	9 367	326	367	34	8 564	300	257	48
S18	8 513	274	354	52	8 806	287	242	29
F1	701	114	31	9	752	123	28	5
F2	798	129	34	9	752	117	26	4
F3	878	77	10	6	859	71	14	8
F4	882	74	13	6	915	70	13	6
F5	874	86	20	11	873	77	14	5
F6	914	87	20	10	936	84	16	7
F7	913	96	20	12	836	74	14	6
F8	877	88	19	9	861	76	12	5
F9	850	84	19	9	896	81	16	8
F10	878	78	15	7	859	72	14	9
F11	862	94	23	12	883	91	17	8
F12	894	90	22	12	967	87	17	9
F13	874	88	22	11	891	76	14	6
F14	911	89	20	10	938	84	16	8
F15	866	86	22	10	1 128	98	17	10
F16	870	82	16	8	1 029	78	12	7
F17	752	125	38	9	861	135	30	5
F18	781	127	38	9	875	136	32	7

Table C8: Major anion concentrations for individual microcosms at T0, T2 and T4

Depth (m)	T0		T2		T4	
	Cl^- (mg/L)	SO_4^{2-} (mg/L)	Cl^- (mg/L)	SO_4^{2-} (mg/L)	Cl^- (mg/L)	SO_4^{2-} (mg/L)
B1	3 310	n.d.	n.m.	n.m.	3 221	n.d.
B2	3 088	n.d.	n.m.	n.m.	3 183	n.d.
B3	3 330	n.d.	n.m.	n.m.	3 176	n.d.
B4	3 474	n.d.	n.m.	n.m.	3 153	n.d.
B5	3 154	n.d.	n.m.	n.m.	3 136	n.d.
B6	3 270	n.d.	n.m.	n.m.	3 200	n.d.
B7	3 152	n.d.	n.m.	n.m.	3 133	n.d.
B8	3 236	n.d.	n.m.	n.m.	3 186	n.d.
B9	3 247	n.d.	n.m.	n.m.	3 228	n.d.
B10	3 216	n.d.	n.m.	n.m.	3 222	n.d.
B11	3 508	n.d.	n.m.	n.m.	3 135	n.d.
B12	3 245	n.d.	n.m.	n.m.	3 220	n.d.
B13	3 279	n.d.	n.m.	n.m.	3 121	n.d.
B14	3 224	n.d.	n.m.	n.m.	3 208	n.d.
B15	3 278	n.d.	n.m.	n.m.	3 157	n.d.
B16	3 327	n.d.	n.m.	n.m.	3 243	n.d.
B17	3 236	n.d.	n.m.	n.m.	3 254	n.d.
B18	3 346	n.d.	n.m.	n.m.	3 410	n.d.
S1	11 000	2 130	10 520	2 030	10 737	2 079
S2	10 900	2 120	10 530	2 035	10 793	2 082
S3	11 100	2 240	10 477	2 105	11 273	2 123
S4	11 000	2 220	10 408	2 063	10 620	1 913
S5	10 800	2 140	10 465	2 049	11 081	1 965
S6	11 100	2 140	10 354	1 980	10 352	1 823
S7	10 700	2 120	10 784	2 099	10 389	1 910
S8	10 800	2 170	10 506	2 093	10 811	2 006
S9	10 700	2 070	10 437	2 002	10 662	1 881
S10	10 500	2 040	10 470	1 904	11 659	1 982
S11	10 600	2 030	10 188	1 918	10 099	1 742
S12	10 900	2 190	10 617	2 131	10 477	1 943
S13	10 800	2 070	10 457	1 894	10 348	1 717
S14	11 100	2 310	10 688	2 133	10 893	2 029

Depth (m)	T0		T2		T4	
	Cl^- (mg/L)	SO_4^{2-} (mg/L)	Cl^- (mg/L)	SO_4^{2-} (mg/L)	Cl^- (mg/L)	SO_4^{2-} (mg/L)
S15	11 400	2 280	10 990	2 056	10 857	1 893
S16	11 100	2 160	10 929	2 153	11 086	2 196
S17	11 400	2 200	11 044	2 140	10 802	2 048
S18	10 600	2 040	11 006	2 140	11 082	2 114
F1	814	n.d.	n.m.	n.m.	859	n.d.
F2	867	n.d.	n.m.	n.m.	864	n.d.
F3	829	n.d.	n.m.	n.m.	863	n.d.
F4	872	n.d.	n.m.	n.m.	883	n.d.
F5	917	n.d.	n.m.	n.m.	914	n.d.
F6	903	n.d.	n.m.	n.m.	952	n.d.
F7	904	n.d.	n.m.	n.m.	880	n.d.
F8	887	n.d.	n.m.	n.m.	894	n.d.
F9	896	n.d.	n.m.	n.m.	922	n.d.
F10	873	n.d.	n.m.	n.m.	868	n.d.
F11	871	n.d.	n.m.	n.m.	902	n.d.
F12	913	n.d.	n.m.	n.m.	940	n.d.
F13	905	n.d.	n.m.	n.m.	916	n.d.
F14	906	n.d.	n.m.	n.m.	927	n.d.
F15	907	n.d.	n.m.	n.m.	1 181	n.d.
F16	884	n.d.	n.m.	n.m.	987	n.d.
F17	873	n.d.	n.m.	n.m.	973	n.d.
F18	879	n.d.	n.m.	n.m.	996	n.d.

n.m. denotes that the value was not measured
n.d. denotes that the value was not detected